FLOW AND SEDIMENT MOVEMENT IN STEPPED CHANNELS

A thesis

submitted in fulfilment

of the requirements for the degree

of

Doctor of Philosophy

in the

University of Canterbury

by

J.G. Whittaker

Lincoln College

1982

ABSTRACT

Laboratory tests were undertaken to establish the formative mechanism for steps and pools in steep mountain streams. They indicated that the formation of steps and pools is associated with high intensity, low return interval events and the processes of armouring/paving and antidune formation. Lower than formative discharges give the structures their step-pool appearance, and under such discharges they are extremely stable.

Step-pool streams may be modelled by a succession of artificial steps or weirs. Wooden steps were placed in a laboratory channel for this purpose, and clear water flow, clear water scour, and sediment transport tests undertaken for a range of discharges and channel slopes.

Three distinct flow regimes were observed for the clear water flow and clear water scour tests. They were stable tumbling flow, unstable tumbling flow, and shooting flow. Sediment transport complicated the regimes from low transport rates.

Unstable tumbling flow (clear water flow) at a low slope was shown to be caused by the breaking of standing waves at a theoretical maximum of 0.142. For higher slopes (and including clear water scour tests), unstable tumbling flow was shown to be associated with the physical system geometry preventing the submerged hydraulic jump from developing fully. However, unstable tumbling flow was also caused at lower discharges by sediment waves which were a feature of some test runs with sediment transport. Even so, unstable tumbling flow is likely to occur under field conditions only rarely.

With clear water scour, the scour dimensions corresponded to the ultimate static limit. That is, no sediment remains suspended by jet action as occurs for the dynamic limit of scour.

For clear water flow and clear water scour, resistance to flow may be predicted by logarithmic equations. Resistance to flow with sediment transport correlated strongly with the average scour hole size.

A sudden increase in average (and maximum) velocities indicated that with sediment transport, the erosive ability of a step-pool system may increase sharply as pools become drowned by sediment. For a given discharge, increasing the sediment transport rate beyond this drowning led to net deposition, but no real increase in average velocity.

With sediment transport, sediment waves and water waves occurred (independently) despite steady inputs of both water and sediment. This behaviour parallels reports of sediment movement as waves in mountain streams. This tendency toward non-uniformity of water and sediment motion suggests that such behaviour may be explicable in terms of recent advances in non-linear thermodynamics.

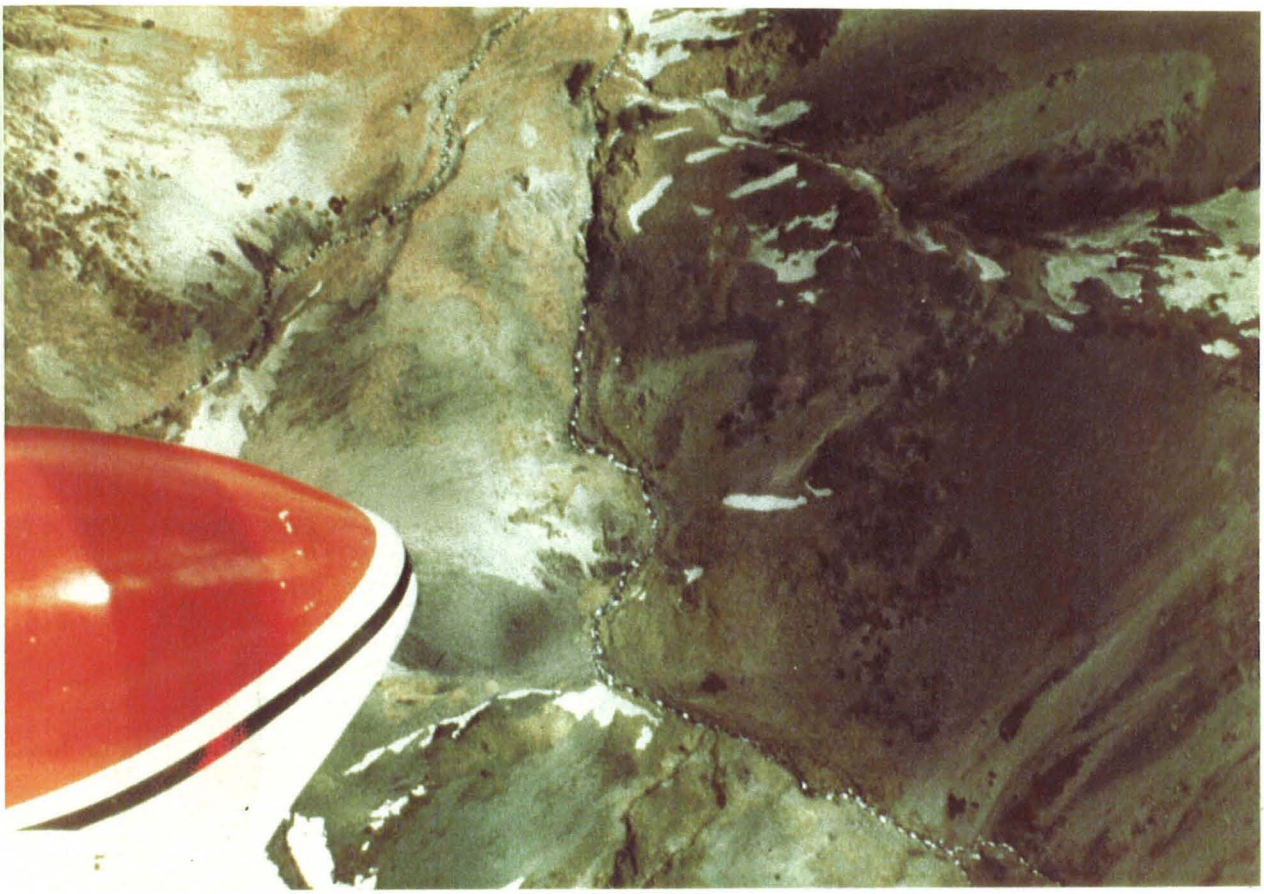

Steps and pools in a steep mountain stream apparent from the air.

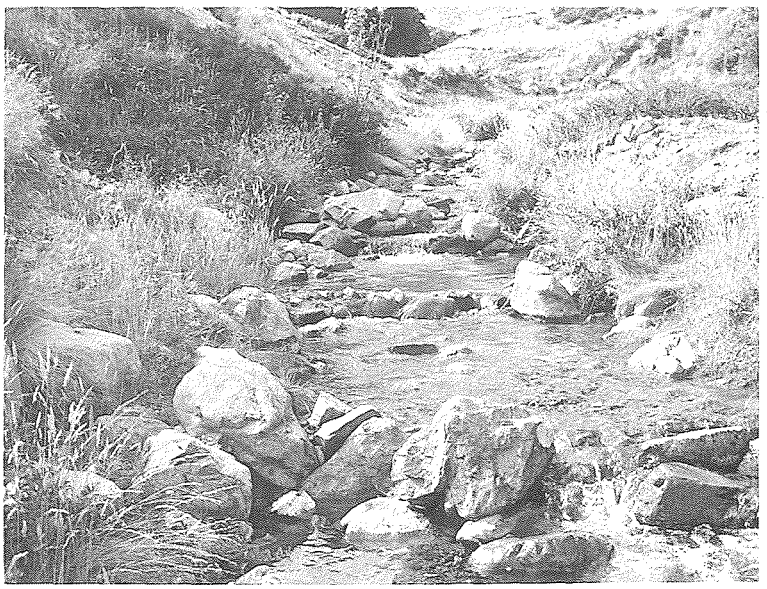

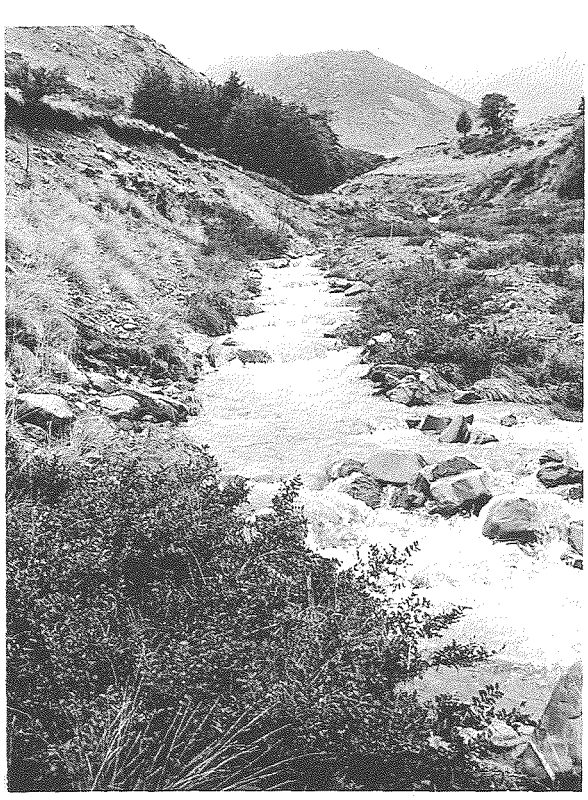

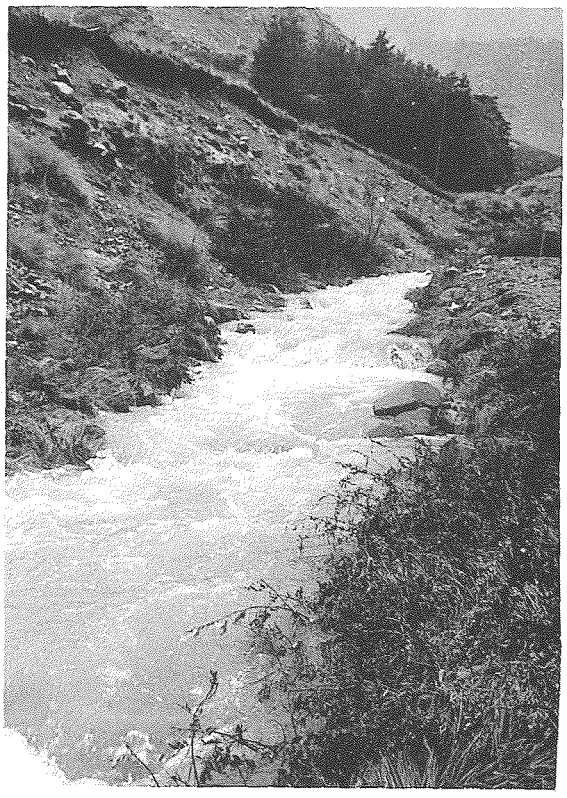

Steps and pools in the Torlesse Stream under varying flow conditions.

ERRATA

Page	Line	Text should read
ABSTRACT	16	...theoretical maximum steepness of 0.142.
XIV	8	...friction factors for discharges ...
12	Fig. caption	...associated bed protuberance.
15	26	$\frac{\partial A}{\partial t} + c \frac{\partial A}{\partial x} = -\beta W \frac{\partial^2 A}{\partial x^2}$ ... 2.12
20	6	...observations of Leopold and Emmett (1976),
21	33/34	...residence time of sediment...
22	6	...Leopold and Emmett (1976) noted...
25	17	...frame (fig. 3.2).
41	16	...(Andrews, 1977; reported by Lisle, 1979), ...
60	16-18	[Remove]... (the point for run 10... region of antidune formation).
71	10	$\sigma = 1 - 1.3 \sin\alpha + 0.08\ h/k$ ...5.16
71	24	$\sqrt{\frac{8}{f}} = \frac{v_m}{v_*} = \phi(\lambda)\left[\frac{\bar{h}}{W}\right]^{7(\lambda-0.08)}\left[\frac{\bar{h}}{k_{50}}\right]^{1/3}$ ...5.17
75	1	...Ishihara et al (1952), and Albertson et al (1960),...
77	25	...5.16 respectively.
89	6/14	... q = 0.004 ... [Comment: The line designating the change in nappe profile in figs. 5.3 and 5.6 is incorrectly drawn].
94	2	...thus $F_1 = 1.672$.
101	11	0.248 0.496 1.768
117	End of page	[Insert: D in mm for equations 6.3 to 6.6]
120	12	...occurs (see section 6.5.2)...
122	4	...Value, a, plus a dimensionless ...
133	8	...were not acting...
133	18	$S' = \frac{H_1 - 0.5 \sin\alpha}{H_1}$
142	19	The length ratio ...
147	6	... 0.172 and 0.248, S...

151	Eq.6.30	$S = \frac{4.52\ q^{0.6}\ H'^{0.5}}{g^{0.5}\ D_{90(m)}^{0.4}} - Tw$ ...6.30
156	4	... clear water flow (fig. 5.17).
159	6	$\sqrt{\frac{8}{f}} = 5.657\ A \log\frac{S_o}{S} + B$
160	4/5	... q = 0.004 ...
162	21	... stream's behaviour
168	Graph abscissa label	$\tan\alpha$
169	8	... to the right in ...
183	Fig. caption	Figure 7.3(b): Plot ...
205	35	... inundation, average ... [Remove: and]
217	12	... Journal of the Hydraulics Div. ...
224	5	... channels. Ph.D. thesis, ...
228	25	... 1981.
241	6	It was found ...
245	15	Further, ...
248	9	... crossings analysis ...
249	3	..., i.e. antidunes, ...
250	21	... close to 0.5; the ...
250	29	... friction factor f_s, ...

TABLE OF CONTENTS

PAGE

PAGE

ACKNOWLEDGEMENTS

The research for this thesis was carried out in the Department of Agricultural Engineering (Lincoln College, University of Canterbury), whose Head is Professor G.T. Ward.

Special thanks and appreciation are due to my Supervisor, Dr T.R.H. Davies. His guidance, encouragement, enthusiasm, helpful criticism and friendship has made the study time much more than a learning experience.

Thanks are also due to Mr M.N.R. Jäggi, who supervised my work during Dr Davies' sabbatical leave in Europe, and who has provided much constructive criticism.

Appreciation is also expressed to the academic and technical staff of the Agricultural Engineering Department. In particular -

Mr Colin Tinker for his assistance with electronics, computing and photographic work;

Messrs Paul Seaton and Ian Clarke for their part in the construction of laboratory apparatus;

Mr Kelvin Nicolle for his assistance with laboratory matters and photographic work;

Dr G.M. Smart (presently working in Zurich, Switzerland) for his encouragement and helpful criticism.

Gratitude is expressed also to Messrs Rob Blakely, Pete Ackroyd, and Dr John Hayward (of the Tussock Grasslands and Mountain Lands Institute, Lincoln College) for the use of Torlesse Stream Catchment data.

I wish to thank Mrs Jan Stewart, Mrs Kathy Brown and Miss Linda Down for typing the manuscript.

Many thanks are due to my wife, Margaret, for her love, encouragement and financial support over the latter part of the project. The encouragement and (financial) support of my parents is also gratefully acknowledged.

For most of the duration of the study, the writer was supported financially by a research grant from the National Water and Soil Conservation Organisation. This support is gratefully acknowledged.

LIST OF FIGURES

FIGURE PAGE

LIST OF TABLES

LIST OF SYMBOLS

a Height of dune above original bed level.

b Width of flume/width between strips in ridge-groove roughness.

b' A function of effective roughness concentration.

c Wave celerity/friction factor.

c_b Bed element shape factor.

c' Position of start of hydraulic jump.

c_* Grain concentration in volume in static debris bed.

e Roughness spacing (equivalent to λ).

f Darcy-Weisbach friction factor f.

g Gravitational acceleration.

h Depth of flow.

$\overline{h}$ Statistical mean depth.

h' Depth of bed datum.

k Mean roughness height/wave number ($= \frac{2\pi}{L}$)

k_n Size of a bed element such that n% of bed elements are larger than k_n.

k_r A Strickler roughness coefficient which indicates grain roughness only.

k_s A Strickler roughness coefficient which indicates total bed resistance/ Equivalent sand grain diameter that gives the same roughness.

k' Actual roughness height experienced by the flow.

m An efficiency for bedload transport (with the Meyer-Peter and Müller bedload formula).

p Grain size distribution of original material.

q Specific discharge/Probability of remaining in the top layer.

$\overline{q}$ An average probability (equivalent to a stability coefficient).

q_1 Specific discharge at which downstream baffle begins to limit development of the scour hole.

q_2 Specific discharge at which depth of scour S begins to decrease with increasing discharge.

q_a Specific discharge at head H_1 computed from the equation for free (unsubmerged) flow.

q_b Specific bedload transport rate.

q_s Specific sediment transport rate.

q_s'' Specific submerged sediment transport rate.

q_{sh} Specific discharge at limit between unstable tumbling flow and shooting flow.

q_{st} Specific discharge at limit between stable tumbling flow and unstable tumbling flow.

q_t Total specific flow rate.

q_{und} Specific discharge of underflow.

(s-1) Excess solids density ratio.

t Time/Thickness of baffles.

u A uniformity coefficient.

v Velocity.

v_c Critical velocity.

v_{max} Maximum velocity.

v_{und} Velocity of underflow.

v_w Absolute velocity of disturbance waves in channel.

v' Approach velocity to roughness element.

v_* Shear velocity.

w_m Fall velocity of sediment.

x Position of any point on a channel.

x' Exponent of the hydraulic radius in the general uniform flow equation.

y Distance from axis of pitot tube to the air-water surface.

y_1 Supercritical (brink) depth of plunging jet.

y_2 Conjugate depth for the hydraulic jump on a horizontal surface.

y_c Critical depth of flow.

y_n Normal depth of flow.

y' Depth at which velocity = 0.

A Wave amplitude/Channel cross-sectional area.

B Boundary shape/Width of scour hole.

C A discharge coefficient/Concentration of tracer solution/Chézy friction factor.

C_D A drag coefficient.

C_L A lift coefficient.

D Median boulder diameter.

DA Drainage area.

D_n Roughness size of sediment such that n% of elements are smaller than.

F Froude number.

F_a Minimum Froude number for antidune formation.

F_f External resisting force.

F_m Maximum Froude number for antidune formation.

F_y Fluctuating forces.

ΣF_m Sum of forces producing motion.

ΣF_r Sum of forces resisting motion.

H Head.

H_1 Upstream head (weir flow).

H_2 Downstream head (weir flow).

H_i Measured energy head at section i.

H_s Differences in height of water surface above and below a hydraulic structure.

H' Fall.

I Measure of the relative area associated with one bed element.

J Channel slope.

J_o $\tan\theta$.

J_r The purely frictional part of the slope.

J' Energy slope due to grain roughness.

J'' Energy slope due to bedform resistance.

L Length between steps/Longitudinal spacing or wavelength of roughness elements.

L_a Length available for hydraulic jump.

L_j Length of hydraulic jump.

L_n Size of bed element long axis such that n% of elements' long axes are shorter than

L_2 Length from change in slope to start of hydraulic jump.

N Number of bed elements larger than a certain size k_n.

N_s Sediment number.

N_{sc} Sediment number at incipient motion conditions.

P Pressure/Wetted perimeter/Probability of grains being transported (Einstein)

Q Discharge.

Q_1 That part of Q whose energy is converted into eddying on the bed.

Q_D Formative discharge.

Q_s Sediment transport (or input) rate.

Q_{sc} Sediment transporting capacity.

Q_{sE} Sediment discharge due to Erosion.

R Hydraulic radius.

Re Reynolds' number.

R_s Hydraulic radius of partial area acting on the bed.

R' Hydraulic radius due to grain roughness.

R'' Hydraulic radius due to form drag.

S Depth of scour.

S_n Size of bed element short axis such that n% of elements short axes are smaller than

S_o Depth of flow at point of maximum scour.

S' Submergence ratio.

T Period of roll waves.

TW Tail water depth.

V Vedernikov number.

W Width of channel (or water surface).

X Distance to the point of maximum scour.

Y_n Size of element cross section axis such that n% of elements' cross axes are smaller than

α Angle of the channel.

α' Coriolos coefficient.

γ (or γ_w) Specific weight of water.

γ_s Specific weight of sediment.

γ_s" Submerged specific weight of sediment.

γ' A shape factor of the channel section.

ζ Some dimensionless inverse function of form loss or scour hole size.

η A function of pressure fluctuations.

θ Relative shear stress/Angle of inclination of plunging jet.

θ' Reduced relative shear stress.

κ Von Kármán's turbulence coefficient.

λ Roughness concentration.

ν Kinematic viscosity of fluid.

π Pi/Dimensionless ratio in Buckingham's Pi theoreum.

ρ Density of fluid.

ρ_s Density of sediment

σ Parameter describing air entrainment.

τ Shear stress.

ϕ A function of/Non dimensional sediment transport rate.

ϕ_a Internal friction angle.

ϕ_b Non dimensional bedload transport rate.

χ A function of the size, shape, and spacing of roughness elements.

ψ Dimensionless flow parameter (equivalent to the inverse relative shear stress.

ψ' Reduced dimensionless flow parameter.

Λ Ratio of model to prototype.

Yalin's nomenclature for Bagnold's work.

cr (Subscript) Critical conditions.

e_b Efficiency for bedload transport.

q_{sb} Specific bedload transport rate.

U_D Velocity in vicinity of the bed.

u_m Mean velocity.

W Ratio of solids to water density.

X Grain size Reynolds' number.

Y A mobility number.

Z A dimensionless granular roughness.

τ_o Shear stress.

ψ Friction angle of channel.

ω Stream power.

ω_o Stream power at incipient motion conditions.

Subscripts

c Critical conditions.

l Air-water phase.

m Mean.

o Initial conditions.

u Values corrected for underflow.

Notation for Appendix 2 is given on page 259.

CHAPTER ONE

INTRODUCTION

1.1 PROBLEM STATEMENT

Excessive sediment supply from upper catchment areas typical of many New Zealand hill regions threatens river control works, hydraulic and other structures, and can cause flooding farther down the river system. Despite the recognition of this problem, little is known of the behaviour of the upland streams transporting the sediment, or of the erosion processes supplying the sediment for transport.

Steep natural channels in such upland regions have a tendency to form apparently well ordered stair-case like structures, which are commonly called step-pool systems. In step-pool systems, water flows over groups of large bed elements that act like weirs, and plunges into pools below these elements. The boundaries of the pools are composed of smaller sediments. While many authors state that step-pool systems are necessarily structured during high intensity, low frequency flood events, no detailed explanation of this process has yet been proposed. An understanding of this formative process is, perhaps, basic to an understanding of other aspects of steep mountain stream behaviour.

The flow in step-pool systems is described as tumbling flow, in which a great part of the flow energy is dissipated by rollers in the pools. The extent of energy dissipation in pools is a measure of the hydraulic roughness of the stream. However, the way in which the ability of the stream to dissipate energy changes with increasing flow rate is not known. It is hypothesised that when the step-pool structure becomes 'drowned' by high flows - that is, its ability to dissipate flow energy by the tumbling overfalls becomes ineffective as high flows shoot straight past the top of the steps - the erosive ability of the stream will increase substantially due to the resultant steeper mean energy slope and greater velocities.

The interaction of erosion (i.e. sediment production) and transport in steep mountain streams is recognised as being very complex (Ashida et al, 1976). On a mountainous watershed, the main causes of sediment yield are surface erosion of bare slopes, landslides, mud-

debris flows, and scouring of the stream bed and banks. These are unsteady phenomena, reflecting an interplay of stream and precipitation runoff. Similarly, sediment transport from these sources is unsteady, varying spatially and temporally. Commenting on the future needs in the sediment field, Wolman (1977) suggested: (p. 51)

> "Both erosion and transport in natural systems vary with time. Perhaps a major need is to understand the way in which discontinuous transport processes take place in channels".

and concluded (p. 54)

> "... as always, we know very little about the sequential micro-processes involved in erosion and sedimentation, but much about the gross impact of some climatic and flow conditions. From both a theoretical and practical point of view, more attention is needed to unsteady or transient phenomena of erosion and transportation".

Certainly, while it is widely accepted that movement of material down slopes is largely controlled by stream bank erosion and undercutting of the toes of slopes occurring when the stream is in flood, little is known of the stream behaviour during these processes.

Similarly, the literature on sediment transport in steep mountain streams reflects general confusion as to the underlying stream processes. The only consistent conclusion to be drawn from different authors is that conventional sediment transport equations are not directly applicable to steep mountain streams. The discontinuous nature of the supply, the storage of sediment within the stream channel, and the morphology of step-pool systems are all recognised as violating assumptions underlying conventional sediment transport formulae.

Consequently, in order to rationalise the behaviour of step-pool streams, an understanding must first be gained of the way in which they are formed. Further, an understanding of the flow processes in step-pool systems is necessary. While this is an end in itself, it is essential for subsequent investigations into erosion and sediment transport (and their interactions) in step-pool systems. In particular, knowledge of when a steep mountain stream will be potentially erosive must be gained. Ultimately a qualitative and quantitative appreciation of risks to downstream fluvial systems and related structures rests on

achieving a satisfactory understanding of the above unknowns.

1.2 OBJECTIVES OF RESEARCH

The work reported herein was undertaken to achieve some understanding of the behaviour of steep mountain streams under a variety of flow and sediment transport conditions. Broadly, the objective of the project was:

> to report and rationalise the behaviour of an idealised step-pool channel stream in response to inputs of water and sediment typical of those occurring in a prototype stream, and to relate this to the known behaviour of step-pool streams in the field.

1.2.1 Specific Objectives and Outline of Methods

From the broad objective, the following specific objectives were formulated, to be achieved as outlined:

Understand the Formation of Step-pool Systems

With a graded sediment (minimum size ≃ 2 mm, maximum size ≃ 50 mm) initially arranged as a plane bed, sediment-moving discharges were to be used to investigate the origin of step-pool systems. Of special interest was the theory that steps and pools (which become apparent at lower flows) originate as antidunes under channel-forming flows. It was also recognised that armouring of the bed surface could be a contributory process. Tests were to be performed at a range of slopes and flow rates.

Longitudinal sediment profiles were to be measured once the bed had attained equilibrium. A zero-crossing analysis would then yield the height and wavelength of bedforms. These characteristics could then be compared to those of antidunes.

Average velocities were to be measured using the salt-velocity technique for a series of low flows as well as the bed shaping flow for each test. This would allow friction factors (a measure of resistance to flow) to be calculated for the shaping flows, and also for the low flows which would give the deformed bed its step-pool appearance.

The bed material size was to be analysed prior to testing. After measuring the longitudinal profile of the equilibrium bed, part of the

bed surface layer was to be sprayed with paint, and the coloured grains removed and sieved. This would give a measured armour layer, which could then be compared to that predicted from the calculated shear stress and sampled bed material.

Understand the Behaviour of an Idealised Step-pool System

A series of 0.285 m high baffle plates were to be established at 0.5 m spacing in the laboratory flume to form an idealised step-pool system. Three sets of tests were then to be performed using this apparathus, namely:

(a) Clear Water Flow. At a series of slopes, for a range of flows, flow regime was to be studied for each test. Average and maximum velocities measured using the salt velocity technique would characterise the erosive ability of the stream. Average velocity would allow calculation of the friction factor for each test. These values were to be compared with conventional resistance equations to see if step-pool systems would be amenable to treatment by conventional hydraulics.

The behaviour of this system would identify any model idiosyncrasies that would have to be allowed for in the following laboratory work.

(b) Clear Water Scour. With the spaces between the baffles initially filled with sediment, the scour field between baffles was to be investigated for a series of slopes, and a range of flows. Again, mean and maximum velocities were to be used to calculate the friction factor and erosive potential. Flow regime was to be compared with that observed for the tests described in (a) above.

(c) Sediment Transport. The tests outlined in (b) were to be repeated, but at each slope-discharge combination, a series of tests would be performed, each with a different sediment transport rate. Modification of the scour field between baffles with transport rate was to be observed (this being the only adjustment available to the system because of imposed flow rate, slope, and sediment input rate). Again, mean and maximum velocities were to be measured.

Attempts would be made to describe the sediment transport rate by an existing equation. (Such an equation would necessarily have a term allowing for channel boundary changes to reflect the only degree of freedom of the system with the given imposed conditions). The stream power approach of Bagnold was anticipated to be the most likely

to be applicable.

1.3 LAYOUT OF THESIS

As can be seen from the objectives outlined above, the laboratory investigations fall into four discrete series of tests. The results for each of the four series of tests, and corresponding analysis, thus stand as discrete entities. For this reason, the thesis has been set out as follows:

Chapter 2 : A literature review of field research relevant to steep mountain streams.

Chapter 3 : A review of the equipment and techniques used in the laboratory investigations.

Chapter 4 : On the origin of step-pool systems.

Chapter 5 : Clear water flow in an artificial step-pool torrent.

Chapter 6 : Clear water scour and associated behaviour of an artificial step-pool torrent.

Chapter 7 : Sediment transport and associated behaviour in an artificial step-pool torrent.

Chapter 8 : Conclusions.

The conclusions presented in Chapter 8 will be general to the project as a whole. However, each chapter will contain its own section on literature (where relevant), tests performed, results, and conclusions. This has been done to preserve clarity by not mingling reporting of the different series of tests.

Symbols used will be as defined in the list of nomenclature. They will also be defined in the text on first appearance. If an alternative meaning is used for a particular symbol, this will be defined in the text also.

CHAPTER TWO

LITERATURE REVIEW : NATURAL STEP-POOL STREAMS

2.1 INTRODUCTION

Physical processes affecting streambed form and composition have been investigated by earth scientists and by hydraulic and hydrologic engineers. The earth sciences have a large body of literature on the development of river systems, river morphology, and erosion and sedimentation processes. Engineers have addressed channel stability and capacity, together with the mechanics and prediction of sediment transport.

Drawing from these different sources, the literature related to steep mountain streams can be classified into five different but overlapping fields. They are:

(a) The geomorphology of steep mountain streams.

(b) The origin of step-pool systems in steep mountain streams (to be dealt with in Chapter 4).

(c) The mechanics of flow in steep mountain streams.

(d) Sediment studies in steep mountain streams and

(e) Sediment transport theories (to be dealt with in Chapter 7).

In the following literature review, (a), (c) and (d) will be investigated in turn. (It is important to note that 'steep' is used as meaning high gradient, rather than that slope that would result in super-critical flow).

2.2 THE GEOMORPHOLOGY OF STEEP MOUNTAIN STREAMS

Longitudinal stream profiles do not usually show a smoothly varying slope, but take the form of reaches of alternatively flatter and steeper slope, associated respectively with deeper and shallower flow sections. Leopold and Wolman (1957) noted that these shallows and deeps are a fundamental characteristic of almost all rivers. Further,

Keller and Melhorn (1978) assert that their existence is largely independent of the material in the channel bed and banks. This is demonstrated by the occurrence of riffles and pools in bed rock as well as in alluvial channels, and by meandering and step formation in supraglacial streams. Leopold et al (1964) comments that there appears to be a latent tendency for the development of riffles and pools even in boulder-bed channels.

This tendency has frequently been reported in steep mountain streams (Ashida et al, 1976, 1981; Day, 1972; Hayward, 1978, 1980; Judd, 1964; Judd and Peterson, 1969; Leopold et al, 1964; Newson, 1981; O'Loughlin, 1969; and Scheuerlein, 1973). In these streams, the alternating sections are often called steps and pools, because of their staircase-like appearance. Thus, despite widely differing channel form, there exists a continuum of channel pattern (Leopold and Wolman, 1957) from low gradient alluvial streams through to steep mountain streams incised in coarse debris.

Steps are formed from large bed elements (Judd, 1964; Judd and Peterson, 1969; Kellerhals, 1973; Newson, 1981). The size of these bed elements may be of the same order as the depth of flow (Day, 1981; Judd, 1964), or even comparable to the width of the channel (Kellerhals, 1972). Judd (1964) and Judd and Peterson (1969) considered the bed to be essentially 'fixed' because of imbrication of the large bed elements. Hayward (1978, 1980) classified step structures into three types as follows:

(a) Boulder steps consist of a group of boulders arranged in a straight or curved line across the channel (fig. 2-1). These are generally found on slopes greater than 5%.

(b) Riffle steps are a collection of larger than average sized sediments which steepen the channel profiles (fig. 2-2), and are found on slopes less than 5%. Riffle steps may contain boulder steps. (Riffle steps lie in the slope range given by Bathurst et al (1981) as being definitive of boulder-bed channels).

(c) Rock steps are found where the channel is confined between bed rock outcrops (fig. 2-3).

Hayward also identified what he called a 'major' and a 'minor' pattern. The minor patterns were found within the major and were most commonly boulder steps. The major patterns were most commonly riffle steps or rock steps. The implication is that the major steps control

Figure 2-1: Boulder steps.

Figure 2-2: Riffle step .

Figure 2-3: Rock steps.

channel grade.

Other authors have referred to boulder steps as being 'transverse ribs' (Boothroyd, 1970; Gustavson, 1974; Koster, 1978; McDonald and Banerjee, 1970, 1971; McDonald and Day, 1978). Transverse ribs are usually found on the riffle portion of low gradient, high width to depth ratio channels with coarse alluvial beds. These channels are often found on glacial outwash fans. Transverse ribs exist as regular pebble, cobble or boulder ridges oriented transversely to flow (McDonald and Banerjee, 1971). The inter-rib areas of the riffle usually contain finer material. The connection with steeper mountain streams was made by McDonald and Banerjee (1971), when data from the No-See-Um Creek (gradient = 7.1%) fitted on a line through data from the Peyto outwash plain (gradient less than 2.2%) on a graph of rib-clast b-axis size versus spacing between ribs.

The structure of bedforms in steep mountain streams may be approached differently to the hierarchical approach of Hayward. Laronne and Carson (1975) investigated a channel ranging in slope from 2% to 9%. They noted frequent large variations in channel width and depth of flow, as well as armouring. [Note: subsequently in this thesis, the loose term armouring will not be used as a description of any imbricated surface. Instead, the definitions of 'armouring' and 'paving' of Bray and Church (1980) will be employed. These definitions are:

> Armouring: Where the population of the bed surface layer material is essentially the same as the population of the subsurface material, when the subsurface bed material size distribution is truncated below 8 mm.
>
> Paving: Where the population of the surface layer material consists of obviously larger sized particles than the population of the subsurface material, when the subsurface bed material size distribution is truncated below 8 mm].

Two main types of bed condition were noted by Laronne and Carson, namely bed protuberances and boulder shadows. Bed protuberances were defined as a single boulder, or a group of boulders dispersed in a section of the bed. Single boulders were seen to occupy about 5 to 10% of the bed area, while groups of boulders were seen to occupy greater than 15%, sometimes with imbrication. These groups were often seen to form transverse ribs.

Almost all bed protuberances were associated with boulder shadows (in both upstream or downstream situations; see fig. 2-4).

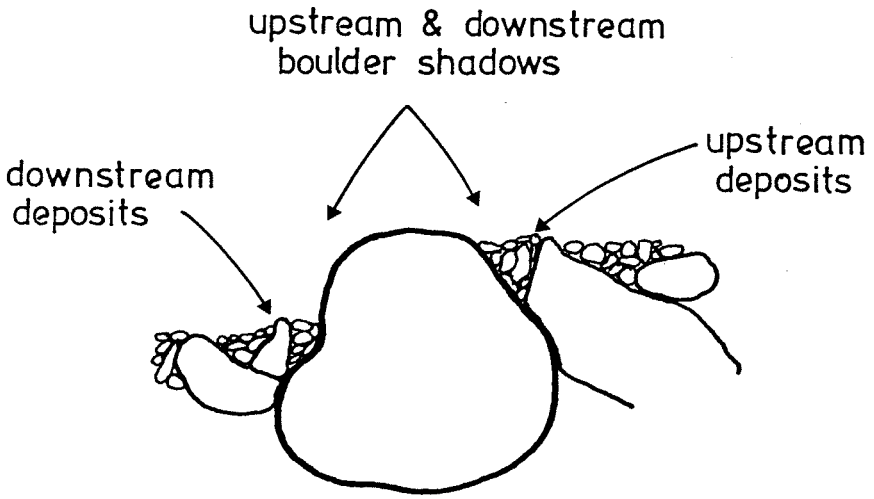

Fig. 2-4: Boulder shadows and associated bed protuberances.

Downstream deposits were found to be predominantly pebbles and fine cobbles, while upstream deposits were mainly small pebbles (10 to 30 mm). Riffle steps may then be viewed as sections of channel with disordered group proturberances.

Most of the channel investigated by Laronne and Carson displayed imbrication of the bed surface material. This imbrication was more stable for the steeper parts of the channel. At lower slopes, interaction of bedload with the armour layer was demonstrated by the selective burial process of labelled bedload particles (see section 2-4-2).

Thus, the bed features classified by Hayward (1978, 1980) can be seen as being determined by the distribution of bed protuberances. Judd (1964) and Judd and Peterson (1969) took a similar approach. After defining a mean plane for the bed of a section of channel, they repres-

ented the intensity of large bed elements with an equation

$$\frac{\sqrt{A}}{k_n} = I\ N^u \qquad \ldots 2\text{-}1$$

where N = number of bed elements larger than a certain size k_n

k_n = size of a bed element such that n% of the bed elements are larger than k_n

A = the area of the cross section of channel

u = a uniformity coefficient

and I = a measure of the relative area associated with one bed element.

This quasi-statistical approach allows recognition of different step types, but avoids the hierarchical distinctions of Hayward.

Many authors recognise that step structure becomes better defined and more regular at steeper slopes (Hayward, 1978, 1980; Heede, 1972(a), 1972(b); Judd, 1964; Judd and Peterson, 1969; O'Loughlin, 1969). Judd, and Judd and Peterson attempted to describe the longitudinal spacing of steps with an equation

$$L = \frac{k_{16}}{C\ J^z} \qquad \ldots 2\text{-}2$$

where L = length between steps

J = slope

k_{16} = a representative bed element height

and C = 2.0, z = 1.0 for average conditions.

In forested catchments, large organic debris in steep mountain streams also forms steps (Beschta, 1981, Heede, 1972(a), 1972(b); Keller and Swanson, 1979). Heede showed that after such organic steps had formed, boulder steps also formed. The result was that in the streams he investigated, more than $\frac{3}{4}$ of the vertical fall was due to steps and pools. Keller and Swanson stated that organic debris contributed between 30% and 80% of falls in channels of around 15% gradient.

2.3 MECHANICS OF FLOW IN STEEP MOUNTAIN STREAMS

Flow in steep mountain streams is characterised by highly variable velocity and intense turbulence, often combined with air entrainment (Hartung and Scheuerlein, 1967; Scheuerlein, 1973). The extremely

large roughness elements in these streams cause ill-defined cross-sections and frequent hydraulic jumps (Kellerhals, 1973). Consequently, the flow has been designated tumbling flow (Judd, 1964; Judd and Peterson, 1969; Kellerhals, 1970, 1972, 1973; Mohanty, 1959; Peterson and Mohanty, 1960). Other authors have commented on the significant energy dissipation that occurs because of the flow patterns of falls and pools in a step-pool stream (Ashida et al, 1976, 1981; Heede, 1972 (a), 1972(b), Newson, 1981).

Most steep mountain streams are geographically remote, and therefore measurements of their basic hydraulic, hydrologic and morphological characteristics are difficult to make. One approach to overcome this difficulty has been to use a hydro-morphic procedure (Day, 1969, 1972) whereby the evaluation of changes in the runoff process can be predicted from channel and basin dimensions. (These can be taken from topographic maps or aerial photographs). Channel width W is related to either drainage area DA (Miller, 1958) or a formative discharge Q_D.

i.e. $$W = \phi_1 \ (DA, \ Q_D, \ J...) \qquad ...2\text{-}3$$

where J = channel slope.

Day (1969), working with channels ranging in slope from 1% to 20%, ignored roughness in his analysis. (Although based on dimensional analysis, this was more like a regime analysis). He began with the continuity equation

$$Q = A.v_m \qquad ...2\text{-}4$$

where Q = flow

A = flow cross-sectional area

and v_m = mean flow velocity.

At a given cross-section, A and v_m vary with discharge as simple power functions (Leopold and Maddock, 1953).

$$v_m = k \ Q^m \qquad ...2\text{-}5$$

$$A = a_A \ Q^{b_A} \qquad ...2\text{-}6$$

(The relationships are usually expressed in terms of v_m, flow depth h, and flow width W as follows:

$$v_m = k \ Q^m \qquad ...2\text{-}5$$

$$h = c\, Q^{f} \qquad \ldots 2\text{-}7$$

and

$$W = a\, Q^{b} \qquad \ldots 2\text{-}8$$

Day used A instead of W because of channel irregularities). Day measured Q and v_m by salt dilution gauging and established an equation for width

$$W = a\, DA^{b}\, J^{c} \qquad \ldots 2\text{-}9$$

J was subsequently found to be insignificant. The equation relating A to Q was then found to have the form

$$A = \phi_2(W)\, Q^{\phi_3(W)} \qquad \ldots 2\text{-}10$$

Kellerhals (1970, 1972, 1973) further developed this theme on the assumption that tumbling flow systems should behave like kinematic flow systems (i.e. the channel at any cross section will be governed by a unique A-Q relation). Confirming that only equations of the form of equation 2-6 gave a good fit to his data, Kellerhals noted that b_A reflected channel type. $b_A = 0.6$ for rough, broad channels, and $b_A = 0.3$ for cascades of pools controlled by parabolic weirs.

He then modelled wave propagation in steep natural channels with this kinematic approach, based on the continuity equation

$$\frac{\partial A}{\partial t} + \frac{\partial Q}{\partial x} = 0 \text{ or } \frac{\partial A}{\partial t} + c\,\frac{\partial A}{\partial x} = 0 \qquad \ldots 2\text{-}11$$

where x = position of any point on the channel

t = time

and c = wave celerity.

However, contrary to the behaviour of kinematic waves, both positive and negative wave fronts were observed to flatten, so a dispersive term βW was added to the equation to give

$$\frac{\partial A}{\partial t} + c\,\frac{\partial Q}{\partial x} = -\,\beta W\,\frac{\partial^2 A}{\partial x^2} \qquad \ldots 2\text{-}12$$

This was solved. However, a computationally simpler model was developed by Kellerhals. In this, the channel was replaced by a cascade of pairs of non-linear reservoirs (for dispersion of waves) and truly kinematic channel segments (for downstream progression of waves).

Bren and Turner (1978), working in a stream of gradient of approximately 8%, and with Reynolds' numbers exceeding 10,000, generated

shock waves over a reach of about 40 m. Kinematic wave theory was found to give a good simulation of the recession hydrograph, and to reproduce features of the rising hydrograph.

Leopold and Maddock (1953) postulated that width W, depth h and velocity v for naturally formed streams are all power functions of discharge Q, i.e.

$$W = a\,Q^{b} \qquad \ldots 2\text{-}8$$

$$h = c\,Q^{f} \qquad \ldots 2\text{-}7$$

$$v = k\,Q^{m} \qquad \ldots 2\text{-}5$$

Further, $Q = a\,Q^{b}.\ c\,Q^{f}.\ k\,Q^{m}$ such that $a.c.k = 1$ and $b + f + m = 1$.

These relationships have been investigated by several authors. Judd (1964), using mean velocity and statistical mean depth $\bar{h}$, found that the average values for the six reaches investigated gave $b + f + m = 1.02$. Heede (1972(a)) assumed that b could be ignored (because width changes so little with discharge), and found average values for f and m of 0.43 and 0.52 respectively (mean channel gradient = 26%). Judd used his results to solve v_m in terms of his statistical mean depth. This resulted in an equation very similar to one relating v_m to channel parameters that was established by dimensional analysis.

Judd and Peterson (1969) noted that with large relative roughness heights, the commonly accepted logarithmic velocity distribution does not hold. However, while non-uniform and unsteady on a small scale, the flow may be macroscopically uniform within a reach providing that the roughness pattern has uniform statistical characteristics within that reach. Judd (1964) used this assumption without stating it. In relating bed characteristics to hydraulic ones, he found that a mean velocity equation of the power form gave best results, viz

$$\frac{v_m}{\sqrt{g\,J\bar{h}}} = c_5\,c_b\,I^{-0.71}\left(\frac{\bar{h}}{W}\right)^{1/3}\left(\frac{\bar{h}}{k_n}\right)^{1/3} \qquad \ldots 2\text{-}13$$

where $c_5 = \phi_4(k_n)$

c_b = a bed element shape factor

$\bar{h}$ = a statistical mean depth

I = an intensity factor

W = width of water surface

and k_n = a bed element size such that n% are larger than k_n.

The equation was tested over a slope range of 1% to 4%.

On this assumption of macroscopic uniformity, Judd and Peterson described the flow in a steep rough channel by the momentum equation

$$\left(\frac{Q\gamma}{g}\right)(v_{m1} - v_{m2}) = P_{m1} - P_{m2} + W\sin\alpha - F_f \qquad ...2\text{-}14$$

where v_{mi}, P_{mi} are the velocity and pressure respectively at section i.

α = slope angle of the channel

F_f = external resistance force

and $W\sin\alpha$ = component of the gravity force acting in the direction of motion.

From the assumption of macroscopic uniformity,

$$P_{m1} = P_{m2},\ v_{m1} = v_{m2}$$

and $W\sin\alpha = F_f$.

Using assumptions about bed element shape, field results, and flume data from simulated natural channels, they obtained the equation

$$\frac{v_m}{\sqrt{g\ J\bar{h}}} = \phi(\lambda)\left(\frac{\bar{h}}{W}\right)^{7(\lambda-0.08)}\left(\frac{\bar{h}}{k_{50}}\right)^{1/3} \qquad ...2\text{-}15$$

where $\lambda = \dfrac{(\Sigma \text{ vertical projected areas of bed elements})}{(\text{Area of the bed})}$

Judd and Peterson observed that for large bed element channels, the Froude number rarely, if ever, exceeded unity.

Like Judd and Peterson, Hartung and Scheuerlein (1967) assumed the flow to be quasi-steady, but further assumed that it could be considered an homogeneous air-water mixture. The flow was represented by the Bernoulli equation

$$\gamma H_i = \gamma_\ell\, y_{\ell i}\cos\alpha + \gamma\frac{v^2_{\ell i}}{2g} \qquad ...2\text{-}16$$

where ℓ (subscript) refers to the air-water phase

α = angle of channel

H_i = measured energy head at point i

and y = distance from the axis of the pitot tube to the air-water surface.

Defining $\sigma_m = \dfrac{\gamma_\ell}{\gamma}$ as a mean value of a parameter describing air entrainment, they deduced

$$v_{\ell m} = c_\ell\sqrt{2g}\,(\sigma_m\, y_\ell)^{1/2}(\sin\alpha)^{1/2} \qquad ...2\text{-}17$$

where m denotes a mean value

and c_ℓ = a resistance factor (which was not independent of roughness, and was defined graphically).

The equation is a variation of the Brahms-Chézy relationship.

Scheuerlein (1973) attempted to solve the same system using a logarithmic formula. (Both Hartung and Scheuerlein (1967) and Scheuerlein (1973) refer to investigations of a large bed element channel of gradient up to 67%). Scheuerlein (1973) citing other authors, reduced their various equations to the common form

$$\frac{1}{\sqrt{f}} = -A \log\left(\frac{k}{R} B\right) \qquad \ldots 2\text{-}18$$

where f = Darcy-Weisbach friction factor

k = mean roughness height

R = hydraulic radius

B = an empirically determined coefficient

$A = \frac{\ell n\ 10}{\kappa\sqrt{8}}$

and κ = Von Kármán's turbulence coefficient.

He then obtained from his data

$$B = \sigma(0.44 + 3\phi) \qquad \ldots 2\text{-}19$$

where σ = an aeration factor

and

$$\phi = k\frac{\tan\alpha}{L} \qquad \ldots 2\text{-}20$$

where L = a longitudinal spacing of roughness elements

and $\tan\alpha$ = channel slope.

While most authors note the role of pools in dissipating fluid energy at low flows, few have considered the behaviour of step-pool systems at high flows. Hayward (1980) and Heede (1972(a)) both postulated the possibility of drowning of the step-pool structure at high flows, with resultant decrease in fluid energy dissipation. However, Heede considered structural submergence rare, while Hayward considered impairment in the dissipation of energy as potentially far more severe when pools are filled with gravel.

2.4 SEDIMENT STUDIES IN STEEP MOUNTAIN STREAMS

Research into sediment movement in steep mountain streams has been limited. However, a body of literature describing some aspects

has been built up by researchers mainly in the Western United States of America. (Streams investigated have been mainly gravel-bottomed riffle-pool streams, which are still considered as steep. Thus the following review will consider these as well as the steeper step-pool channels). A consistent feature in the literature is that sediment transport in steep mountain streams is typified by temporal and spatial variations of orders of magnitude, even under constant flow conditions. This variation has led many researchers to attempt to develop sediment runoff prediction formulas which have considered the watershed as a black box. Inputs to the models have been macroscopic factors such as climate and topography (Ashida et al, 1976). Hayward (1980) points out the inappropriateness of some of these models, specifically those attempting to relate sediment delivery rate to climate and relief.

Another common method of predicting bedload transport rate, that of assuming it to be a certain percentage of the suspended sediment transport rate, is also seen to be incorrect. Jarocki (1957, quoted by Gregory and Walling, 1973) estimates that bedload accounts for 70% of the total sediment from alpine streams. Kellerhals (1972) confirms that bedload makes a significant contribution to total sediments in mountain streams in Alberta. By contrast, MacPherson (1971) found that at Bragg Creek (Alberta), bedload accounted for less than 1% of total annual sediment yield. Hayward (1980) reported suspended sediment in the Torlesse Stream to account for only 10% of the total annual sediment yield.

Ashida et al (1976) observed that even though the main sediment sources and grain size distributions may be known (as they were for their study basin), the complicated transport phenomena make any quantitative discussion equally complex.

Despite these problems, several consistent features emerge from all these studies. First, sediment production is from limited sites within the catchment. Secondly, this sediment is stored in the stream channel. Once this stored sediment moves through a channel reach, the transport rate drops considerably (for the same flow) until there is another input from one of the sediment production sites. This effect is modified at lower slopes where interaction of bedload and the armour layer occurs. Further, especially at higher slopes, the streams are seldom transporting bedload at capacity. This is due to paving or armouring, as well as the above two reasons.

Any attempts to model sediment transport in steep mountain streams must, then, be able to calculate bedload transport rates as a function of hydraulic conditions, sediment inflows and streambed scour and deposition (accounting for changes in streambed elevation and composition) (Jackson, 1981).

Based on observations of Emmett (1976), Jackson (1981) proposed a bed-material routing model operating in two distinct phases. Phase 1 involves the transport of bed material over a stable armoured bed. Phase 11 bedload transport occurs at flows which are greater than those required to entrain riffle armour, and includes larger riffle sediments in addition to Phase 1 sediments. This model, while developed for low gradient riffle and pool rivers, can also be applied to steeper step-pool streams.

2.4.1 Sediment Movement in Step-Pool Streams

The paved beds of step-pool streams are extremely stable, and only break down under very high flow rates. Ashida et al (1981) calculated that the critical flow required to destroy a paved bed at steep slopes is about 4 m^3/s. A 25 yr flood with peak discharge of about 2.1 m^3/s (Hayward, 1980) destroyed small sections of paved bed in the Torlesse Stream.

Thus the main mode of transport in the step-pool system is Phase 1 type where bedload moves along a paved channel. Because the sediment inputs are usually of a bulk nature, the sediment is stored in the channel and tends to move through the step-pool system as discrete waves. Sediment yield is often measured at or near the mouth of a catchment or watershed. Any one particular flood hydrograph may or may not move a sediment wave within the channel through the sampling station. Hayward (1980) reported highly variable sediment yields for storms of the same magnitude. If the sediment wave is at or near the sampling station, the measured transport rate will correlate highly with the rising limb of a flood hydrograph. Ashida et al (1976) noted that if the stored sediment was of sufficient quantity, then sediment transport rate approached an equilibrium state such that a bedload formula may have been appropriate.

However, if the sediment wave is some distance from the sampling site, there is a time lag before sediment yield occurs under the rising limb of the hydrograph. Antecedent low flows may have sorted the stored

sediment, moving available smaller sizes further down the channel. During a flood these are sampled before the main bulk of the sediment wave moves through the sampling station (Ashida et al, 1976).

The extreme case is where antecedent flows have swept the channel clean of stored sediment before a flood event. Under such conditions, Ashida et al (1976) measured lag times of about 10 to 12 hours, the time taken for material to travel 500 m from the supply area. Hayward (1978, 1980) measured the progress of sediment waves through the Torlesse stream, and similar waves were also noted by Nanson (1974). Implicit in the above is that most bedload movement occurs over very short periods of time. Hayward calculated that 90% of sediment transport for the Torlesse stream occurred in 1% of total time.

Thus bedload transport in step-pool systems is supply regulated (Ashida et al, 1976, 1981; Hayward, 1980; Nanson, 1974) and not controlled by bed and hydraulic variables (Griffiths, 1980; Nanson, 1974). Storage in the pools causes complex hysteresis in the sediment transport process (Ashida et al, 1981). If the paved channel surface is destroyed, sediment discharge increases rapidly.

2.4.2 Sediment Transport in Riffle-Pool Gravel Bedded Streams

Gravel-bedded riffle-pool streams occur at lower slopes than step-pool streams. The major difference is that the channel of riffle-pool streams is armoured, not paved. Because the armour layer forms under high frequency, low intensity flow events, it breaks down under about a two year flood, with consequent strong channel bed/bedload interaction. Milhous and Klingeman (1973) assert that for these streams, the armour layer is the most important single factor limiting the availability of stream bed sediment and in controlling the relationship between stream flow and bedload discharge. Large temporal variations in bedload transport occur (Beschta, 1981).

As in the case of step-pool streams, waves of sediment may be stored in the stream channel, specifically in the pools (Meade et al, 1981). As well, the bulk of sediment transport of many of these streams occurs over short periods of time (Bennet and Nordin, 1977). The residence of time of sediment in riffle-pool streams tends to be long (as compared to step-pool streams). Including the interaction of stored sediment with the channel bed, Dietrich and Dunne (1978) estimated the channel residence time for sediment in Rock Creek (Oregon Coast Range)

to be approximately 620 years. Megahan (1976) estimated that for small forested catchments in central Idaho, an average of only 10% of stored sediment appeared as annual yield over the period 1972-1974.

Phase 1 transport occurs in riffle-pool streams during floods of low magnitude, i.e. flows insufficient to disrupt the bed armour. Emmett (1976) noted for these conditions bedload of mostly sand sized particles, while Bennet and Nordin (1977) reported sediment moving in intermittent waves over the top of the armoured layer.

However, as soon as the flow disrupts the armour layer, and Phase 11 transport begins, sediment transport factors become highly variable as a result of interactions between flow conditions, sediment transport, and stream bed composition and form (Jackson, 1981). As the armour layer breaks down, gravel sizes from the armour layer are transported as bedload. Fines trapped in or beneath the armour layer become available for transport (as suspended or bedload, depending on the particle size) as sections of the bed experience rapid scour (Bennet and Nordin, 1977; Beschta, 1981; Edwards, 1980; Jackson, 1981). So, on the rising limb of the hydrograph, transport rate will increase with flow. Scour and fill occur at different times at different sections of the channel. Because of this, relatively large fluctuations or pulses in the transport rate occurs on the receding hydrograph limb (Beschta, 1981).

As the flow drops, the armour layer will reform. Its composition will be determined by hydrograph shape, the existing substrate, bed material, and material in transport (Jackson, 1981). The complexity of this reformation is reflected in the variety of structures and lenses of different sized materials (Edwards, 1980) occurring in the substrate. Further, as the armour forms, fines from suspended material and bedload filter into sheltered positions and pores in the armoured structure. Because of the unique combination of conditions encountered during the formation of each armour layer, its grain size distribution will vary from one flood event to another (Milhous and Klingeman, 1971, 1973). Similarly, the critical flow for subsequent disruption of the armour layer will vary.

2.4.3 A Model and General Features

A sediment routing model that is applicable to both step-pool and riffle-pool streams is that of Ashida et al (1976), developed for

the Hirudani watershed of the Ashiaraidani experimental basin (Northern Japan). The two-phase nature of sediment transport is implicit in the option 'Channel Erosion'. The model can be generalised as follows (fig. 2-5).

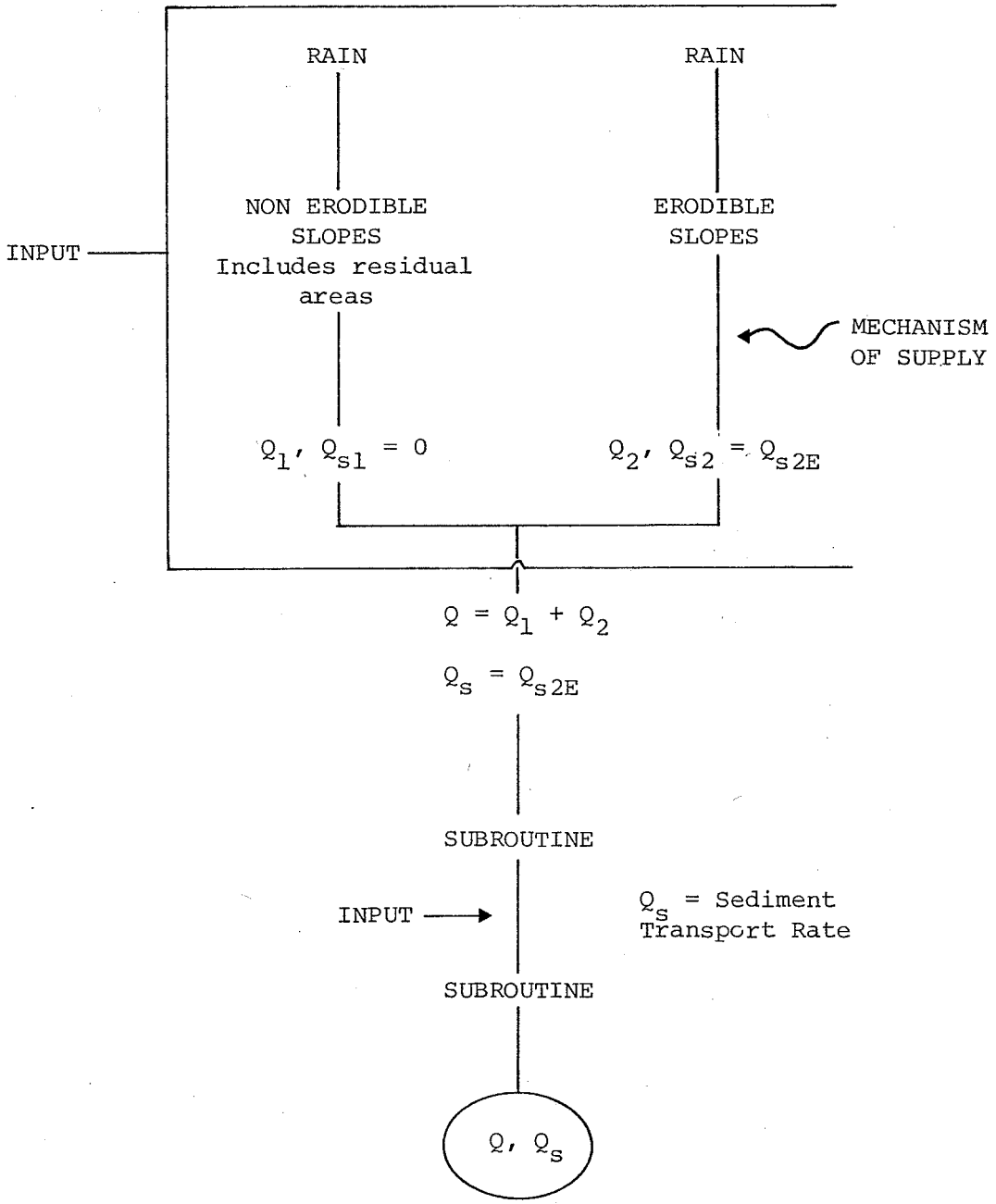

Fig. 2-5 Generalised Sediment Routing Model (After Ashida et al, 1976).

Inputs from other watersheds may be added in series with the channel process SUBROUTINE as shown.

The step nature of input to the model is not inappropriate. Ashida et al (1976, 1981) list the mechanisms of sediment supply to the channel as: surface erosion of bare slopes, land slides, mud debris flows and scouring of channel bed and banks. In their 1976 study they

divided the Hirudani watershed into three sub-watersheds based on sediment supply sites and mechanisms. Petrographical analysis of sediment yield enabled the contribution of each of the supply sites in the sub-watersheds to be identified. Nanson (1974) identified the main sediment supply to Bridge Creek (a small, steep tributary to the North Saskatchewan River, Alberta, Canada) to be from spring-thaw activated debris flows of glacial deposits in the middle and lower parts of the basin into the entrenched stream.

The movement of bedload (or suspended load) through the channel is modelled by the option SUBROUTINE (fig. 2-6)

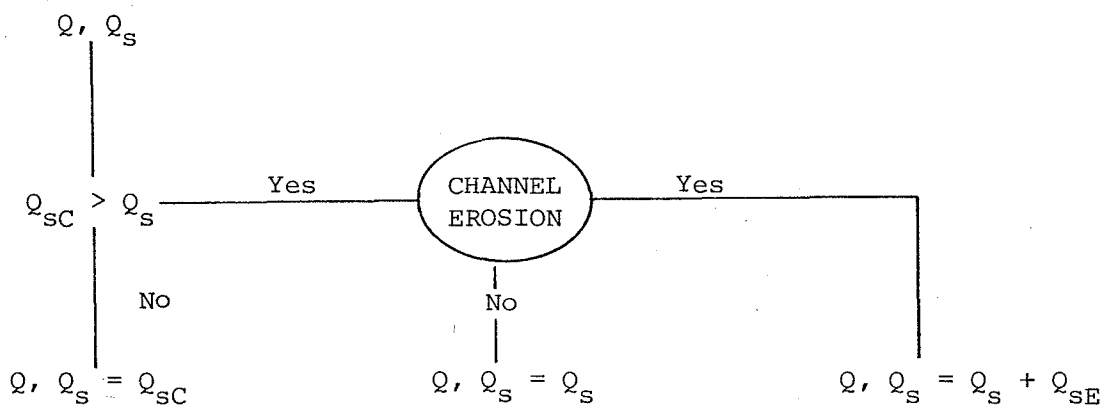

Q = Flow rate

Q_s = Sediment discharge

Q_{sE} = Sediment discharge due to erosion

Q_{sC} = Sediment transporting capacity.

Fig. 2-6 Detail of option SUBROUTINE in Routing Model (after Ashida et al, 1976).

The actual mechanics of sediment movement are not given by SUBROUTINE. A feature of the bedload transport in most of the streams discussed above was that for conditions where flow and average bedload transport rates were essentially constant, instantaneous bedload rates fluctuated markedly. This is probably caused by the mechanism of bedload movement through a step-pool reach as particularly influenced by channel morphology (Ashida et al, 1981), and is examined in Chapter 7.

CHAPTER THREE

LABORATORY APPARATUS

3.1 TILTING FLUME

The primary laboratory component was a 10 m long tilting, recirculating channel (fig. 3-1). The channel was designed by the writer, who assisted in the initial major construction. All subsequent work on the channel was done by the writer.

The main structural component of the flume is a 9.5 m long 203 x 152 x 9.5 RHS section. This was oriented with the major section dimension vertical. An angle-iron frame was welded to both sides to enable side-walls to be attached inside (fig. 3-2). A full-depth viewing section of perspex 4.5 m long was included in the middle of both side-walls of the channel. The rest of the channel side-walls, as well as the channel bottom, were made of marine plywood coated with fibre-glass. The channel depth is approximately 0.6 m, and the internal channel width 0.132 m.

The flume is hinged at the lower end, the support being a splayed frame (fig. 3-1). Slope adjustment is made at the upper end of the channel. The channel is lifted via an attached hinged yoke by a chain-hoist suspended from the tower structure (fig. 3-3). At the desired slope, the channel rests on a steel bar located in holes through the tower members. The slopes of the channel corresponding to positions of the bar are given in Table 3-1.

TABLE 3-1 FLUME SLOPES

Position Number	α^{o}	Slope J (tan α)
1	1.54	0.027
2	3.60	0.063
3	5.62	0.098
4	7.72	0.136
5	9.77	0.172
6	11.84	0.210
7	13.93	0.248

Figure 3-1: The laboratory channel.

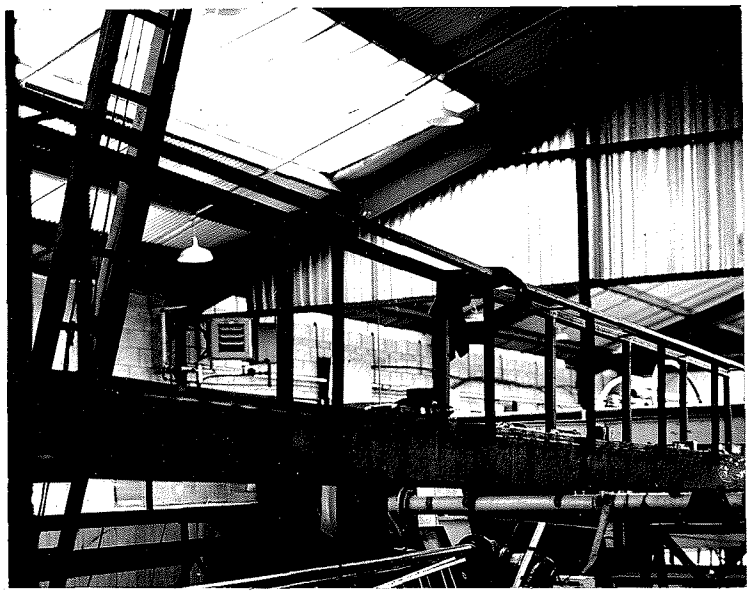

Figure 3-2: Angle-iron side-wall frame.

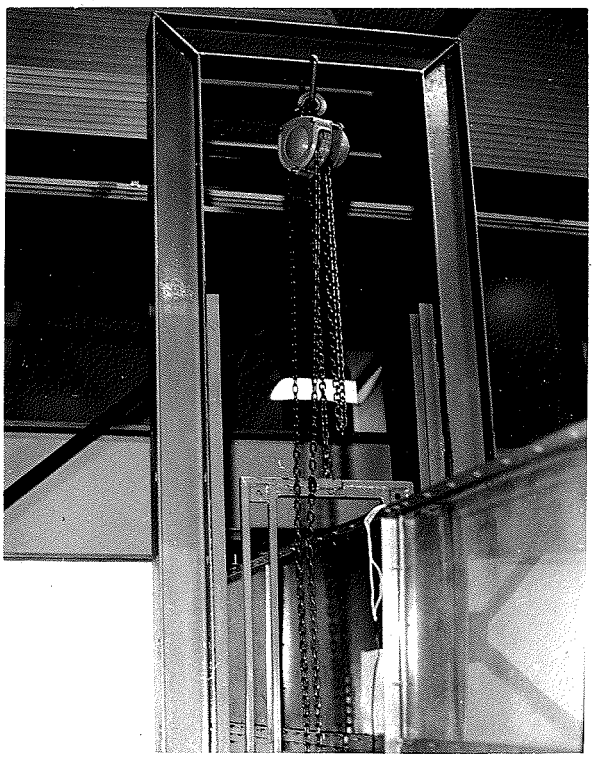

Figure 3-3: Lifting arrangement.

Figure 3-4: Location of lifting yoke in towe

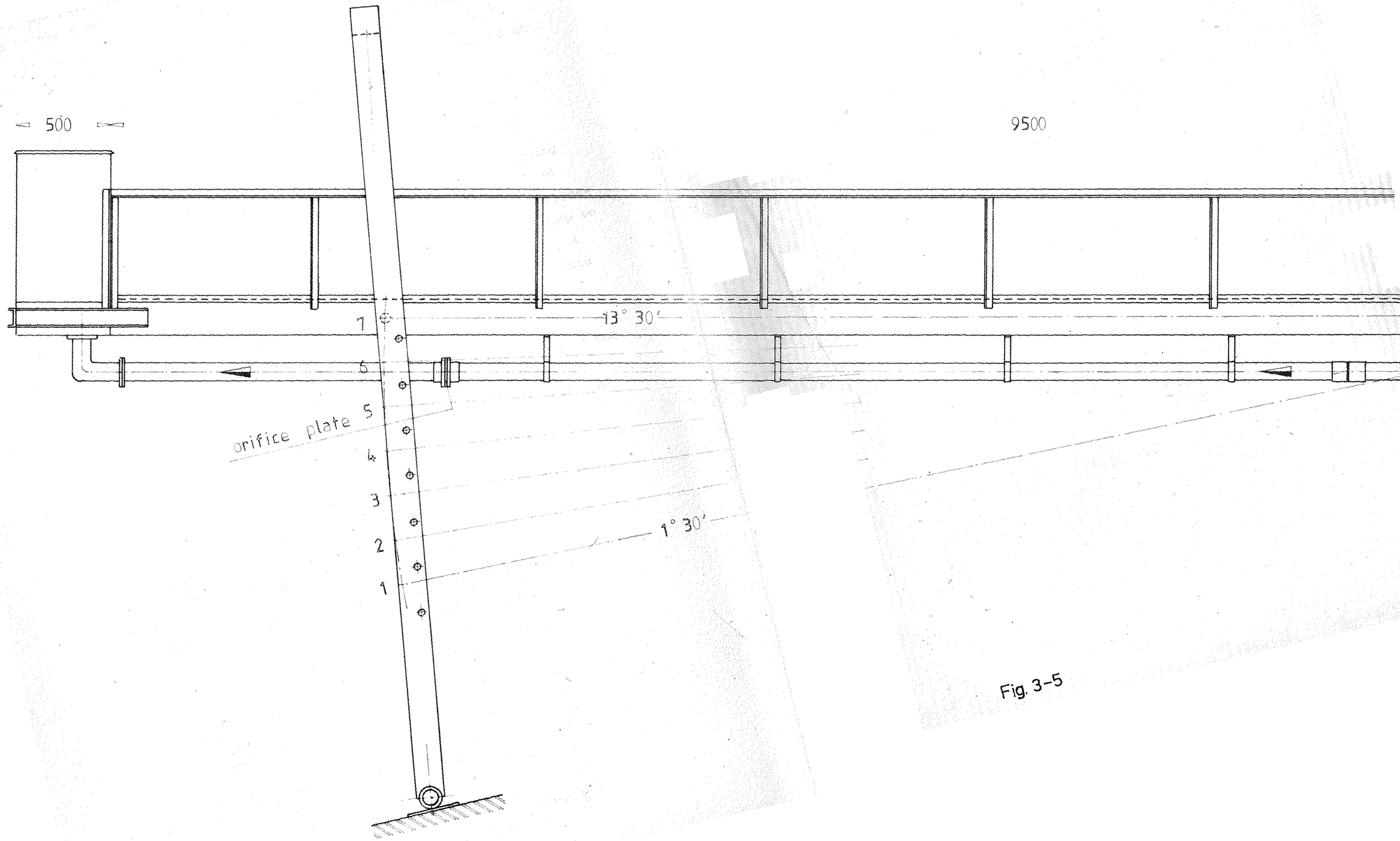

Fig. 3-5

channel

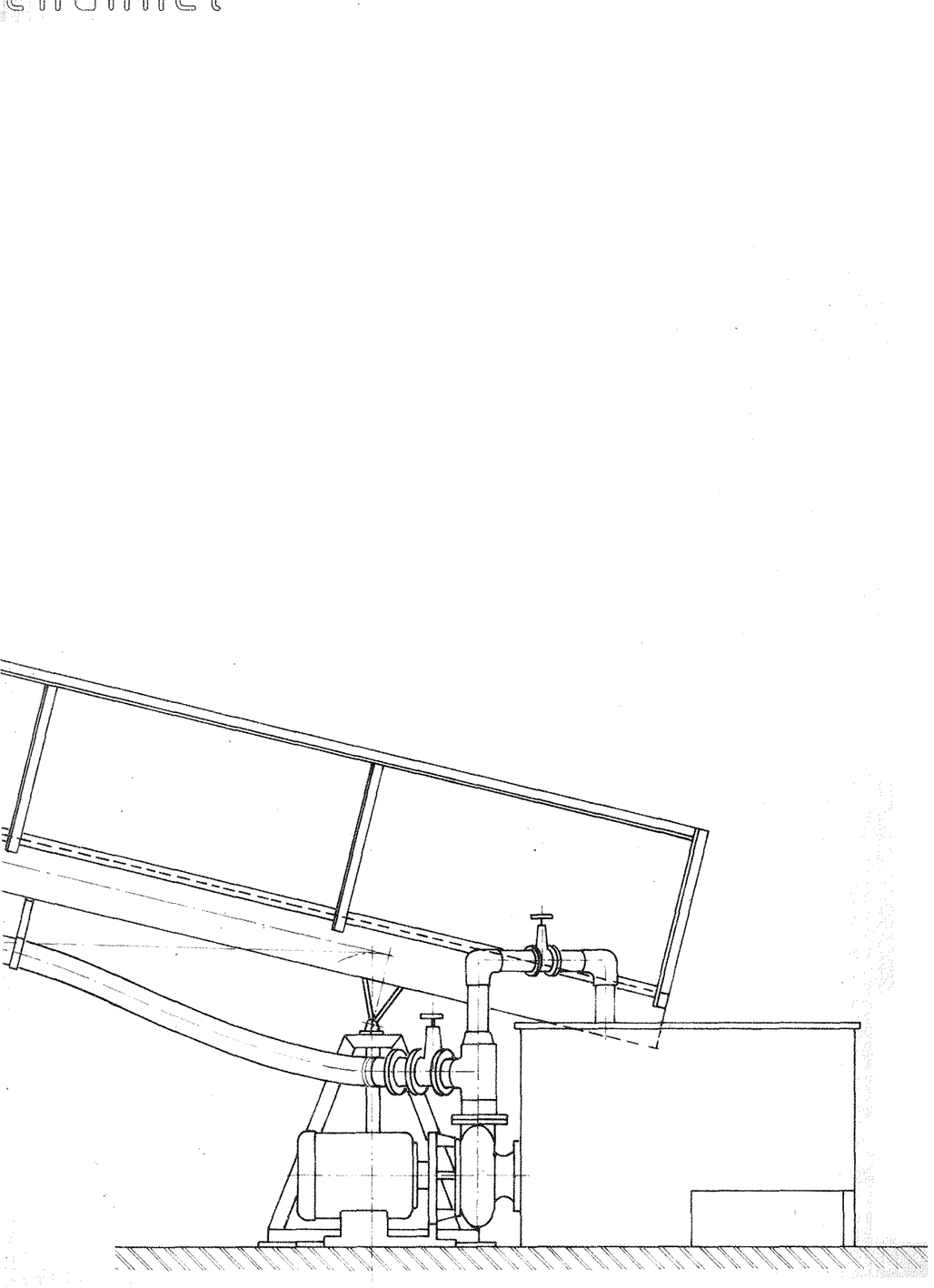

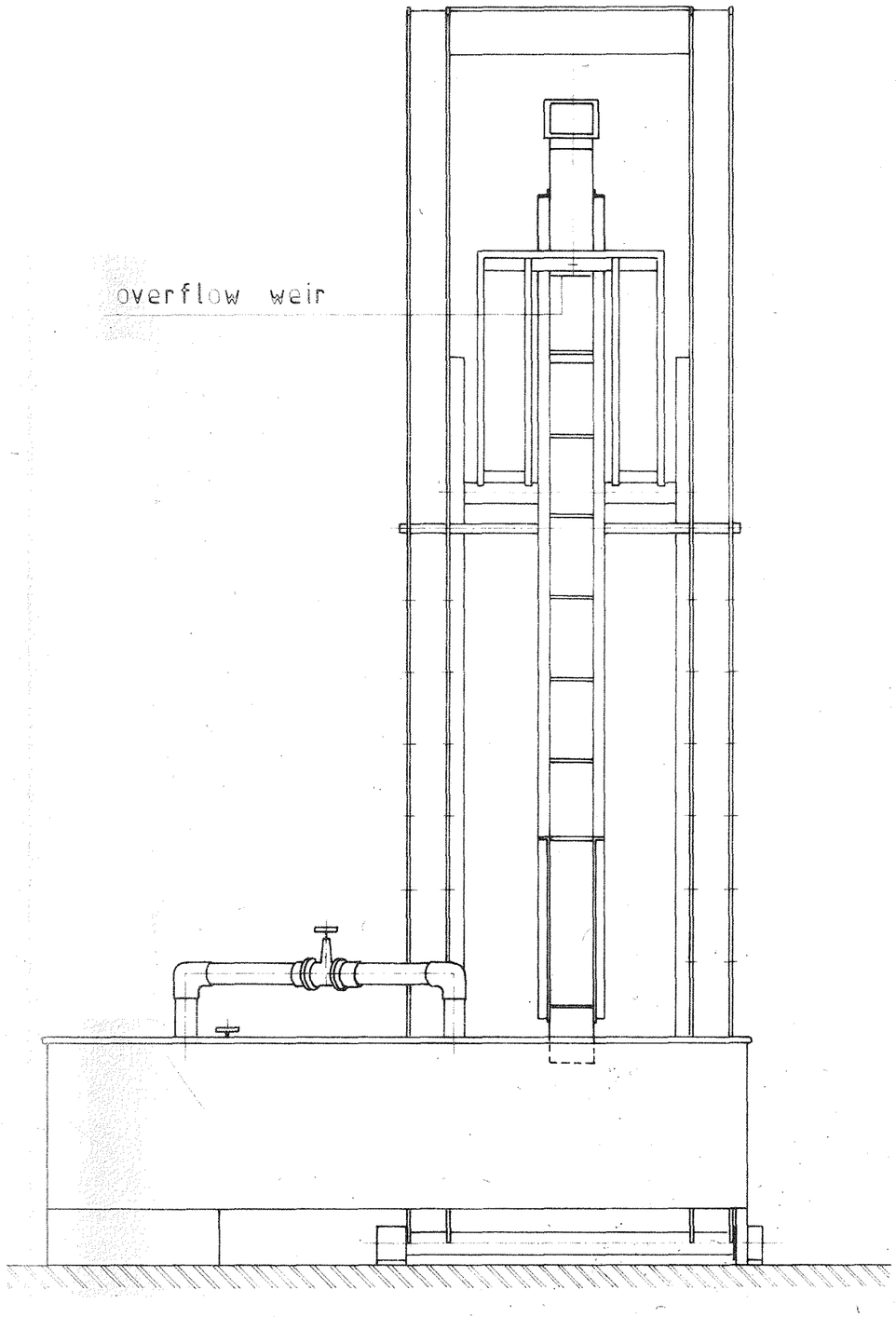

scale: 1 : 20

The tower is itself hinged at the floor, with the flume being located by the yoke structure running in a piece of channel (fig. 3-4) attached to the tower. The whole flume assembly is shown in fig. 3-5.

For the series of tests in which the channel was used as an idealised model of step-pool streams, steps of Australian hardwood were inserted perpendicular to the channel bed. These were 0.033 m thick, 0.285 m high, extended the full width of the channel, and were placed at 0.5 m centres (fig. 3-6).

3.2 WATER SUPPLY AND CONTROL

The flume uses a Davies centrifugal pump driving a recirculating water supply. The tail tank acts as a sump. Flow rate is controlled by a 100 mm butterfly valve, in conjunction with an 80 mm valve on a bypass circuit back into the tail tank (fig. 3-7). The bypass allows the pump to work at near capacity when small flow rates are needed in the flume. A steel plate 1 m square was installed in the tail tank (placed on concrete blocks, and therefore removable) above the pump inlet to prevent air entrainment at that point.

Water passes from the pump through a supply pipe located below the flume into a head tank of the same width as the flume at the inlet end of the channel. In the head tank, the flow is turned by the internal construction (fig. 3-8) and proceeds into the channel over a weir.

Figure 3-6: Hardwood steps in channel.

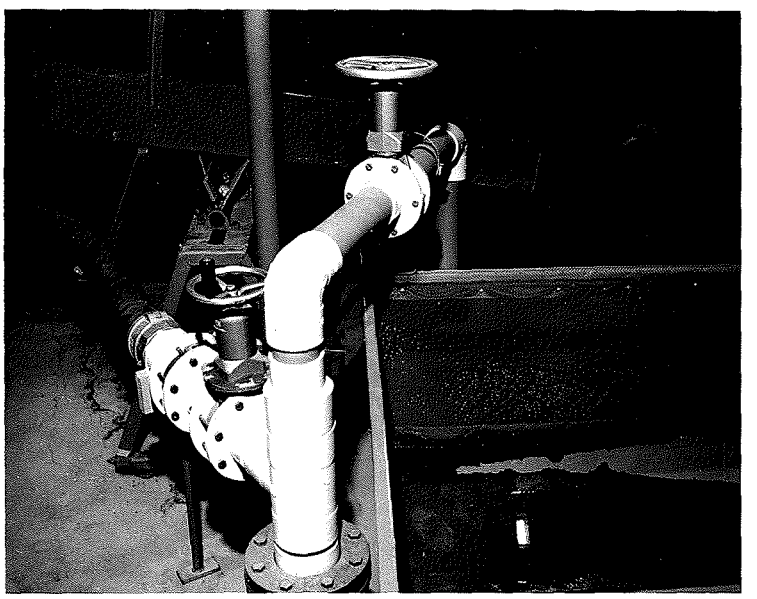

Figure 3-7: Valves and bypass for flow control.

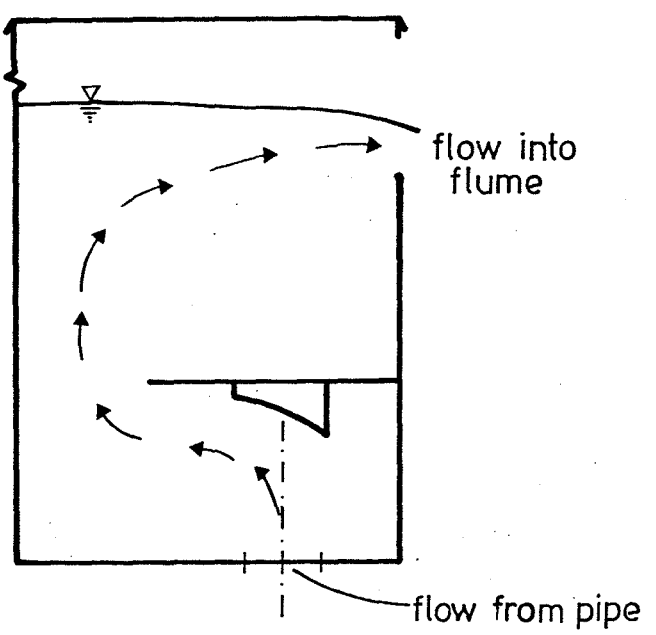

Figure 3-8: Internal construction of head tank.

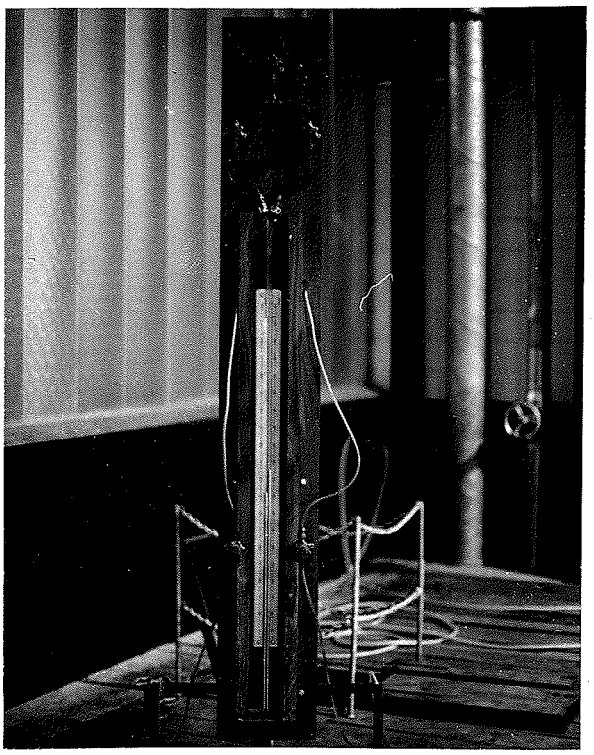

Figure 3-9: Manometer board used for calculating flow rate.

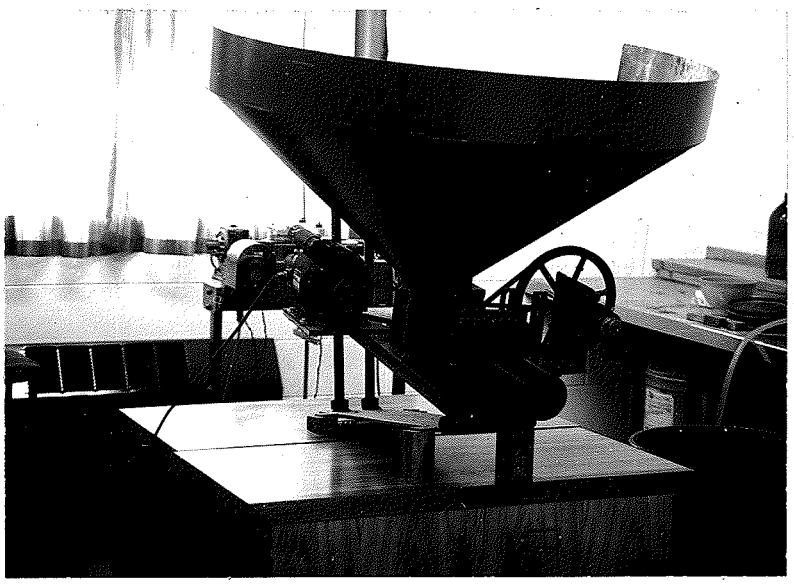

Figure 3-10: Sediment feed machine.

Flow rate is measured by a vertical manometer board (fig. 3-9) measuring pressure difference either side of an orifice plate in the supply pipe beneath the channel. Three orifice plates and their installation were designed to BS 1042:1943, to cover the range of flow rates used.

3.3 SEDIMENT INPUT

For the series of tests involving sediment transport, it was necessary to construct a sediment feed device. This machine works on a rotating tube principle, where sediment moves by gravity from a hopper into a rotating tube. The angle and rotational velocity of the tube determine the sediment supply rate. The equipment (which was constructed principally by the writer) is shown in fig. 3-10.

The lower steel base plate is attached to the top of the channel just below the head tank, with the feed tube pointing upstream. The angle of the rotating tube is altered by the two screws shown. These move the upper steel plate (upon which the machine is mounted) in a circular arc about the hinge point which was located below the feed tube. In this way, the angle of the flume can be accommodated without affecting the machine's performance. The tube is powered by a ¼ HP motor via a system of pulleys and belts. These were selected to convert the output rotational velocity of the motor to an appropriate rotational velocity for the tube. The tube itself runs in two wooden bearings, and is located by a flange at the hopper end. The side angle of the hopper is equal to the angle of repose for granular sediments to ensure steady supply to the tube.

The input rate of sediment to the flume was measured by sampling the output from the tube over a certain time period, and then weighing the sampled sediment. This output was found to be very even with time, even with a changing level of sediment in the hopper. One limitation of the sediment feed machine was that it would only feed dry sediment. Feed rate was sensitive to moisture content. For this reason, after a test run had been completed, sediment was removed from the tail tank and air-dried before being stored in the hopper, or standby drums.

3.4 BEDLOAD MEASUREMENT

A stainless steel mesh basket was positioned at the downstream end of the flume to measure bedload transport rates. It is suspended from a chain hoist attached to a swivelling arm (fig. 3-11). When the bedload

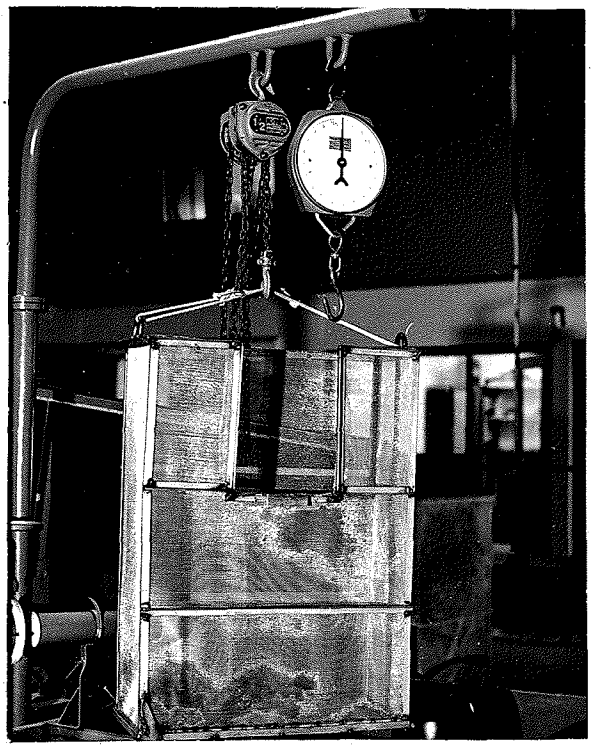

Figure 3-11: Apparatus for measuring sediment transport rate.

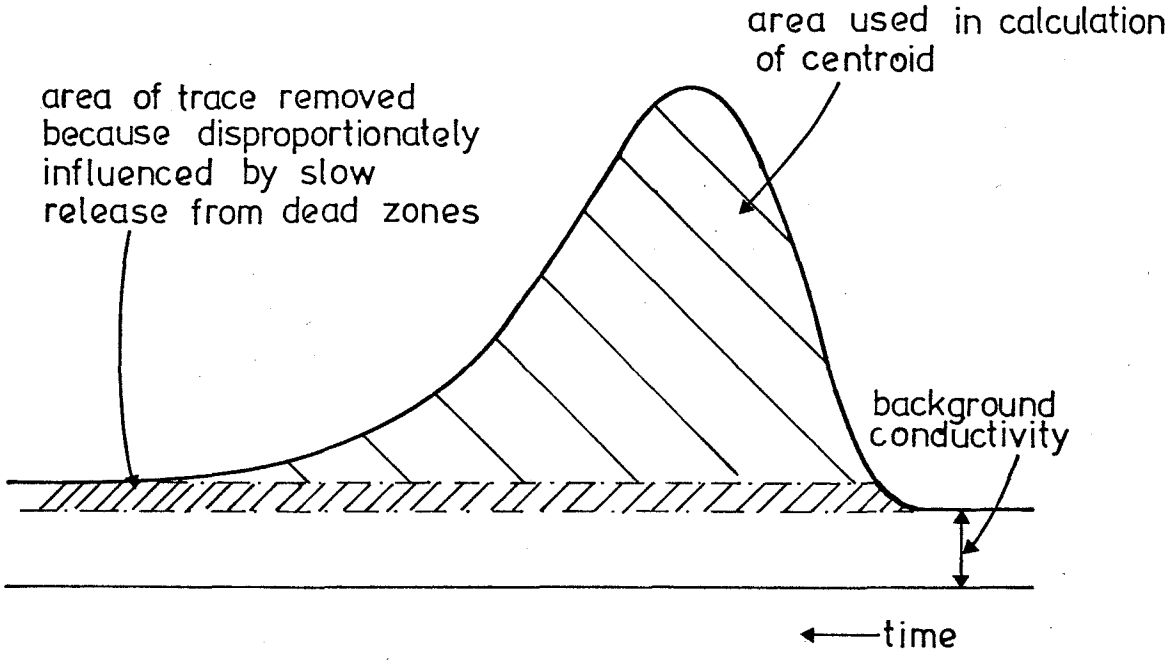

Figure 3-12: Area used for calculation of conductivity curve centroid.

had been sampled for a desired time period t, the basket was swung out of the flow. It was then raised, pulled forward, and lowered onto the spring balance shown. The weight of the basket was known, and subtracted from the total weight. This enabled calculation of the bedload transport rate.

The basket was then transferred back to the chain hoist, and positioned above the tail tank alongside the flume. A pin at one end of the bottom of the basket was removed. The bottom, hinged at the other end, then swung down, depositing the sampled sediment in the bottom of the tail tank. A screen across the middle of the tail tank (visible in fig. 3-7) prevented this sediment, as well as that not sampled (which obviously went straight into the tank) from entering the pump.

3.5 MEASUREMENT OF MEAN VELOCITY

The salt-velocity method, devised by C.M. Allen and E.A. Taylor, is based on the fact that salt in solution increases the electrical conductivity of water (U.S.D.I. Bureau of Reclamation, 1981). A quantity of electrolyte is introduced into the stream at a point x_o. Its time of passage between two downstream points, distances $x = x_1$ and $x = x_2$ from the injection point, is monitored by conductivity meters attached to electrodes placed in the flow.

As soon as the solution is introduced into the channel, it will begin to diffuse about its centre of concentration under the influence of turbulence and velocity gradients so that at downstream points, a solution wave of finite length will be detected. The increments of conductivity C(t), over the initial or 'background' conductivity C(o) of the natural stream water will be proportional to the concentration of solution present at location x and time t, C(x,t) (Church and Kellerhals, 1970). The mean velocity of all 'marked' particles corresponds to the mean stream velocity if the tracer is well distributed laterally (Day, 1977). The mean velocity of a tracer cloud, and thus of the natural stream, is therefore measured by the centroid $\bar{x}$ of the C(x) curve observed at a given time $\bar{t}$. In practice, one observes C(t) for two given locations x_1 and x_2. At location x_1, the mean travel time is

$$\bar{t}_1 = \frac{\int_{\infty}^{\infty} C_1(t)\, dt}{\int_{\infty}^{\infty} \frac{C_1(t)}{t}\, dt} \qquad \ldots 3\text{-}1$$

where $\bar{t}_1$ corresponds to the centroid of C(t) at x_1.

The mean velocity between points x_1 and x_3 is

$$v_m = \frac{x_2 - x_1}{\bar{t}_2 - \bar{t}_1} \qquad \ldots 3\text{-}2$$

(Church and Kellerhals, 1970)

Church and Kellerhals (1970) give several assumptions for the method.

(a) The volume of introduced solution is small, so that an uncharacteristic surge is not produced in the flow.

(b) The introduced solution has dispersed uniformly across the channel section before reaching x_1, so that the propagation of the solution downstream is truly representative of the stream's mean velocity.

(c) The measuring electrodes must be so placed in the channel that a representative set of measurements of conductivity for determining mean velocity can be obtained.

The difficulty in applying the method to steep natural channels occurs because these channels are irregular with many zones of back water or dead water where there is no net downstream flow. When marked particles enter these zones, they are observed to be trapped for considerable periods of time before they are released and re-entrained in the flow. This temporary storage has a significant effect on longitudinal dispersion, providing a tail with a low concentration of tracer particles for a considerable distance downstream (Sabol and Nordin, 1978).

The effect of dead zones was especially important in the series of tests performed with the artificial steps in the channel. However, some observations may be made on dispersion of tracer clouds in this situation. As the cloud moves along the channel, tracer particles periodically enter dead zones. If the tracer cloud were allowed sufficient time in any one locality, the solute masses in the flow zone and dead zone(s) would be in direct proportion to the respective zone volumes (Valentine and Wood, 1977). This would result in the mean velocity of the cloud U_m being a constant proportion of the mean discharge velocity.

i.e. $$U_m = \left(\frac{y_n}{y_n + \xi h'} \right) \text{ x mean discharge velocity} \quad \ldots 3\text{-}3$$

where y_n = normal depth of flow

ξ = proportion of the bed covered by dead zones

and h' = depth of dead zones.

(Valentine and Wood, 1979)

In the tests described herein, while dead zones were often of the same order of magnitude as the flow zone, insufficient time elapsed to allow this proportionality to be established. Thus, with less tracer removed from the flow zone, the velocity given by the centroids of the conductivity curves was more representative of the mean velocity of the flow zone than indicated by equation 3-3. Further, in the analysis used to determine average velocities (see Appendix 1), the effect of the long tail caused by the slow release of tracer from dead zones was reduced by eliminating it from calculation of the conductivity curve centroid (fig. 3-12). This again reduced the influence of dead zones in calculating the mean flow zone velocity.

Another approximation made was that of the 'frozen cloud' assumption. The approximation is based on the assumption that during the passage of the tracer cloud past the probe, it does not disperse. This has been shown to be acceptable in its effect on accuracy of results (Valentine and Wood, 1979). In the context of the tests reported herein, the effect of this assumption is minor compared to other assumptions used in the analysis of mean velocity.

For the tests described herein, about 10 ml of salt solution or hydrochloric acid was used as the tracer for each run. Because such a small volume of tracer was used, an uncharacteristic surge was not generated in the flow.

Thus, the velocities calculated from the centroids of conductivity curves are held to be reasonably accurate approximations of the mean stream flow velocity for idealised step-pool systems.

Calkins and Dunne (1970), using the salt-velocity method in small mountain streams, found the velocity obtained by this technique to give a better representation of average stream velocity than that computed by the continuity equation at 3 channel cross sections.

Maximum velocities were calculated by measuring the distance between the initial rise of the upstream and downstream conductivity curve traces. This distance was assumed to correspond to the fastest time t taken by tracer particles (and thus water particles) between the probe stations. Maximum velocity was thus calculated by dividing the distance between the probe stations by t.

The equipment used in the tests is shown in fig. 3-13. The probes were pairs of one inch wide strips of sheet aluminium bonded to the side of the channel. These were insulated from the metal construction of the channel. Conductivity readings were relayed through a dual channel conductivity meter to a two-channel chart recorder, which traced out the changing conductivity values on a moving sheet of paper. The resultant curves were used in the analysis of mean flow velocities (Appendix 1). The use and potential of this particular apparatus in the laboratory environment has been considered by Davies and Jäggi (1981). They noted that the accuracy of the technique was very high, and limited mainly by the accuracy of analysis of the time-conductivity curves. Like Davies and Jäggi (1981), the writer measured flow independently and was thus able to estimate a value of mean depth, allowing calculation of channel resistance to flow.

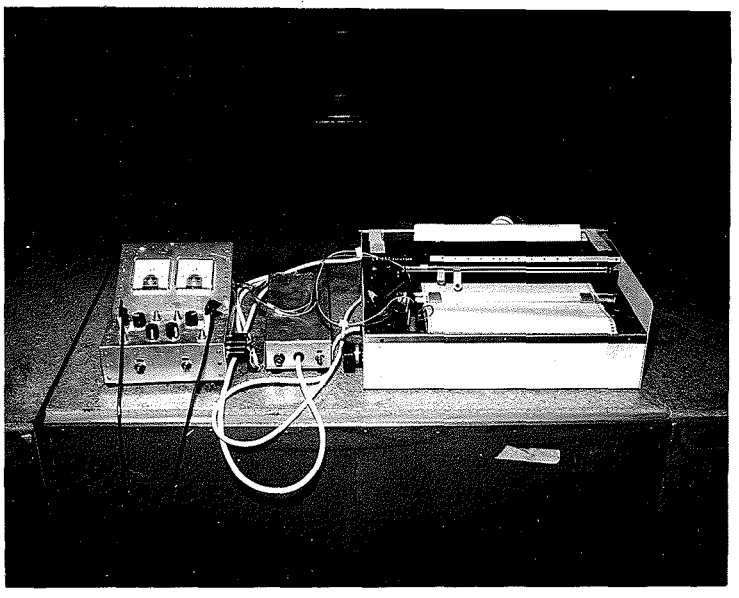

Figure 3-13: Conductivity measurement apparatus.

CHAPTER FOUR

THE ORIGIN OF STEP-POOL SYSTEMS IN MOUNTAIN STREAMS

4.1 COMMENT

The tests reported in this chapter were performed under the supervision of Mr. M.N.R. Jäggi, who conceived the idea of a dual anti-dune armouring formative process. The results corresponding to initial conditions found in table 4-1 were calculated by him. All other work is that of the writer. This work 'On the Origin of Step-Pool Systems' by J.G. Whittaker and M.N.R. Jäggi has been accepted for publication by the Journal of the Hydraulics Division, A.S.C.E. A copy of the submitted manuscript of the paper is in Appendix 2.

4.2 INTRODUCTION

Any theory attempting to explain the origin of step-pool systems must take into account that they are disequilibrium bedforms in the sense proposed by Allen (1976) and Middleton and Southard (1975). The structures are not created by the low flows which give the visual step-pool appearance since these are not capable of moving the rocks forming the steps. Rather, their formation is associated with flow conditions during high-intensity, low frequency flood events (Leopold and Maddock, 1953; Judd and Peterson, 1969; Kellerhals, 1970).

A necessary condition for step-pool formation is heterogeneity of bed material size (Leopold et al, 1964). Such material may be derived from a variety of sources, for example weathering of steep cliffs, glacial deposits (Miller, 1958; Kellerhals, 1970), or tributary streams (Graf, 1979), as well as that transported from upstream. Thus both the material size and its source are independent variables (similarly for steps formed by fallen logs). This coarse material is restructured into an armoured or paved step-pool pattern. Step-pool formation may also be affected by the influence of past and present climatic/hydrologic regimes. Some mountain streams investigated have, in the past, been subjected to much higher flows than those experienced at present. However, apparently immovable bed material such as that reported by Miller

(1958) may still be capable of responding to a low-interval flood. Hence, it can be seen that step-pool systems are not generally in equilibrium with 'normal' flow conditions. In this context, some existing theories of step-pool origin will now be examined.

4.3 SOME THEORIES ON THE ORIGIN OF STEP-POOL SYSTEMS

4.3.1 The Antidune Theory

Step-pool sequences in steep cobble or boulder channels have been considered to be generically similar to transverse ribs, which are commonly found on the riffle portion of much flatter, shallow gravel channels in environments such as glacial outwash fans (McDonald and Banerjee, 1971; Church and Gilbert, 1975). Many authors consider these transverse ribs to be relict antidunes (Boothroyd, 1970; Boothroyd and Ashley, 1975; Church and Gilbert, 1975; Gustavson, 1974; Koster, 1978). Shaw and Kellerhals (1977) found a striking similarity between gravel bedforms in the field and gravel antidunes developed in the laboratory. Boothroyd and Ashley (1975) cited the laboratory results of Fahnestock and Haushild (1972) to support the idea that transverse ribs are a form of antidune in a gravel-sand mixture.

The difficulty in equating transverse ribs (and thus steps) with antidunes lies not in the validity of the proposal (Whittaker and Jäggi, in press), but in the mechanisms proposed to explain the formation of transverse ribs by antidunes. Antidunes are formed in association with a standing wave, where the waveform of the bed is in phase with the form of the water surface (Kennedy, 1961). Transverse ribs on outwash areas are reported to have formed when material introduced locally generated an accompanying surface wave (Koster, 1978). This introduced material is atypical of the bed material and so the bed forms are not true antidunes as proposed by Kennedy (1961). The mechanism proposed by Koster (1978) involves growth of a ribbed sequence proceeding upstream in response to a water disturbance migrating upstream in discrete steps. According to Kennedy (1961), however, an antidune wavetrain propagates downstream, regardless of the direction of movement of the antidunes.

A variation on this theme is a mechanism proposed by McDonald and Day (1978) in which transverse ribs are formed by a process where a hydraulic jump travels upstream in an episodic fashion. Pebbles

accumulate just downstream of the hydraulic jump during the intervals when it is stationary. However, supercritical flow rarely occurs in regions where transverse ribs form; indeed if ever in the large bed element channels described by Judd and Peterson (1969). As pointed out by McDonald and Day (1978), it is difficult to transfer their formative mechanism to natural channels, and it has never been reported in the field literature.

The environment in which steps occur differs from the glacial outwash areas where transverse ribs are commonly found, in that the areas between steps do not exhibit a totally different bed material to that composing the steps. By contrast, inter-rib areas do tend to exhibit a totally different bed material to that composing the ribs. However, the gravel antidunes of Shaw and Kellerhals (1977) provide a reasonable explanation for transverse rib formation. But, as will be demonstrated, only step features at lower slopes are fully so explained. Whittaker and Jäggi (in press) show that armouring or paving is also involved in the formation of step-pool systems.

4.3.2 The Dispersion and Sorting Theory

Yang (1971) developed a theory that riffle-pool sequences occur because '.. natural streams minimise their time rate of potential energy expenditure per unit mass of water in accordance with the law of least time rate of energy expenditure'. Yang further suggested that in riffles, where the local energy gradient is higher than average, there would be a high rate of shearing of bed material with flood flows. Bed elevation would consequently increase with migration of coarse material to the surface due to a grain dispersion process reported by Bagnold (1954).

Recognising the continuum of bed forms (Leopold and Wolman, 1958) from riffle-pool sequences to step-pool systems, Yang's theory is limited to the step-pool sequences at slopes less than about 5%, where, as for riffle-pool sequences, bed material is in motion at moderate flood flows. But to achieve the dispersion reported by Bagnold (1954), the whole bed would have to experience shearing motion to a considerable depth. This would occur only under debris flow conditions.

Similarly, shearing and dispersion of bed material at higher slopes only occurs for debris flows, as shown by Takahashi (1978) and Mizuyama (1981). At such higher slopes, these may provide the deposits in which new step-pool systems can form, but they obliterate any existing

structures.

4.3.3 The Velocity (or Shear Stress) Reversal Theory

This theory, although developed for riffles and pools, can be applied to the riffle-step and pool sections of mountain streams (i.e. gradients less than about 5%). Keller (1971) measured bottom velocities in pools and riffles for different discharges. He reported that with increasing discharge, there was a greater increase of bottom velocity in the pools than in the riffles. He concluded from extrapolation of this data that at high flows, bottom velocities in pools would exceed those over riffles (hence the so-called 'velocity reversal'). This reversal would supposedly then move coarse grains quickly from a riffle, through the subsequent pool, to be deposited in the next riffle, thus maintaining these features.

There is no evidence that this reversal actually occurs. The data used does not show a velocity reversal, only a velocity equalisation. The reversal of mean velocity (Andrews, 1977) reported by Lisle (1979), rests on defining a riffle and pool as a depositing or scouring section respectively, rather than as the actual morphological features. With armour layer disruption, this definition may be incorrect.

Lisle (1979) found that a reversal of mean bed shear stress occurred. Mean bed shear stress was defined as

$$\tau_m = \gamma RJ \qquad \ldots 4\text{-}1$$

where γ = specific weight of water

R = hydraulic radius

and J = water surface slope.

The reversal occurred when, as flow increased to about bankfull stage, the depth of flow in the pool stayed greater than that over the riffle, while the water surface slope values for riffle and pool converged. One source of doubt as to whether Lisles' measurements are truly representative is that the pool and riffle sections were separated by a kilometer of channel length.

In phase 1 transport, where bedload moves over a stable armoured bed (see section 2-4), such a shear stress situation easily explains movement of sediment stored in pools (as noted by Silverston and Laursen, 1976). Lisle hypothesised that with phase 11 transport, where flow

disrupts the armoured bed layer adding bed material to the existing bedload, riffles erode preferentially with subsequent movement of sediment through the pool to the next riffle. An alternative explanation is that when the armour layer is destroyed, and bed material over the whole bed is available for transport, a selective portion may be moved preferentially (Bagnold, 1968). Bagnold showed that bedload derived from bed material had a narrower size distribution than the bed stock. Excesses of both fine and coarse material were left on the bed. Given these circumstances, the riffle-pool structures would essentially be left intact. The preferentially eroded size is about 4 mm (Bagnold, 1980), which could explain the absence of comparable sediment sizes commented on by Lisle.

It must be noted that both Keller's and Lisle's hypotheses explain only the maintenance of pre-existing riffle-pool sequences.

As with the dispersion theory of Yang (1971), the reversal theories do not apply to step-pool structures on slopes greater than about 5%. For these higher slopes, very high flows in the Torlesse stream were observed by the writer to form large standing waves, rather than the water surface slope equalisation noted for riffle-pool gravel rivers. Judd and Peterson (1969) hypothesised such waves for step formation in large bed element channels.

4.4 TESTS

Tests were performed to clarify the formative processes of step-pool sequences. Bed deformation and grain sorting processes were expected to occur under appropriate flow conditions. It was throught that either or both tendencies would eventually stabilise the bed for flows capable of deforming an initially plane bed.

4.4.1 Test Procedure

The laboratory tests were performed in a tilting, re-circulating channel, 10 m long, 0.132 m wide and 0.6 m deep. A graded sediment ranging between 2 mm and 50 mm in size (fig. 4-5) initially arranged as a plane bed had a sediment-moving discharge passed over it. No sediment was fed at the upstream end of the flume; thus parallel and rotational degradation occurred as the bed was eroded. Tests were

performed at slopes ranging from 0.027 to 0.248. Because of the steep slopes used, the change in slope associated with rotational degradation was, where it occurred and the bed also stabilised, comparatively small. For most of the selected discharges the bed achieved a stable condition (i.e. sediment motion ceased).

In many of the test runs stabilisation was associated with increased resistance to flow. This increase was due to an increase in form resistance as well as paving of the bed. To estimate resistance to flow, measurements of average flow velocity were made, using the salt-velocity technique (see section 3-5).

When the bed had stabilised under the deforming flow, to what are subsequently referred to as final conditions, the discharge was reduced to study the low flow appearance of the bed. This allowed a visual comparison with the field situation, commensurate with the disequilibrium concept mentioned above.

At the completion of each run, the longitudinal profile of the bed was measured. Bed armouring was seen to be a significant factor, so areal bed samples were taken. A portion of the bed surface was sprayed with paint, the painted stones were removed by hand, and a sieve analysis of these stones was performed. The area sampled extended over at least one bedform, and therefore represents an average and not a local grain size distribution.

Discharge measurements were made with a calibrated orifice plate inserted in the return pipe. A summary of experimental data is found in table 4-1.

4.5 EXPERIMENTAL OBSERVATIONS

Within the range of slopes (2.5% to 25%) for which experimental flume runs were performed, two clearly defined cases were observed.

At lower slopes, for relatively high flow rates, antidunes formed which were similar to those reported by Shaw and Kellerhals (1977) (fig. 4-1). As the flow rate was subsequently reduced, a hydraulic jump formed in the existing trough region. The visual impression at a low flow rate was more that of a riffle-pool sequence (fig. 4-2), although the wavelength was clearly determined by that of the original antidunes. Fig. 4-3(a) illustrates conceptually a run with a progression from bed forming flow to a low flow.

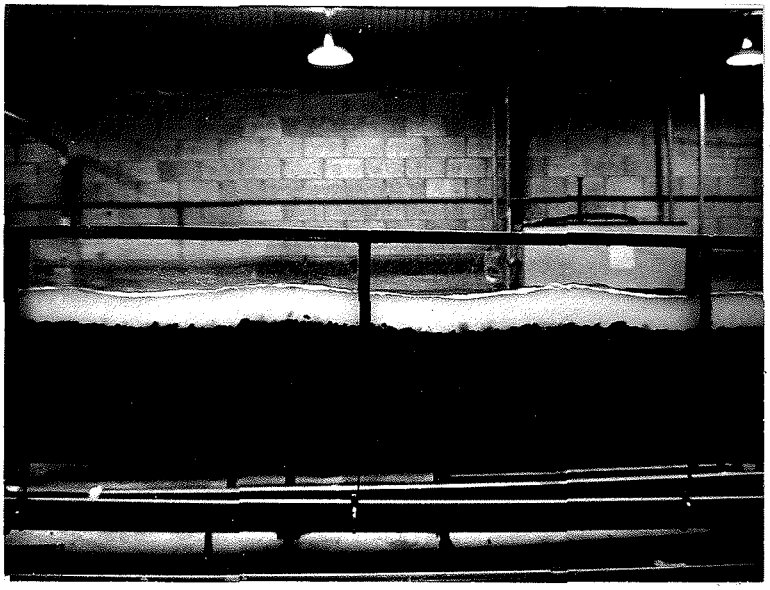

Figure 4-1: Gravel antidunes.

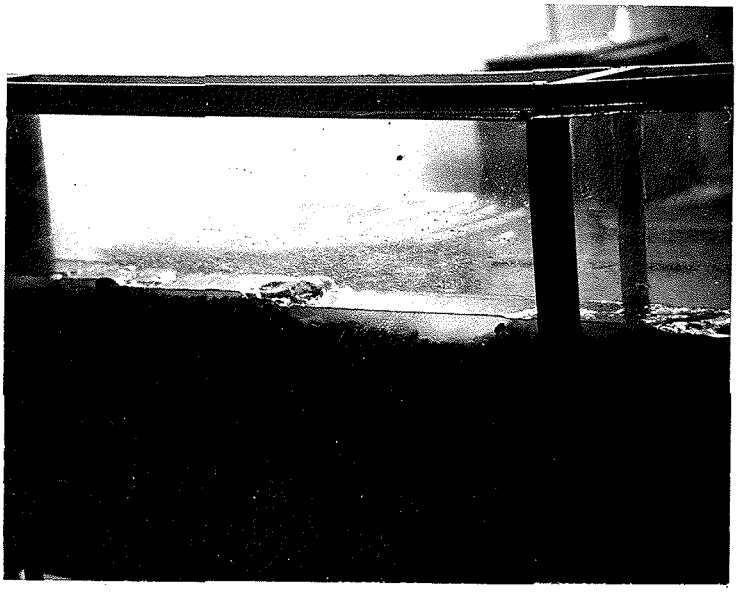

Figure 4-2: Riffle-pool aspect at lower than formative flow rate.

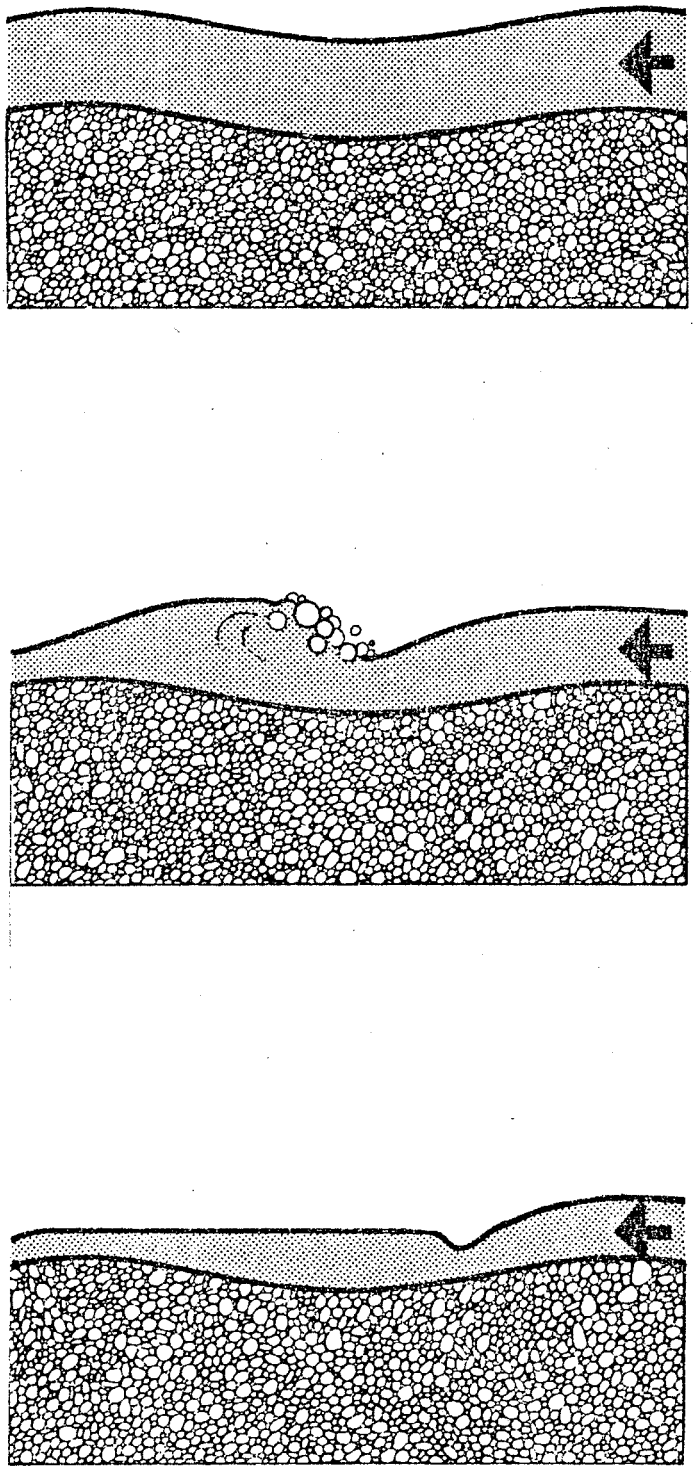

Figure 4-3(a): Conceptualisation of progression from antidune flow to the tumbling flow of a step-pool system.

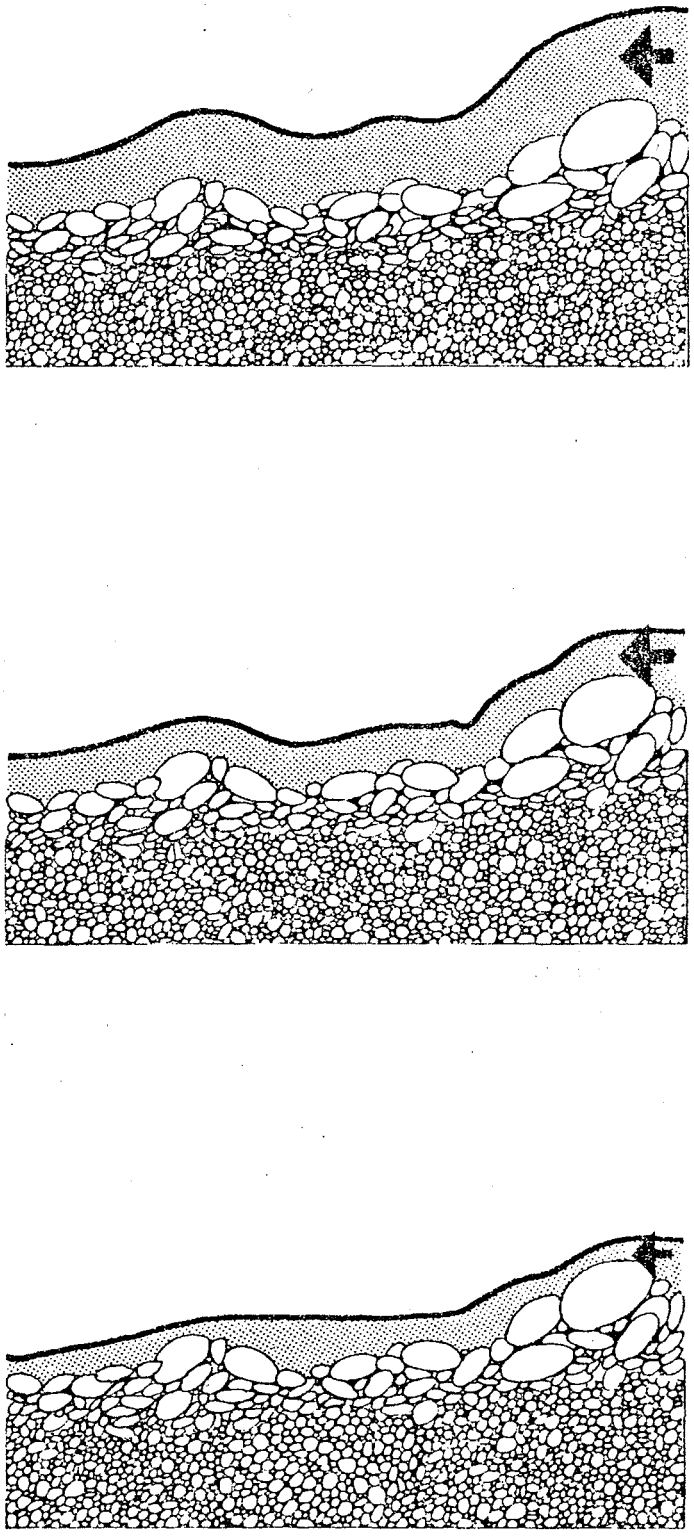

Figure 4-3(b): Conceptualisation of progression from rough flow to the tumbling flow of a step-pool system.

At higher slopes and smaller flows, the coarser grains had a considerable effect on the bed deforming process. The flow initially formed regular antidune wavetrains, but with some degradation the flow pattern subsequently developed increasingly in response to the (random) location of larger individual roughness elements. These larger elements anchored some of the waves, preventing migration. Some of the 'steps' so formed occasionally broke down, setting in motion a short-lived 'slug' of sediment. At a low flow rate, relative to the deforming flow, the flow pattern closely resembled step-pool sequences as seen in natural situations (see fig. 4-3(b); this figure was prepared from a video recording of a run).

The transition slope between the two above cases was about 0.075.

4.6 RESULTS

The main results of the tests are listed in table 4-1. A sidewall correction procedure, for estimating friction losses, was applied after Gessler (1965).

From the test results the friction factor f_u, the mean bed shear stress τ_m, and the hydraulic radius with respect to the bed R_u, were calculated. For a comparison of the results f_o, h_o, and R_o values were computed for the plane bed case at the beginning of the tests. Because of the rapid initial bed deformation, it was not possible to measure these parameters. Thus, for computation of resistance to flow in this case, the Keulegan logarithmic resistance law was used. The occurrence of wake interference losses in the lee of larger roughness elements necessitated the use of a roughness height of 3.5 D_{84} in the Keulegan formula (Hey, 1979). Thompson and Campbell (1979), noting this blocking effect, have suggested $k_s = 4.5\,D$ where D is the median boulder diameter.

Because of the high gradients in the tests, $\sin\alpha$ was used for the energy slope instead of $\tan\alpha$ (Scheuerlein, 1973).

4.6.1 Grain Sorting Effects

In widely graded materials, the flow causes grain sorting. In theory this leaves a coarser top layer by preferentially eroding more of the finer material sizes than the coarser. Gessler (1965, 1970) approached the problem from a probabilistic perspective. For every grain

TABLE 4-1 RESULTS OF TESTS ON THE FORMATION OF STEPS AND POOLS

RUN	SLOPE (SINα)	Q_{Du}	v_u	h_u	R_u	f_u	τ_m	F_u	h_o	R_o	f_o	F_o	$\frac{f_u}{f_o}$
1	0.098	0.0039	0.423	0.070	0.069	2.94	65.84	0.663	0.038	0.037	0.52	1.650	5.65
2	0.098	0.0041	0.439	0.071	0.070	2.77	66.72	0.683	0.040	0.039	0.49	1.606	5.65
3	0.098	0.0045	0.411	0.083	0.082	3.70	78.12	0.592	0.042	0.040	0.47	1.639	7.87
4	0.098	0.0054	0.447	0.091	0.089	3.42	85.48	0.614	0.046	0.044	0.42	1.715	8.14
5	0.085	0.0062	0.477	0.098	0.096	2.80	79.60	0.631	0.049	0.047	0.39	1.776	7.18
7	0.163	0.0010	0.513	0.015	0.015	0.71	23.20	1.829	0.020	0.020	1.45	1.167	0.49
8	0.172	0.0008	0.622	0.010	0.010	0.34	16.32	2.719	0.018	0.017	1.94	1.102	0.17
10	0.238	0.0004	0.459	0.007	0.006	0.60	15.75	2.477	0.013	0.013	4.57	0.922	0.13
11	0.022	0.0148	0.887	0.126	0.106	0.23	22.91	0.971	0.098	0.077	0.10	1.407	2.33
12	0.025	0.0182	1.274	0.108	0.083	0.10	20.24	1.505	0.108	0.082	0.10	1.503	1.02
14	NO UNDERFLOW VALUES TAKEN FOR THIS SLOPE												
15	0.168	0.0012	0.398	0.023	0.023	1.87	37.00	1.145	0.019	0.018	1.13	1.512	1.66
16	0.241	0.0008	0.231	0.026	0.026	8.93	59.54	0.647	0.015	0.015	1.87	1.489	4.78
17	0.025	0.0147	1.228	0.091	0.071	0.09	17.32	1.581	0.094	0.074	0.10	1.495	0.89
18	0.026	0.0118	1.057	0.084	0.069	0.13	17.65	1.416	0.081	0.066	0.11	1.502	1.15

there is a probability q of remaining in the top layer, where q is a function of the flow conditions. If p is the grain-size distribution curve for the original material, then

$$dp_a = \frac{q\ dp}{\int_0^1 q\ dp} \qquad ...4\text{-}2$$

defines the grain-size distribution of the resultant top layer. Further, an average probability $\bar{q}$ is defined (Gessler, 1970) where

$$\bar{q} = \int_0^1 q\ dp_a \qquad ...4\text{-}3$$

If this value exceeds 0.5, then a stable top layer can be formed. The analysis (after Gessler, 1965) for predicting the armoured or paved top layer was applied to a sample of the original material used in the tests (see Appendix 3). Results are shown in fig. 4-4(a) to (ℓ), compared with the corresponding measured top layer. Table 4-2 lists the values of $\bar{q}$ corresponding to initial conditions. For slopes greater than 0.075, all values of $\bar{q}$ are far lower than the limit of 0.5 given for bed stabilisation.

TABLE 4-2 BED ARMOURING STABILITY COEFFICIENT

Run No. (1)	$\bar{q}$ (2)
1	0.240
2	0.238
3	0.145
4	0.174
5	0.183
7	0.213
8	0.224
10	0.183
11	0.495
12	0.492
17	0.430
18	0.458

The effect of the sampling procedure and corresponding correction procedures have been discussed by Kellerhals and Bray (1971), and later by Proffit and Sutherland (1980). In fig. 4-5(a) to (ℓ) the measured armour or pavement grain size distribution curves (areal sampling) are modified to allow comparison with the original bed material curve (volume sampling).

4.6.2 Wavelength of Observed Bedforms

Kennedy (1961, 1963) developed an analysis of antidune bedforms, which related the Froude number F of the flow to the wave number k ($k = \frac{2\pi}{L}$, where L is the wavelength of the bedform) and the flow depth h. He found that the region for possible antidune formation is delineated by equations for maximum and minimum Froude numbers F_m and F_a respectively. These two defining envelopes are shown in fig. 4-6, with the appropriate region shown bounded by ABC.

The experimental values of the bed wavelength L were calculated from a zero-crossings analysis of the measured longitudinal bed profile. Photographs of runs taken at slopes less than 0.075 gave wavelengths that were a little different from those indicated by a zero-crossings analysis; the rough sediment profile yielded more zero-crossings than the fluid flow pattern showed. Both values of wavelength are shown in table 4-3. Using the value h_o (the computed flow depth at the beginning of the tests) for the determination of F and k, results were obtained as shown in fig. 4-6. The points (except for run 10) lie close to the region of antidune formation.

When the value h_u is used (together with the corresponding Froude number F_u) in the plotting of F versus $kh = \frac{2\pi h}{L}$, the points for runs 1 to 5, 11, 12, 17 and 18 fall outside (although reasonably close to) the antidune region (fig. 4-6).

The points for runs 7, 8, 10, 15 and 16 lie in the region of antidune formation. This confirms the observation that regular antidune wavetrains formed at slopes greater than 0.075. Further, despite modification by the presence of larger individual roughness elements, the computed values of kh indicate that the final condition bedforms still correspond to antidunes.

Froude numbers were calculated from the formula

TABLE 4-3 WAVELENGTH OF BEDFORMS

Run no. (1)	Wavelength in meters			Standard deviation in meters (5)
	average (2)	max. (3)	min. (4)	
1	0.171	0.497	0.045	0.104
2	0.169	0.640	0.049	0.119
3	0.227	0.814	0.038	0.163
4	0.247	0.903	0.082	0.170
5	0.258	0.618	0.049	0.134
6	unstable conditions			
7	0.225	0.759	0.065	0.169
8	0.239	0.686	0.091	0.153
9	unstable conditions			
10	0.272	0.700	0.061	0.186
11	(0.585) 0.402	1.026	0.120	0.248
12	(1.091) 0.502	1.062	0.110	0.268
13	unstable conditions			
14	(0.632) 0.416	0.979	0.104	0.255
15	0.286	1.107	0.084	0.236
16	Longitudinal profile not measured			
17	(0.642) 0.433	1.215	0.124	0.299
18	(0.546) 0.457	1.352	0.188	0.280

(figures in brackets based on photographs)

$$F = \frac{v_u}{\sqrt{gh \frac{\cos\alpha}{\alpha'}}} \qquad \ldots 4\text{-}4$$

which allows for steep slope effects. The coriolis coefficient α' was determined from the mean of values given by the equations of Obrazosvskiy and Morozov (Golubtsov, 1976). In fig. 4-6, points corresponding to the final depth h_u were plotted only if there was a substantial differerence from the values determined for the initial depth h_o.

4.6.3 Steepness of Observed Bedforms

Bedforms are not only characterised by their wavelength, but also by their steepness, i.e. the ratio of their height to their wavelength. In a more general way this value has been called roughness spacing or concentration when considering isolated roughness elements and their concentration on the bed (Rouse, 1965).

For the tests performed, each maximum height between successive upward zero-crossings was divided by the distance between the same upward zero-crossings, and the mean of the resultant steepness values taken to give the results shown in table 4-4. The steepness values have been designated e, where e was used by Sutherland and Williman (1977) for effective roughness concentration.

4.6.4 Resistance to Flow

During formation of step-pool systems (as simulated by these tests), bedform generation and grain sorting tended to increase resistance to flow for most runs. The grain sorting resulted in an armoured or paved stable bed, with larger grains acting as isolated roughness elements. The increase in resistance to flow can be characterised by the ratio $\frac{f_u}{f_o}$. Values of the ratio are listed in table 4-1.

The tests with low slope and high discharge showed no appreciable change in resistance. For runs 7, 8 and 10 (which correspond to the lowest flow(s) at slopes 0.172 and 0.248) the values of $\frac{f_u}{f_o}$ indicate that resistance to flow decreased from initial to final conditions. However, other runs for slopes of 0.098, 0.172 and 0.248 all indicate that resistance to flow increased from initial to final conditions.

After the bed had been modified by the bed forming flow, the flow rate was reduced to a series of low flows that visually produced the tumbling flow pattern. Friction factors for these reduced flows are given in table 4-5.

TABLE 4-4 ROUGHNESS SPACING

Run no. (1)	Roughness spacing e			Standard deviation (5)
	average (2)	max. (3)	min. (4)	
1	0.146	0.436	0.031	0.074
2	0.138	0.311	0.040	0.078
3	0.118	0.288	0.031	0.068
4	0.126	0.217	0.086	0.051
5	0.100	0.190	0.011	0.039
6	unstable conditions			
7	0.149	0.335	0.040	0.063
8	0.129	0.250	0.045	0.057
9	unstable conditions			
10	0.130	0.356	0.039	0.071
11	0.065	0.136	0.022	0.030
12	0.046	0.087	0.022	0.019
13	unstable conditions			
14	0.051	0.125	0.012	0.027
15	0.127	0.293	0.036	0.063
16	Longitudinal profile not measured			
17	0.052	0.141	0.020	0.029
18	0.055	0.116	0.017	0.023

TABLE 4-5 VALUES OF VELOCITY AND FRICTION FACTOR FOR DISCHARGE LESS THAN FORMATIVE DISCHARGES

RUN	LOW FLOW	Q_u (m^3/s)	v_u	f_u	RUN	LOW FLOW	Q_u	v_u	f_u
1	A	0.00165	0.144	31.99	8	A	0.00037	0.287	1.60
	B	0.00222	0.187	19.59	10	A	0.00009	0.842	0.025
	C	0.00122	0.090	96.20	11	A	0.00121	0.220	1.46
2	A	0.00325	0.283	8.23	15	A	0.00037	0.212	3.75
	B	0.00263	0.227	12.98	17	A	0.00085	0.201	1.53
	C	0.00175	0.126	50.47	18	A	0.00163	0.289	1.02
3	A	0.00306	0.257	10.34					
	B	0.00260	0.205	17.38					
	C	0.00175	0.095	117.64					
4	B	0.00267	0.137	59.74					
	C	0.00188	0.125	55.67					
5	A	0.00332	0.274	7.97					
	B	0.00267	0.136	53.34					
7	A	0.00058	0.397	0.872					
	B	0.00033	0.384	0.593					

4.7 DISCUSSION OF RESULTS

4.7.1 Grain Sorting Effects

Fig. 4-4(i) to (ℓ) shows the results for runs 11, 12, 17 and 18. It can be seen that Gessler's (1965) method of analysis predicted a top layer grain size distribution coarser than that measured. The predicted distributions for initial and final conditions are virtually identical because there was very little change in shear stress over the duration of the bed shaping process. Despite the discrepancy between the measured and predicted distributions, the observed stabilisation of the bed is in agreement with Gessler's prediction, since the values of $\overline{q}$ are close to his theoretical value for stability of 0.5.

On correcting the measured armour layer to enable comparison with the original bed material using the Proffitt and Sutherland (1980) correction (Kellerhals and Bray's (1971) correction over-compensates), it is apparent that insignificant coarsening had occurred (see fig. 4.5(i) to (ℓ)). For these runs (which were all at slope = 0.027), the action of the flow on the bed surface consists of a rearrangement of the bed material, rather than a coarsening. The bed surface is thus armoured as defined by Bray and Church (1980). This suggestion is supported by the very low bedload transport rates that occurred.

For the other test runs (all at slopes greater than 0.075), fig. 4-4(a) to (h) shows that there is reasonably good correlation between the measured and predicted bed surface grain distributions. That there is little difference between the distributions predicted for initial or final conditions shows that Gessler's (1965) method is, for these tests, reasonably insensitive to changes in shear stress. The distributions calculated from initial conditions tend to give better correlation with the measured distributions. The plots of runs 1 and 2 (Fig. 4-4(a) and (b) respectively) appear to contradict this, but the contradiction is in fact due to the omission of coarser sieve sizes in the grain size distribution analysis for these runs. Fig. 4-5(a) to (h) shows that coarsening occurred for most of these runs. Thus, at slopes greater than 0.075, the action of the flow has caused the bed surface to become paved (as defined by Bray and Church, 1980).

However, the $\overline{q}$ values in table 4-2 indicate that stability should not have occurred for these runs at higher slopes. That the beds did stabilise is in part due to the increase in resistance that

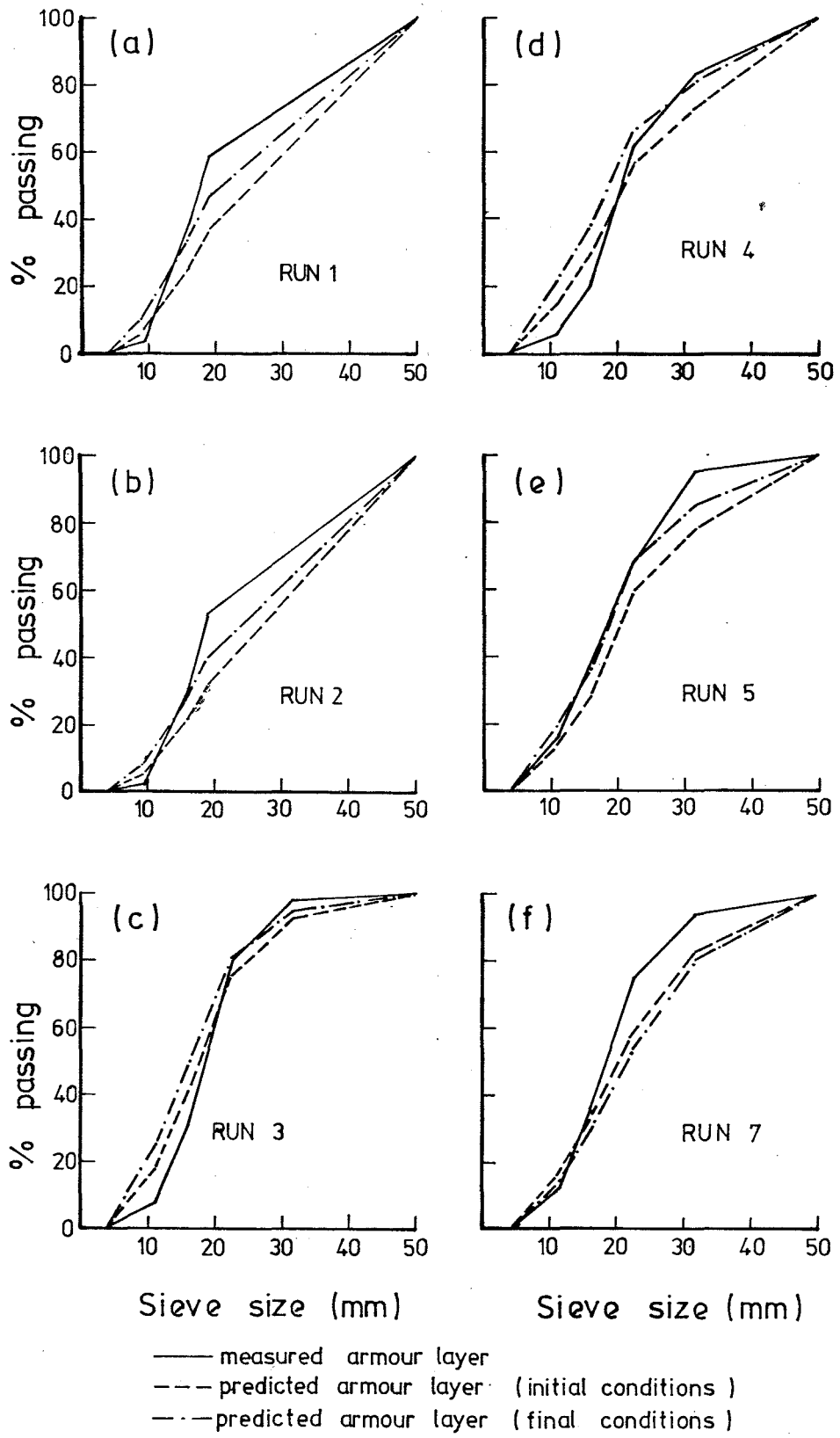

Figure 4-4: Plot of measured and predicted armour layer distributions.

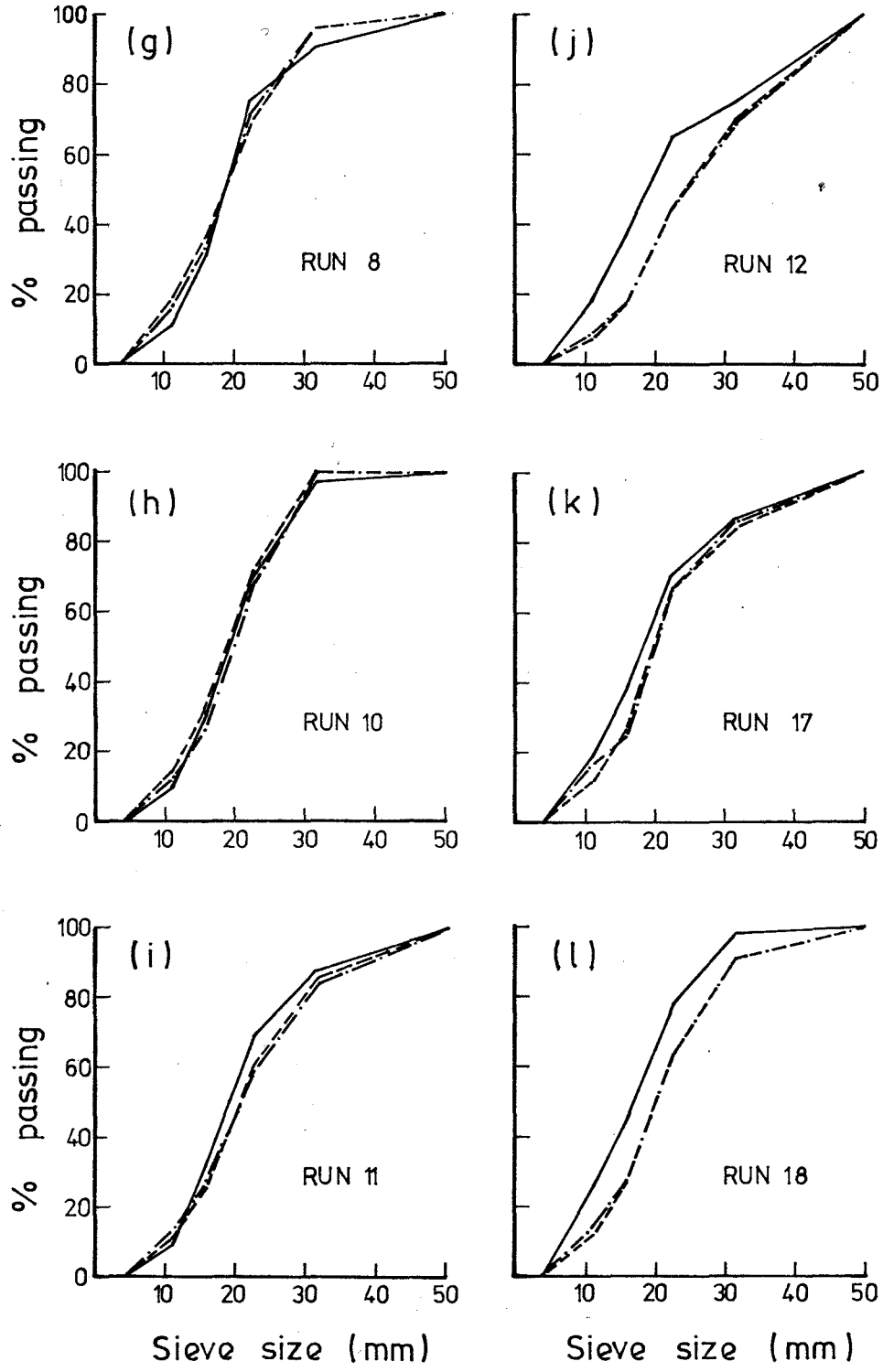

Figure 4-4: (continued.....)

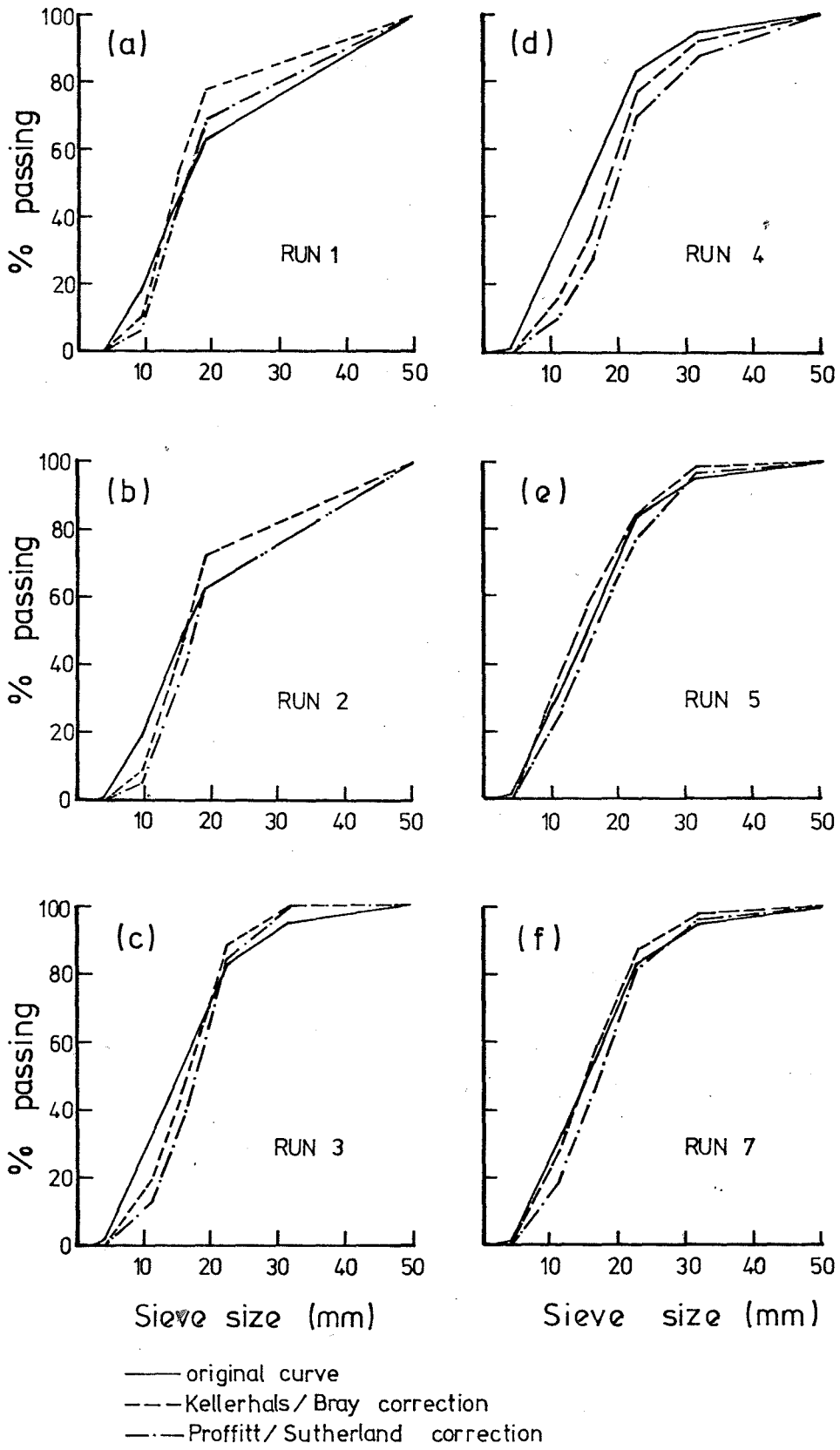

Figure 4-5: Plot of original material distribution compared with corrected measured armour layer distribution.

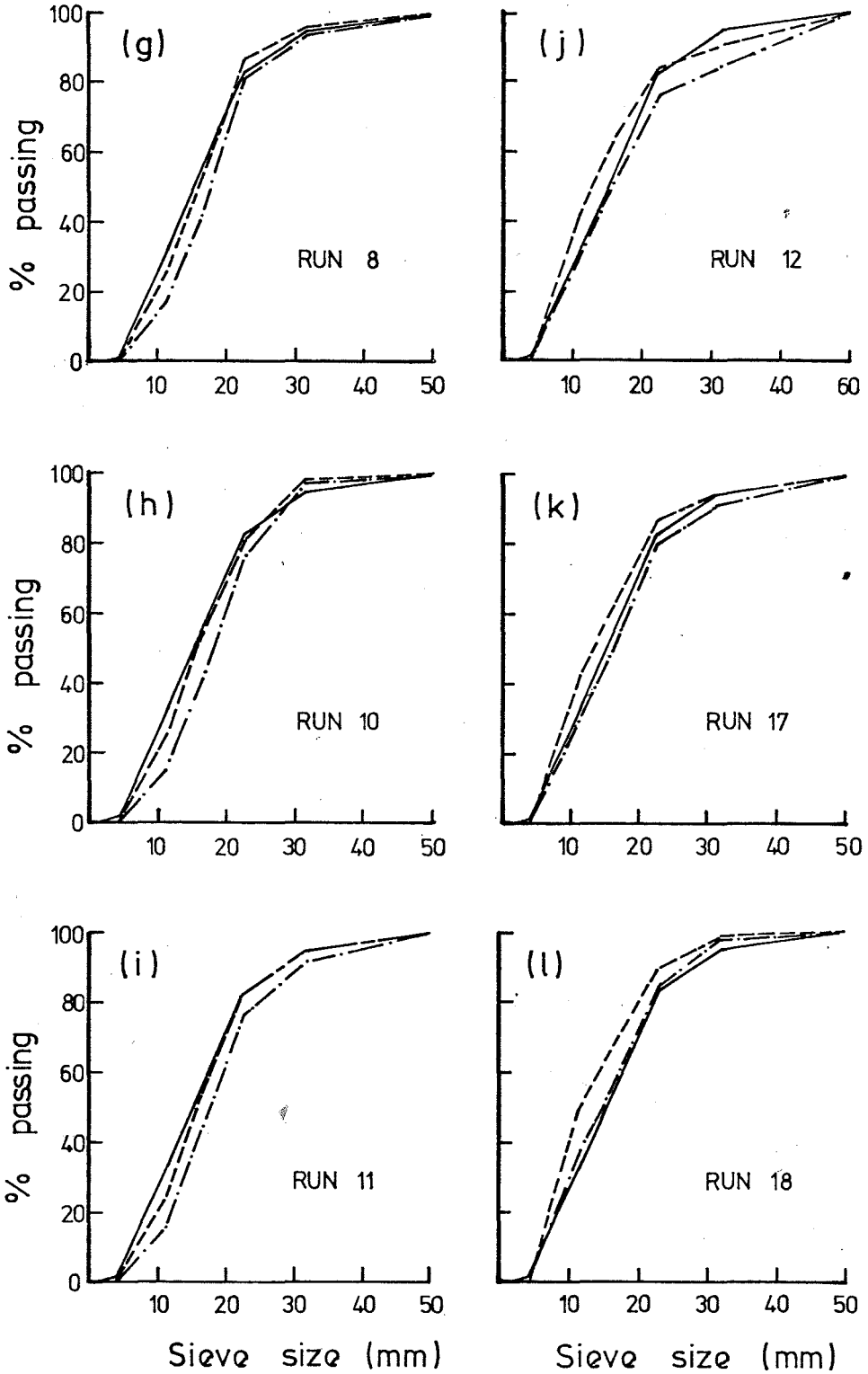

Figure 4-5: (Continued....)

accompanied the paving (see section 4.7.4). A further factor not accounted for in Gessler's analysis, is that for the small flow depths occurring in these runs, there is an increase in the critical shear stress required for incipient motion of each grain. This increase in the critical value of Shield's parameter can be as much as 250% (Ashida and Bayazit, 1973).

4.7.2 Wavelength of Observed Bedforms

In the tests reported herein, it was observed that the bedforms developed quickly in response to the imposed flow. It was then assumed that the wavelength measured at final conditions reflected the wavelength existing at initial conditions. The large bed elements modified the bed waves during the duration of the tests by affecting their steepness through locally anchoring material rather than by distoring their wavelength. By using the final wavelength in this way as an indicator of the initial wavelength, it can be seen from fig. 4-6 that the bedforms at the beginning of each test run were antidunes (the point for run 10 being the only point that does not lie close to the region of antidune formation). For runs at slope 0.027, antidunes occurred. The points in fig. 4-6 for these tests (runs 11, 12, 17 and 18) corresponding to initial and final conditions lie to the right of the region of antidune formation. However, when the wavelengths from the photographs are used, the points lie much closer. Within the precision of measurement, these bed waves conformed to the equations of Kennedy (1961, 1963).

The points corresponding to final conditions for the tests at slopes 0.098, 0.172 and 0.248 (i.e. runs 1 to 5, 7, 8, 10, and 15) lie close to or in the region of antidune formation. Thus, although the bed waves were modified in appearance by the larger bed elements, they still conformed to the equations of Kennedy (1961, 1963) for antidunes.

4.7.3 Steepness of Observed Bedforms

An ideal steepness, corresponding to a local maximum of the resistance coefficient (Davies and Sutherland, 1980), has been reported for artificial roughness elements and lower regime bedforms (Davies, 1980; Rouse, 1965; Yalin, 1977 pp. 269-271). Upper regime bedforms i.e. antidunes, tend to a steepness that lies within the range given by Rouse (1965) as corresponding to a maximum of resistance for artificial roughness elements, but this steepness is only temporarily

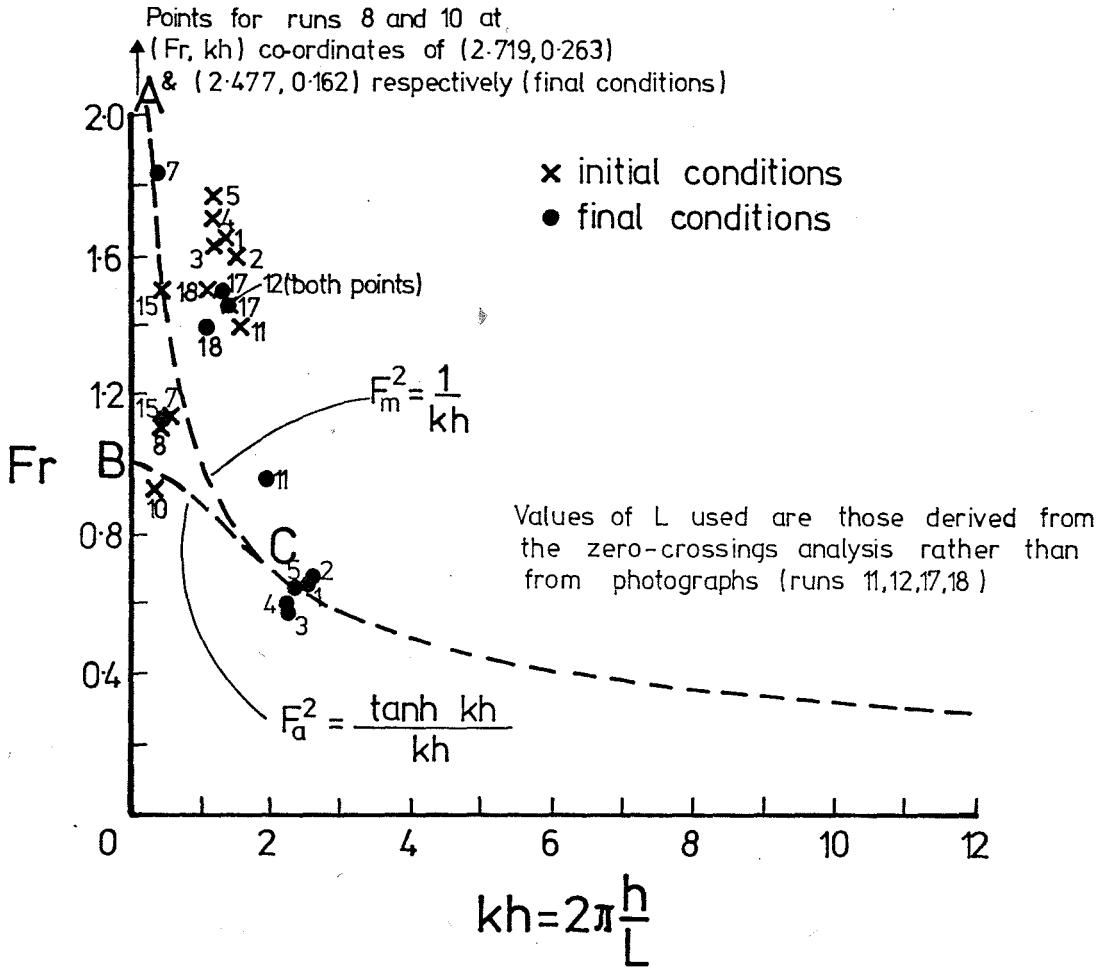

Figure 4-6: Plot of dimensionless wave number kh vs Froude number F.

achieved when the surface waves are on the point of breaking, i.e. at e = 0.142. At this point the antidunes break and wash out. The ideal steepness is reached cyclically, and usually only occurs over a portion of the bed. The mean steepness of antidunes thus tends to be less than the 'ideal' value. In line with this, for runs 11, 12, 17 and 18 where 'classic' antidunes formed, the average e value lies well outside the range given by Rouse (1965) as corresponding to the maximum roughness effect of many roughness forms. A photograph of an individual breaking antidune in run 14 showed a value of e = 0.151, close to the theoretical maximum of e = 0.142. Thus, for these runs, the e values reflect an average condition where some of the bed is essentially plane, and some of it will have antidunes of maximum amplitude or less.

For an armoured or paved surface, Sutherland and Williman (1977) found a tendency toward an ideal steepness. They used a zero crossings analysis to define element size (height) as the maximum difference in elevation between successive upward zero-crossings. The mean height of all elements is a measure of the effective roughness size of the surface. Mean steepness was referred to by Sutherland and Williman (1977) as effective roughness concentration e. The average e value for runs 1 to 5, 7, 8, 10 and 15 was 0.127. This is lower than the mean value of 0.19 obtained by Sutherland and Williman (1977). However, the maximum steepness for long square roughness elements and rectangular bar roughness elements occurs at a roughness concentration of just less than 0.1 and just greater than 0.1 respectively (Koloseus and Davidson, 1966b). The bedforms of these test runs could be considered to resemble rectangular elements. The e value of 0.127 then reflects a compromise between the value of 0.1 due to the bedforms and the value of about 0.2 reported to characterise an armoured or paved surface. Judd and Peterson (1969) noted that the high gradient, rough channels they investigated tended to give a maximum resistance to flow at e = 0.1 They also suggested that a compromise of e values corresponding to different roughness element shapes would give a truer reflection of reality.

4.7.4 Resistance to Flow

The values of the Darcy-Weisbach friction factor f found in the above tests after stabilisation are extremely high. However, they are similar to values obtained by other researchers for flow in similar channels, as reported by Scheuerlein (1973).

For runs 11, 12, 17 and 18, armouring of the bed surface occurred, i.e. the bed surface did not coarsen. f values for initial and final conditions indicate that the antidunes did not increase resistance to flow.

The values of $\frac{f_u}{f_o}$ for runs 1 to 5, 15 and 16 indicate that the resistance to flow of the bed increased over the duration of the tests. This increase in resistance was caused by paving, which coarsened the bed surface grain size distribution. Runs 1 to 5 also show that as flow increases, $\frac{f_u}{f_o}$ increases. That is, the final bed condition relative to the initial bed condition offers proportionally more resistance to flow as discharge increases. However, paving also occurred for runs 7, 8 and 10, whereas the values of $\frac{f_u}{f_o}$ indicate that the paved bed offered less resistance to flow than the plane bed under initial conditions. This is even more puzzling in that the formula of Hey (1979) tends to underestimate the friction factor at very small flow depths (MacMurray, in prep). This inconsistency is considered to be caused by the fact that underflow comprised the bulk of the total flow for these runs (note that the flow values given in table 4-1 are for total flow minus underflow). Thus the velocity derived for the surface flow (obtained by correcting the salt velocity for the slower underflow component; see comment in Appendix 2) is possibly a little inaccurate. The trend given by runs 7 and 8, however, is correct in that with increasing flow $\frac{f_u}{f_o}$ increases.

4.8 CONCLUSIONS

It has been possible to simulate, in a laboratory flume, a bed shaping process which, after flow reduction, resulted in step-pool sequences resembling those found in mountain streams. On the basis of these simulations, it is postulated that the step-pool structures in the bed of a mountain stream are generated during high flows and not by the low flows which give them the step-pool appearance. Thus, under usual flow conditions, the channel bed of steep mountain streams can be seen as being extremely stable.

The deforming process leading from an initially plane bed to step-pool formation is basically the same process as that which produces antidunes. At slopes less than 0.075 'classic' antidunes formed, and armouring of the bed surface occurred for all flows. At slopes greater

than 0.075, paving of the bed occurred in conjunction with bedforms that conformed to equations describing antidunes. The paving was associated with an increase in resistance to flow.

Thus the formation of step-pool structures involves a combination of antidune and armour layer (or paved layer) formation. Values of steepness of the bedforms tend to suggest that the deformations are those which give a maximum value of resistance coefficient.

CHAPTER FIVE

CLEAR WATER FLOW THROUGH A STEP-POOL SYSTEM

5.1 INTRODUCTION

The extreme irregularity of a boulder-strewn channel is sometimes simulated by means of a succession of discrete weirs (Rouse, 1965; Kellerhals, 1970, 1972, 1973). Rouse further states that this is a reasonable procedure if one realises that the simulated roughness must eventually become not merely a form of flow impedence but a type of non-uniformity that inherently involves the Froude number. Thus, in the present tests, a series of baffles was installed in the experimental flume at 0.5 m intervals to model step-pool systems in steep mountain streams.

The objectives of the clear water flow series of tests were as follows:

(1) to study flow behaviour through an idealised step-pool system in order to gain a basis for understanding the behaviour of step-pool systems in the field. Specifically, average velocity was to be measured by the salt-velocity method to facilitate computation of resistance to flow in the idealised system, in order to understand energy dissipation in field step-pool systems,

and (2) to identify and examine any idiosyncrasies of the model not apparent in the field situation. In particular, idealised systems using regular sills or baffles were known to induce flow unsteadiness in the form of roll waves.

To provide an adequate base for discussion of the present results, a literature review follows which covers aspects of roughness in channels, flow regimes, and flow instabilities.

5.2 LITERATURE REVIEW

5.2.1 Roughness in Open Channel Flow

General: The friction factor c is the ratio of the average velocity of the flow v_m to the shear velocity v_*

$$c = v_m/v_* \qquad \ldots 5\text{-}1$$

(Note that the Chézy friction factor $C = c\sqrt{g}$).

In the case of two-dimensional flow,

$$v_* = \sqrt{gJh} \qquad \ldots 5\text{-}2$$

Alternatively, resistance to flow is represented by the Darcy-Weisbach friction factor f

$$f = \frac{8}{c^2} \qquad \ldots 5\text{-}3$$

From equation 5-2, it can be shown that

$$F = c\sqrt{J} \qquad \ldots 5\text{-}4$$

and thus

$$f = \frac{8J}{F^2} \qquad \ldots 5\text{-}5$$

which shows that roughness or friction factor is a function of Froude number F.

Traditionally, roughness in open channels has been represented by an equation

$$\frac{1}{\sqrt{f}} = A \log \frac{R}{y'} + B \qquad \ldots 5\text{-}6$$

where, for this equation

$A = 2$

$B = 0.79$ (if width to depth ratio large)

R = hydraulic radius

and y' = depth at which velocity = 0.

y' has usually been considered to be related to k_s, where k_s is the equivalent sand grain diameter that would give the same roughness characteristics (Nikuradse, 1932).

Flow in Rough Channels: The Nikuradse equivalent grain size roughness value was used for other roughness types than sand grains in an attempt to derive a single representative friction factor function. Equation 5-6 implies that f is independent of Reynolds number Re. However, Morris (1959) noted that f may be an increasing or decreasing function of the Reynolds number, depending on the nature of the channel

roughness. It was thus seen that a more complete description of the roughness characteristics was necessary (Morris, 1959; Sayre and Albertson, 1963; Rouse, 1965).

Morris (1955) noted that the chief source of friction loss in a fluid flowing over a rough surface was the generation, spreading, and subsequent dissipation of vortices from the wake and separation zones behind each element. This suggested that the longitudinal spacing of roughness elements L was the roughness dimension of greatest importance in rough conduit flow. Morris (1955) proposed three different flow regimes, namely

(a) isolated roughness flow,

(b) wake interference flow,

and (c) quasi-smooth (or skimming) flow.

Morris (1959) expanded this classification to the following

(a) smooth turbulent flow,

(b) normal turbulent flow,

(c) semi-smooth turbulent flow (i.e., isolated roughness flow),

(d) hyper-turbulent flow (i.e., wake interference flow),

and (e) quasi-smooth flow.

Morris developed different equations to predict the resistance to flow for each of these regimes.

Artificial Roughness Element Channels: It is implicit in this type of approach that the friction factor depends on the size, shape, and spacing of roughness elements making up the channel bed. To incorporate these factors into an analysis of resistance to flow in rough channels, many authors have used artificial roughness elements. Schlichting (1936) was the first to attempt this style of analysis and the type of element he studied over the greatest range of spacing was the sphere. His results for spheres are plotted in fig. 5-1 (after Rouse, 1965).together with points determined by Koloseus (1958), Koloseus and Davidian (1966b), and O'Loughlin and MacDonald (1964). (O'Loughlin and MacDonald used cubes arranged in the Schlichting pattern, and the same pattern turned through 90°, as well as sand in controlled concentrations. Concentration λ is the ratio of the sum of areas projected normal to the flow to the bed area of the channel.) It is immediately evident that there is an optimum concentration of about 15% to 25% which produces the greatest resistance to flow.

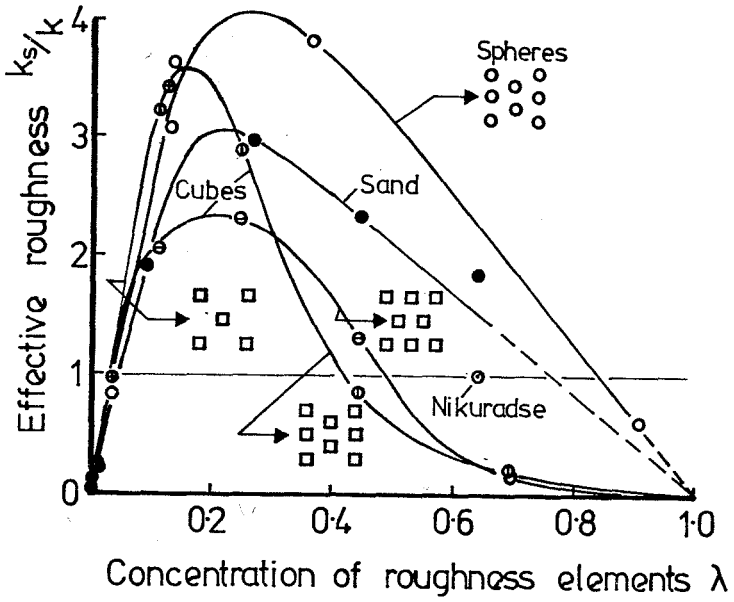

Fig. 5-1 Effective roughness as a function of form, pattern, and concentration of roughness elements (After Rouse, 1965).

Below a value of λ of about 15%, the resistance varies in direct proportion to the concentration, and the proportionality coefficient varies approximately with the relative drag of the individual elements. So the resistance to flow for fully developed roughness of height k, and concentration λ is

$$\frac{1}{\sqrt{f}} = A \log \frac{R}{Dk\lambda} + B \qquad \ldots 5\text{-}7$$

$$(\lambda < 0.15)$$

where ,

D = function of both the shape and arrangement of roughness elements,

and A, B = constants.

Koloseus and Davidian (1961, 1966a) found

$$\frac{1}{\sqrt{f}} = 2 \log \left(\frac{0.14 \left(\frac{4h}{k}\right)}{\lambda^{0.9}} \right) \qquad \ldots 5\text{-}8$$

Adachi (1964) added 'incomplete wake interference flow' as a transitional regime between the wake interference and isolated roughness regimes of Morris' (1955) classification. He then reduced those classifications to two cases.

Ridge Roughness - causes incomplete wake interference flow and isolated roughness flow,

and Groove Roughness - causes complete wake interference flow and skimming flow.

He used relative roughness h/k in his empirical log resistance formula, with L/b (b = width between strips) for groove roughness instead of L/k as had been done for ridge roughness (Morris, 1955).

Knight and MacDonald (1979) compared the results of several authors with their own. In general, the friction factor was seen to decrease with increasing Reynolds number. Maximum bed resistance to flow was found to occur at a relative spacing of $L/k \cong 8$.

However, the studies mentioned so far have all involved small values of relative roughness k/h. Bathurst (1978) classified three types of flow on the basis of relative roughness k/h, namely

(a) $k/h < 0.1$ - small-scale roughness,

(b) $0.1 < k/h < 0.3$ - transitional,

and (c) $k/h > 0.3$ - large-scale roughness.

Bayazit (1975) noted that equation 5-6 may not be valid for large values of k/h, while Rouse (1965) warned that such flows could no longer be considered uniform and thus the velocity distribution is not logarithmic. Bayazit (1975) and O'Loughlin and MacDonald (1964) found that friction factor increases substantially when relative roughness exceeds 0.3.

Sayre and Albertson (1963) analysed data for the transitional and small-scale roughness cases, and found that a logarithmic equation was still applicable. They postulated the equation

$$c = \frac{2.30}{\kappa} \log \frac{y_n}{\chi} \quad \ldots 5\text{-}9$$

where κ = von Kármán turbulence coefficient

y_n = normal depth of flow

and $\chi = \phi$ (size, shape, and spacing of roughness elements).

From $c = \frac{2.30}{\kappa} \log \frac{y_n}{k} + c_2$ ... 5-10

and equation 5-9, they found

$$c_2 = -6.06 \log \frac{\chi}{a} \quad \ldots 5\text{-}11$$

where, for this equation, a = constant.

Sayre and Albertson (1963) found that they could consider the channel bottom as the reference datum for close-spaced roughness elements, unlike some authors who had had to consider depth of flow from the water surface to some other reference level. Further, the data indicated that κ was independent of roughness pattern, provided the conditions of wake interference and uniform roughness prevailed.

Raju and Garde (1970) also worked in the transitional and small-scale roughness zones, but with low Froude numbers so that the Froude number effect due to wave resistance could be ignored. They found that the total resistance of a rough bed (L/k from 2.5 to 4.5) may be estimated from

$$\frac{1}{\sqrt{C_D}} = c_1 \log \frac{h}{k} + c_2 \quad \ldots 5\text{-}12$$

where C_D = a drag coefficient.

Comparing this with

$$\frac{v_m}{v_*} = 6.06 \log \left(\frac{h}{k} \right) + c_3 \quad \ldots 5\text{-}13$$

they found that the depth datum may be set at the flume bottom for L/k from 5 to 40, but for L/k less than 5, the datum needs to be set at a higher level.

For large-scale roughness, some researchers still used a logarithmic law (Scheuerlein, 1973) while others opted for an empirical power law to describe resistance to flow (Mohanty, 1959; Herbich and Shulits, 1964). In these large-scale roughness channels, despite the gross effect

on the water surface due to the roughness elements, the flow can be considered quasi-steady and uniform in a macroscopic sense (Hartung and Scheuerlein, 1967). Scheuerlein (1973) defined

$$\sqrt{\frac{1}{f}} = -A \log \left(\frac{k}{R} B\right) \quad \ldots 5\text{-}14$$

where $A = \frac{\ln 10}{\kappa \sqrt{8}}$

and $B = \sigma (0.44 + 3 \phi)$ ... 5-15

where $\phi = \frac{k \tan \alpha}{L}$

and $\tan \alpha$ = channel slope.

Here, σ is an aeration factor and

$$\sigma = 1 - 1.3 \sin \alpha + 0.08 \, h/k. \quad \ldots$$

Herbich and Schulits (1964) differentiated two cases:

(a) flow depth greater than roughness element height and

(b) flow depth less than roughness element height.

They presented graphical relations relating a resistance coefficient K (inverse of Manning's n in S.I. units) to λ and F for various values of slope.

While some of these studies were undertaken specifically to model boulder bed channels (Herbich and Shulits, 1964; Hartung and Scheuerlein, 1967; Scheuerlein, 1973), other authors attempted to work directly from field data.

Field Studies of Boulder-Bed Channels: Judd and Peterson (1969) showed resistance to flow to be a function of channel shape, roughness, spacing (or concentration) λ, and relative roughness. They derived

$$\sqrt{\frac{8}{f}} = \frac{v_m}{v_*} = \phi(\lambda) \left(\frac{\bar{h}}{w}\right)^{7(\lambda - 0.08)} \left(\frac{\bar{h}}{k_{50}}\right)^{1/3} \quad \ldots$$

where W = channel width.

Bathurst (1978) noted that with large-scale roughness, the total resistance was the sum of the profile drag of each roughness element. He theorised

$$\sqrt{\frac{8}{f}} = \frac{v_m}{v_*} = \left(\frac{1}{\frac{1}{2}C_D \lambda \left(\frac{v'}{v_m}\right)^2} \right)^{\frac{1}{2}} \quad \ldots 5\text{-}18$$

where C_D = a drag coefficient

and v' = approach velocity to roughness element,

but then derived the following equation

$$\sqrt{\frac{8}{f}} = \left(\frac{R}{0.365\ D_{84}} \right)^{2.34} \left(\frac{W}{h}\right)^{7(\lambda-0.08)} \quad \ldots 5\text{-}19$$

Bathurst differentiated very steep channels (characterised by steps and pools) from conditions of large-scale roughness with associated macro-uniformity. In Bathurst et al. (1981), this is clarified further by defining the large-scale roughness channels as boulder bed channels found at slopes greater than about 0.3% but less than about 7%. These boulder bed channels thus correspond to the region of riffle steps (Hayward, 1980). Bathurst et al. (1981) derived for these channels

$$\sqrt{\frac{8}{f}} = \left(\frac{0.28}{b'} F\right)^{\log(0.755/b')} \left[13.434 \left(\frac{W}{Y_{50}}\right)^{0.492} b'^{\,1.025\left(\frac{W}{Y_{50}}\right)^{0.118}} \right]$$

$$\times \left(\frac{A_w}{Wh'}\right) \quad \ldots 5\text{-}20$$

where b' is a function of the effective roughness concentration such that

$$b' = a \left(\frac{h}{S_{50}}\right)^c \quad \ldots 5\text{-}21$$

where a, c = constants varying with bed material

and S_{50} = size of element short axis, which is bigger than or equal to 50% of short axes.

$$Y_{50} = \frac{L_{50} + D_{50}}{2} \quad \ldots 5\text{-}22$$

Y_{50} is the cross stream axis size, while L_{50} is the long axis of the bed material.

and $\frac{A_w}{Wh'}$ = relative roughness area where

h' = depth of bed datum.

Hey (1979) noted that many authors gave a general form of resistance equation for gravel bed channels, and he proposed

$$\sqrt{\frac{1}{f}} = 2.03 \log \left(\frac{a\ R}{3.5\ D_{84}} \right) \quad \ldots 5\text{-}23$$

where a varies with the cross-sectional geometry of the flow.

Thompson and Campbell (1979) proposed

$$f = \left((1-0.1 \frac{k_s}{R}) \quad 2 \log_{10} (12 \frac{R}{k_s}\ )\right)^{-2} \quad \ldots 5\text{-}24$$

where $k_s = 4.5\,D$, with D equal to the median boulder diameter.

At high relative roughness $\frac{k}{h}$ it appears that Hey's (1979) and Thompson and Campbell's (1979) equations under-estimate f (Bathurst et al., 1981; MacMurray, in prep.). Further, the large-scale roughness equations are held to be inapplicable to step-pool streams (Bathurst et al., 1981; Bathurst, in press).

5.2.2 Steep Streams Modelled by Steps and Pools

Mohanty (1959) described three flow regimes for step-pool channels

(a) tranquil,

(b) tumbling,

and (c) rapid.

Mohanty reported that for any regime, each roughness element acts as a partial or full control, while flow is macroscopically uniform at a scale much greater than step length. He also found instability in the transition regions between rapid and tumbling, and rapid and tranquil regimes. Peterson and Mohanty (1960) stated that roll waves formed in these transition zones, and noted that in tumbling flow, the roughness elements acted as critical flow weirs. Al-Khafaji (1961) introduced a new regime

(d) unstable tumbling flow

as well as three transitional ones. Al-Khafaji used plots of q vs J (for different $\frac{L}{k}$ values) to show the major flow regimes.

Morris (1968) summarised all the information in a detailed report. He varied size, spacing, and shape of roughness elements to determine an optimum geometry for dissipating fluid energy on steep slopes.

Unstable tumbling flow was characterised by the occurrence of roll waves. The following section summarises some attempts to explain their occurrence, in comparison with the analysis of the more common type of roll wave caused by instability in uniform flow.

5.2.3 Instability in Open Channel Flow

Uniform open channel flow will become unstable when the velocity of flow is very high or the channel slope is very steep (greater than 2 or 3%). Under these conditions, instability of the free surface is characterised by the formation of a series of roll waves (Chow, 1959).

The phenomenon of roll wave formation was first reported by Cornish (1910). Many attempts have been made to develop a criterion for instability of uniform flow to explain the formation of roll waves. Jeffreys (1925) used a non-linear shallow water equation and the Chézy resistance law to establish the criteria

$$v_m = 2\sqrt{gh} \qquad \ldots 5\text{-}25$$

That is, the initial instability occurs at a Froude number of 2. Keulegan and Patterson (1940) used the same approach, but with Manning's resistance law instead of Chézy's. Their criterion was then

$$v_m = 1.5\sqrt{gh} \qquad \ldots 5\text{-}26$$

or instability for F greater than 1.5.

Ishihara et al. (1952), working with a smooth sheet flow, considered the Manning and Chézy equations inapplicable, and found roll waves at flow velocities smaller than those of Jeffreys (1925) or Keulegan and Patterson (1940). Mayer (1959) described two types of waves. Roll waves were found in the laminar flow regime, where surface tension was found to be vital for their formation. Further, the surface velocity was less than the wave velocity. Slug waves formed at the boundary between supercritical laminar and subcritical turbulent flow. The data for both types was found to lie on a single curve of a plot of $F/\sqrt{J}$ vs Reynolds number. Mayer (1959) found that instabilities occurred for $F > 2$, but

in line with Ishihara et al. (1952), Albertson et al. (1960) reported that the unstable limit occurs at F < 1 for laminar flow.

Vedernikov (1945) used the Saint-Venant approximations to establish a criterion for instability called the Vedernikov number V.

$$V = \frac{x' \gamma' v_m}{v_w - v_m} \qquad \ldots 5\text{-}27$$

(Chow, 1959)

where x' = the exponent of the hydraulic radius in the general uniform flow equation. Thus, x' = 2 for laminar flow, 0.5 for turbulent flow if the Chézy formula is valid, and 0.667 for turbulent flow if the Manning formula is used.

v_w = absolute velocity of disturbance waves in channel,

and γ' = a shape factor of the channel section defined by

$$\gamma' = 1 - R \frac{dP}{dA} \qquad \ldots 5\text{-}28$$

where R = hydraulic radius

P = wetted perimeter

and A = the flow cross-sectional area.

$v_w - v_m$ is equal to the celerity c of the waves, or to the critical velocity v_c (Chow, 1959). Thus, the Vedernikov number may be reduced to

$$V = x' \gamma' F \qquad \ldots 5\text{-}29$$

When the Vedernikov number is less than unity, the flow will be stable; when V is equal to or exceeds unity, unsteady flow will develop and roll waves will form.

Dressler (1949) showed that roll waves could not occur when the resistance to flow was zero, or exceeded a certain value. Rouse (1938) also stated that large roughness and/or bed irregularities would prevent the formation of roll waves.

Koloseus and Davidian (1966(a)) used the ratio F/F_s (similar to, but not the same as, the Vedernikov number) to define the stability limit:

where $\frac{F}{F_s} > 1$ unstable
$\frac{F}{F_s} < 1$ stable ... 5-30

They found that F_s increased as the ratio of flow width to flow depth decreased. They postulated that for a rough channel, a single relation could describe stable sub- or super-critical flow. The relation was

$$\frac{1}{\sqrt{f}} = 2 \log \left[\frac{0.14 \frac{4h}{k}}{\lambda^{0.9}} \right] \quad \ldots 5\text{-}31$$

where λ = roughness concentration.

The unstable data coalesced when the degree of instability was considered. The resultant equation was

$$\frac{1}{\sqrt{f}} = 2 \log \left[\frac{0.14 \left(\frac{4h}{k} \right)}{\lambda^{0.9} \left(\frac{F}{F_s} \right)^{2/3}} \right] \quad \ldots 5\text{-}32$$

Koo (1963, 1967), working with large roughness values, attempted the same coalescing by plotting $\frac{1}{\sqrt{f}}$ against $\frac{\frac{h}{k}}{F/\sqrt{J}}$. However, Al-Khafaji (1961) had questioned the usefulness of $F/\sqrt{J}$ for such channel roughnesses.

A common feature of roll waves is that they break in the forward direction. The waves of Koo (1963, 1967), Mohanty (1959), Al-Khafaji (1961) and the present tests, all break in the backward direction. Whether the latter waves are the same as the roll waves predicted by uniform flow stability analyses is made even more questionable by the following description by Al-Khafaji (1961):

> ".... It was found that at the instant roll waves started there existed a minimum depth in the neighbourhood of the middle of each cycle where the velocity was a maximum. When this depth approached the height of the roughness the wave started to form."

Koo (1963, 1967) found F_s to be 1.35. However, in his derivation of F, he used the depth over the roughness elements. In stable tumbling flow his roughness elements would have acted as critical depth sections. A local Froude number of about 1.3 is not at all unusual

in these situations if depth measured is the brink depth.

Thus, there appear to be several sorts of instability in open channel flow. The most usual instability is that investigated by the use of shallow water theory. Very large roughnesses also generate instability. A further type described by Foley and Vanoni (1977), and Schumm et al. (1982) is due to the breaking of antidune waves, and is thus a two-phase phenomenon.

5.3 TESTS

For this series, tests were performed at slopes of 0.027, 0.098, 0.172 and 0.248. At each slope, a series of flows was passed down the channel. Average and maximum velocities were measured using the salt-velocity technique. Observations were made of flow regimes. Photographs were taken to provide a visual record of each test run. Negatives of the test runs were projected onto a screen and tracings of the flow profiles were made.

5.4 RESULTS

The results for these tests are listed in Table 5-1.

5.4.1 Flow Regime

In these tests, three distinct flow regimes were observed. They were stable tumbling, unstable tumbling, and shooting flow, and are shown in fig. 5-2(a) to (c). The existence regions of the different regimes are shown in fig. 5-3.

5.4.2 Average and Maximum Velocities

Plots of average and maximum velocity are shown in figs. 5-15 and 5-16 respective.

5.4.3 Friction Factor and Average Shear Stress

The average shear stress τ_m and the Darcy-Weisbach friction factor f were calculated for each test using the wall correction procedure outlined by Gessler (1965). The average velocity was used for the velocity

TABLE 5-1 RESULTS OF CLEAR WATER FLOW TESTS

Run Number	J	q ($m^3 s^{-1}/m$)	v_m (m/s)	v_{max} (m/s)	h (m)	R (m)	τ_m (N/m^2)	f	F
1	0.098	0.003	0.008	0.022	0.370	0.370	357.57	46897.39	0.005
2	0.098	0.009	0.033	0.081	0.281	0.281	271.45	2018.51	0.026
3	0.098	0.014	0.050	0.101	0.284	0.284	274.25	891.80	0.039
4	0.098	0.019	0.066	0.132	0.287	0.287	277.03	513.44	0.051
5	0.098	0.022	0.072	0.162	0.302	0.302	291.46	452.30	0.054
6	0.098	0.026	0.101	0.272	0.261	0.260	251.68	197.37	0.082
7	0.098	0.030	0.106	0.479	0.279	0.278	268.99	191.10	0.083
8	0.098	0.035	0.123	0.347	0.281	0.280	270.76	142.25	0.097
9	0.098	0.040	0.139	0.529	0.285	0.284	274.46	113.32	0.108
10	0.098	0.045	0.149	0.529	0.301	0.300	289.77	104.70	0.112
11	0.098	0.051	0.190	0.628	0.267	0.266	256.63	56.87	0.152
12	0.098	0.065	0.232	0.559	0.280	0.278	268.64	39.83	0.182
13	0.098	0.111	0.409	2.514	0.270	0.266	256.76	12.30	0.326
14	0.098	0.091	0.368	2.011	0.246	0.243	234.46	13.86	0.308
15	0.098	0.144	0.472	2.285	0.305	0.299	283.99	10.38	0.354
16	0.098	0.163	0.599	2.514	0.272	0.265	255.68	5.71	0.476

Run Number	J	q ($m^3 s^{-1}/m$)	v_m (m/s)	v_{max} (m/s)	h (m)	R (m)	τ_m (N/m^2)	f	F
17	0.027	0.003	0.010	0.042	0.266	0.266	70.41	5962.23	0.007
18	0.027	0.007	0.025	0.088	0.279	0.279	73.81	983.65	0.018
19	0.027	0.022	0.079	0.718	0.283	0.282	74.59	95.37	0.058
20	0.027	0.039	0.135	0.914	0.290	0.287	76.05	33.53	0.097
21	0.027	0.048	0.161	1.257	0.301	0.297	78.72	24.29	0.114
22	0.027	0.055	0.179	1.257	0.306	0.302	79.87	19.94	0.126
23	0.027	0.071	0.221	1.117	0.321	0.315	83.37	13.66	0.152
24	0.027	0.080	0.275	1.117	0.290	0.282	74.79	7.91	0.198
25	0.027	0.093	0.326	1.257	0.286	0.277	73.23	5.51	0.237
26	0.027	0.127	0.477	1.396	0.265	0.250	66.23	2.33	0.360
27	0.027	0.160	0.623	1.571	0.257	0.236	62.49	1.29	0.477

Run Number	J	q (m^3 s^{-1}/m)	v_m (m/s)	v_{max} (m/s)	h (m)	R (m)	τ_m (N/m^2)	f	F
52	0.172	0.011	0.040	0.087	0.282	0.282	468.75	2343.75	0.033
53	0.172	0.020	0.073	0.168	0.275	-	-	-	-
54	0.172	0.028	0.096	0.251	0.287	0.287	476.60	410.29	0.079
55	0.172	0.038	0.130	0.245	0.293	0.292	486.21	230.87	0.105
56	0.172	0.044	0.152	0.305	0.288	0.287	477.67	165.18	0.124
57	0.172	0.050	0.169	0.296	0.297	0.296	492.40	138.74	0.135
58	0.172	0.056	0.180	0.318	0.311	0.310	515.46	127.70	0.141
59	0.172	0.078	0.272	1.257	0.286	0.284	472.80	51.31	0.222
60	0.172	0.094	0.302	2.793	0.311	0.309	513.65	45.20	0.236
61	0.172	0.126	0.559	2.514	0.225	0.221	368.12	9.42	0.515
62	0.172	0.162	0.684	3.142	0.237	0.232	385.68	6.60	0.614

Run Number	J	q ($m^3\ s^{-1}/m$)	v_m (m/s)	v_{max} (m/s)	h (m)	R (m)	τ_{m_2} (N/m^2)	f	F
76	0.248	0.012	0.048	0.114	0.247	0.247	583.03	2067.24	0.043
77	0.248	0.024	0.090	0.168	0.266	0.266	627.53	623.93	0.079
78	0.248	0.034	0.120	0.219	0.279	0.279	657.88	363.67	0.103
79	0.248	0.041	0.142	0.437	0.290	0.289	683.56	270.44	0.119
80	0.248	0.048	0.161	0.234	0.301	0.300	709.26	219.99	0.132
81	0.248	0.054	0.168	0.258	0.321	0.320	756.27	213.85	0.134
82	0.248	0.066	0.224	0.437	0.294	0.293	691.89	110.21	0.187
83	0.248	0.075	0.261	0.479	0.287	0.286	674.86	79.19	0.220
84	0.248	0.085	0.261	0.393	0.324	0.323	761.86	89.20	0.208
85	0.248	0.093	0.295	1.479	0.314	0.312	737.77	67.64	0.238
86	0.248	0.125	0.408	2.285	0.307	0.305	719.26	34.63	0.333
87	0.248	0.138	0.488	1.955	0.282	0.279	659.19	22.12	0.416
88	0.248	0.159	0.447	1.933	0.356	0.353	833.14	33.30	0.339

(Note: Channel width b = 0.132 m,
therefore Q = (q x 0.132) m^3/s)

Figure 5-2(a): Stable tumbling flow.

Figure 5-2(b): Unstable tumbling flow.

Figure 5-2(c): Shooting (or rapid) flow.

value in the calculation. The Darcy-Weisbach friction factors are shown in fig. 5-17.

5.5 DISCUSSION OF RESULTS

5.5.1 Flow Regime

The following description of the four major flow regimes is taken from Morris (1968).

Tranquil Regime

This regime occurs at mild bed slopes ranging up to a maximum of 1% to 3%, depending on the discharge and the size and spacing of bed elements. The flow is characterised by surface smoothness, although at higher discharges the flow tends toward surface instability.

Stable Tumbling Regime

This regime occurs at steeper slopes. The larger the bed element spacing the smaller is the slope at which tumbling flow begins. The range of the stable tumbling regime is a function of channel slope, discharge, size and spacing of roughness elements. For a given bed geometry, the range of discharges producing this flow decreases with slope up to about 8%, then starts increasing (but at a decreasing rate with increasing slope).

The flow in this regime is characterised by alternate acceleration and deceleration between supercritical and subcritical velocities in every cycle from bed element to bed element. The qualitative criterion for the regime is, then, a series of hydraulic jumps. Critical depth occurs over each roughness element.

Unstable Tumbling Regime

This regime is also a function of channel slope, discharge, and roughness geometry. For a given slope, it occurs at discharges higher than those for stable tumbling flow and lower than for the rapid regime. In this regime, pulsating surges appear as waves superimposed over the normal flow. These waves increase in height as they travel downstream, and break backwards, rather than forwards as occurs with roll waves caused by amplified instability in uniform flow.

Rapid Regime

This regime occurs at the same slopes as stable and unstable tumbling flow, but at higher discharges. The lower limit of the regime

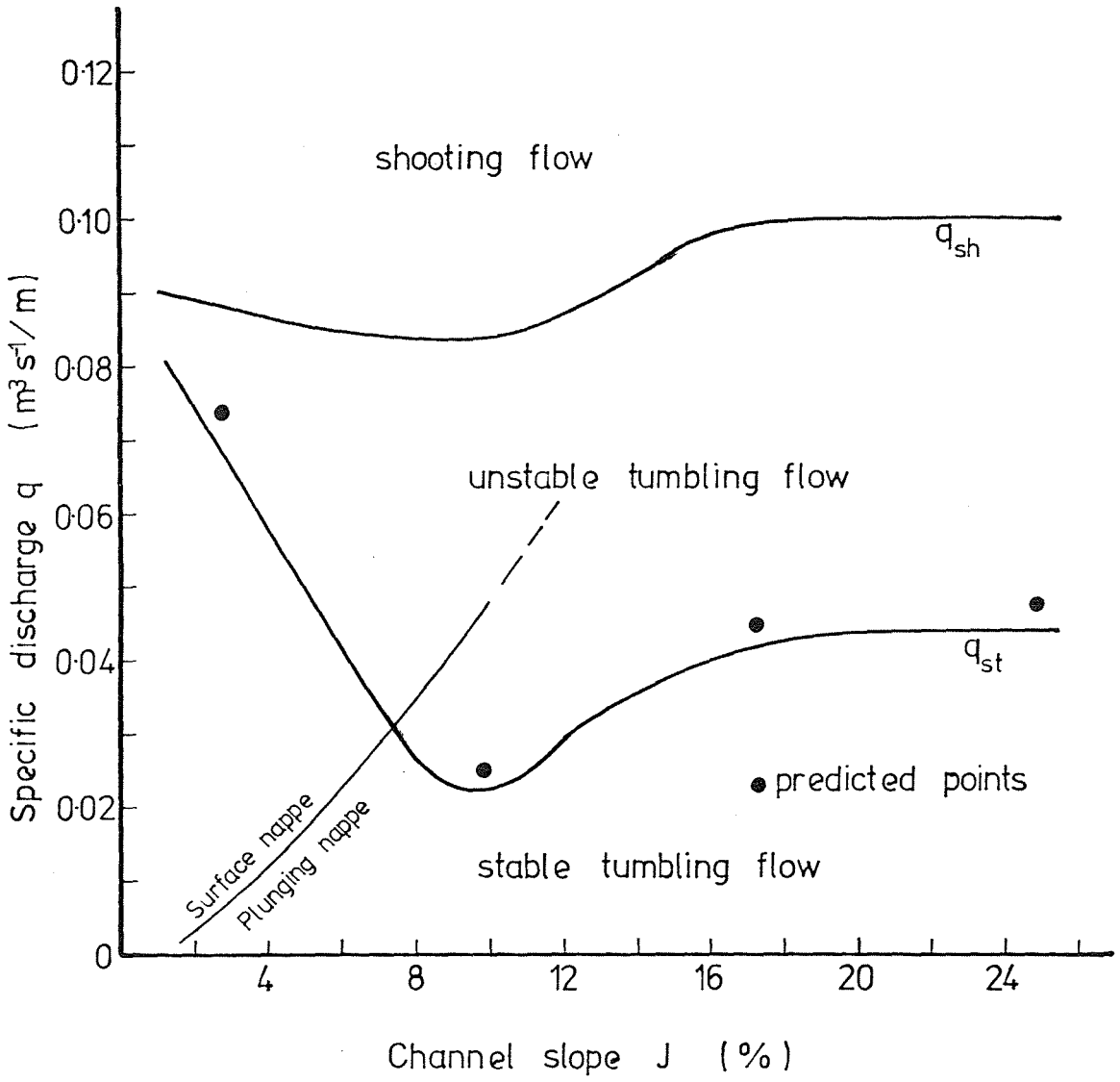

q_{st} = specific flow rate at limit between stable tumbling and unstable tumbling flow

q_{sh} = specific flow rate at limit between unstable tumbling and shooting flow

Figure 5-3: Existence regions of flow regimes.

increases markedly with increased spacing of bed elements.

In this regime, water skims over the roughness elements. The eddies between the roughness elements are of large magnitude.

As can be seen from fig. 5-2, the roughness elements used in the present tests were rectangular, having dimensions of 0.285 m x 0.132 m x 0.033 m. Designating height of the element (0.285 m) by k, distance between the baffles (0.5 m) by L, and thickness of the baffles (0.033 m) by t, the following dimensionless variables were obtained

$$\frac{L}{k} = 1.754 \qquad \ldots 5\text{-}33$$

and

$$\frac{t}{k} = 0.116 \qquad \ldots 5\text{-}34$$

Koo (1963) used $\frac{L}{k} = 5$, and $\frac{L}{k}$ from 3 to 10 (1967), while Al-Khafaji (1961) used $\frac{L}{k}$ from 5 to 15. Their flow regime data presented in plots of q vs J showed the same general shape as fig. 5-3, with unstable tumbling flow reaching a maximum extent at a slope of about 5 to 10% (this varied with shape of roughness element used). Both used square cross-section roughness elements, which were most susceptible to roll wave generation at $\frac{L}{k} = 5$ (Koo, 1967; Morris, 1968). Morris (1968) performed tests for a variety of different cross-section shapes at $\frac{L}{k} = 5$ and found that they reduced to some extent the range of unstable tumbling flow.

The existence regions for the flow regimes shown in fig. 5-3 thus belong to this general family of curves mentioned, modified due to the relatively close spacing and large bed element size.

Formation of Roll Waves

Flow through the system for slope = 0.027 was observed to be qualitatively different to that occurring at the slopes of 0.098, 0.172 and 0.248.

The steps in the channel act as weirs. Cox (1928) noted that flow over a weir could be either of two types, namely plunging nappe or surface nappe. At low flows, the nappe plunges (fig. 5-4(a)), while at higher flows it rides of the surface of the downstream pool (fig. 5-4(b)). The change from plunging to surface nappe occurs at a submergence ratio S'. $S' = \frac{H_2}{H_1}$, (see fig. 5-4) of about 0.2 for $\frac{k}{H_1} > 4.5$ (Vennard and Weston, 1943; Villemonte, 1947), which increases with decreasing $\frac{k}{H_1}$ for $\frac{k}{H_1} < 4.5$.

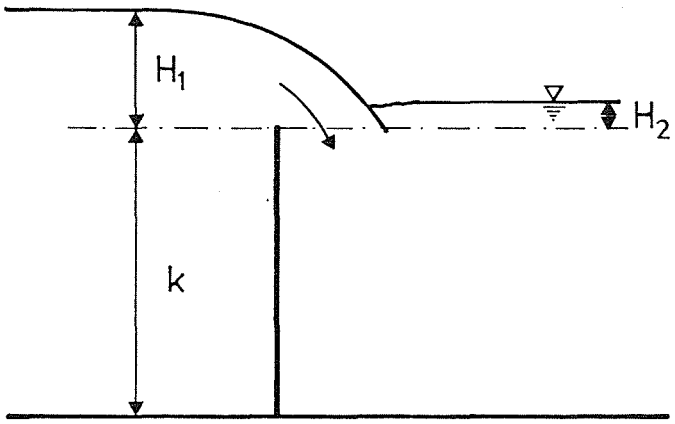

(a) plunging nappe profile

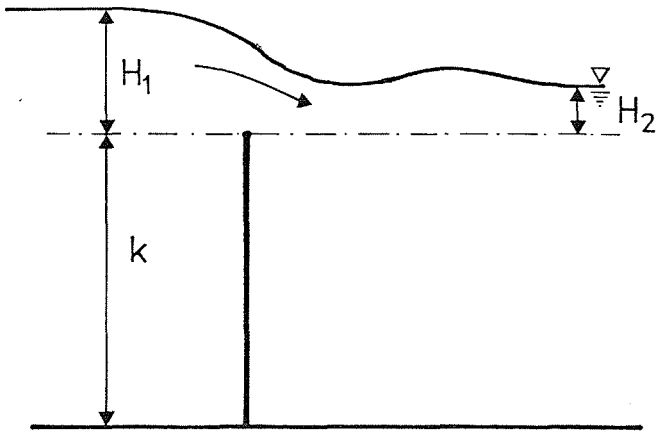

(b) surface nappe profile

Figure 5-4: Alternative nappe profiles.

The flow rates at which this change in nappe profile would occur were calculated for slopes = 0.027, 0.04, 0.06, 0.08 and 0.098. These points are shown on fig. 5-3 (for slopes = 0.172 and 0.248, $k/H_1 < 4.5$, and the flow rate would need to be even higher than indicated by the trend for slopes = 0.027 through 0.098).

For slope = 0.027, only run 17 had a flow rate less than q = 0.006 $m^3 s^{-1}/m$, the value for the change in nappe form. Run 17 and run 18 are shown in fig. 5-5(a) and (b) respectively. The change in nappe profile is clearly observable. The surface nappe probably corresponds to an undular hydraulic jump, as opposed to the submerged hydraulic jump (plunging nappe) that characterised stable tumbling flow for most of the tests performed. This suggests that at lower slopes, a flow sub-regime should be delineated, namely stable tumbling surface flow (see fig. 5-6).

As discharge increased beyond q = 0.006 $m^3 s^{-1}/m$ at slope = 0.027, the wavelength of oscillations of the surface nappe lengthened until the flow pattern was characterised by a standing wave over each step. The length between steps then defined the wavelength, and with increasing discharge the flow pattern could alter only by increasing the wave amplitude A. Steepness (i.e. A/L) was measured on the tracings for these runs; the results are listed in table 5-2.

TABLE 5-2 STEEPNESS OF STANDING WAVES

(J = 0.027)

Run	Steepness
21	0.077
22	0.092
23	0.130
24	0.164

The flow pattern for run 23 was observed to be on the verge of becoming unstable, and the corresponding discharge was considered to be the lower limit for unstable tumbling flow.

The maximum steepness for an irrotational wave has been theoretically calculated to be 0.142 (Milne-Thomson, 1968, p 406). Kennedy (1961) states that this value refers to gravity waves in a fluid of infinite depth, but

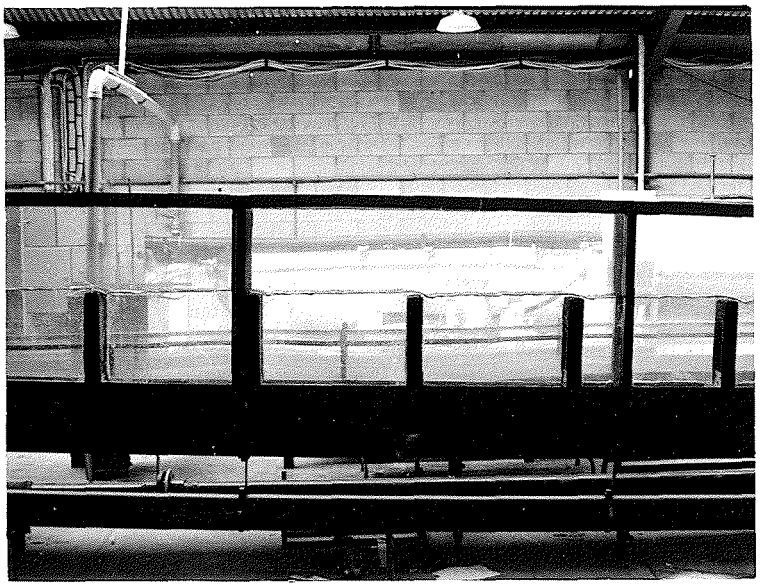

(a) Run 17 - Plunging nappe.

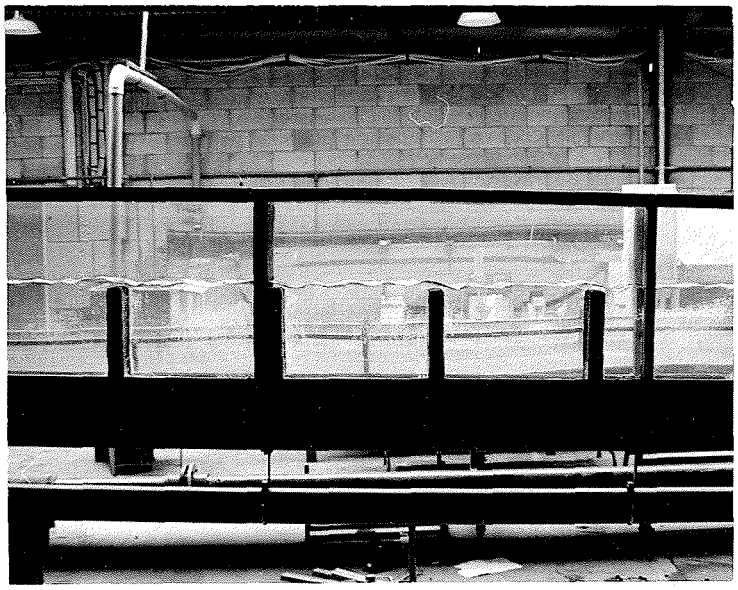

(b) Run 18 - Surface nappe.

Figure 5-5: Observed change in nappe profile.

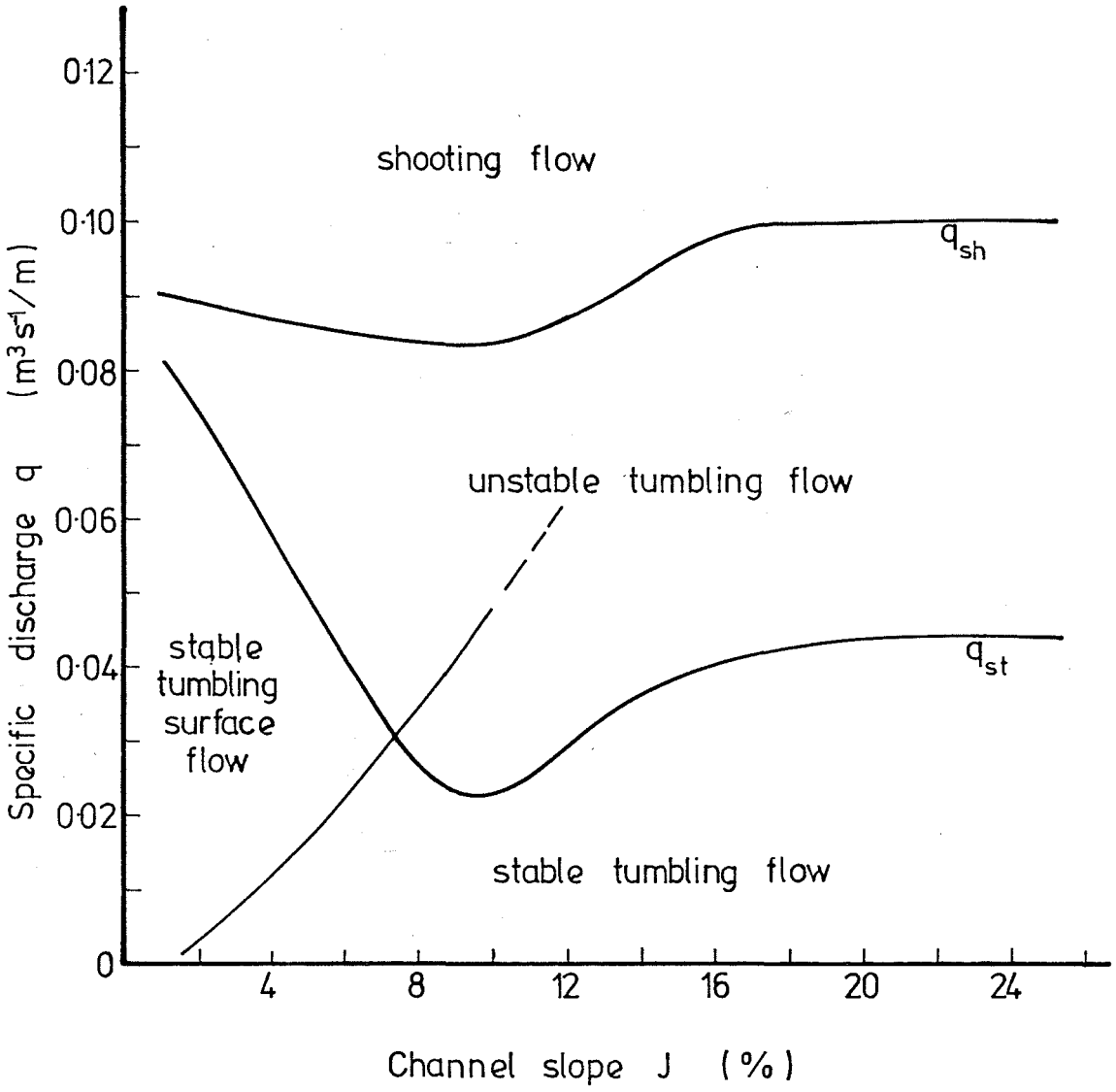

Figure 5-6: Existence regions of flow regimes with delineated sub-regime.

found (as did Foley and Vanoni, 1977) that antidune waves in a fluid of finite depth broke at this steepness value. Brater and King (1976, p 10-18) state that waves in shallow water usually break before their steepness reaches 0.142.

The standing waves store water, and when the waves break this stored water is released as a surge (Foley and Vanoni, 1977; Schumm et al., 1982). Thus, the unstable tumbling flow observed in the present tests at slope = 0.027 can be seen to be caused by the breaking of standing waves on reaching a theoretical maximum possible steepness of 0.142 (see Fig.5-3

However, it is obvious from fig. 5-3 that this is not the mechanism operating at slopes = 0.098, 0.172 and 0.248. Fig. 5-3 shows that unstable tumbling flow occurs at lower discharges than those at which the nappe profile would change from plunging to shooting. The following mechanism was found to be responsible for the observed unstable tumbling flow at these slopes.

In the stable tumbling flow (with a plunging nappe) regime, the sills act as critical flow structures. For this, the upstream head H is equal to $\frac{3}{2}$ y_c (Henderson, 1966). Further, the plunging jet in the model step-pool system may be considered to be bounded on its underside. That is, the jet may be considered to be running on a very steep slope (fig. 5-7).

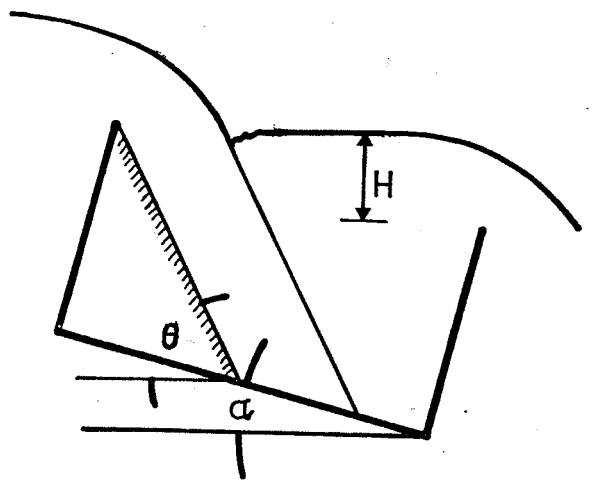

Figure 5-7: Assumed flow behaviour of plunging jet.

This assumption is reasonable since a submerged high velocity jet persists for a considerable distance (Moore, 1943). The situation can be considered as a variation of a hydraulic jump on a sloping surface. For a sloping surface with a horizontal apron, the following case occurs when the end of the hydraulic jump is at the boundary of the sloping surface and apron (fig. 5-8).

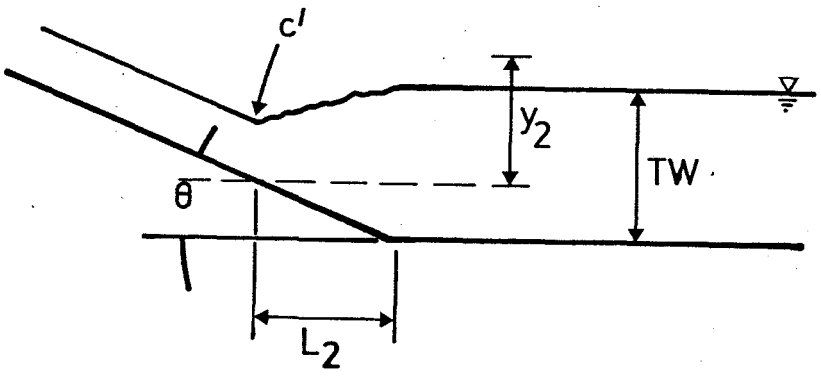

Figure 5-8: Hydraulic jump on a sloping surface.

In fig. 5-8, the following variables were introduced:

y_2 = conjugate depth for the hydraulic jump on a horizontal surface,

TW = tail water depth,

L_2 = length from change in slope to start of the hydraulic jump,

y_2 was calculated from the formula

$$F_1^2 = \frac{1}{2} \frac{y_2}{y_1} \left(\frac{y_2}{y_1} + 1 \right) \qquad \ldots 5\text{-}35$$

(Henderson, 1966)

The sills were seen to act as critical depth meters, and so y_1 was taken as the brink depth, i.e. $y_1 = 0.71\ y_c$, and thus $F_1 = 1.616$.

The above case occurs when a jump, initially formed on a horizontal apron, is made to encroach on the upstream slope by an increase in the tail water depth TW beyond y_2. For the case as shown in fig. 5-8, the length L_2 is given by the empirical equation

$$\frac{L_2}{y_2} = 0.82\ J_o^{-0.78} \qquad \text{... 5-36}$$

(After Henderson, 1966)

where $J_o = \tan \theta$.

Any further increases in TW are matched by exactly equal rises in the level of point c' (fig. 5-8), and thus by horizontal movements equal to those amounts divided by J_o.

Therefore,

$$\frac{L_2}{y_2} = 0.82\ J_o^{-0.78} + \frac{(\frac{TW}{y_2}) - 1.3}{J_o} \qquad \text{... 5-37}$$

(Henderson, 1966)

This can be solved for tail water depth thus:

$$TW = y_2\left[J_o\ (\frac{L_2}{y_2} - 0.82\ J_o^{-0.78}) + 1.3\right] \qquad \text{... 5-38}$$

The step-pool system that was used for the present tests imposed a tail water depth, since the sills acted as critical flow sections. In fact, it appears from a comparison of calculated and measured TW values (from tracings) that the geometry of the plunging jet was dictated by the tail water depth. This can be seen in fig. 5-9. This shows that for slope = 0.098, there was a continual decrease in θ with increasing discharge. However, this trend for slopes = 0.172 and 0.248 is distorted; θ tends to a limit value at a certain critical flow. The reason can be seen in the following development.

Bakhmeteff and Matzke (1938) measured the length of hydraulic jumps on slopes to be $6y_2$. However, fig. 15-21 of Chow (1959, p 428) shows that this corresponds to flow on a nearly horizontal surface at a Froude number of about 7.5. Jump length decreases with steeper slopes, and with decreasing Froude number (the curves are only estimated for $F < 4$).

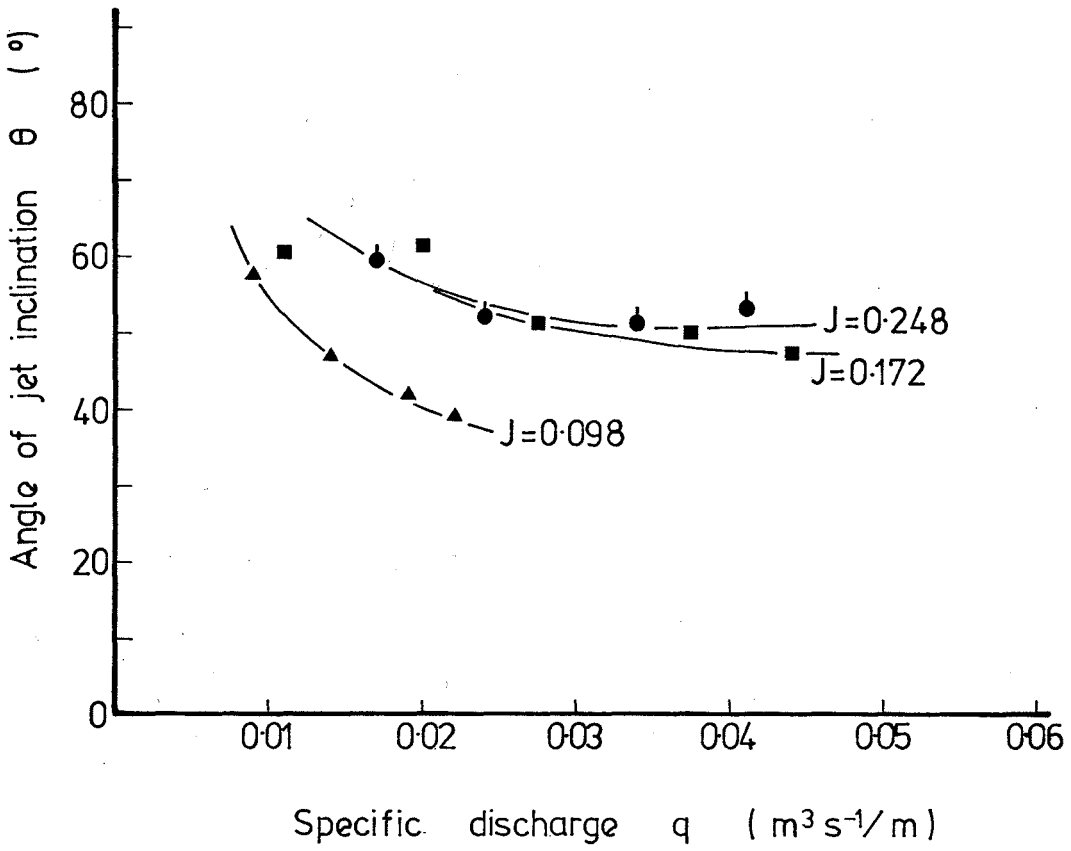

Figure 5-9: Angle of plunging jet for varying discharge.

Kindsvater (1944) measured the length of the jump as equal to the length of the surface roller (his tests were performed at slope = 0.167). He found that for Froude numbers of about 2, the length of the jump L_j was equal to about 3.5 y_2. For the tests reported herein, the value $\frac{L_j}{y_2}$ = 3.5 was used.

For low discharges, the flow situation was as follows (fig. 5-10).

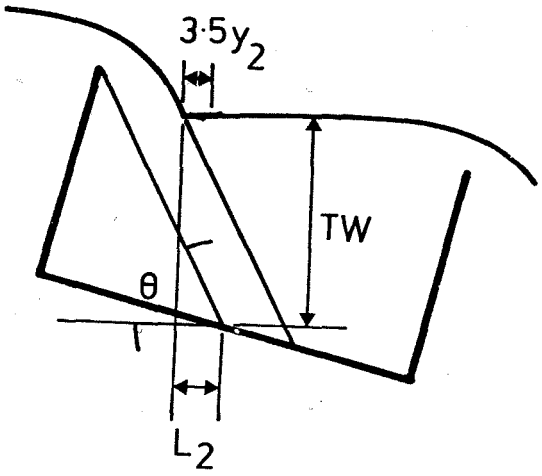

Figure 5-10: Flow situation at low discharges ($3.5y_2 < L_2$).

For slope = 0.098, 3.5 y_2 was never greater than L_2, and so θ decreased with increasing flow. However, TW appears to dictate θ and thus L_2. For slopes = 0.172 and 0.248, at a certain flow (= ϕ slope) tail water depth constrains the jet to an almost constant value of θ The flow rate at which this occurs corresponds to 3.5 y_2 = L_2. Beyond this flow rate, the flow situation was as shown in fig. 5-11.

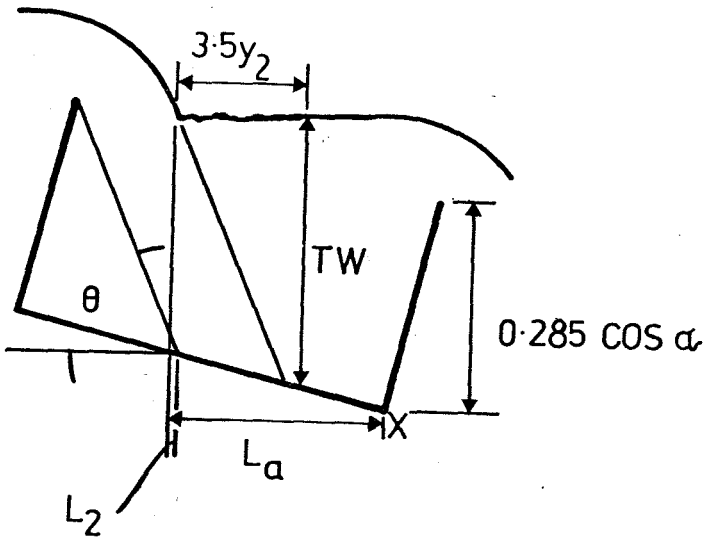

Figure 5-11: Flow situation with $3.5y_2 > L_2$

The situation shown in fig. 5-11 was still stable, but equation 5-38 no longer predicted TW accurately. It can be seen, however, that with increasing flow, TW can only increase to the value of 0.285 cos α + H. This will correspond to where the end of the jump (as given by $3.5y_2$) will be at X. Then the ratio $\frac{3.5y_2}{L_a}$ will equal 1, and TW will have reached the maximum depth possible under the physical constraints. Any further increases in flow rate pushes $3.5y_2$ further than X, and the TW depth required can only be accommodated by increasing H. But this results in H being greater than $\frac{3}{2} y_c$, and a flow instability is established. The new depth will correspond to $\frac{3}{2} y_c$ for a higher flow q', and so discharge will increase over the step. This now exceeds the incoming flow, and the pool is drained reducing H until $3.5 y_2 < L_a$ again. Pool outflow is now less than inflow, causing H to increase again. Thus the flow oscillates; the perturbations in flow are amplified as they pass through successive pools, and become roll waves.

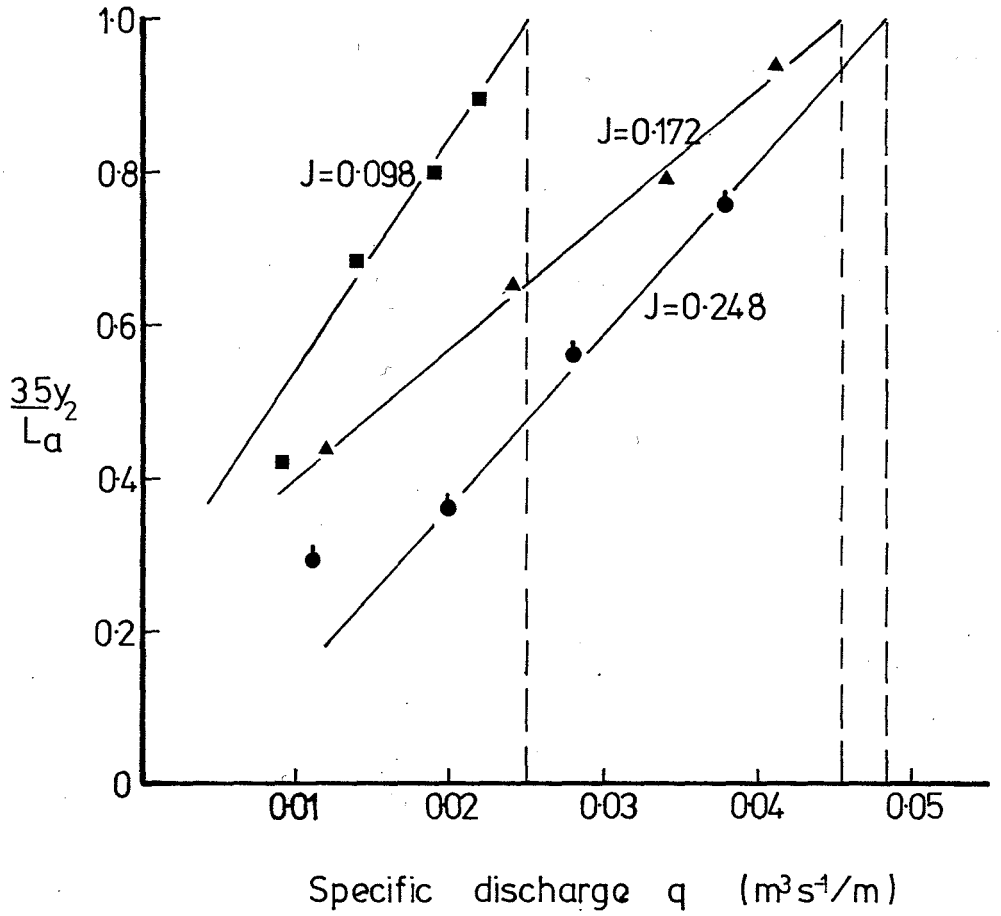

Figure 5-12: Plot of $\frac{3.5y_2}{L_a}$ vs specific discharge.

Fig. 5-12 shows the ratios $\frac{3.5y_2}{L_a}$ plotted against specific discharge for slopes of 0.098, 0.172 and 0.248. From the graph, the critical discharges for the onset of instability can be estimated. These are plotted in fig. 5-3, and show very close agreement with the observed critical discharges for the slopes mentioned above.

The description of the flow profile given by Al-Khafaji (1961) for the onset of unstable tumbling flow (section 5-2-3) corresponds to the profiles observed by the writer at the limit described above.

Comparison with Other Formative Mechanisms for Roll Waves

Roll waves caused by instability in uniform flow do not develop when resistance to flow exceeds a certain value (Rouse, 1938; Dressler, 1949). This value can be calculated using the Vedernikov number. (The following development is adapted from Ligget, 1975.) The Vedernikov number can be written

$$V = x' \gamma' F \qquad \ldots 5\text{-}29$$

where $\gamma' = 1 - R\frac{dP}{dA}$ ... 5-28

V is unity at the stability limit.

For a rectangular natural channel

$$A = Wh \ , \quad P = W + 2h$$

and $$\frac{dP}{dA} = \frac{2}{W} \ ,$$

$$R = \frac{Wh}{W + 2h}$$

assuming a sufficiently wide channel

$$R \simeq h$$

and $\frac{dP}{dA}$ tends to zero.

Therefore, for stability, $F < {}^{1}/_{x'}$ ... 5-39

For the Chézy relation, $x' = 0.5$. Further, the Chézy relation may be written

$$v_m = c\sqrt{gJh} \qquad \ldots 5\text{-}40$$

where Chézy friction factor $C = c\sqrt{g}$.

From equation 5-40

$$J = \frac{v_m^2}{gh}\ \frac{1}{c^2} \qquad \ldots 5\text{-}41$$

that is, $J = \frac{F^2}{c^2}$ (equivalent to equation 5-4).

From equation 5-39, for stability

$$c^2 \frac{1}{x'^2} > J \qquad \ldots 5\text{-}42$$

which gives $\frac{1}{c^2} \geqslant \frac{1}{4} J \qquad \ldots 5\text{-}43$

(this is also given by Thomas, 1940; Dressler, 1949; Mayer, 1959; and Albertson et al., 1960).

Therefore, using equation 5-3, the flow will be stable if

$$f \geqslant 2J \qquad \ldots 5\text{-}44$$

However, the channel in the present tests was not sufficiently wide to assume that $\frac{dP}{dA}$ tends to zero.

Instead, $\gamma' = (1 - \frac{2R}{b}) \qquad \ldots 5\text{-}45$

Therefore, for stability

$$1 \geqslant x' (1 - \frac{2R}{b}) F \qquad \ldots 5\text{-}46$$

or $F \leqslant \frac{1}{x' (1 - {}^{2R}/_{b})} \qquad \ldots 5\text{-}47$

Then $\frac{1}{x'^2 (1 - \frac{2R}{b})^2 c^2} \geqslant J \qquad \ldots 5\text{-}48$

and so the flow will be stable if

$$\frac{f}{\left(1 - \frac{2R}{b}\right)^2} \geq 2J \qquad \ldots 5\text{-}49$$

The critical $\frac{f}{\left(\frac{1-2R}{b}\right)^2}$ values for which the flow will become unstable are given in table 5-3. Also shown are the smallest values of $\frac{f}{\left(\frac{1-2R}{b}\right)^2}$ observed in the tests.

TABLE 5-3 CRITICAL VALUES OF $\frac{f}{\left(\frac{1-2R}{b}\right)^2}$ FOR STABILITY OF FLOW

J	2 J (critical)	Lowest $\frac{f}{\left(\frac{1-2R}{b}\right)^2}$
0.027	0.054	0.195
0.098	0.196	0.631
0.172	0.344	1.048
0.245	0.496	1.768

The lowest $\frac{f}{\left(\frac{1-2R}{b}\right)^2}$ values for the tests correspond to the highest flow rate at each slope. These values indicate that the flow is still stable. Clearly, the roll waves observed in the writer's tests are not the same as those investigated by Thomas (1940), Dressler (1959) Mayer (1959) and others. This is confirmed in that the roll waves of the writer, Mohanty (1959), Peterson and Mohanty (1960), Al-Khafaji (1961), Koo (1963, 1967) and Morris (1968) all broke backwards, in contrast to the roll waves resulting from instability in uniform flow which break forward.

The period of the roll waves investigated herein decreased with increasing q (fig. 5-13). The arrival of roll wave peaks at the downstream conductivity probe were clearly marked on the conductivity traces (see Appendix 1).

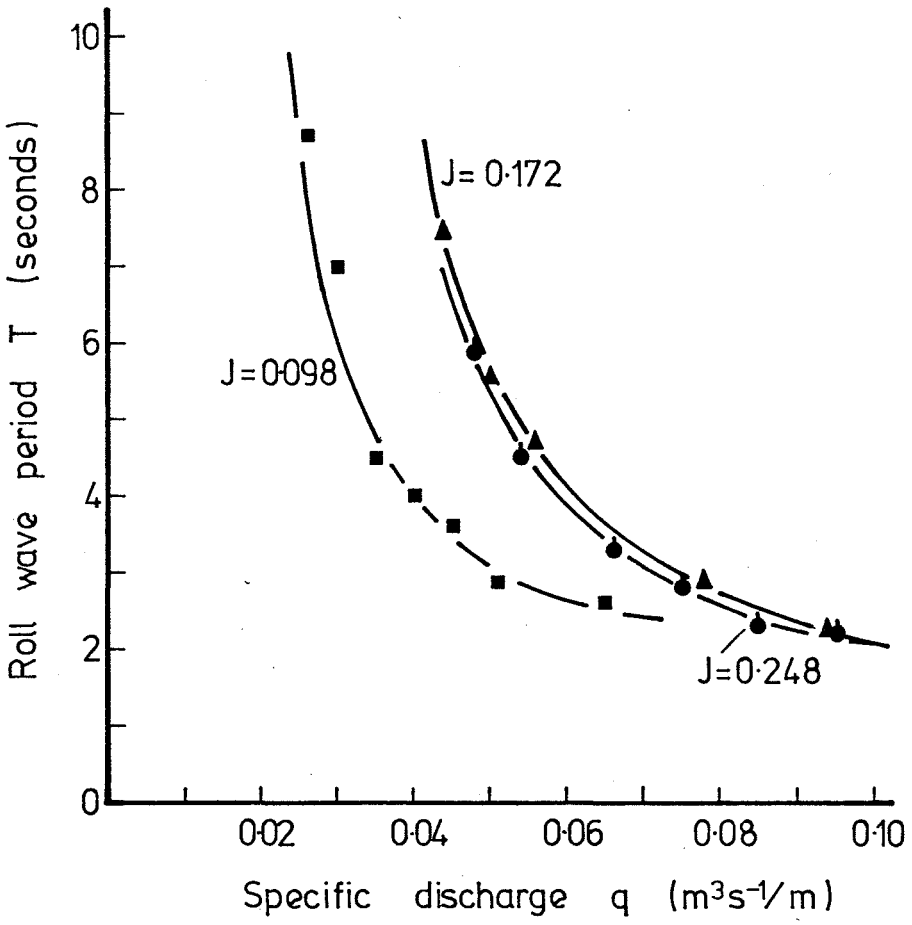

Figure 5-13: Period of roll waves plotted versus specific discharge.

The travelling waves of 5 to 8 feet amplitude observed by Holmes (1936) would be of the unstable uniform flow type, and the dry channel between wave crests is as predicted by Rouse (1938). However, the travelling waves observed by Knighton (1981) in a supraglacial meltwater stream are of the type obtained in the writers' tests. Knighton noted that the quasi-regular step and pool sections in the observed streams had associated supercritical and subcritical flow respectively. It is probable that, as melt flow increased, thermal degradation of the channel would have lagged, and the dimensions accorded the hydraulic jump by the pool would have become too small, resulting in the observed instability.

Morris (1968), citing Koo (1967), stated that unstable tumbling flow would occur when the Froude number corresponding to uniform flow in the channel upstream from the elements became greater than 1.35. The present results show that this is incorrect (see table 5-1).

Observations on the Rapid Flow Regime

Unstable tumbling flow resulted in an oscillating flow pattern (fig. 5-14(a) and (b)).

When a roll wave passed through a pool, a large eddy occurred between the steps. Rapid or shooting flow was defined for these tests to be when the flow situation shown in fig. 5-14(b) occurred for more than 50% of the time. The writer has so far been unable to quantitatively establish the nature of the mechanism causing the *release* of water to form each roll wave, and so is unable to predict the onset of rapid flow.

Morris (1968) asserts that in the rapid regime, the flow depth is less than critical, and therefore the flow is supercritical. Values of F given in table 5-1 (calculated using the average velocity, determined from the salt-velocity technique and adjusted for steep slope effects following Chow (1959, p 211)) indicate that this is not necessarily true. It may occur with smaller roughness elements. Measurements of depth to establish whether the depth was less than critical is considered dubious in the light of the extremely rough surface to the flow.

5.5.2 Average and Maximum Velocities

Average velocity versus specific discharge is plotted in fig. 5-15. The most striking feature of fig. 5-15 is that at low flow rates (up to about q_{st}, the flow at which unstable flow begins), for a specified flow rate there is practically no difference in average velocity values for the four channel slopes. For higher flow rates, the average velocity values

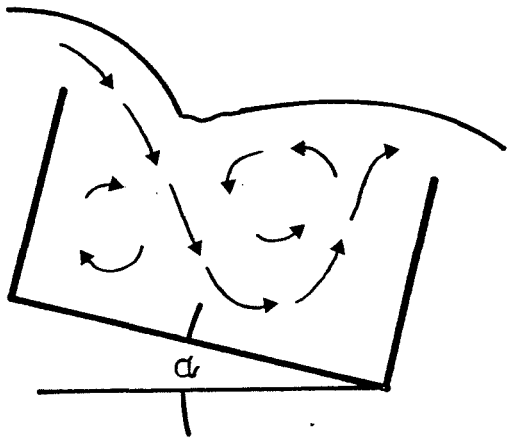

(a) Plunging jet

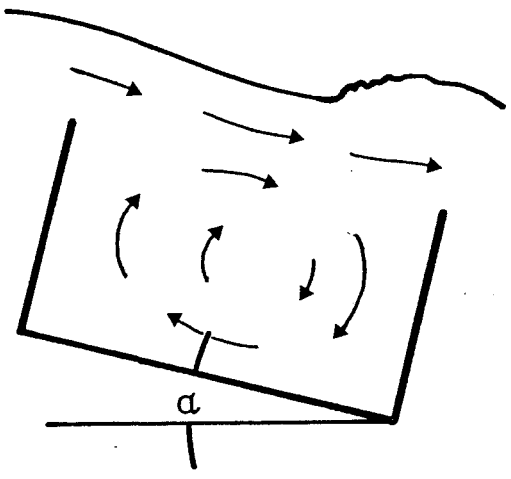

(b) Roll wave passing through pool

Figure 5-14: Oscillating flow pattern with unstable tumbling flow.

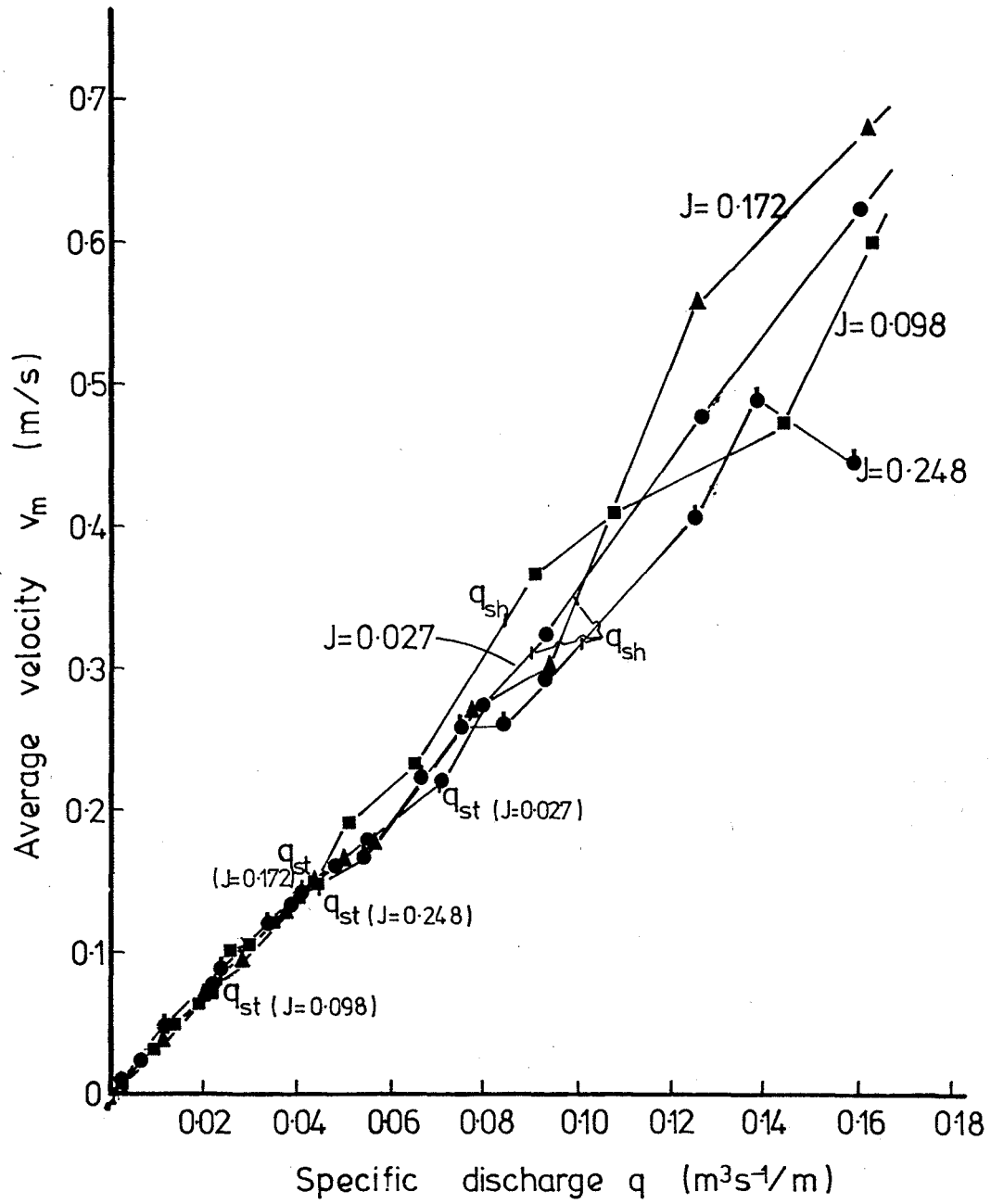

Figure 5-15: Plot of average velocity versus specific discharge.

show considerable scatter. If the average velocities for slope = 0.027 are ignored, a trend appears which is repeated in fig. 5-16. At higher discharges, average and maximum velocities initially increase with increasing slope as the gravity component of the motivating force increases. However, as slope increases still further, the flow appears to experience greater resistance, and average and maximum velocities decrease.

From fig. 5-16, it can be seen that maximum velocities decrease with increasing channel slope at discharges ranging into the unstable tumbling regime. The effect of the surface nappe regime for slope = 0.027 is clearly seen in its much higher maximum velocities over these discharges. However, at slope = 0.027, there is only a gradual increase in maximum velocity through the unstable and rapid regimes. For slopes = 0.098, 0.172 and 0.248, there appear to be limiting flows within the unstable tumbling regime beyond which maximum velocities suddenly increase. For higher discharges, the trend with slope is as described above.

Experience indicates that sediment discharge is strongly correlated with velocity (Vanoni, 1975, p.177). Bagnold (1960) correlated sediment discharge with stream power (per unit bed area), $\tau_o v_m$, the product of bed shear stress and mean velocity. In his 1966 paper, Bagnold equated the rate of doing work in transporting sediment with the available power times an efficiency (Graf, 1971, p.209). Yang (1972, 1976) and Yang *et al.* (1976) defined unit stream power as stream power per unit weight of water, Jv_m. He claimed this quantity to be more highly correlated with sediment transport than any other.

While mean velocity correlates with an average measure of the ability of a stream to transport sediment, maximum velocity gives an indication of the maximum size of sediment a stream may be capable of moving. The potential of a stream for eroding and transporting sediment may be termed its erosive potential. Thus, average and maximum velocities may be considered to indicate the erosive potential of a stream.

In an artificial step-pool channel, average velocity values show that the erosive potential would increase only mildly with increasing flow rate. Maximum velocities, however, show that for the higher discharges in the unstable tumbling regime, there is a marked increase in erosive potential.

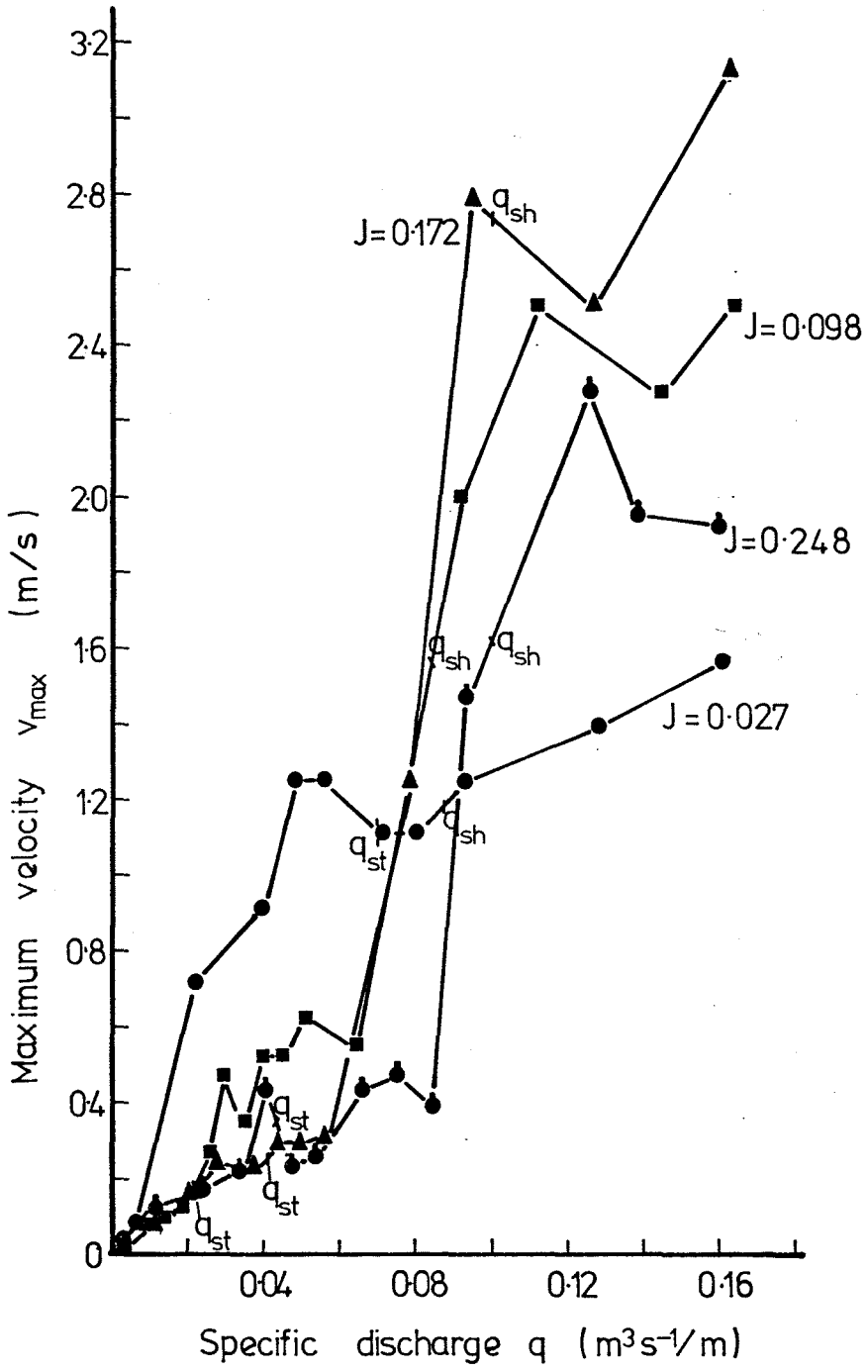

Figure 5-16: Plot of maximum velocity versus specific discharge.

5.5.3 Resistance to Flow

A plot of Darcy-Weisbach friction factor f versus specific discharge is shown in fig. 5-17. It can be seen that f initially diminishes rapidly with flow, but at higher discharges (in the rapid regime) approaches an essentially constant value. f values corresponding to flows in the unstable tumbling regime provide a transition between these two trends.

The f values are extremely high (much higher than those of various authors summarised by Scheuerlein (1973)). Beven et al. (1979) evaluated an f value of 1328 for a mountain stream, so the present values seem reasonable. Resistance to flow is a measure of the rate of fluid energy dissipation, and considerable fluid energy is known to be dissipated in the pools of step-pool systems. The calculated f values reflect this energy dissipation . It is for this reason that Bathurst (1978) asserted that the large-scale roughness channels for which he derived his power resistance laws are functionally different from step-pool streams. Thus, the power resistance laws of Bathurst (1978) and Bathurst et al. (1981) are inapplicable to step-pool systems.

An analysis was attempted, however, to see if the roughness could be predicted by an empirical formula similar in form to other resistance laws.

From tracings of projected photographs, an average depth of flow h' from the flume bottom was obtained. Depending on flow regime, the hydraulic radius R obtained from measurements of q and v_m differed from h'. Thus, the actual roughness height experienced by the flow is less than k = 0.285 m, and may be designated by k', where

$$k' = \left[k - (h' - R) \right] \qquad \ldots 5\text{-}50$$

The relevant values are listed in table 5-4.

The difference noted between R and h' reflects the presence of dead zones in the flow. Plots of $\sqrt{\frac{8}{f}}$ versus $\log \left(\frac{R}{k'} \right)$ (see fig. 5-18) indicated that a resistance law could be derived of the form

$$\sqrt{\frac{8}{f}} = 2\sqrt{8}\,(A) \log \left(\frac{R}{k'} \right) + B \qquad \ldots 5\text{-}51$$

where A, B = ϕ (energy slope J'; J' = sin α).

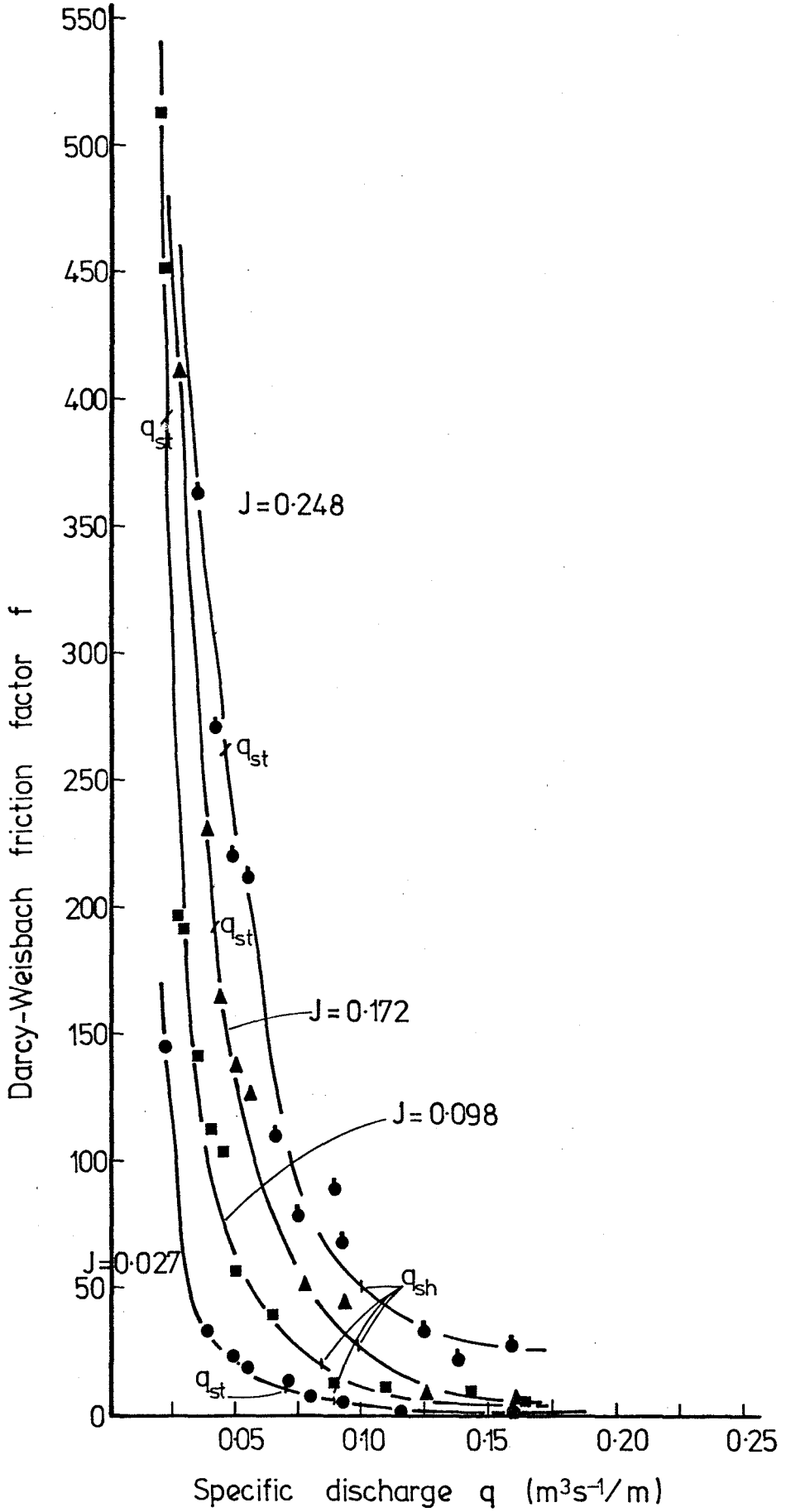

Figure 5-17: Plot of Darcy-Weisbach friction factor f versus specific discharge.

TABLE 5-4 VALUES OF AVERAGE DEPTH OF FLOW FROM FLUME BOTTOM h', AND ACTUAL ROUGHNESS HEIGHT k'

Run Number	h'	k'		Run Number	h'	k'		Run Number	h'	k'
1	0.265	0.390		17	0.283	0.265		56	0.302	0.270
2	0.289	0.277		18	0.294	0.270		57	0.335	0.246
3	0.295	0.274		19	0.311	0.256		58	0.359	0.236
4	0.302	0.270		20	0.323	0.249		59	0.357	0.212
5	0.301	0.286		21	0.332	0.250		60	0.349	0.245
6	0.301	0.244		22	0.336	0.251		61	0.383	0.123
7	0.304	0.259		23	0.343	0.257				
8	0.297	0.269		24	0.355	0.212		76	0.260	0.272
9	0.308	0.261		25	0.376	0.186		77	0.284	0.267
10	0.314	0.271		26	0.384	0.151		78	0.297	0.267
11	0.315	0.236		27	0.397	0.124		79	0.309	0.265
12	0.332	0.231						80	0.340	0.245
13	0.351	0.200		52	0.295	0.272		83	0.344	0.227
14	0.339	0.189		53	0.303	-		86	0.374	0.216
15	0.361	0.223		54	0.315	0.257		88	0.356	0.282
16	0.363	0.187		55	0.314	0.263				

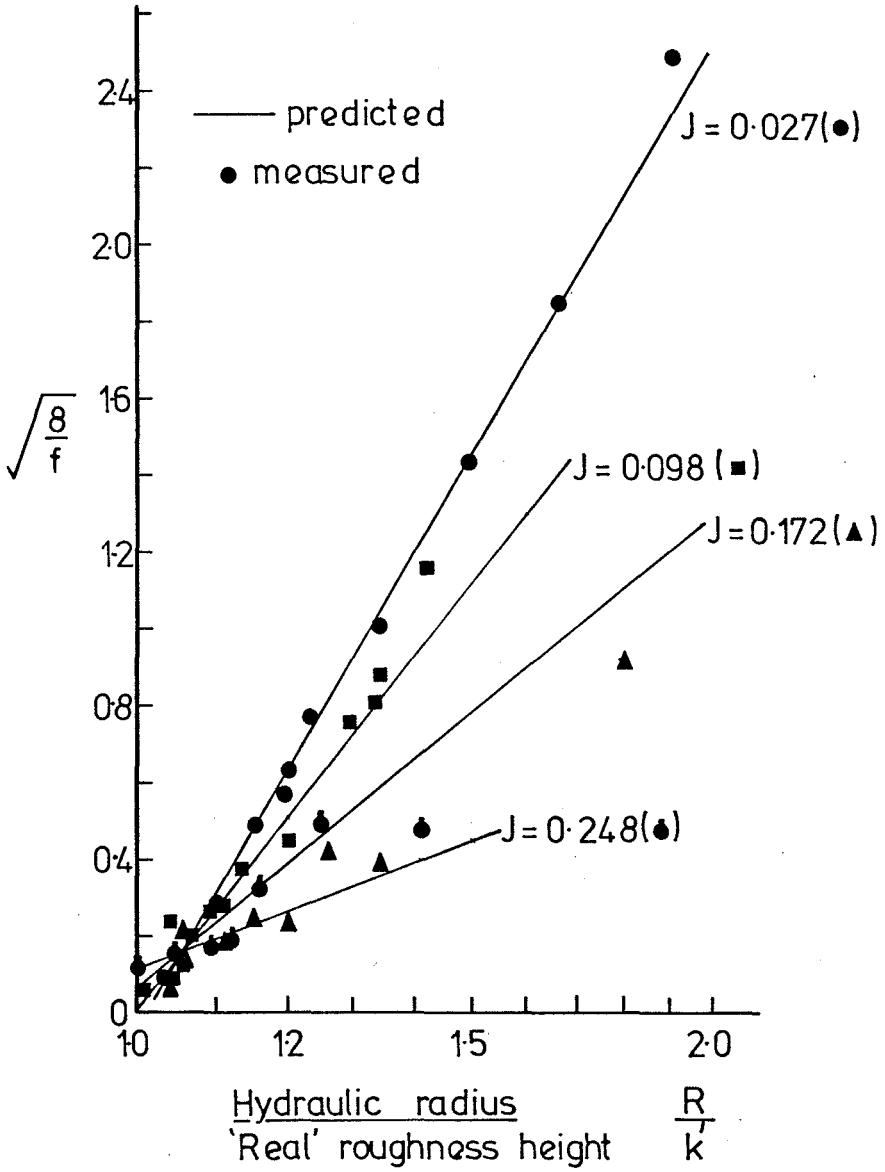

Figure 5-18: Plot of $\sqrt{\frac{8}{f}}$ versus log $\left(\frac{R}{k'}\right)$.

This was evaluated to be

$$\sqrt{\frac{8}{f}} = 5.657\ (1.676 - 5.715\ J')\ \log\ (\frac{R}{k'})$$

$$+\ (0.630\ J' - 0.057) \qquad ...5\text{-}52$$

That is

$$\sqrt{\frac{8}{f}} = 5.657\ A\ \log\ (\frac{R}{k'}) + B \qquad ...5\text{-}53$$

where $A = (1.676 - 5.715\ J')$

and $B = (0.630\ J' - 0.057)$

B may prove to be a function of λ. λ was not varied in the tests reported herein, and so could not be treated as an independent variable.

The predicted values are contrasted with the calculated values in fig. 5-18.

It is of interest that the data for shooting flow indicate that the active flow depth still extended considerably below the crests of the roughness elements. The interaction of the main flow with the large eddy (fig. 5-14(b)) explains why for rapid flow, F never exceeded unity. Thus, rapid flow need not be supercritical, despite Morris' (1968) assertion to the contrary.

5.6 CONCLUSIONS

The main conclusions for the tests of clear water flow through an artificial step-pool system are as follows:

(1) Three flow regimes were observed, namely

(a) stable tumbling flow,

(b) unstable tumbling flow,

(c) rapid or shooting flow.

(2) At low slopes, flow in the stable tumbling regime may be in the surface nappe form, rather than the plunging nappe form which characterises stable tumbling flow at higher slopes. Further, the unstable flow developing from the surface nappe flow is caused by the breaking of standing waves at a steepness of about 0.142, as predicted by theory.

(3) Unstable tumbling flow (at slopes where the stable tumbling flow is of the plunging nappe form) is caused by constraints on the full development of the submerged hydraulic jump imposed by the physical boundaries of the step-pool system. The onset of unstable tumbling flow can be predicted on this basis.

(4) Unstable flow in step-pool systems is a different phenomenon to the instabilities occurring in uniform flow at Froude numbers of approximately 1.6 or greater. This is further supported by the observation that step-pool systems exceed the roughness limits that are a theoretical upper bound to the development of uniform flow instabilities.

(5) Over the stable tumbling flow range, average velocity increases with increasing discharge but is independent of slope. Some slope effects are apparent for discharges in the rapid flow regime.

(6) An inverse relation between maximum velocity and slope occurs over the range of discharges corresponding to the lower portion of the unstable tumbling regime. There is a sudden increase in maximum velocity with discharge over the latter portion of the unstable tumbling regime. For rapid flow, the same slope effects are apparent as for average velocity.

(7) The trends in average and maximum velocities suggest that an artificial step-pool channel may suddenly increase its potential erosivity over the upper portion of the range of discharges producing unstable tumbling flow.

(8) Resistance to flow decreases with increasing discharge until an essentially constant value (which is a function of slope of the channel) is attained for rapid flows.

(9) The resistance to flow can be empirically predicted using a variation of the traditional logarithmic resistance law. Energy slope of the channel is an important variable in the derived function.

CHAPTER SIX

CLEAR WATER SCOUR IN A STEP-POOL SYSTEM

6.1 INTRODUCTION

It was established in the preceding chapter that step-pool systems can be modelled by a succession of discrete weirs. Flow in such a system was the subject of Chapter 5. While the results obtained with discrete weirs are indicative of the behaviour of a natural step-pool channel, this model can be made much more realistic by the inclusion of gravel between the weirs or steps. This was done, and the model behaviour investigated.

The objectives of this clear water scour series of tests were as follows:

(1) To study flow behaviour through an idealised step-pool system containing gravel in order to understand the behaviour of step-pool systems in the field. Average velocities were to be used to compute resistance to flow and energy dissipation.

(2) To investigate the phenomenon of scour in a step-pool system.

and (3) To ascertain whether roll waves are influenced by the presence of gravel, and to define the conditions under which roll waves might occur in field step-pool systems.

A literature review on the subject of scour follows to facilitate discussion of scour observed in the tests.

6.2 THE MECHANICS OF SCOUR

Rouse (1939) noted that scour, like any general problem in unsteady, non-uniform flow, depends on geometric, flow, fluid and sediment characteristics. He considered the relative motion between sediment and fluid to be related to the normal settling velocity of individual grains. This assumption was assimilated into the work of other authors, e.g. Johnson (1950), Thomas (1953) and Doddiah et al (1953). Rouses' (1939)

experiments involved an impinging jet. Schoklitsch (1935) noted the influence of jet form on scour.

Rouse (1939) derived the equation

$$\frac{S}{a} = \log \left[\frac{w_m t}{a} \left(\frac{w_m}{v} \right)^3 \right]^{\left(\frac{v}{w_m} - 1 \right)} \qquad \ldots 6.1$$

where S = depth of scour below original bed level

a = height of dune above original bed level

w_m = fall velocity of sediment

v = velocity of jet

and t = time.

It is implicit in this equation that the rate of scour is an exponential function of time. Consequently, for uniform material where grading effects are not present, no equilibrium of scour can be expected, other than that imposed by physical boundaries. This concept of an ever increasing scour with time due to exponential growth was echoed by Johnson (1950), Thomas (1953), and Doddiah et al (1953). These authors also emphasised the influence of the depth of water over the scouring bed on the final scour hole dimensions.

Johnson (1950) noted that, with high tail water, a dune built up above the original bed just downstream of the scour hole and restricted growth of the scour hole by preventing the escape of suspended grains. With low tail water, the dune was always removed by the flow, and no restriction on escape of the grains occurred. Schoppmann (1975) measured turbulence intensities in the scour zone. He showed that large eddies generated in the shear zone of the scour hole were responsible for transport of suspended grains out of the scour hole.

Thomas (1953) investigated scour at the base of a free overfall (fig. 6-1).

A comparison of his results with the equation of Schoklitsch (1935) (equation 6.3) showed only moderate agreement. Thomas found that the depth of scour increased rapidly with increasing discharge, and more slowly with increasing height of fall. Both of these trends are indicated by equation 6.3.

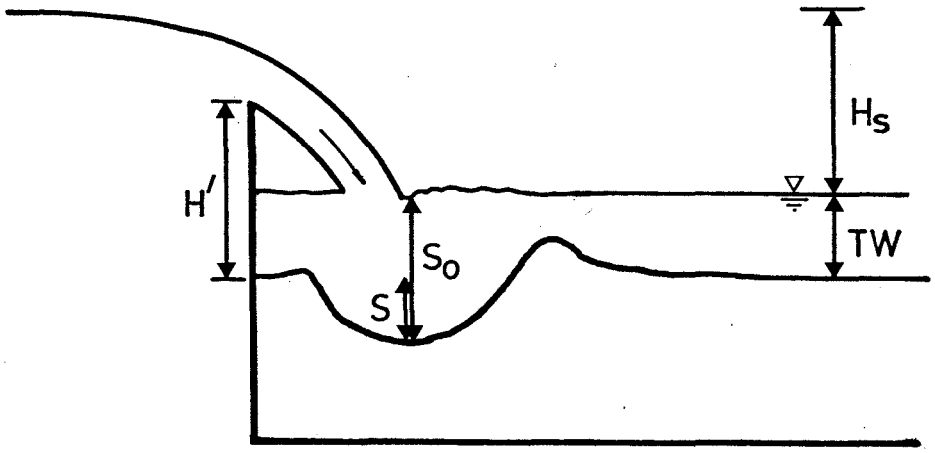

Figure 6-1: Scour at the base of a free overfall.

Doddiah et al. (1953) demonstrated that for scour from vertical jets, scour hole development was unaffected by whether the jet was hollow or solid (for a given area and velocity of jet). Further, for both scour by vertical jets and scour at the base of a free overfall, scour increased with increasing depth of water over an erodible bed until the depth reached a critical value. Any further increase in depth diminished the scour, probably indicating the high tail water condition noted by Johnson (1950).

Laursen (1952) defined the rate of scour as the difference between the rate of supply and the rate of removal of sediment from the scouring zone. This can be represented by

$$\frac{d[\phi(B)]}{dt} = Q_{sc}(B) - Q_s \qquad \ldots 6.2$$

where B = boundary shape

$\phi(B)$ = a function of

$Q_{sc}(B)$ = transport capacity of the flow

and Q_s = rate of supply of sediment.

Further, he reasoned that the enlargement of the flow section would result in a reduction of velocity along the scour zone boundary with a consequent reduction in capacity for transport. The rate of scour then decreases as the difference between the flow's capacity for transport and the rate of sediment supply decreases. Implicit in the foregoing statement is the notion of a limiting extent of scour. The rate of scour will equal zero when the transport capacity is equal to the supply rate. Laursen then showed that this limit would be approached asymptotically. This concept of a limiting extent to scour was subsequently assimilated by other authors e.g. Li (1955), Novák (1961), Johnson (1967), and Vanoni (1975). Rajaratnam and Beltaos (1977) assert that scour development breaks with the logarithmic relation and begins to approach the limit asymptotically when the scour depth is three quarters of its final value. By plotting dimensionless coordinates, Laursen (1952) also established that scour profiles exhibited similarity during development.

Novák (1955) listed some equations for scour downstream of an overfall. They were

$$S = \frac{4.75}{D_{90}^{0.32}} H_s^{0.2} q^{0.57} - TW \qquad ...6.3$$

(after Schoklitsch)

$$S = \frac{3.68}{D_{90}^{0.42}} H'^{0.225} q^{0.54} - TW \qquad ...6.4$$

(after Veronese)

$$S = 6 H'^{0.25} q^{0.5} \left(\frac{TW}{D_{90}}\right)^{0.33} - TW \qquad ...6.5$$

(after Jaeger)

and

$$S = \frac{22.88}{D_{90}^{0.4}} H'^{0.5} q^{0.6} - TW \qquad ...6.6$$

(after Eggenberger-Müller)

where S = depth of scour

H_s = difference in height of water surface above and below the hydraulic structure

H' = fall (see fig. 6-1)

q = specific discharge

D_{90} = sediment diameter; than which 90% of grains are smaller

and TW = tail water depth.

Novák (1955) investigated the effect of stilling basin design on the depth of scour, and found that an effective design decreased scour to about 50% of that predicted by equations 6.3, 6.4, and 6.5, and to about 12% of that predicted by equation 6.6. The difference between equations 6.3, 6.4 and 6.5, and 6.6 is that scour depth S is defined for different limits. The equations of Schoklitsch, Veronese, and Jaeger give the scour value for a dynamic limit, where material is still in suspension in the scour zone. The equation of Eggenberger-Müller, however, defines the ultimate static limit, where the dune has been removed and all sediment in suspension has escaped from the scour zone (Johnson, 1967). Thus the Eggenberger-Müller formula can be considered to be a low tail water equation (Johnson, 1950), and the other three to be high tail water equations.

Novák (1961) noted that the passage of bedload strongly influences the formation of scour downstream of a stilling basin. He found that with no bedload, the scour depth approaches its final value asymptotically, while for the bedload case the scour depth reaches a final value in a lesser time which decreases as bedload transport rate increases.

Carstens (1966) provided a radical departure from conventional scour analysis in attempting to unify different scour situations. He reasoned that a particle's motion would depend on whether or not the vector sum of lift and drag forces was of greater magnitude than the particle's submerged weight. A force ratio was defined as $\frac{\Sigma F_m}{\Sigma F_r}$

where ΣF_m = sum of forces producing motion

and ΣF_r = sum of forces resisting motion.

Further

$$\frac{\Sigma F_m}{\Sigma F_r} = \frac{k_1 \sqrt{C_L^2 + C_D^2}}{k_2} \frac{v^2}{(s-1) g D_m} \qquad ...6.7$$

where k_1, k_2 = constants

C_L = lift coefficient

C_D = drag coefficient

v = flow velocity

$(s-1)$ = excess solids density ratio

and D_m = mean diameter of sediment.

The sediment number N_s was then defined as

$$N_s = \frac{v}{\sqrt{(s-1) g D_m}} \qquad ...6.8$$

so that $\frac{\Sigma F_m}{\Sigma F_r} = \phi$ (sediment grain geometry) N_s^2.

Assuming that sediment transport is a function of the force ratio, Carstens hypothesised a dimensionless form of sediment transport

$$\frac{Q_s}{v\ B\ D_m} = \phi\left[(N_s^2 - N_{sc}^2), \frac{S}{L}, \text{ disturbance geometry, sediment grain geometry, ...}\right] \quad ...6.9$$

where Q_s = sediment transport rate

B = width of scour hole

N_{sc} = lowest value of sediment number for which scour will occur

v = reference flow velocity

L = a characteristic dimension of the obstruction

and S = scour depth.

This equation was applied to a variety of situations, all of which yielded the basic form

$$\frac{Q_s}{(N_s^2 - N_{sc}^2)^{5/2}\ v\ B\ D_m} = \phi[\text{disturbance geometry}, \frac{S}{L}, \text{ sediment grain geometry...}] \quad ...6.10$$

for sediment transport rate; and

$$\frac{S}{L} = \left[(N_s^2 - N_{sc}^2)^{5/2}\right]\left(\frac{Dg}{L}\right)\left(\frac{vt}{L}\right)\phi[\text{disturbance geometry, sediment grain geometry,...}] \quad ...6.11$$

for scour depth.

Raudkivi and Ettema (1977) investigated the effect of sediment grading on local scour, finding that armouring due to sediment grading reduced scour. The maximum depth of clear water scour was seen to be a function of the standard deviation of the grain size distribution of the bed material.

6.2.1 Scour in a Step-Pool Channel

In a channel with a series of steps or sills, the length between sills is critical for formation of the scour hole (Apmann and Blinco, 1969). If L, the length between sills, is too short, the point of maximum scour depth moves closer to the downstream sill (Volkart, 1972; Volkart et al, 1973). If L is longer than some critical length L_c, the scour hole dimensions will be independent of length L (Apmann and Blinco, 1969). This points to an error in Volkart's (1972) analysis,

in which he evaluated an equation for depth of scour S (see fig. 6-2).

$$S = 1.25 \frac{q^{0.5} J^{0.5} L^{0.667}}{D_{90}^{0.42}} \frac{\gamma_w}{\gamma_s'' g^{0.25}} \qquad ...6.12$$

where q = specific discharge

J = slope of plane of top of sills

L = length between sills

γ_w = specific weight of water

γ_s'' = submerged specific weight of sediment.

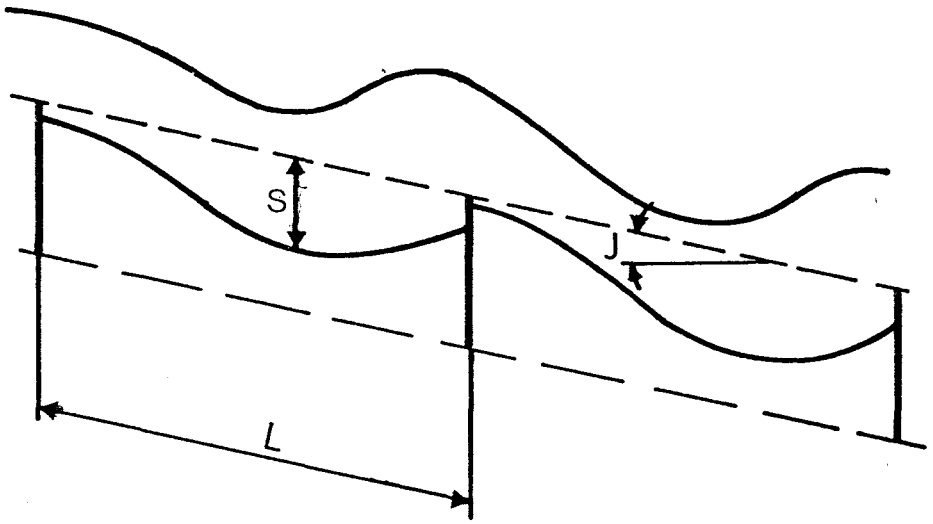

Figure 6-2: Definition diagram for Volkart's scour tests (After Volkart, 1972).

For scour uninfluenced by the downstream sill, S is independent of L. For scour influenced by the downstream sill, a complex distortion of the scour field occurs (see section 6.5.1) and therefore equation 6.12 is not realistic. The factor $L^{0.667}$ probably reflects the influence

of D_{90} via the dimensionless ratio $\frac{L}{D_{90}}$ that Volkart used in his analysis. Apmann and Blinco (1969) noted that scour also occurs both upstream and downstream of sills (fig. 6-3).

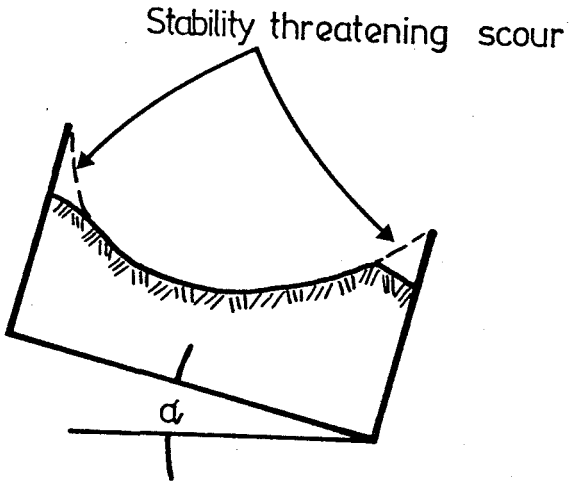

Figure 6-3: Scour upstream and downstream of sills.

Schmid (1972, 1973) began his analysis with the same 'bedload-balance' approach as Laursen (1952). He then noted that an equation for bedload transport in scour development could be developed as an analogy to the bedload transport formula of Meyer-Peter and Müller (1948). The Meyer-Peter and Müller formula may be written as

$$\frac{q^{0.667}_J}{D_g\, g^{0.33}} = a + b\,\frac{q_s{}''^{0.667}}{\gamma_s{}''^{0.667}\, D_g\, g^{0.33}} \qquad \ldots 6.13$$

where $q_s{}''$ = specific submerged bedload transport rate

$\gamma_s{}''$ = submerged specific weight of sediment

J = slope

and D_g = characteristic particle size of the bedload material.

i.e. a dimensionless transport quantity equals a dimensionless limiting value, a plus a dimensionless bedload transport quantity. Schmid (1972, 1973) evaluated a dimensionless transport quantity for scour

$$\frac{q^{0.667} H_s^{0.333}}{g^{0.333} D_{90}^{0.333}} \frac{1}{S_{omax}} = c_1 \qquad ...6.14$$

where c_1 = a dimensionless limiting value.

For $S_o < S_{omax}$, a dimensionless bedload quantity was added, resulting in the general equation

$$\frac{q^{0.667} H_s^{0.333}}{g^{0.333} D_{90}^{0.333}} \frac{1}{S_o} = c_1 + c_2 \left(\frac{q_s}{D_{90}^{1.5} g^{0.5}} \right)^{0.333} \qquad ...6.15$$

Equation 6.15, considering Schmid's value for c_1 of $c_1 = 0.521$, represents a dynamic limit of scour (Johnson, 1967).

6.3 TESTS

In this series of tests, 4 mm diameter gravel filled the spaces between the steps of the laboratory channel. Tests were performed at slopes of 0.027, 0.098, 0.172 and 0.248. At each slope, a series of flows was passed down an initially plane bed. For each flow rate, when bedload transport had ceased (i.e. the scour between steps had reached equilibrium), the average and maximum velocities through the scour system were measured using the salt velocity technique. Photographs were also taken to allow the dimensions and shape of the scour hole to be measured.

6.4 RESULTS

The results for these tests are listed in table 6-1.

6.4.1 Flow Regime

With gravel between the steps, distinct flow regimes were observed. These were stable tumbling, unstable tumbling, and shooting flow. They are

TABLE 6-1 EXPERIMENTAL RESULTS FOR CLEAR WATER SCOUR TESTS

Run No.	J	q (m^3s^{-1}/m)	v_m (m/s)	v_{max} (m/s)	h (m)	R (m)	τ_{m_2} (N/m^2)	f	F	S (m)	X (m)	S_o (m)	% Scour
1	0.027	0.056	0.462	0.558	0.121	0.155	30.32	1.14	0.516	0.073	0.231	0.165	18.81
2	0.027	0.072	0.517	0.558	0.140	0.131	34.74	1.04	0.537	0.072	0.232	0.189	18.22
3	0.027	0.119	0.662	0.914	0.180	0.164	43.43	0.79	0.606	0.074	0.254	0.196	18.99
4	0.027	0.148	0.717	0.838	0.207	0.186	49.36	0.77	0.612	0.071	0.250	0.211	18.38
5	0.027	0.184	0.855	0.897	0.215	0.188	49.69	0.54	0.716	0.075	0.279	0.235	18.89
6	0.027	0.030	0.412	0.555	0.072	0.069	18.19	0.86	0.596	0.027	0.103	0.045	3.26
7	0.027	0.044	0.489	0.546	0.091	0.086	22.69	0.76	0.630	0.049	0.181	0.079	10.46
8	0.098	0.021	0.216	0.287	0.096	0.095	92.17	15.80	0.289	0.142	0.175	0.150	27.87
9	0.098	0.008	0.166	0.251	0.047	0.047	45.22	13.13	0.244	0.071	0.082	0.069	6.30
10	0.098	0.015	0.204	0.287	0.073	0.073	70.12	13.48	0.313	0.122	0.133	0.117	19.14
11	0.098	0.034	0.235	0.305	0.145	0.144	139.10	20.15	0.256	0.166	0.210	0.198	41.37
12	0.098	0.043	0.274	0.419	0.158	0.157	151.30	16.12	0.286	0.154	0.220	0.195	39.92
13	0.098	0.066	0.418	0.513	0.157	0.154	149.22	6.83	0.437	0.129	0.237	0.177	35.85
14	0.098	0.098	0.578	0.785	0.169	0.165	159.07	3.81	0.583	0.135	0.431	0.201	35.82
15	0.098	0.164	0.943	1.142	0.174	0.165	159.46	1.43	0.937	0.148	0.467	0.270	29.67
16	0.172	0.009	0.144	0.234	0.063	0.063	104.51	40.32	0.251	0.121	0.087	0.092	16.24
17	0.172	0.016	0.168	0.205	0.098	0.098	162.48	46.05	0.235	0.174	0.122	0.162	29.87
18	0.172	0.038	0.200	0.262	0.189	0.188	313.09	62.62	0.201	0.225	0.210	0.241	56.81
19	0.172	0.051	0.219	0.322	0.233	0.232	385.77	64.35	0.198	-	-	-	-

TABLE 6-1 CONTD.

Run No.	J	q ($m^3 s^{-1}/m$)	v_m (m/s)	v_{max} (m/s)	h (m)	R (m)	τ_{m_2} (N/m^2)	f	F	S (m)	X (m)	S_o (m)	% Scour
20	0.172	0.086	0.471	0.558	0.182	0.180	298.81	10.78	0.482	0.215	0.464	0.313	58.26
21	0.172	0.181	0.917	1.570	0.187	0.181	300.94	2.86	0.927	0.194	0.464	0.320	40.71
22	0.172	0.133	0.755	1.005	0.177	0.173	287.11	4.03	0.784	0.162	0.467	0.278	36.49
23	0.248	0.011	0.121	0.193	0.090	0.090	211.51	115.57	0.183	0.181	0.118	-	19.21
24	0.248	0.025	0.170	0.258	0.145	0.145	341.61	94.56	0.202	0.229	0.154	-	50.53
25	0.248	0.054	0.240	0.437	0.220	0.219	516.85	71.79	0.231	0.222	0.248	-	67.52
26	0.248	0.075	0.348	0.679	0.214	0.213	502.16	33.17	0.340	0.232	0.467	-	66.63
27	0.248	0.119	0.690	1.092	0.172	0.169	399.51	6.71	0.752	0.184	0.467	-	49.01
28	0.248	0.169	0.835	1.795	0.202	0.198	466.81	5.36	0.840	0.201	0.467	-	46.33
29	0.027	0.013	0.345	0.670	0.039	0.038	9.96	0.67	0.679	-	-	-	-
30	0.027	0.033	0.460	0.773	0.071	0.067	17.80	0.67	0.671	-	-	-	-
31	0.027	0.046	0.504	0.670	0.090	0.085	22.38	0.70	0.653	-	-	-	-

shown in fig. 6-5(a) - (c), while the existence regions are shown in fig. 6-6.

6.4.2 Percentage Scour and Dimensions of the Scour Hole

Negatives of photographs of each run for the lower three slopes were projected onto a screen and the scour pattern traced on paper. The percent scour was evaluated as the ratio of the area of scour divided by the total area bounded by the steps. The respective areas were planimetered from the tracings. Values obtained were averaged over the number of steps visible in the clear-sided section of the flume for each test run. Results are listed in table 6-1, and are plotted in fig. 6-16, with standard errors shown. For slope = 0.248, the scour pattern was traced directly from the flume, and the relevant areas planimetered to give the percent scour (see fig. 6-16).

From tracings of the scour and flow patterns, the depth of maximum scour S, the distance to the point of maximum scour X, and the depth of flow at the point of maximum scour S_o were measured. The results are shown in fig. 6-13, 6-14, and 6-15 respectively. S, X and S_o are defined as shown in fig. 6-4.

No values of S_o were available for slope = 0.248, due to failure of photographic arrangements.

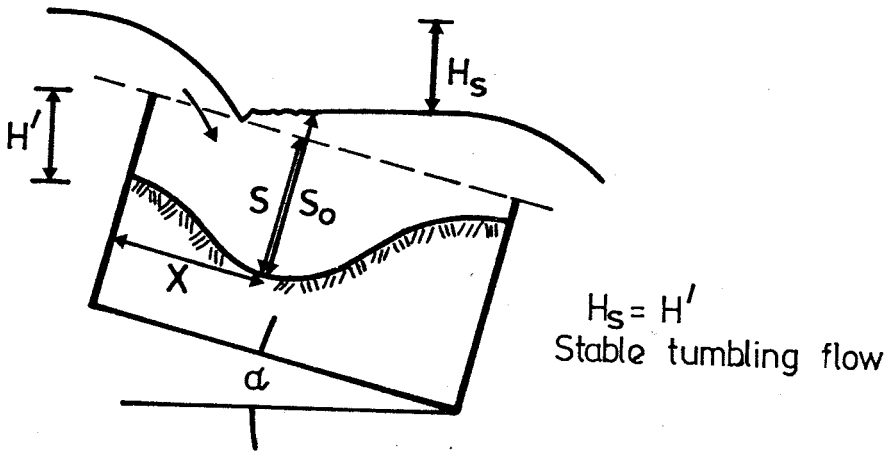

Figure 6-4: Definition diagram for terms used to describe scour.

6.4.3 Average and Maximum Velocities

Average and maximum velocities are shown in fig. 6-22 and fig. 6-23 respectively.

6.4.4 Friction Factor and Average Shear Stress

The average shear stress τ_m and the Darcy-Weisbach friction factor f were calculated for each test run using the wall-correction procedure as outlined in Gessler (1965). The average velocity v_m, average depth h, and channel slope J were used for the velocity value , depth value, and slope value respectively in these calculations. Values obtained are listed in table 6-1. The Darcy-Weisbach friction factors are shown in fig. 6-24.

6.5 DISCUSSION OF RESULTS

6.5.1 Flow Regime

Three distinct flow regions were observed, namely stable tumbling, unstable tumbling and shooting flow (see fig. 6-5). The characteristics of the flow in each of these flow regimes are described in section 5.5.1.

Fig. 6-6 shows the existence regions of these regimes on a plot of discharge versus channel slope. The curves defining the limit values q_{st} and q_{sh} were estimated from test runs and have the same shape as those found for clear water flow. The clear water flow curves for these boundaries are compared to the clear water scour curves in fig. 6-7. This shows that the major difference in curves between the two flow types is that the region of occurrence of unstable tumbling flow has changed; at all slopes unstable tumbling flow for clear water scour occurs at a higher discharge (by an essentially constant amount) than that at which unstable tumbling flow begins for clear water flow. This difference is obviously the result of sediment between the steps. Inspection of photographs (fig. 6-5) shows that the sediment produces a flow geometry quite different to that of the clear water flow test runs (see fig. 5-2). The question thus arises as to whether the mechanism responsible for flow instability is the same in both cases.

Mechanism for Flow Instability

(a) Slope = 0.027. As was shown for clear water flow, at slope = 0.027 a change in nappe profile from plunging to surface occurs at

Figure 6-5(a): Stable tumbling flow (clear water scour).

Figure 6-5(b): Unstable tumbling flow (clear water scour).

Figure 6-5(c): Shooting (or rapid) flow (clear water scour).

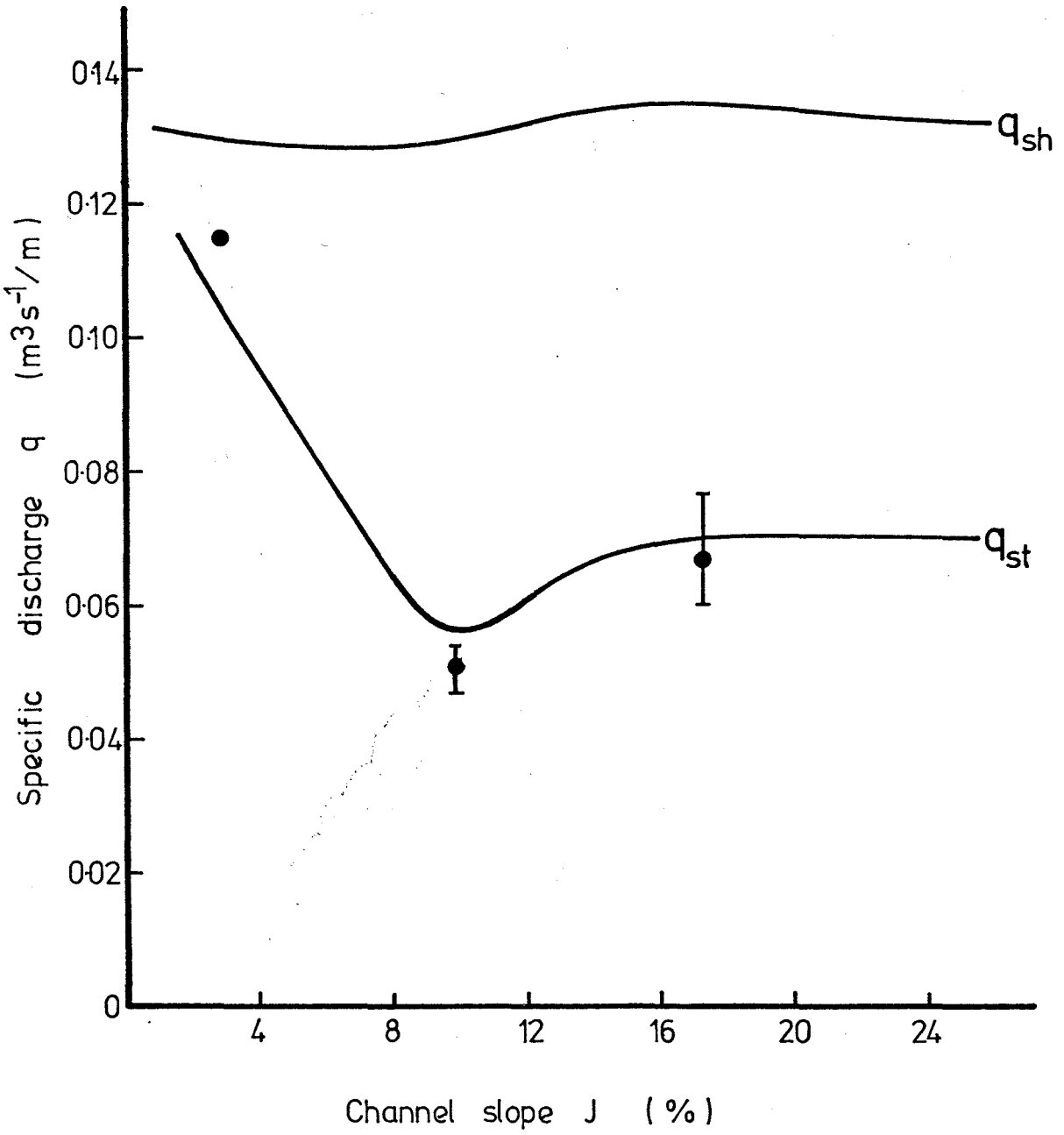

Figure 6-6: Existence regions of flow regimes (clear water scour).

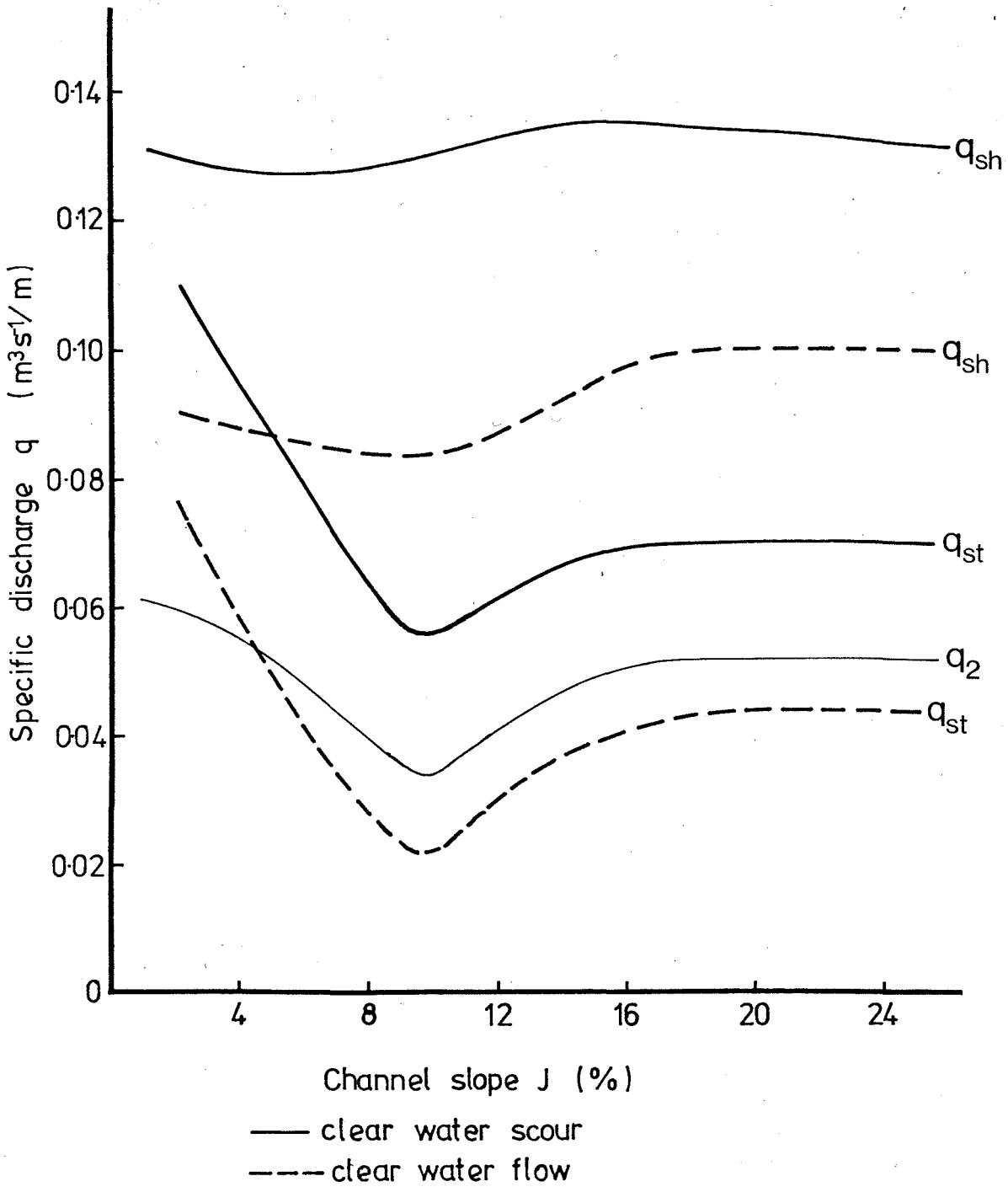

Figure 6-7: Comparison of regions of existence of flow regimes for clear water flow and clear water scour.

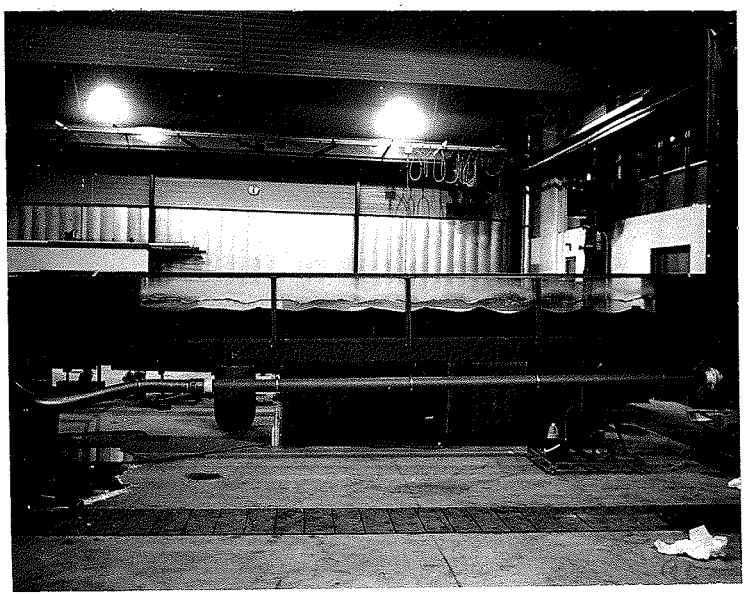

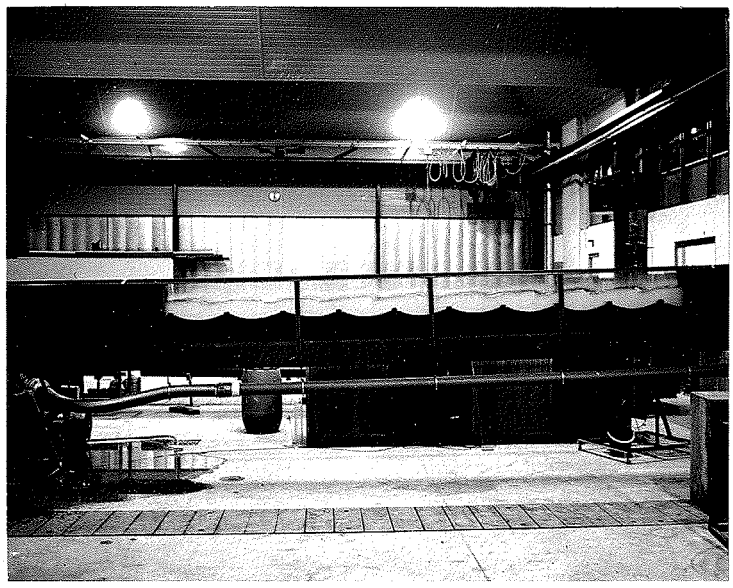

Figure 6-8: Scour profiles of runs at slope of 0.027.

very low flow rates. It was not possible to calculate values for the change in nappe profile as k (here considered equal to S) < 4.5 H_1. However, the scour profiles of the runs are clearly determined by the surface nappe profile (see fig. 6-8).

For discharges approaching the transition between stable tumbling and unstable tumbling flow, standing waves did not develop as they did for the clear water flow case. Further, it was obvious that the sills are not acting as critical flow structures as they do at slopes = 0.098, 0.172 and 0.248, but as submerged weirs.

Flow over a submerged rectangular weir is given by the formula

$$\frac{q}{q_a} = \left[1 - \left(\frac{H_2}{H_1}\right)^{3/2}\right]^{0.385} \qquad \ldots 6.16$$

(Brater and King, 1976)

where q_a = specific discharge at head H_1 computed from the equation for free (unsubmerged) discharge

and H_1, H_2 are shown in fig. 6-9.

From equation 6-16, the factor $\frac{H_2}{H_1}$ is the submergence ratio S'. For the tests reported here

$$S' \frac{H_1 - 0.5 \sin\alpha}{H_1} \qquad \ldots 6.17$$

(Note that H_1 is equivalent to H as used in Chapter 5.)

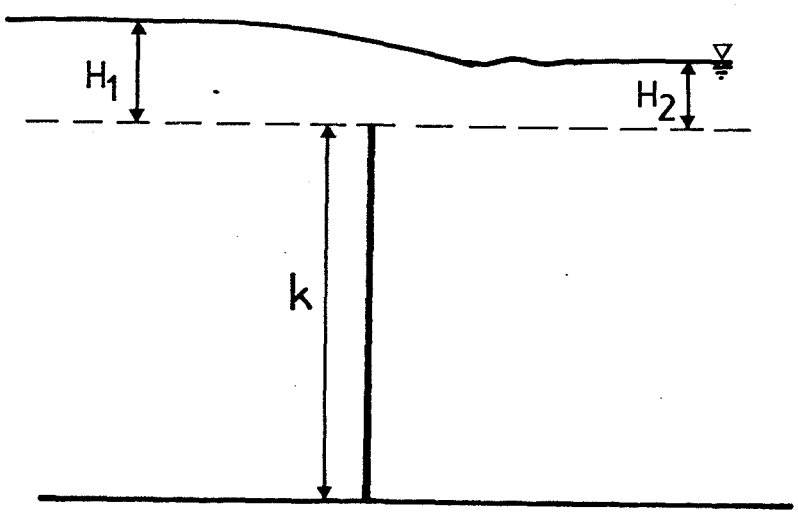

Figure 6-9: Flow over a submerged weir.

For J = 0.027,

$$S' = \frac{1 - 0.013}{H_1} \qquad ...6.18$$

Further

$$q_a = C\, H_1^{3/2} \qquad ...6.19$$

where C = a discharge coefficient.

The equation attributed to Kindsvater and Carter (Brater and King, 1976) was used to evaluate C:

$$C = 3.22 + 0.40 \frac{H}{k} \qquad ...6.20$$

where k is shown in fig. 6-9.
For the analysis, depth of scour S was equated with k, and H_1 was measured from the tracings of the test runs. Good agreement was found between the predicted and measured specific flow rate (table 6-2).

TABLE 6-2 COMPARISON OF CALCULATED AND MEASURED SPECIFIC FLOW RATES

RUN	q (measured)	q (predicted)
7	0.044	0.047
1	0.056	0.053
2	0.072	0.076

For discharges greater than about q = 0.06 m^3s^{-1}/m, S (and thus k) is essentially constant (see fig. 6-12) because the downstream step limits any further scour development. Values of H_1 for runs 1, 2 and 7 were plotted (see fig. 6-10) versus specific discharge and the curve extrapolated to allow estimation of H_1 for higher discharges. For six estimated values of H_1, corresponding weir flow rates were calculated (table 6-3).

TABLE 6-3 CALCULATED SUBMERGED WEIR DISCHARGES

q	H_1 (est)	C	q_a	S'	q (calc)
0.08	0.125	3.887	0.172	0.896	0.083
0.09	0.135	3.940	0.195	0.904	0.092
0.10	0.142	3.977	0.213	0.908	0.098
0.11	0.150	4.020	0.234	0.913	0.106
0.12	0.156	4.052	0.250	0.917	0.111
0.13	0.162	4.084	0.266	0.920	0.117

The calculated values indicate that, given the observed trend in H_1, the submerged steps become incapable of passing the flow rate imposed.

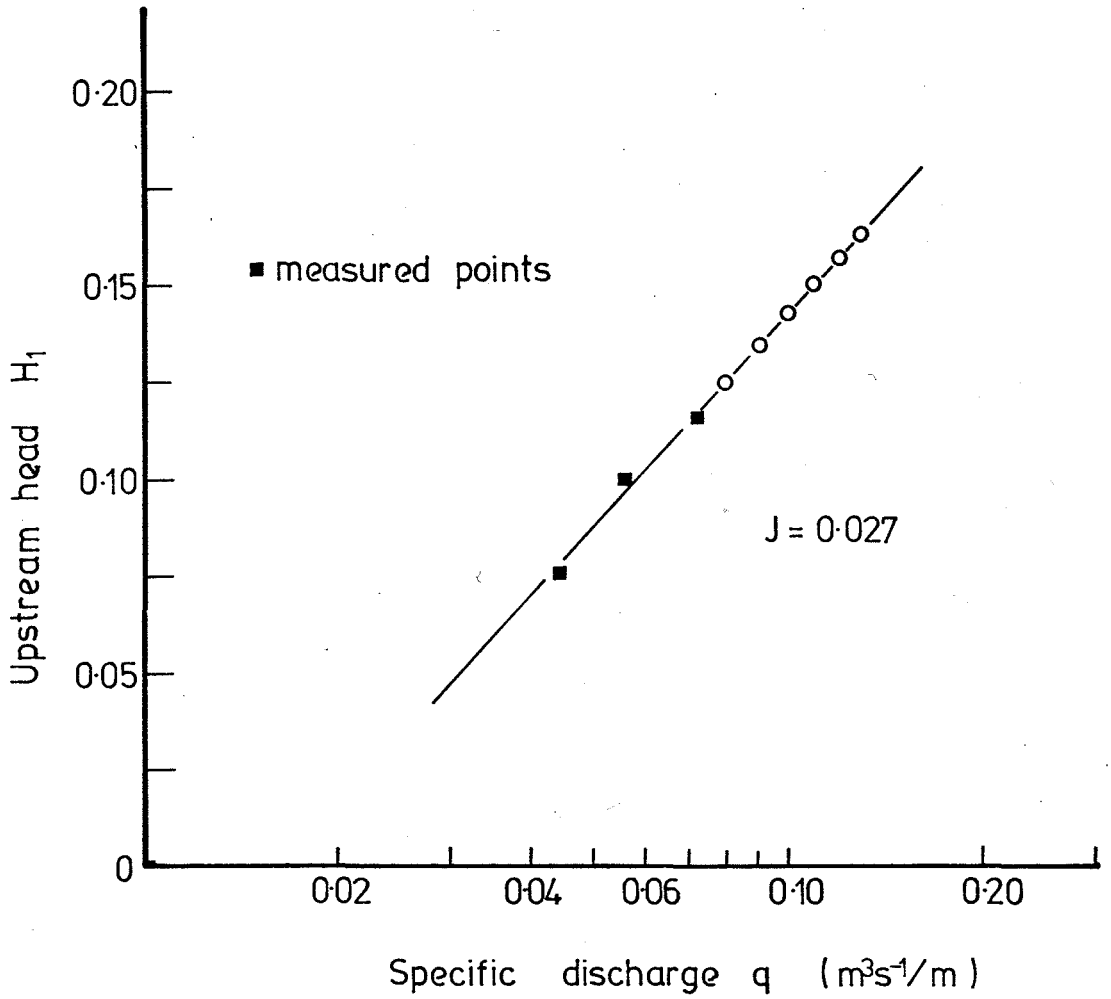

Figure 6-10: Extrapolation of upstream head H_1 values to higher flow rates.

Thus it is possible that an instability will develop. The value of specific discharge at which this instability will begin is estimated to be about q = 0.115 m^3s^{-1}/m, and is shown on fig. 6-6.

(b) Slope = 0.098, 0.172. The scour hole shapes for stable tumbling runs at slopes = 0.098, 0.172 and 0.248 are indicative of scour caused by a plunging nappe. As with clear water flow, the steps act as critical depth devices. Thus a hydraulic jump forms in the pool region. The situation can be visualised as shown in fig. 6-11.

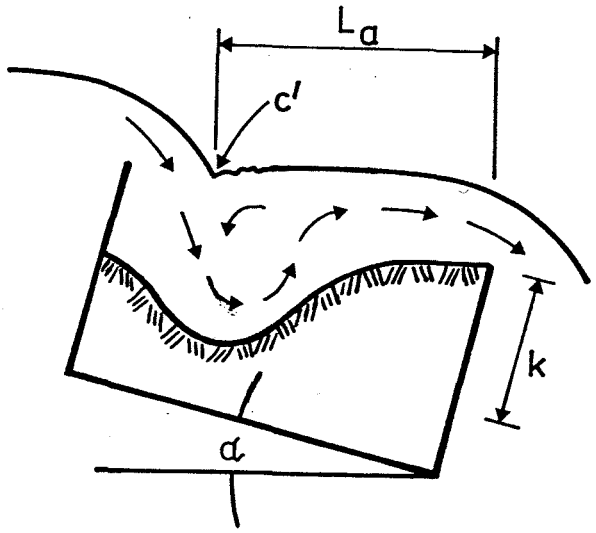

Fig. 6-11 : Plunging Nappe Scour.

This could be considered to be acting as a hydraulic jump at an abrupt rise (where the height of the rise = k). Forster and Skrinde (1950) give an equation for the length L_j of a hydraulic jump at an abrupt rise as

$$L_j = 5\ (k + y_c) \qquad \ldots 6.21$$

They note that if L_j is shorter than that given by equation 6.21,

the jump will be submerged. This was found to be the case for the present test runs. Thus, the length of the submerged jump may be considered to be $L_j = 3.5\ y_2$ (Kindsvater, 1944). As in the clear water flow case, a critical discharge will be reached when $3.5\ y_2 = L_a$. This criterion may be considered to correspond to the onset of unstable tumbling flow.

Values of the ratio $\frac{3.5\ y_2}{L_a}$ are plotted versus specific discharge in fig. 6-12. For slope = 0.098, the points indicate that a critical value of $\frac{3.5\ y_2}{L_a} = 1$ is reached at about $q = 0.05\ m^3 s^{-1}/m$ (a measure of precision is indicated). This is near the value observed for the onset of unstable tumbling flow. It is probable that the limited length available for complete jump development triggers the instability.

The change in slope of the curve in fig. 6-12 at about $q = 0.035\ m^3 s^{-1}/m$ is to be expected. For $q > 0.035\ m^3 s^{-1}/m$, distance to the point of maximum scour is essentially constant (fig. 6-14), while depth of scour decreases (fig. 6-13) with increasing discharge. Thus, with increasing flow, point c' (fig. 6-12) will move rapidly toward the downstream step reducing L_a, while $3.5\ y_2$ increases.

For slope = 0.172, the values of $\frac{3.5\ y_2}{L_a}$ follow closely those for slope = 0.098. However, for $q > 0.04\ m^3 s^{-1}/m$, while distance to the point of maximum scour increases slightly (fig. 6-14), scour depth S also increases slightly (fig. 6-13). Thus, with increasing discharge point c' (fig. 6-11) will not move toward the step as rapidly as occurred for slope = 0.098. The anticipated trend in $\frac{3.5\ y_2}{L_a}$ with increasing discharge is shown in fig. 6-12. The trend indicates that the critical value of $\frac{3.5\ y_2}{L_a}$ will be reached at about $q = 0.07\ m^3 s^{-1}/m$, although the range of possible values is large.

The range of values of q corresponding to $3.5\ y_2 = L_a$ for slopes = 0.098 and 0.172 indicate that the limited length available for the hydraulic jump provides a reasonable explanation for the onset of unstable tumbling flow. Measurements were not available for slope = 0.248.

Applicability to the Field Situation

For all the slopes investigated, the onset of unstable tumbling flow was preceded by a range of flow rates over which the downstream step

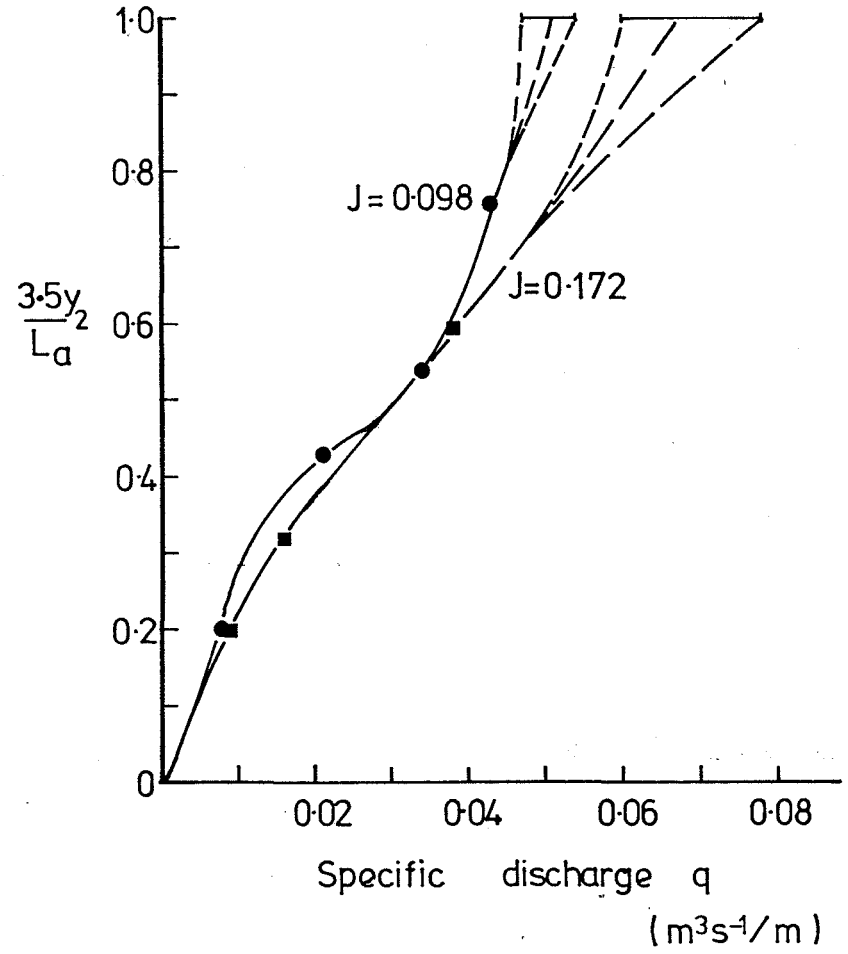

Figure 6-12: Plot of $\frac{3.5y_2}{L_a}$ versus specific discharge.

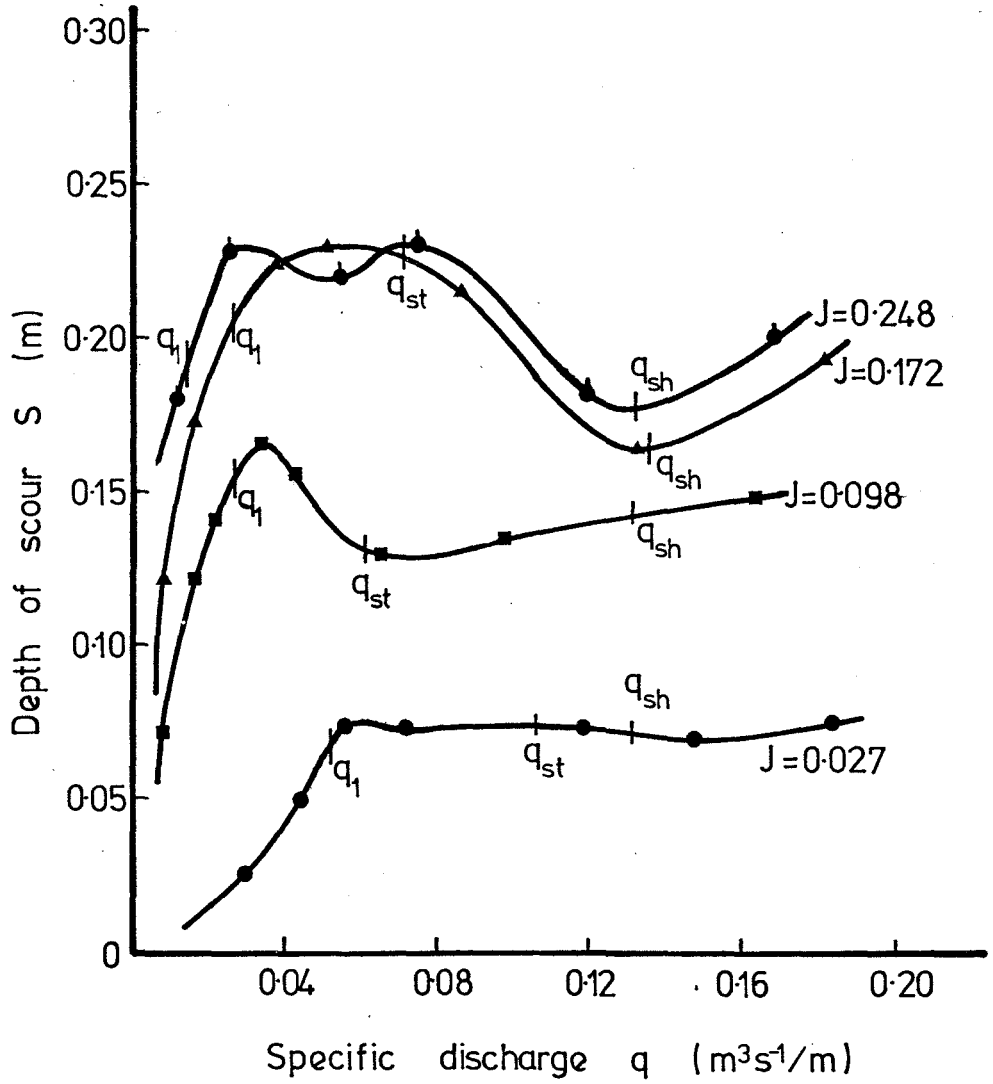

Figure 6-13: Plot of depth of scour S versus specific discharge.

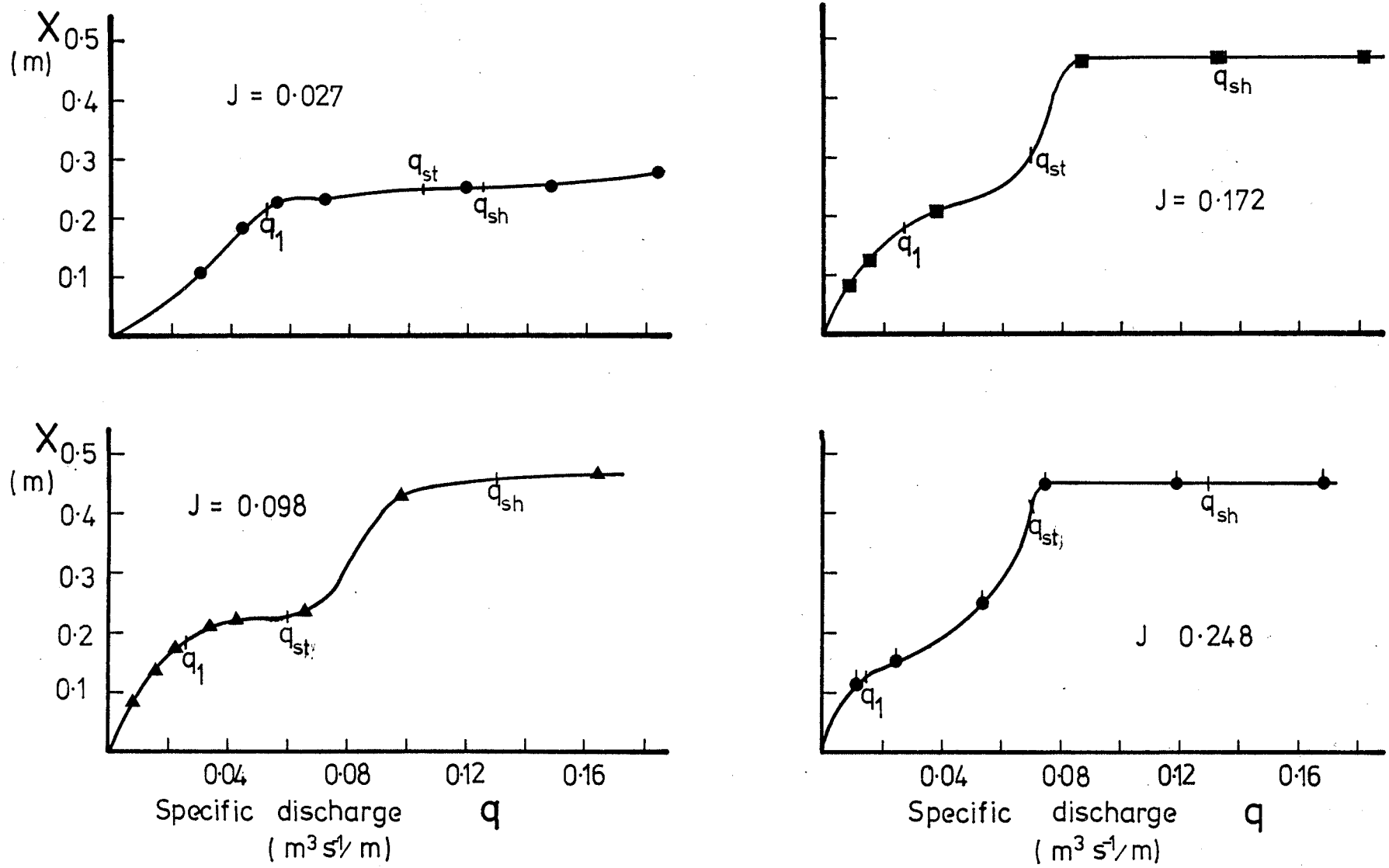

Figure 6-14: Plot of distance to the point of maximum scour X versus specific discharge.

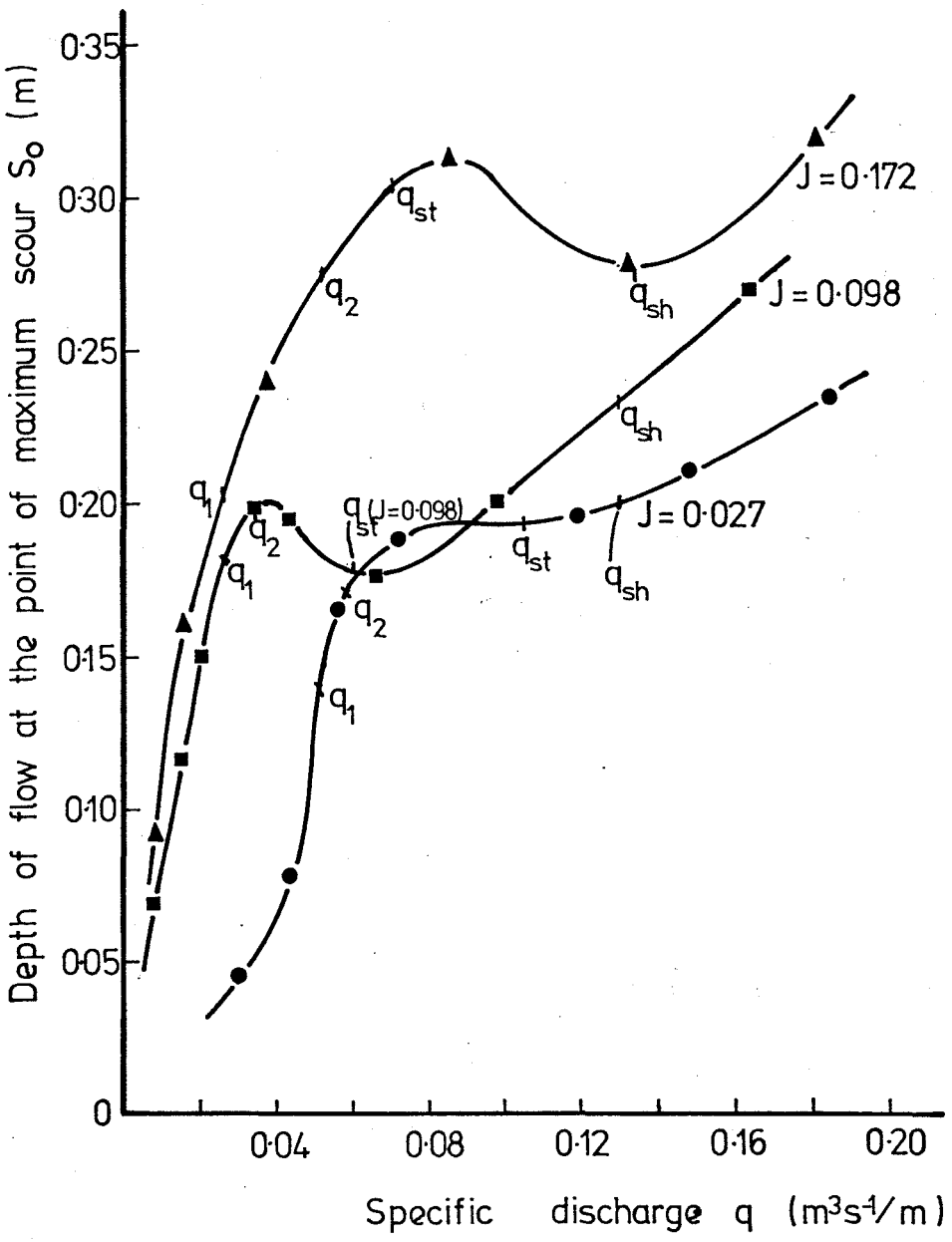

Figure 6-15: Plot of depth of flow at the point of maximum scour S_o versus specific discharge.

influenced the development of the scour hole. For slopes = 0.098, 0.172 and 0.248 (and also to a small extent for slope = 0.027) scour occurred in front of the upstream step, and behind the downstream step (see fig. 6-3) over this range of flows.

In a natural stream, this would correspond to removal of the deposits immediately upstream of the steps (low flow scour usually results in removal of any deposits immediately downstream of steps). Paving of the stream channel makes the stream bed very stable, and the deposits immediately upstream of steps are consequently difficult to remove.

The laboratory model may be considered to be Froudian, that is, it has fully developed turbulent free surface flow which is independent of Reynold's number effects. If Λ represents the ratio of model to prototype, then

$\Lambda_g = 1$ (gravity has the same effect in both model and prototype)

$\Lambda_s = 1$ (densities are the same in both model and prototype)

and $\Lambda_J = 1$ (slopes are the same in both).

This length ratio may be chosen freely as Λ_ℓ, and consequently the velocity ratio is

$$\Lambda_v = \sqrt{\Lambda_\ell}$$

Data from the Torlesse Stream was used to allow scaling to determine field flow rates corresponding to q_1, the flow rate at which the downstream step begins to influence development of the scour hole. Step length was used to establish a length ratio, given a step length of 0.5 m in the model. Data are shown in table 6-4.

TABLE 6-4 FIELD DATA FROM THE UPPER TORLESSE STREAM SYSTEM

Slope	Step Length	Stream Width	Λ_ℓ
0.104	3.06	1.70	0.163
0.164	2.88	1.48	0.174

(There is considerable variation in field step lengths at any given slope). Now, for a Froude number similarity model

$$q_{prototype} = \frac{q_{model}}{\Lambda_\ell^{1.5}}$$

Thus, for slope = 0.104, a field flow at which the downstream step would begin to limit development of the scour hole (assuming armouring effects are not apparent) is

$$q_1 = 0.365 \ m^3 s^{-1}/m$$

or $$Q_1 = 0.620 \ m^3/s$$

For slope = 0.162, this flow rate is

$$q_1 = 0.276 \ m^3 s^{-1}/m$$

or $$Q_1 = 0.408 \ m^3/s$$

The Upper Torlesse Stream is one of two main tributaries feeding the Torlesse Stream proper. In the Torlesse Stream, a 25 yr flood (April, 1978) developed a peak flow of about 2.1 m^3/s (Hayward, 1978, 1980). Allowing for a reduction in the Upper Torlesse (because of its tributary status) and for paving of the stream channel, it can be anticipated that this flow would probably not be equivalent to q_1 in the model.

Using the model discharges at which unstable tumbling flow began, scaling indicates prototype flows of 1.55 m^3/s and 1.43 m^3/s for slopes = 0.104 and 0.162 respectively. Again allowing for paving effects and the tributary status of the Upper Torlesse Stream, unstable tumbling flow is unlikely to occur in the field. Unstable tumbling flow is further discouraged by the irregularity of the field step-pool structures (Rouse, 1938), since steps of greater than average length can absorb a flow instability originating in a shorter pool upstream.

6.5.2 Clear Water Scour

Most equations derived to predict the process of local scour predict the depth of flow in the scour hole S_o rather than the depth of scour S. These equations show that S_o increases with increasing specific flow rate q. Similarly, except when the tailwater depth TW is such as to disperse the scouring jet before it reaches the erodible bed, S increases as q increases. This is intuitively obvious from the general form of most equations, which is

$$S_o = W' \frac{q^{\alpha} H'^{\beta}}{D_g^{\gamma} g^{\delta}} \qquad \ldots 6.22$$

(Schmid, 1972)

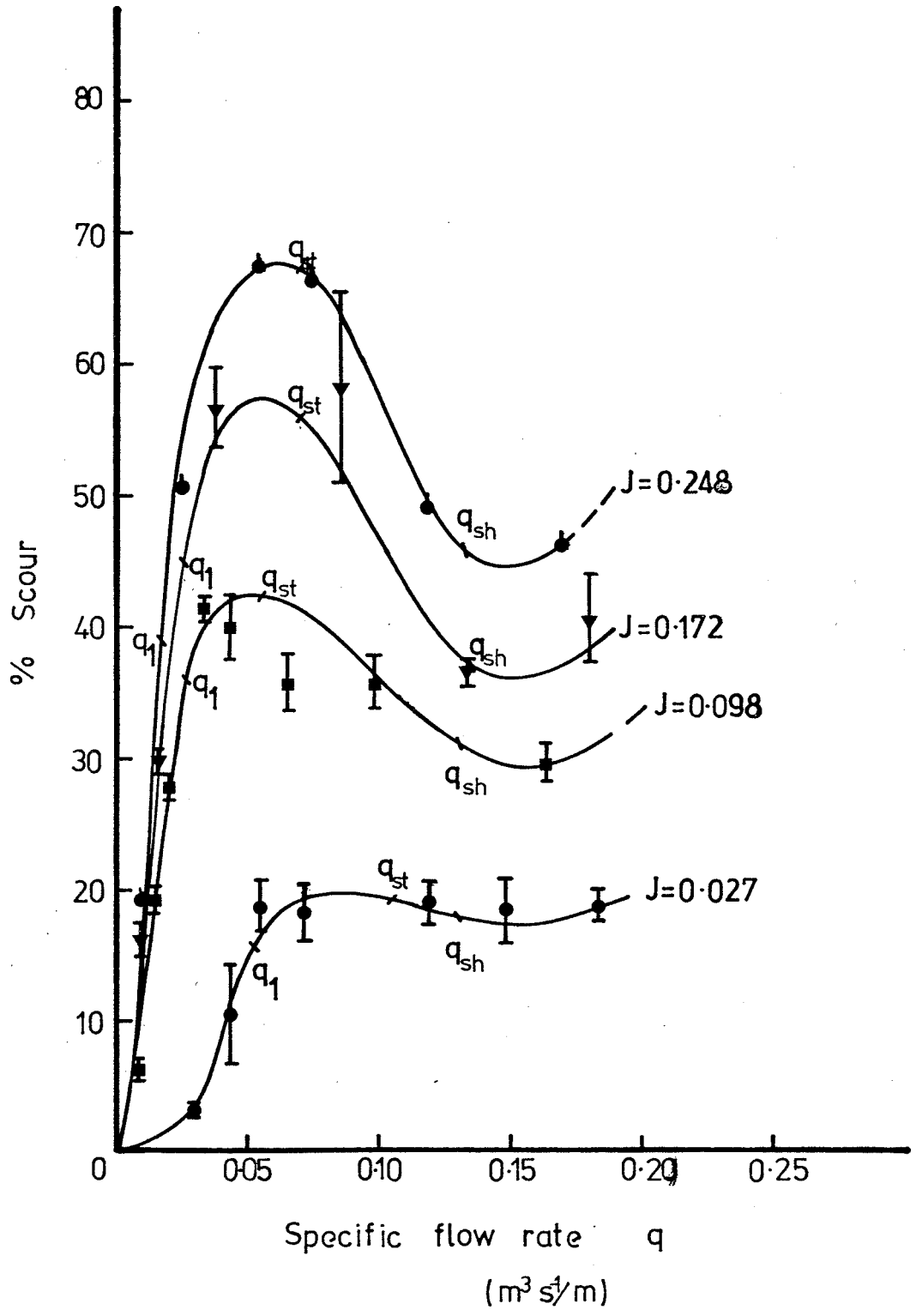

Figure 6-16: Plot of % scour versus specific discharge.

where H' = fall height

W' depends on the form of the scouring jet

D_g = a representative diameter of the bed material

$\alpha, \beta, \gamma, \delta$ are constants > 0

and g = gravitational acceleration.

Thus the curves shown in fig. 6-13 and 6-15 are surprising. One may have expected S_o to decrease as S decreased due to dispersion effects caused by increasing tail water depth with increasing discharge, and then increase with further increase in q as TW increase overshadowed the decrease in S. But under these conditions, S would decrease to zero as tail water totally dispersed the eroding jet before it impinged on the erodible bed. However, fig. 6-13 shows that after an initial increase, S decreases with q, and then increases again beyond a certain value of q. This trend is mirrored by the % scour curves shown in fig. 6-16. Thus the behaviour of scour in the stepped system deviates from previous scour investigations.

For reasonably low flow rates, the scour hole produced for the plunging nappe case is as shown in fig. 6-17.

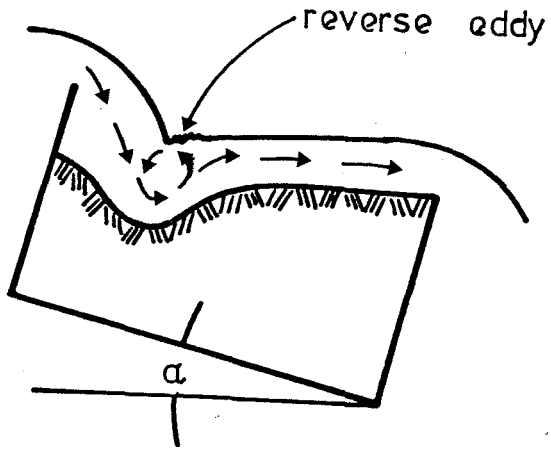

Figure 6-17: Scour hole shape (plunging nappe) for low flow rates.

As q increases, S, S_o and X all initially increase. However, at a certain value of q (say q_1, where $q_1 = \phi$ (slope)), the downstream sill or baffle begins to limit development of the scour hole as noted by Apmann and Blinco (1969). The situation develops as shown in fig. 6-18.

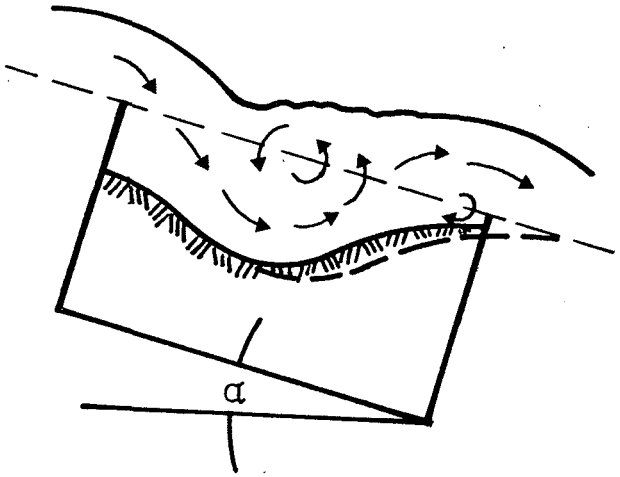

Figure 6-18: Scour hole shape as influenced by the downstream baffle.

The baffle forces the main scouring jet to rise before it can erode the scour hole to the dimensions that would have resulted (dashed line) had the baffle been farther downstream. The values of S and X are further influenced by the small positive (clockwise) eddy just upstream of the downstream baffle, which moves sediment from behind the baffle back into the scouring zone.

The baffle effect is clearly seen in figs. 6-13, 16-14, and 16-15. For each slope (except slope = 0.027, where S remains essentially constant for all $q > q_1$) the flow rate $q_2 (> q_1)$ at which S begins to

decrease with increasing q parallels the flow rate at which unstable tumbling flow begins (see fig. 6-7).

As q increases still further, another threshold value (q_{st}) is attained. At this point, the flow forced upward by the downstream baffle suddenly becomes unstable, as described in section 5.5.1. Consequently, for slopes of 0.098, 0.172 and 0.245, S and X are further decreased as the main eddy in the pool reverses due to the passage of the wave caused by this instability. This effect is shown in fig. 6-19.

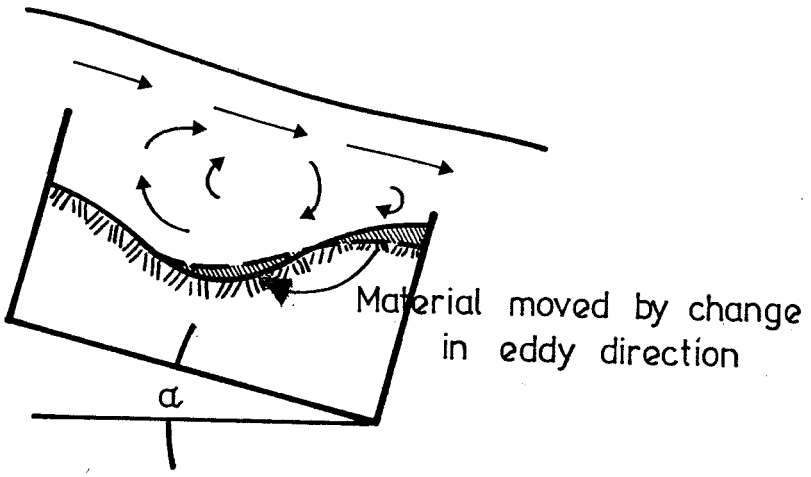

Figure 6-19: Change in shape of scour hole due to passage of roll wave.

With increasing flow rate, the period of these waves decreases. The two oscillating flow patterns result in the threshold scour hole shape shown in fig. 6-20.

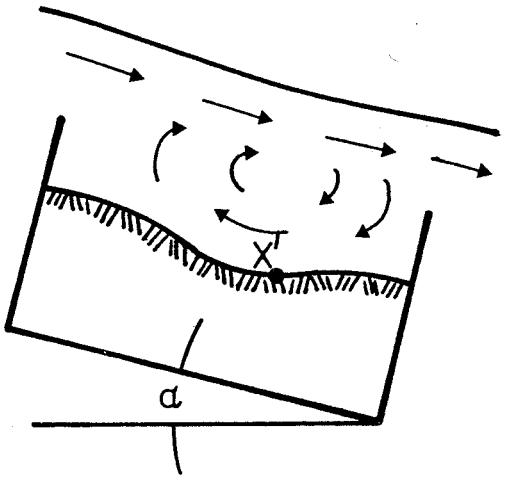

(a) Roll wave passing through pool

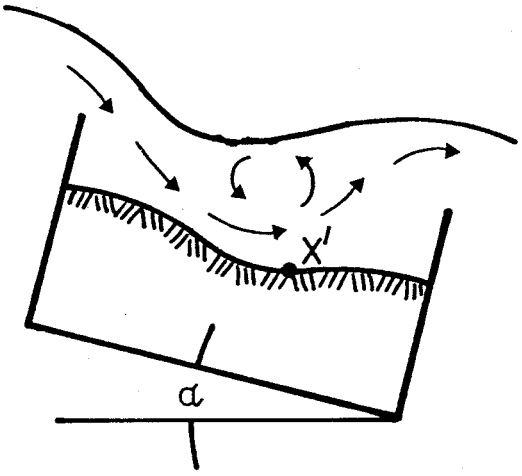

(b) Plunging nappe

Figure 6-20: Threshold scour hole shape resulting from oscillating flow pattern due to unstable tumbling flow.

The threshold shape (Volkart, 1972) shown corresponds, for slopes = 0.172 and 0.248, to a local minimum in S (at X'; see fig. 6-13) and including slope = 0.098 results, to a local minimum in % scour (see fig. 6-16). If flow is increased slightly, the scour field beyond X' erodes, and the following scour shape results (fig. 6-21).

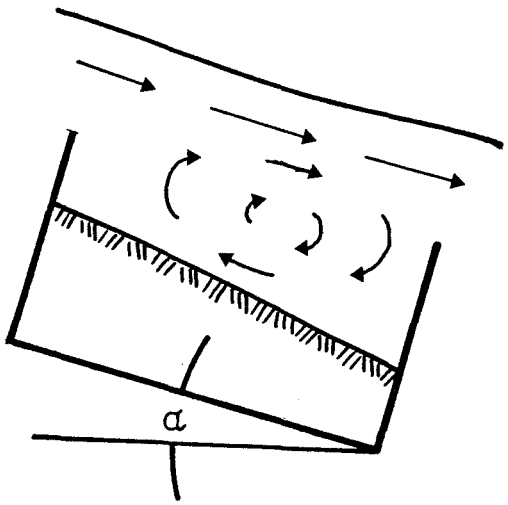

Figure 6-21: Final scour hole shape.

The large positive eddy flow pattern dominates, and the flow is shooting. (Shooting flow was, for these tests, defined as the flow state in which the large positive eddy as shown in fig. 6-20(a) occurred for 50% of the time or more). Accompanying this change in shape was the sudden increase in X to L, the length between steps. This is clearly seen in fig. 6-14. As q increases further, S and % scour again increase (see figs. 6-13 and 6-16).

Fig. 6-15 shows that for slope = 0.027, S_o maintains a constant value for $q > q_1$ (as does S) but begins to increase again as

the flow becomes shooting, reflecting the increase in tailwater depth while depth of scour remains essentially constant. For slope = 0.098, the S_o curve mirrors the trends of the S curve, with the tailwater depth strongly influencing S_o in the unstable tumbling and shooting flow regimes.

For slope = 0.172 S_o decreases from about q_2 (fig. 6-15), but begins to increase again as the flow becomes shooting.

It can be seen that only those tests for which the values of S_o, S and X were not influenced by the downstream baffle can be analysed in a way comparable to most existing analyses.

Most scour formulae from different authors have the form of equation 6-22.

Schmid (1972), from the Buckingham π-theorem and dimensionless variables

$$\pi_1 = \frac{S_o}{H_s}, \quad \pi_2 = \frac{q}{H_s \sqrt{gH_s}} \quad \text{and} \quad \pi_3 = \frac{H_s}{D_{90}}$$

used the scour results of Kotoulas (1967) to derive the equation

$$S_o = W' \frac{q^{0.667} H_s^{0.333}}{g^{0.333} D_{90}^{0.333}} \qquad \ldots 6.23$$

An analysis of all present tests where the downstream baffle did not distort the scour values, using the scour dimensionless variables as Schmid, resulted in the following equation

$$S_o = 0.162 \frac{q^{0.981} H_s^{0.866}}{g^{0.491} D_{90}^{1.337}} \qquad \ldots 6.24$$

$(R^2 = 0.930)$

One S_o value for J = 0.248 was used. It was estimated from a polaroid photograph of run 23.

Because only one sediment size was used in the tests, D_{90} may be treated as a constant, and so

$$S_o = 40.5 \frac{q^{0.981} H_s^{0.886}}{g^{0.491} D_{90}^{0.337}} \qquad \ldots 6.25$$

The exponent values differ markedly from those obtained by other researchers. However, the scour hole shapes for tests performed at slope = 0.027 were visibly different from those obtained at the other slopes, because of the different nappe form. When the values for slope = 0.027 were eliminated, and a multiple regression analysis performed, the following equation was obtained.

$$\log \frac{S_o}{H_s} = 0.852 \log\left(\frac{q}{H_s\sqrt{gH_s}}\right) + 0.773 \log\left(\frac{H_s}{D_{90}}\right) - 0.167 \qquad \ldots 6.26$$

$$R^2 = 0.993$$

Thus
$$S_o = 0.680 \frac{q^{0.852} H_s^{0.495}}{g^{0.426} D_{90}^{0.773}} \qquad \ldots 6.27$$

Again treating D_{90} as a constant yields

$$S_o = 7.72 \frac{q^{0.852} H_s^{0.495}}{g^{0.426} D_{90}^{0.333}} \qquad \ldots 6.28$$

The values of the exponents are similar to those of Schmid, although the constant multiplier is several times larger. However, written as

$$S = 7.72 \frac{q^{0.852} H_s^{0.495}}{g^{0.426} D_{90}^{0.333}} - TW \qquad \ldots 6.29$$

the equation is very similar to that of Eggenberger-Müller (Nóvak, 1955)

i.e.
$$S = 22.88 \frac{q^{0.6} H'^{0.5}}{D_{90}^{0.4}} - TW \qquad \ldots 6.6$$

(Note for the present tests, H_s would be equivalent to Eggenberger-Müller's H').

Introducing $g^{0.5}$ into equation 6.6, one obtains

$$S = 7.3 \frac{q^{0.6} H'^{0.5}}{g^{0.5} D_{90}^{0.4}} - TW \qquad \ldots 6.30$$

A further development of the Eggenberger-Müller formula by Franke (1960) resulted in

$$S_o = 2.42 \frac{(H' + TW)^{0.5} q^{0.667}}{D_{90}^{0.5} g^{0.333}} \quad \ldots 6.31$$

This is defined by Johnson (1967) as corresponding to the ultimate limit of scour, where all suspended material in circulation in the scour hole is eventually removed. (This contrasts with the dynamic limit as suggested by Laursen (1952), where the scouring jet is capable of keeping material moving within the scour hole, but not in lifting it completely out). Thus the results obtained by the writer and described by equation 6-28 indicate that the ultimate static scour limit has been reached. It should be noted that S (i.e. S_o - TW) defined in equation 6-29 is equivalent to S as defined in fig. 6-1. This is a little different from S as defined in fig. 6-4.

Depths of scour for the surface nappe case may be predicted from the submerged weir analysis presented in section 6.5.1. If q and submergence S' (and thus H', given J = tanα) are known, the unsubmerged discharge q_a can be calculated from equation 6-19. Then k (in the clear water scour case, k = depth of scour S as shown in fig. 6-11) can be calculated from equation 6.10 having used equation 6.19 to calculate the discharge coefficient C.

The free overfall scour studies of most investigators have been performed such that there has been no imposed structural constraint to the scouring process. Schmid (1972) stated that for his step-stair scour tests (writer's free translation) '...the maximum distance between two steps is limited by the maximum length of scour expected, because the overflow jet should not impact on the following step crest'. By contrast, the scour tests of Volkart (1972) included tests where the downstream step influenced the scour dimensions. An inconclusive attempt was made to analyse the present tests using Volkart's method. Until the effects of the downstream baffle on scour are quantified, the results given above for $q > q_1$ remain unable to be analysed.

6.5.3 Average and Maximum Velocities

It is immediately evident from fig. 6-22 that slope has an effect on average velocity. Average velocity decreases with increasing slope up to specific discharges of about $q = 0.11\ m^3s^{-1}/m$. This is due to the increase in scour depth (with consequent increase in fluid energy dissipation) with increasing slope at any discharge. Beyond this dis-

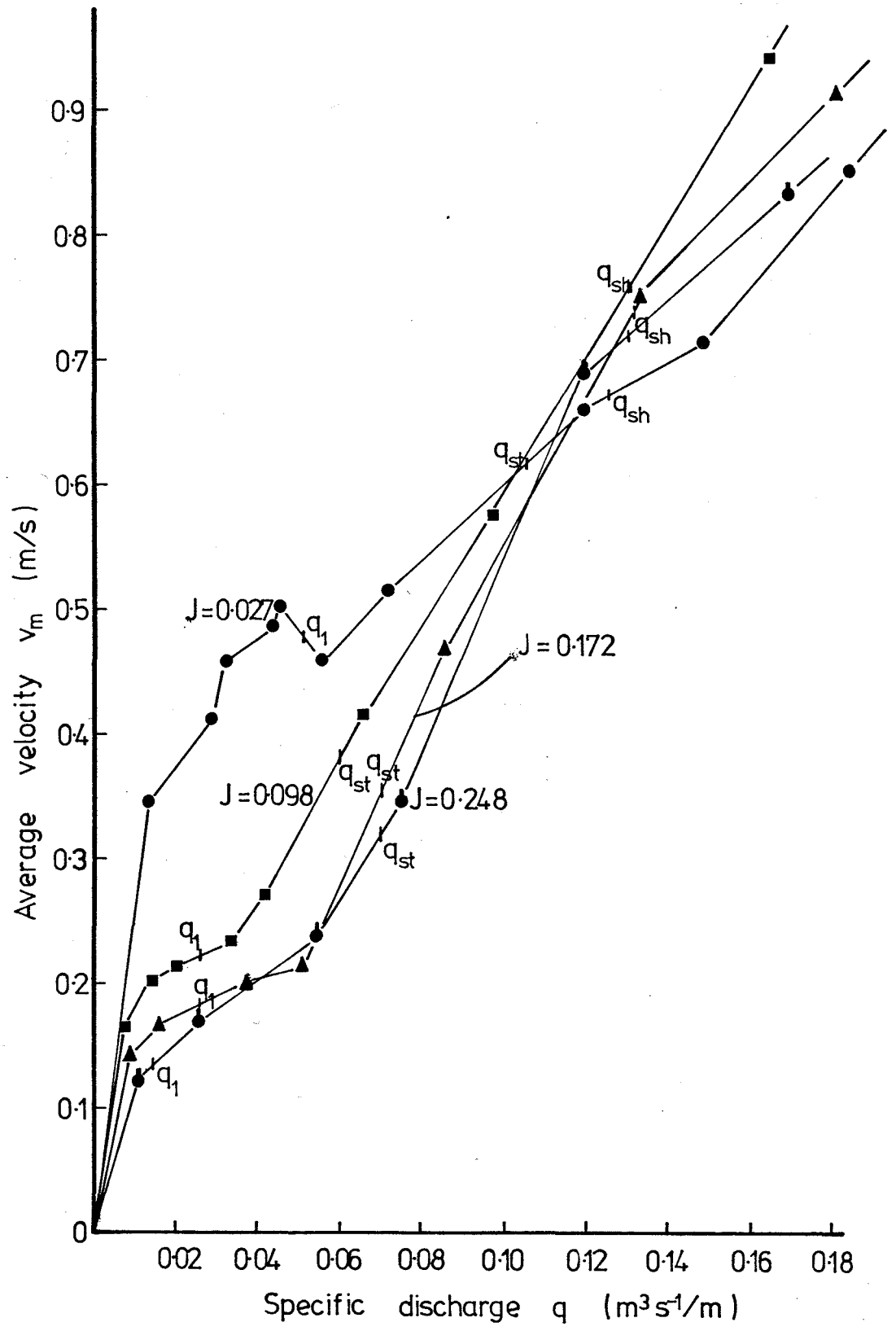

Figure 6-22: Plot of average velocity v_m versus specific discharge.

charge, the average velocities for slope = 0.027 are less than the values for the other slopes.

For all slopes, there is an initially rapid increase in average velocity with discharge, followed by a lessening in the rate of change of average velocity with discharge up to a q value (a function of slope) marked q_1 in fig. 6-22. This is the specific discharge at which the downstream sill begins to limit development of the scour hole. For $q > q_1$, average velocity begins to increase almost monotonically with increasing discharge. The zone of unstable tumbling delineated (fig. 6-22) seems to have an insignificant effect on this trend.

For maximum velocities (shown in fig. 6-23) the trend in the values for slope = 0.027 is clearly different to the trend in the values at other slopes. For discharges up to $q = q_1$, there is essentially little change in maximum velocity (although there is considerable scatter in the data). Maximum velocity then increases with increasing flow up to about the stable tumbling/unstable tumbling flow limit, reflecting the static scour hole shape over this range of flows. For flows in the unstable tumbling and shooting flow regimes, there is again very little change in maximum velocities.

For slopes = 0.098, 0.172 and 0.248, there is no clear trend with changing slope. However, over the complete range of discharge, maximum velocities increase with increasing flow rate.

The average and maximum velocities are indicative of the erosive ability of the stream. For slope = 0.027, the stream will be least erosive over the range of flows up to q_1. Beyond this value, both maximum and average flow velocities indicate a sudden increase in erosive potential.

In general, some authors recommend avoiding the unstable tumbling flow regime because roll waves increase a channel's erosive capacity (Chow, 1959; Morris, 1968; Peterson and Mohanty, 1960; Schumm et al, 1982). For slopes = 0.098, 0.172 and 0.248, it can be seen that it is not just the unstable tumbling and shooting flow regimes that should be avoided because of erosive danger. The discussion above shows that a channel begins to increase in erosive potential as soon as the downstream step begins to affect development of the scour hole. As shown in section 6.5.1, in the Torlesse Stream, this probably corresponds to a flood of more than a 25 yr return period.

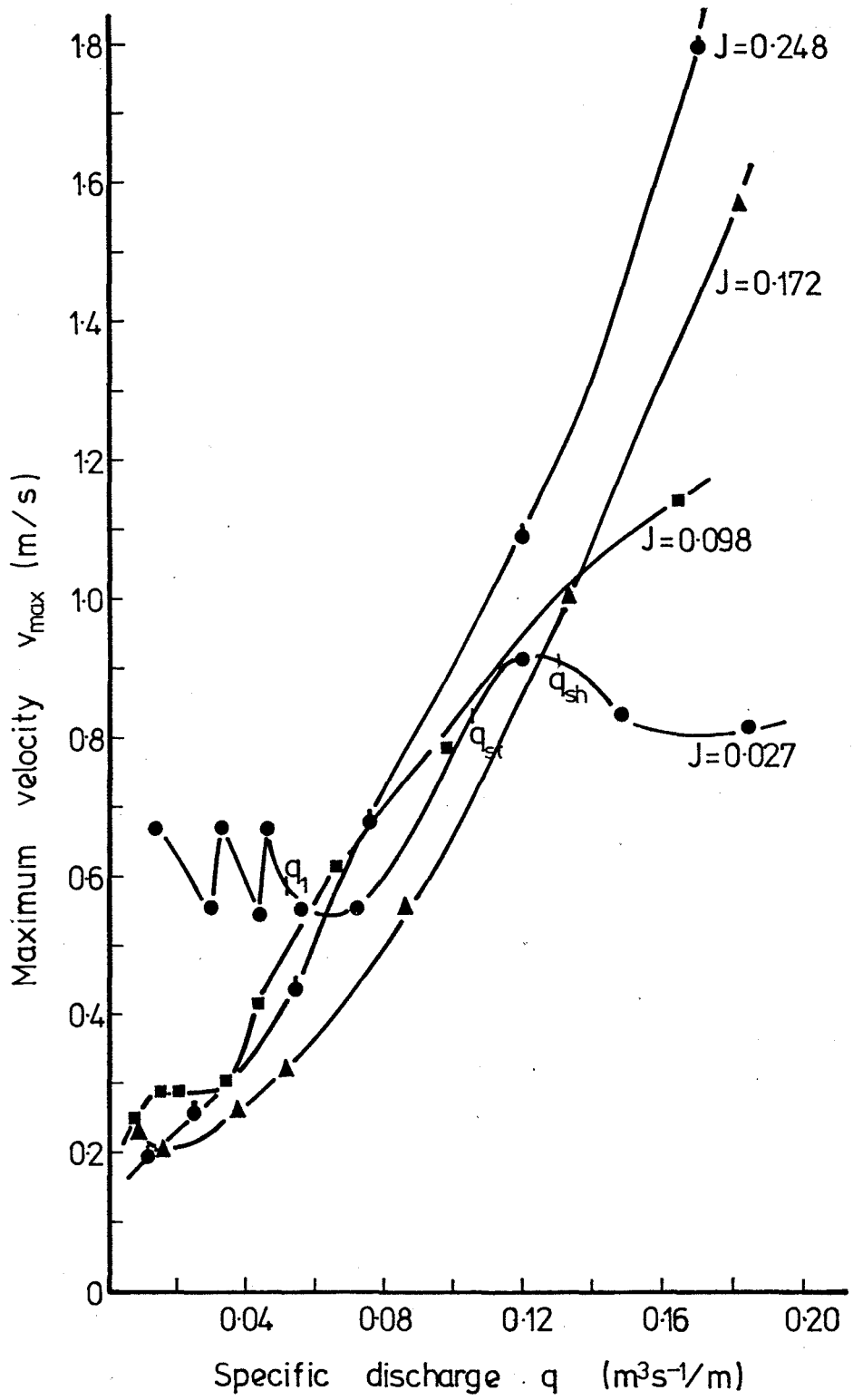

Figure 6-23: Plot of maximum velocity v_{max} versus specific discharge.

6.5.4 Resistance to Flow

The Darcy-Weisbach friction factors f shown in fig. 6-24 for clear water scour exhibit an interesting difference in trend from those for clear water flow (fig. 5-16). At low flows, there is an initial increase in f for slopes = 0.027, 0.098 and 0.172, followed by the same type of decrease noted in the clear water flow case.

For slopes = 0.027, 0.098 and 0.172, resistance to flow increases up to a point between q_1 and the discharge at which unstable tumbling flow q_{st} begins (see fig. 6-24). The increase in resistance to flow corresponds to increasing depth of scour. The flow rate at which friction factor f reaches a maximum corresponds closely to the flow rate q_2 at which depth of scour S attains a maximum value (see fig. 6-13). Beyond this flow rate, f decreases. The slowing in the decrease of f with increasing flow rate can be attributed to the increase in S in the shooting flow regime for the slope of 0.172 and 0.248 and in the unstable tumbling and shooting flow regimes for the slope of 0.098.

Fig. 6-25 shows a plot of $\sqrt{\frac{8}{f}}$ versus q. As in fig. 6-24, two distinct trends are apparent. In order to predict resistance to flow empirically, it was clear that two expressions would have to be evaluated: one corresponding to the stable tumbling flow test runs in which f increased ($\sqrt{\frac{8}{f}}$ decreased) with increasing flow, and one corresponding to the test runs where f decreased ($\sqrt{\frac{8}{f}}$ increased) with increasing flow.

Stable Tumbling Flow; f Increasing

A logarithmic equation was considered to be the most suitable form for expressing resistance to flow.

Depth of flow at the point of maximum scour S_o may be considered to be a function of the hydraulic radius R. Further, depth of scour S may be considered to be equivalent to the effective roughness height k'. As S_o and S are both reasonably easily measured in the field, it was decided to use $\frac{S_o}{S}$ as the independent variable rather than $\frac{R}{k'}$.

As noted in section 6.5.2, scour depth S as measured in these tests is a little different to scour depth S as shown in fig. 6-1. Thus an equation using field values of S will differ from one derived using model values. However, $S_{field} = \phi(J)\ S_{model}$, and so the form of the equation derived using model values of scour depth will still be applicable to the field situation.

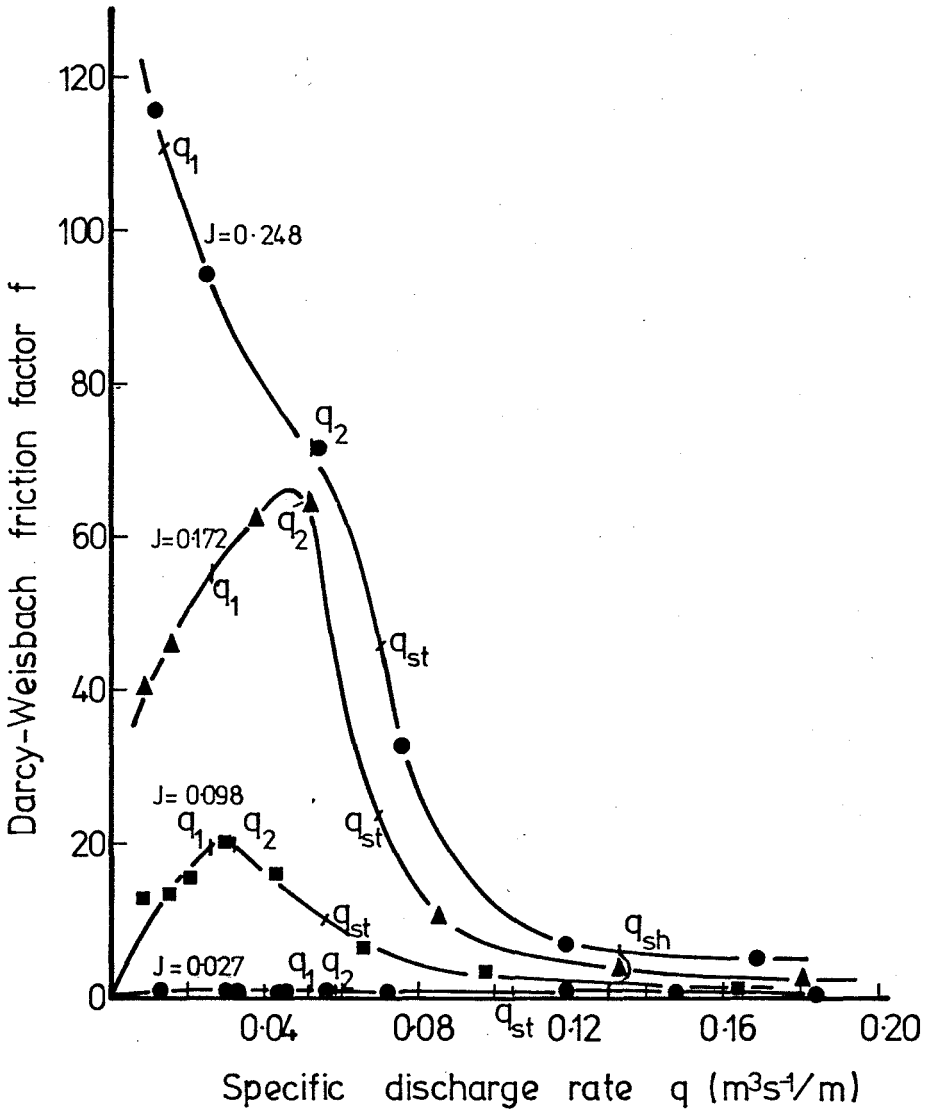

Figure 6-24: Plot of Darcy-Weisbach friction factor f versus specific discharge.

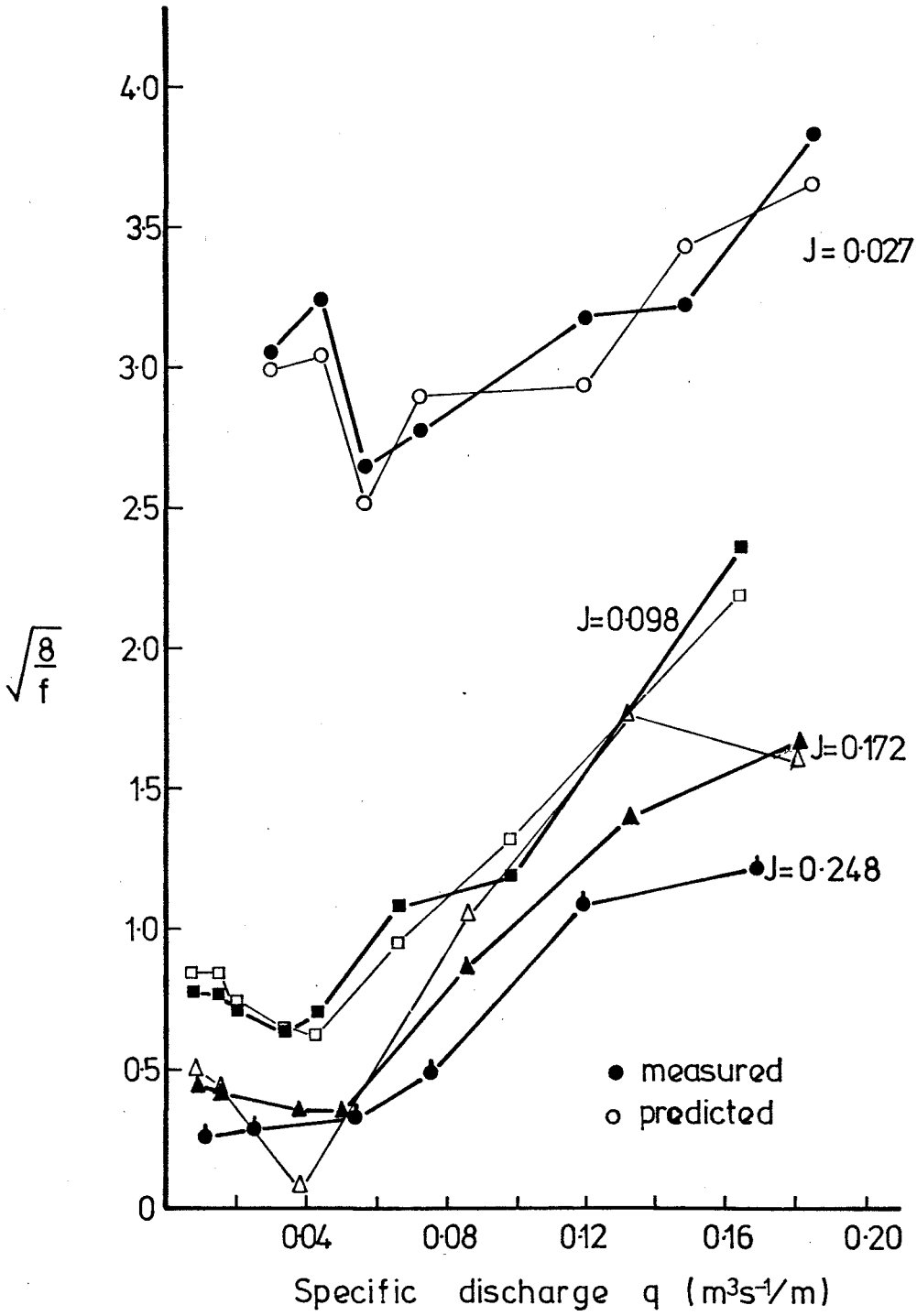

Figure 6-25: Plot of measured and predicted $\sqrt{\frac{8}{f}}$ values versus specific discharge.

It was decided to use difference in elevation H' (i.e. fall) instead of slope. Thus, the system is defined as in fig. 6-4 (note that H' = 0.5 sinα). No values of S_o were available for slope = 0.248.

An equation was obtained by multiple regression

$$\sqrt{\frac{8}{f}} = 5.657\ (7.177\ H' - 0.742)\ \log \frac{S_o}{S} + \frac{0.022}{H'^{1.197}} \qquad \ldots\ 6.32$$

Then

$$\sqrt{\frac{8}{f}} = 5.607\ A\ \log \frac{S_o}{S} + B \qquad \ldots\ 6.33$$

where $A = (7.177\ H' - 0.742)$

and $B = \frac{0.022}{H'^{1.197}}$

The fit of predicted and measured values shows reasonable agreement (fig. 6-25).

Unstable Tumbling and Shooting flows; f Decreasing

In the following derivation of the equation, no values of S_o were available for the slope of 0.248.

The equation found to give a good fit to the data was

$$\sqrt{\frac{8}{f}} = 5.657\ (1.751)\ \log \frac{S_o}{S} + (-\ 395.011\ H'^2 + 48.71\ H' - 1.832) \qquad \ldots\ 6.34$$

or

$$\sqrt{\frac{8}{f}} = 5.657\ (1.751)\ \log \frac{S_o}{S} + B$$

where $B = (-\ 395.011\ H'^2 + 48.71\ H' - 1.832)$.

A comparison of predicted and measured values is shown in fig. 6-25.

6.6 CONCLUSIONS

The main conclusions for the tests of clear water scour in an artificial step-pool channel are as follows:

(1) Three flow regimes were observed, namely

(a) Stable tumbling flow

(b) Unstable tumbling flow

(c) Shooting or rapid flow.

(2) At the slope of 0.027, flow of magnitude greater than q = 0.006 $m^3 s^{-1}/m$ in the stable tumbling regime was of the surface nappe form. Stable tumbling flow at the slopes of 0.098, 0.172 and 0.248, was characterised by the plunging nappe profile.

(3) At the slope of 0.027, flow in the stable tumbling regime was able to be predicted from measured values of S', H', and H_1 by the use of equations describing submerged weir flow. Further, at this slope, the onset of unstable tumbling flow was shown to occur as a result of the inability of the steps, acting as submerged weirs, to pass the imposed discharge.

(4) Unstable tumbling flow for the slopes of 0.098 and 0.172 (and thus, by implication, for J of 0.248) was seen to be associated with the flow at which the length of the submerged hydraulic jump (3.5 y_2) exceeded the distance from the start of the jump to the downstream step L_a.

(5) It was shown that unstable tumbling flow was unlikely to be encountered in the field, due to paving, to irregularity of step spacing, and to the high flow required (of the order of a 25 yr flood in one case).

(6) Above a certain flow rate that is a function of slope, scour hole shape was shown to be strongly influenced by the downstream step. Deviations from the expected trend in shape were attributable to this influence (either directly, or indirectly through flow regime which is dictated by channel geometry).

(7) For plunging nappe flows where the scour hole shape was not influenced by the downstream step, an empirical equation relating depth of scour to fluid, sediment, and channel properties was obtained. The equation

$$S = 7.72 \frac{q^{0.852} H_s^{0.495}}{g^{0.426} D_{90}^{0.333}} - TW \qquad \ldots 6.29$$

indicates that the predicted scour depth conforms to the ultimate static limit of scour.

(8) Average and maximum velocities suggest that a step-pool torrent will become potentially more erosive as the downstream step begins to limit the development of the scour hole.

(9) Resistance to flow was shown to increase with increasing discharge to the point at which the downstream step influence was strong enough to cause depth of scour to decrease. With increasing discharge, resistance to flow then decreased.

(10) Empirical equations were obtained to predict resistance to flow for the increasing and decreasing resistance cases respectively. Both were of the form

$$\sqrt{\frac{8}{f}} = 5.657\ A \log \frac{S_o}{S} + B$$

where $B = \phi$ (slope)

and $A = \phi$ (slope) for increasing resistance

or $=$ const for decreasing resistance.

CHAPTER SEVEN

SEDIMENT TRANSPORT IN AN ARTIFICIAL STEP-POOL TORRENT

7.1 INTRODUCTION

It has previously been established that the extreme irregularity of a boulder bed channel may be simulated by means of a succession of discrete weirs. A more realistic picture of step-pool stream behaviour is given when sediment is introduced between the weirs. This chapter details a further step in rendering the model more realistic still : sediment transport through the simulated step-pool system.

A single sediment size was used for these tests to prevent armouring or paving. Thus the tests are still very much an idealisation of the natural situation.

The objectives of the sediment transport series of tests were as follows:

(a) Average and maximum velocities were to be measured to see when, with sediment transport, flow through a step-pool system would become potentially erosive.

(b) To investigate the applicability of conventional sediment transport formulae to a step-pool system.

(c) Flow regimes were to be observed to see if the model gave a reasonable representation of a natural step-pool streams behaviour.

[Some material from this chapter has been prepared as a paper entitled 'Erosion and sediment transport processes in step-pool torrents' by J.G. Whittaker and T.R.H. Davies. The paper is being presented to the first I.A.H.S. Scientific General Assembly, Exeter, U.K. (July 1982) in the Symposium 'Recent developments in the explanation and prediction of erosion and sediment yield'. A copy of the manuscript is found in Appendix 4].

7.2 SEDIMENT TRANSPORT THEORIES

Yalin (1977) writes '... in spite of intense research activity, our knowledge of the mechanics of sediment transport, i.e. of the

quantitative and universally applicable laws governing the motion of the transporting fluid and the transported sediment remains remarkably meagre'. This is certainly true for sediment transport in step-pool systems.

As discussed above, bedload transport rates in steep mountain streams are not controlled only by the availability of transportable bed material. A sediment transport model must, then, calculate transport rates as a function of hydraulic conditions, sediment inflows, and changes in storage of the sediment being transported (Jackson, 1981).

However, most theoretical sediment transport relationships are confined to cohesionless granular materials and to steady and uniform flows, which can only be treated as two-dimensional (Yalin, 1977). Because of these restraints, it is recognised that theoretical sediment transport relationships are inapplicable to steep mountain streams (Beschta, 1981; Hayward, 1978, 1980; Jackson, 1981). In spite of this, certain sediment transport relationships can be modified to account for some of the peculiarities of such streams.

The 'Swiss formula' of Meyer-Peter and Müller (1948, 1949) can be expressed as follows for the case of a steady and uniform two-dimensional flow

$$\frac{\gamma Jh}{\gamma_s D} = 0.047 + 0.025 \left(\frac{\gamma}{g}\right)^{1/3} \frac{q_s^{2/3}}{\gamma_s D} \qquad \ldots 7.1$$

The original expression of Meyer-Peter and Müller was not only restricted to plane beds and two-dimensional flows. The term $\frac{\gamma Jh}{\gamma_s D}$ was prefexed by the multiplier m where

$$m = \frac{Q_1}{Q} \left(\frac{J_r}{J}\right)^{3/4} \qquad \ldots 7.2$$

Here J and Q are the slope and flow rate of the channel respectively; Q_1 is that part of Q whose energy is converted into eddying on the bed; J_r is the purely frictional part of the slope. In general, $m \leq 1$.

Ashida et al (1976, 1981) recognised that the rollers in the pools at the bottom of steps consume considerable energy, and therefore the effective slope for transportation of sediment should be much flatter than actual topographical inclination. Further, they found that when storage of sediment within the channel exceeded a certain value, sediment

transport approached a sort of equilibrium, where flow rates and sediment discharges were related, i.e. a bedload formula could be used. Consequently, they suggested modifying the Meyer-Peter and Müller formula for these conditions, i.e. $m < 1$. In this sense, m can be considered an 'efficiency' of bedload transport.

Hayward (1978, 1980) found that for the Torlesse Stream, Bagnold's (1966) concept of stream power and efficiency of the stream power for bedload transport showed close agreement with measured values. Conventional bedload prediction equations were found to over-estimate sediment yields by up to several orders of magnitude. The proportion of stream power expended in bedload transport in 'average conditions' was found to be less than 1%.

Using the symbols of Yalin (1977), Bagnold (1956) gave this efficiency as e_b where

$$e_b = (\tan \psi_o) \frac{q_s}{[\tau_o - (\tau_o)_{cr}]\, u_D} \qquad ...7.3$$

where $\tan \psi_o$ = friction slope of the channel

q_s = specific transport rate

and u_D = velocity in the vicinity of the bed.

Then

$$q_s = \frac{e_b}{\tan \psi_o} [\tau_o - (\tau_o)_{cr}]\, u_D \qquad ...7.4$$

but $\tau_o\, u_D$ is stream power ω

$$q_s = \frac{e_b}{\tan \psi_o} [\omega - \omega_o] \qquad ...7.5$$

However, in his 1966 paper, Bagnold derived the equation (considering only the bedload part)

$$q_{sb} = \tau_o\, u_m \frac{e_b}{\tan \psi_o} \qquad ...7.6$$

where u_m = mean velocity of flow.

Then

$$q_{sb} = \omega \frac{e_b}{\tan \psi_o} \qquad ...7.7$$

But $e_b = \phi_1$ (X, Y, W) (Yalin, 1977)

where $X = \frac{v_* D}{\nu}$, the grain-size Reynolds number

$Y = \frac{\rho v_*^2}{\gamma_s D}$, a mobility number

$W = \frac{\rho_s}{\rho} = 2.65$

and ϕ_1 = a function of

Thus e_b cannot be chosen arbitrarily. Using flume data, Bagnold (1977) showed that

$$q_{sb} = \frac{1}{\tan \psi_o} \frac{[\omega - \omega_o]^{3/2}}{\omega_o^{1/2}} \times \left(\frac{h}{D}\right)^{-2/3} \qquad ...7.8$$

where ω_o, the value of ω at the onset of sediment motion was introduced to remove curvature from a log-log plot of q_{sb} versus ω.

so $$e_b = \left(\frac{[\omega - \omega_o]}{\omega_o}\right)^{1/2} \left(\frac{h}{D}\right)^{-2/3} \qquad ...7.9$$

implying $$e_b = \phi_2 (X, Y, Z, W) \qquad ...7.10$$

where $Z = \frac{h}{D}$, a dimensionless granular roughness.

From a fairly incomplete graph, Leopold and Emmett (1976) tentatively proposed efficiencies ranging from 25% for fine sand to about 1% for particles of 30 mm to 50 mm.

Bagnold (1977) implied that at high slopes ω would be augmented by an additional element $q_{sb}J$ due to the gravity component acting directly on the solids. This makes the formula inapplicable to streams at high slopes, other than step-pool mountain torrents. The formula is still applicable to mountain torrents because flows of super-saturated solids are far more difficult to instigate in step-pool beds than on a steep plane bed. Obviously then, for torrents the efficiency e_b will be affected by the falls and pools; however, the relationship between this effect on e_b due to falls and pools and the increase due to the component $q_{sb}J$ is not known.

A different approach to the effect of deviating from the plane bed assumption was used by Jäggi (1978), who presented the Meyer-Peter and Müller formula in the dimensionless form

$$\frac{gRJ}{(s-1)g\ D} = 0.047 + 0.25 \left[\frac{q_b}{(s-1)^{0.5}\ g^{0.5}\ D^{1.5}}\right]^{0.667} \qquad ...7.11$$

or $$\theta = 0.047 + 0.25\ \phi^{0.667} \qquad ...7.12$$

where $$\theta = \frac{gRJ}{(s-1)g\ D} \text{ and } \phi = \frac{q_b}{(s-1)^{0.5}\ g^{0.5}\ D^{1.5}}$$

Considering the effect of form roughness (of which steps and pools may be considered to be gross components), Meyer-Peter and Müller reduced the product $R_s J$ (where R_s = hydraulic radius of partial area acting on the bed) by the factor

$$\left(\frac{k_s}{k_r}\right)^{1.5}$$

Here k_s is a Strickler roughness coefficient which indicates total bed resistance, while k_r is the grain roughness only. The exponent 1.5 was determined empirically. R_s was introduced to account for the effect of cross-sectional or bank roughness, and thus can be considered to be the result of a wall correction procedure. (For the evaluation of R_s, see Jäggi (1978)).

Instead of θ being used, θ' is determined as

$$\theta' = \frac{\left(\frac{k_s}{k_r}\right)^{1.5} R_s\ J}{(s-1)\ D_m} \qquad ...7.13$$

Jäggi (1978) states that the region of validity of the Meyer-Peter and Müller equation is

$$0 < \theta' < 0.2$$

With $\left(\frac{k_s}{k_r}\right)^{1.5} \simeq 0.75$, this limits the applicability of the formula to slopes of less than 2% (Jäggi, 1978). Jäggi simplified Einstein's (1942, 1950) bedload formula to

$$P = 1 - \frac{1}{\sqrt{\pi}} \int_{-(0.143\ \psi-2)}^{0.143\ \psi-2} e^{-t^2}\ dt = \frac{43.5\ \phi_b}{1 + 43.5\ \phi_b} \qquad ...7.14$$

where P is the probability of grains being transported. The probability integral is tabulated in specialised literature, and from such tables

Einstein has diagramatically presented the formula as a relation between ψ and ϕ_b.

$$\psi = \frac{\rho_s - \rho}{\rho} \frac{D}{RJ} = \frac{(s-1)g\ D}{gRJ} = \frac{1}{\theta} \qquad ...7.15$$

To account for the loss due to form drag, Einstein introduced reduced inverse relative shear stress

$$\psi' = \frac{(s-1)\ D}{R'\ J} \qquad ...7.16$$

Here
$$R' + R'' = R_s \qquad ...7.17$$

(see also Yalin, 1977, p 133)
where R" = part of the hydraulic radius due to form drag.

Jäggi (1978) states the region of validity of Einstein's relaionship as $0 < \theta' < 1.0$, i.e. the Einstein formula can be used at slopes of up to about 20% for typical values of R' in rivers.

For riffle-pool gravel bed rivers (such as discussed in section 2.4), the Meyer-Peter and Müller formula is disadvantaged in that it assumes that all grains are in motion (Jäggi, 1978), which does not allow for formation of an armour layer. If gradation of transported material is small, Einstein uses D_{35} as a representative grain size in his formula. However, if there is a significant difference between D_m and D_{35}, bedload can be calculated step-wise using

$$D = \sqrt{D_1 D_2} \qquad ...7.18$$

where D_1 and D_2 are the limiting diameters of the part of the sediment under consideration. For low transport rates, an armour layer could presumably be evaluated.

Ashida et al (1981) recognised that sediment transport occurs in modes other than that of simple bedload. They listed the primary modes of sediment transport mathematically as

$$\tau_{*c} = 0.4 \times 10^{1.72\ I} \qquad ...7.19$$

$$I = \frac{c_* (\rho_s - \rho) \tan \phi_a}{c_* (\rho_s - \rho) + \rho(1 + \frac{h}{D})} \qquad ...7.20$$

$$I = \frac{c_* (\rho_s - \rho) \tan \phi_a}{c_* (\rho_s - \rho) + \rho(1 + K^{-1})} \qquad ...7.21$$

$$I = \frac{c_* \ (\rho_s - \rho) \ \tan \phi_a}{c_* \ (\rho_s - \rho) + \rho} \qquad \ldots 7.22$$

$$I = \tan \alpha \qquad \ldots 7.23$$

where c_* = grain concentration in volume in the static debris bed

h = depth of flow

D = diameter of grain

$I (\tan \alpha)$ = channel slope

τ_{*c} = Shield's value of critical tractive force

ρ_s and ρ = densities of grain and fluid respectively

ϕ_a = internal friction angle

and K = an experimental constant.

By plotting these equations, the various types of transport mode are delineated (fig. 7-1).

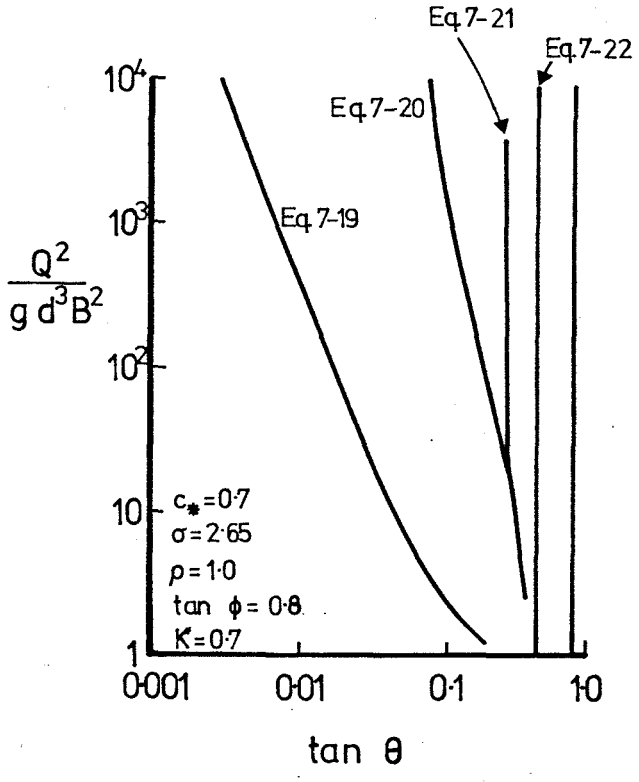

Figure 7-1: Criteria for various modes of sediment transport (After Ashida et al., 1981).

Ashida et al (1981) note that the region to the right of a particular curve is for the occurrence, not the movement; e.g. a debris flow can sometimes reach downstream areas with rather mild slope. As noted in an earlier paper (i.e. Ashida et al, 1976) when commenting on applying the Meyer-Peter and Müller formula to bedload prediction, the effective slope for sediment transport in step-pool streams should be much flatter than the topographic inclination of the channel.

Thus, equation 7.19 would need to be moved to the left in the diagram according to the extent of the energy dissipation in the pools. Mizuyama (1981) describes the characteristics of the three types of debris flow arising from the classification.

Type 1 : Mild Slopes; sediment concentration in the moving layer is high, but the surface flow is clearly seen. Although this is sometimes regarded as individual transport on a mild slope, in steeper slopes it is regarded as mass movement because the moving sediment layer has a velocity distribution.

Type 3 : The bore of the flow is clearly seen, with coarser materials gathering in the front of the flow. The surface flow can not be seen.

Type 2 : This is a variation of Type 3. At the front of the flow a bore forms, but stops, creating a dune. This builds, until the flow moves on (to stop again etc).

Type 1 is considered to be a transitional debris flow, or an intermediate phenomenon between debris flow and bedload transport.

All the above relations are concerned with sediment transport processes in the stream channel itself. However, as noted in Chapter 2, sediment supply is often a limiting factor, and so any transport formula adjusted for energy dissipation in pools will only given an upper envelope of actual transport occurring in the field. Griffiths (1980) developed a stochastic model of bedload yield from step-pool streams taking this into consideration. He predicted the total expected bedload yield from a given basin, in a prescribed interval, through the convolution of a Poisson number of events with an exponential probability of bedload yield. The exponential distribution is defined from

regional flood frequency relations, an empirical bedload transport formula, and flow records from a nearby basin within the same hydrologic regime as the one under consideration. Griffiths recognised that the application required input data from a nearby reference catchment, but despite this difficulty, emphasised the potential of the methodology for dealing with bedload transport in mountain watersheds.

7.3 TESTS

In this series, tests were performed at slopes of 0.027, 0.098, 0.172 and 0.248. At each slope, several values of flow rate were investigated. For each flow rate, a series of sediment transport rates were introduced. When equilibrium had been established, i.e. the sediment output rate from the flume equalled the sediment input rate, average (and maximum) velocities were measured using the salt-velocity technique. Photographs were also taken to allow the extent, dimensions and shape of the scour to be determined.

7.4 RESULTS

The results for this series of tests are listed in table 7.1.

7.4.1 Flow Regime

The flow regimes discussed in section 6.5.1 provide initial conditions for the regimes realised with sediment transport. Slope and sediment transport rate influenced regime markedly, resulting in the regimes shown in fig. 7-2(a) to (c).

One clear feature of fig. 7-2 is the occurrence of sediment waves which form despite constant sediment input. Observations of the trends in the form of the scour hole with sediment transport are listed in Appendix 5.

7.4.2 Scour with Sediment Transport

Values of % scour for this series of tests were evaluated by the procedure described in section 6.4.2. The results are listed in table 7.1, and % scour is plotted against transport rate in fig. 7.3(a) to (d).

TABLE 7.1 RESULTS OF SEDIMENT TRANSPORT TESTS

Run Number	Slope J	Specific Discharge $q(m^3s^{-1}/m)$	Sediment Transport Rate Q_s (kg/min)	Mean Velocity v_m (m/s)	Maximum Velocity v_{max} (m/s)	Depth h (m)	Hydraulic Radius R(m)	Froude Number F	Friction Factor f	Depth of Scour S(m)	Depth of Flow at Max Scour S_o(m)	% Scour
65	0.098	0.022	0.000	0.185	0.296	0.117	0.116	0.224	26.29	0.135	0.148	-
64	0.098	0.022	1.525	0.216	0.347	0.100	0.099	0.283	16.46	0.102	0.124	16.39
81	0.098	0.022	2.139	0.269	0.529	0.083	0.082	0.387	8.79	0.093	0.114	14.83
1	0.098	0.022	2.791	0.390	0.503	0.057	0.056	0.677	2.85	0.087	0.102	12.15
2	0.098	0.022	3.678	0.577	0.718	0.039	0.038	0.933	0.88	0.078	0.093	10.80
4	0.098	0.022	5.352	0.644	0.773	0.035	0.034	1.427	0.63	0.051	0.059	6.02
3	0.098	0.022	5.852	0.790	-	0.028	0.027	1.957	0.33	0.045	0.051	5.57
5	0.098	0.021	9.096	0.616	1.005	0.034	0.033	1.385	0.67	0.024	0.033	-0.30
6	0.098	0.023	11.197	0.753	-	0.030	0.029	1.802	0.39	-	-	0.54
66	0.098	0.039	0.965	0.267	0.437	0.145	0.144	0.291	15.59	0.146	0.180	35.52
67	0.098	0.039	4.862	0.306	0.591	0.126	0.125	0.357	10.29	0.104	0.128	20.75
68	0.098	0.039	8.775	0.501	0.914	0.077	0.075	0.749	2.32	0.046	0.072	4.80
69	0.098	0.039	11.878	0.907	0.914	0.043	0.041	1.813	0.38	0.043	0.067	4.05
7	0.098	0.058	2.329	0.404	0.523	0.144	0.142	0.441	6.71	0.124	0.186	31.07
8	0.098	0.058	3.991	0.492	0.613	0.118	0.116	0.594	3.69	0.114	0.155	27.34
9	0.098	0.058	5.688	0.516	0.644	0.113	0.110	0.636	3.21	0.101	0.142	22.82

TABLE 7.1 CONTD.

Run Number	Slope J	Specific Discharge $q(m^3s^{-1}/m)$	Sediment Transport Rate Q_s (kg/min)	Mean Velocity v_m (m/s)	Maximum Velocity v_{max} (m/s)	Depth h (m)	Hydraulic Radius R(m)	Froude Number f	Friction Factor f	Depth of Scour S(m)	Depth of Flow at Max Scour S_o(m)	% Scour
10	0.098	0.058	9.611	0.627	0.698	0.092	0.089	0.857	1.76	0.082	0.131	15.90
11	0.098	0.058	13.098	0.711	0.761	0.081	0.078	1.036	1.20	0.081	0.110	13.84
12	0.098	0.091	1.441	0.542	0.628	0.168	0.164	0.548	4.32	0.112	0.192	28.19
13	0.098	0.091	3.059	0.547	0.739	0.166	0.162	0.557	4.19	0.106	0.194	26.03
14	0.098	0.091	4.975	0.623	0.810	0.146	0.142	0.676	2.82	0.096	0.159	22.14
15	0.098	0.091	7.665	0.666	0.866	0.137	0.133	0.746	2.31	0.089	0.160	20.77
16	0.098	0.091	12.558	0.811	0.897	0.113	0.108	1.000	1.27	0.086	0.141	18.21
17	0.098	0.127	2.202	0.739	0.966	0.171	0.165	0.741	2.33	0.096	0.169	23.89
18	0.098	0.127	3.683	0.839	1.092	0.151	0.144	0.895	1.59	0.091	0.166	21.88
19	0.098	0.127	5.817	0.834	1.142	0.152	0.146	0.887	1.62	0.082	0.148	18.97
20	0.098	0.127	8.153	0.850	1.092	0.149	0.142	0.913	1.52	0.084	0.139	17.98
21	0.098	0.127	12.939	0.915	1.396	0.138	0.131	1.021	1.21	0.068	0.127	15.09
78	0.027	0.033	0.000	0.468	0.838	0.070	0.066	0.687	0.64	0.032	0.055	4.59
77	0.027	0.033	0.599	0.754	1.117	0.044	0.039	1.396	0.15	0.017	0.047	2.02
70	0.027	0.033	1.318	0.757	1.142	0.043	0.038	1.418	0.14	0.009	0.036	-0.85

TABLE 7.1 CONTD.

Run Number	Slope J	Specific Discharge $q(m^3s^{-1}/m)$	Sediment Transport Rate Q_s (kg/min)	Mean Velocity v_m (m/s)	Maximum Velocity v_{max} (m/s)	Depth h (m)	Hydraulic Radius R(m)	Froude Number F	Friction Factor f	Depth of Scour S(m)	Depth of Flow at Max Scour S_o(m)	% Scour
22	0.027	0.033	1.827	0.835	1.142	0.040	0.035	1.622	0.11	0.006	0.040	-0.84
23	0.027	0.033	3.642	0.826	1.256	0.040	0.035	1.604	0.11	DEPOSITION		-8.93
80	0.027	0.077	0.000	0.562	0.718	0.138	0.128	0.588	0.86	0.064	0.175	16.07
79	0.027	0.077	0.377	0.761	0.966	0.102	0.091	0.926	0.33	0.037	0.115	7.41
71	0.027	0.077	1.377	0.801	1.047	0.097	0.086	0.999	0.28	0.035	0.083	6.12
24	0.027	0.077	2.181	0.903	1.256	0.086	0.074	1.196	0.19	0.039	0.088	6.78
25	0.027	0.077	5.052	1.127	1.675	0.069	0.056	1.667	0.09	0.013	0.066	0.36
26	0.027	0.077	7.312	1.106	1.675	0.070	0.057	1.624	0.10	DEPOSITION		-2.63
76	0.027	0.109	0.571	0.771	0.897	0.141	0.125	0.798	0.45	0.050	0.147	13.18
72	0.027	0.109	1.414	0.928	1.092	0.117	0.100	1.054	0.25	0.051	0.134	11.92
27	0.027	0.109	2.545	0.986	1.196	0.110	0.093	1.155	0.20	0.036	0.104	7.42
28	0.027	0.109	5.810	1.140	1.675	0.095	0.077	1.437	0.13	0.018	0.091	2.04
29	0.027	0.109	8.809	1.237	1.675	0.088	0.069	1.620	0.10	DEPOSITION		-4.38
73	0.027	0.138	0.000	0.759	0.931	0.182	0.162	0.691	0.60	0.070	0.206	18.02
75	0.027	0.138	0.864	0.910	1.196	0.152	0.131	0.907	0.33	0.060	0.186	13.62

TABLE 7.1 CONTD.

Run Number	Slope J	Specific Discharge $q(m^3s^{-1}/m)$	Sediment Transport Rate Q_s (kg/min)	Mean Velocity v_m (m/s)	Maximum Velocity v_{max} (m/s)	Depth h (m)	Hydraulic Radius R(m)	Froude number F	Friction Factor f	Depth of Scour S(m)	Depth of Flow at Max Scour S_o(m)	% Scour
31	0.027	0.138	1.363	0.875	1.142	0.157	0.136	0.858	0.38	0.048	0.166	10.99
74	0.027	0.138	2.137	0.988	1.322	0.140	0.118	1.026	0.26	0.034	0.136	7.52
30	0.027	0.138	2.933	1.107	1.322	0.124	0.101	1.221	0.18	0.031	0.124	6.66
32	0.027	0.138	6.822	1.179	1.795	0.117	0.094	1.339	0.14	DEPOSITION		-3.19
33	0.027	0.140	9.424	1.330	1.795	0.105	0.080	1.595	0.10	DEPOSITION		-4.19
48	0.172	0.012	2.253	0.118	0.372	0.101	0.101	0.162	96.32	0.101	0.097	11.44
49	0.172	0.012	3.995	0.136	0.479	0.087	0.087	0.201	62.44	0.082	0.080	8.86
50	0.172	0.012	6.730	0.148	0.558	0.080	0.080	0.229	48.47	0.064	0.073	5.79
51	0.172	0.012	10.102	0.184	0.558	0.065	0.065	0.315	25.45	0.046	0.054	3.02
52	0.172	0.012	13.460	0.309	0.628	0.038	0.038	0.692	5.26	0.035	0.041	0.99
39	0.172	0.017	1.355	0.161	0.347	0.105	0.105	0.217	53.74	0.148	0.141	22.41
40	0.172	0.017	3.408	0.157	0.347	0.106	0.106	0.211	57.05	0.121	0.120	16.77
41	0.172	0.017	5.089	0.192	0.402	0.087	0.087	0.284	31.28	0.098	0.102	11.18
42	0.172	0.017	7.335	0.212	0.529	0.079	0.079	0.330	22.29	0.092	0.098	10.89
43	0.172	0.017	11.384	0.246	0.591	0.068	0.068	0.412	14.87	0.071	0.081	7.72

TABLE 7.1 CONTD.

Run Number	Slope J	Specific Discharge $q(m^3s^{-1}/m)$	Sediment Transport Rate Q_s (kg/min)	Mean Velocity v_m (m/s)	Maximum Velocity v_{max} (m/s)	Depth h (m)	Hydraulic Radius R(m)	Froude Number F	Friction Factor f	Depth of Scour S(m)	Depth of Flow at Max Scour S_o(m)	% Scour
34	0.172	0.028	1.706	0.187	0.299	0.149	0.148	0.212	56.49	0.174	0.179	33.41
35	0.172	0.028	3.592	0.211	0.375	0.132	0.131	0.254	39.28	0.167	0.171	33.56
36	0.172	0.028	5.999	0.214	0.314	0.130	0.129	0.259	37.60	0.135	0.151	33.27
37	0.172	0.028	8.781	0.279	0.457	0.100	0.099	0.386	16.99	0.111	0.128	16.71
38	0.172	0.028	11.068	0.279	0.529	0.100	0.099	0.386	16.99	0.103	0.126	13.70
44	0.172	0.049	1.401	0.236	0.375	0.208	0.207	0.226	49.44	0.225	0.259	61.61
45	0.172	0.049	3.438	0.269	0.419	0.181	0.180	0.276	33.08	0.202	0.232	52.02
46A	0.172	0.049	6.150	0.278	0.419	0.177	0.176	0.289	30.28	0.188	0.218	47.28
46	0.172	0.049	9.265	0.287	0.457	0.171	0.170	0.303	27.44	0.177	0.206	43.80
47	0.172	0.049	11.549	0.315	0.558	0.157	0.156	0.347	20.90	0.171	0.199	41.11
53	0.248	0.012	2.403	0.112	0.324	0.111	0.111	0.145	182.93	0.135	0.115	20.67
54	0.248	0.012	3.816	0.130	0.503	0.091	0.091	0.195	101.56	0.114	0.097	17.98
55	0.248	0.012	6.785	0.150	0.558	0.075	0.075	0.259	57.36	-	-	-
56	0.248	0.012	10.619	0.149	0.718	0.079	0.079	0.240	67.09	-	-	-
57	0.248	0.012	14.091	0.157	0.718	0.075	0.075	0.259	57.36	-	-	-

C/T

TABLE 7.1 CONTD.

Run Number	Slope J	Specific Discharge $q(m^3 s^{-1}/m)$	Sediment Transport Rate Q_s (kg/min)	Mean Velocity v_m (m/s)	Maximum Velocity v_{max} (m/s)	Depth h (m)	Hydraulic Radius R(m)	Froude Number F	Friction Factor f	Depth of Scour S(m)	Depth of Flow at Max Scour S_o(m)	% Scour
59	0.248	0.027	2.780	0.191	0.437	0.139	0.139	0.232	71.78	0.190	0.178	38.24
60	0.248	0.027	6.223	0.183	0.372	0.145	0.145	0.217	81.58	0.166	0.155	30.59
61	0.248	0.027	9.358	0.193	0.419	0.137	0.137	0.236	69.29	0.151	0.152	27.96
62/63	0.248	0.027	13.201	0.226	0.419	0.117	0.117	0.299	43.12	0.132	0.134	24.13

Also listed in table 7.1 are scour depth S, and depth of flow at the point of maximum scour S_o.

7.4.3 Average and Maximum Velocities

Values of average and maximum velocities for each test are listed in table 7.1. Further, average velocities are plotted versus sediment transport rate in fig. 7-10, while maximum velocities are plotted versus sediment transport rate in fig. 7-11.

7.4.4 Resistance to Flow

Darcy-Weisbach friction factor f was calculated for each test using the wall correction procedure as outlined in Gessler (1965). Average velocity was used for the velocity value in the calculation. Values are listed in table 7.1, and are plotted in fig. 7-12 versus sediment transport rate.

7.5 DISCUSSION OF RESULTS

7.5.1 Flow Regime

The distinct flow regimes observed for the clear water flow and clear water scour cases break down very quickly as sediment transport is introduced to the model.

Slope = 0.027

The flow regimes observed for slope = 0.027 are shown in fig. 7-2(a). An interesting feature is the increase in the stable tumbling flow regime zone with increasing Q_s, with a consequent decrease in the zone of unstable tumbling flow. Sediment waves, shown as a regular variation in the degree of pool infilling formed at low sediment transport rates.

Slope = 0.098

The regimes shown in fig. 7-2(b) are radically different from those occurring at slope = 0.027. The zone of unstable flow is much larger, although the intensity of the instability decreases with increasing sediment transport rate. Interestingly, flow instability occurs at higher values of Q_s for test runs which were initially of the stable tunbling regime.

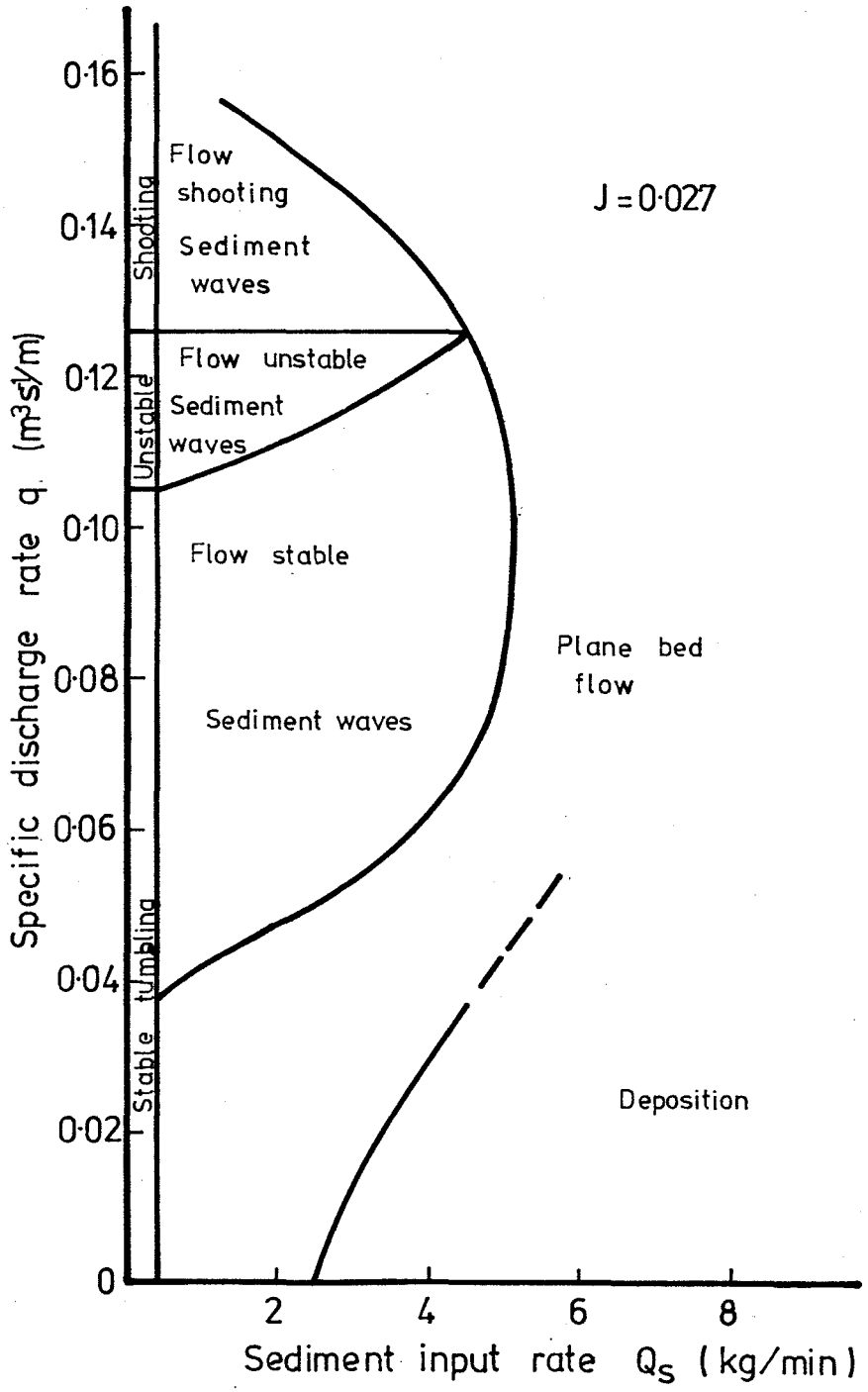

Figure 7-2(a): Flow regimes with sediment transport (J = 0.027).

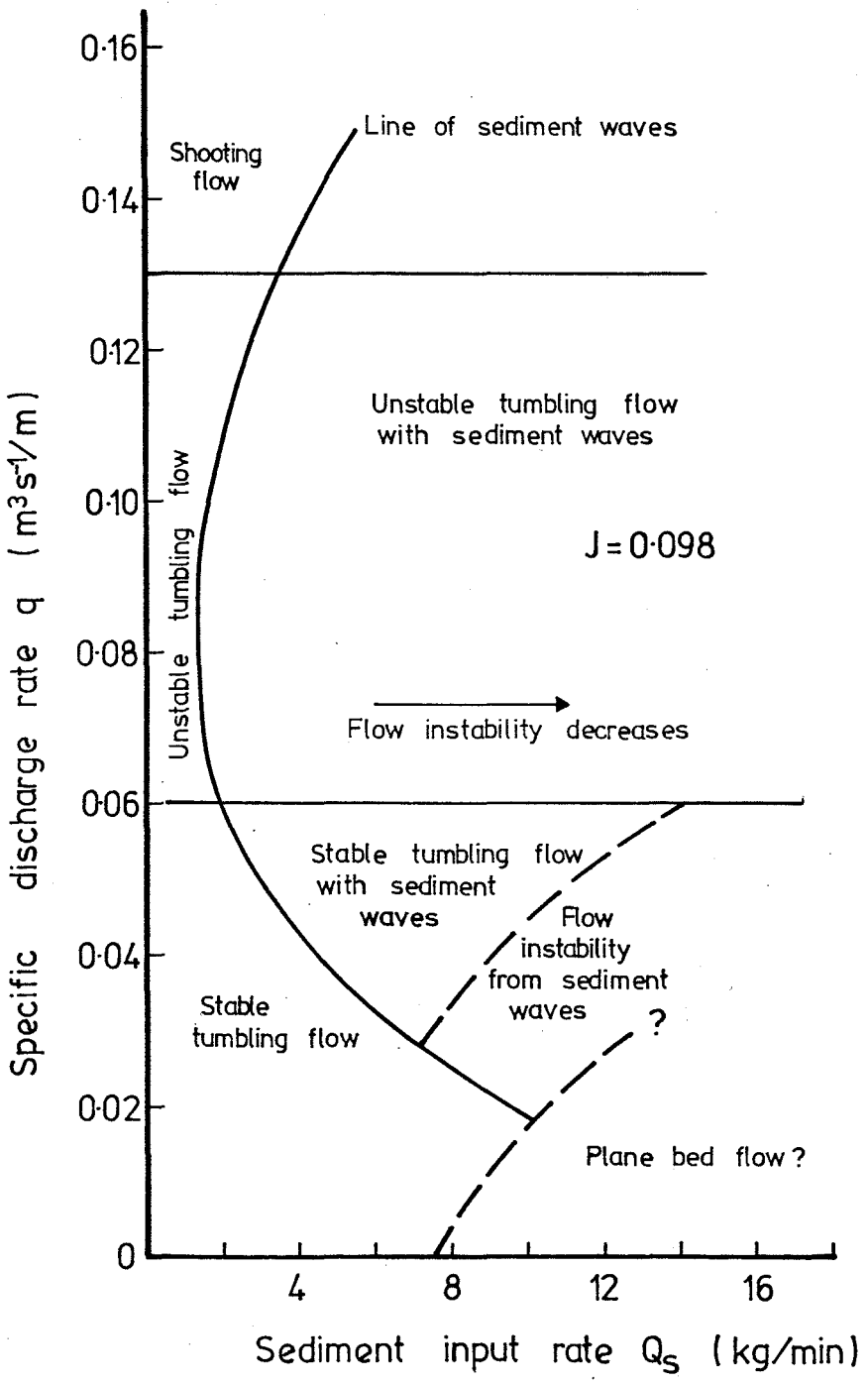

Figure 7-2(b): Flow regimes with sediment transport (J = 0.098).

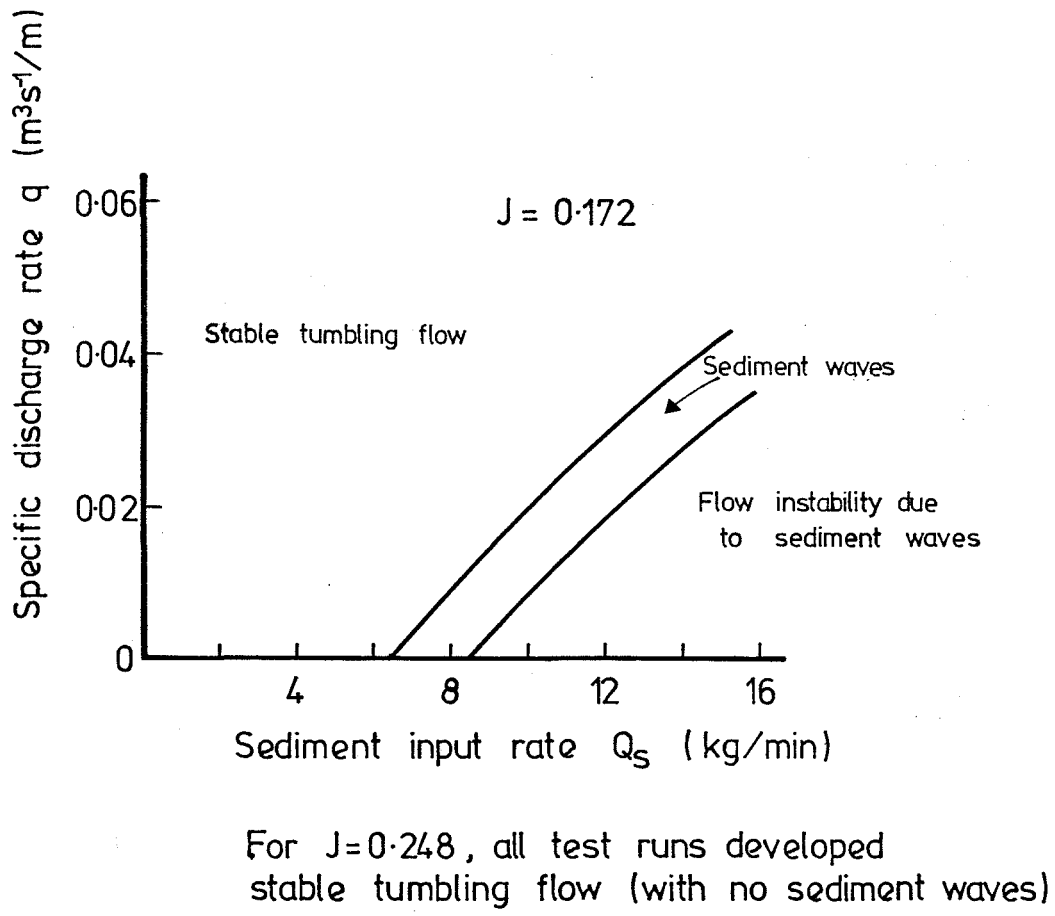

Figure 7-2(c): Flow regimes with sediment transport (J = 0.172).

Slopes = 0.172 and 0.248

All the flow-sediment transport rate combinations for J = 0.248 showed the flow to be stable tumbling, with no accompanying sediment wave formation.

Fig. 7-2(c) shows that for tests performed at slope = 0.172, sediment waves forming under stable tumbling flow triggered a flow instability at low flow rates.

General

Roll waves in an alluvial environment are seen to be dangerous because of their potential erosivity (Morris; 1968; Schumm et. al, 1982). Therefore, it is of interest to evaluate the likelihood of roll waves occurring in alluvial channels. The present tests indicate that for steep slopes, they will occur even at low flow rates if the sediment transport rate is sufficiently high (see fig. 7-2(c)). However, as flow rate increases, a much higher sediment transport rate is required to produce unstable flow.

Input of sediment to a steep mountain stream is usually of a bulk nature, and usually only occurs at reasonably high flow rates. With much sediment available for transport fig. 7-2(b) and (c) indicate that flow instability may occur under such flow conditions, and on the receding limb of the hydrograph.

However, sediment from a bulk input travels through a steep mountain stream as a discrete wave. Any flow instability generated would occur only in the vicinity of such a wave. The likelihood of their incipient generation is reduced by the random step length common in mountain streams (Rouse, 1938). If roll waves did form, they would be absorbed by the non-sediment-inundated channel immediately downstream of the sediment wave. The laboratory tests thus indicate that unstable flow could only occur rarely in natural streams with sediment input.

7.5.2 Scour

Fig. 7-3(a) to (d) shows % scour versus sediment transport rate for different flow rates and slopes.

Slope = 0.027

At this slope (fig. 7-3(a)) % scour decreases rapidly with increasing sediment transport rate. Flow regime plays an important part in this

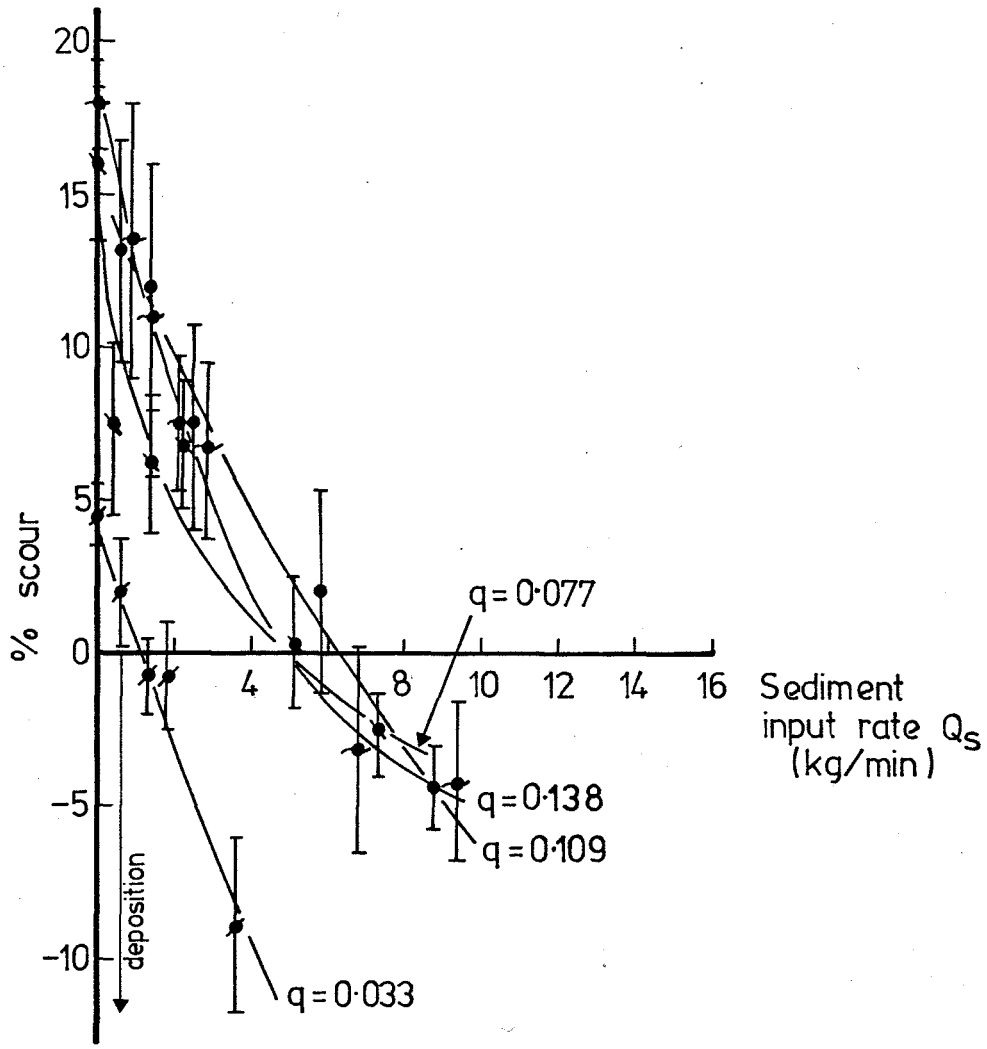

(a) J = 0·027

Figure 7-3(a): Plot of % scour versus sediment input rate (J = 0.027).

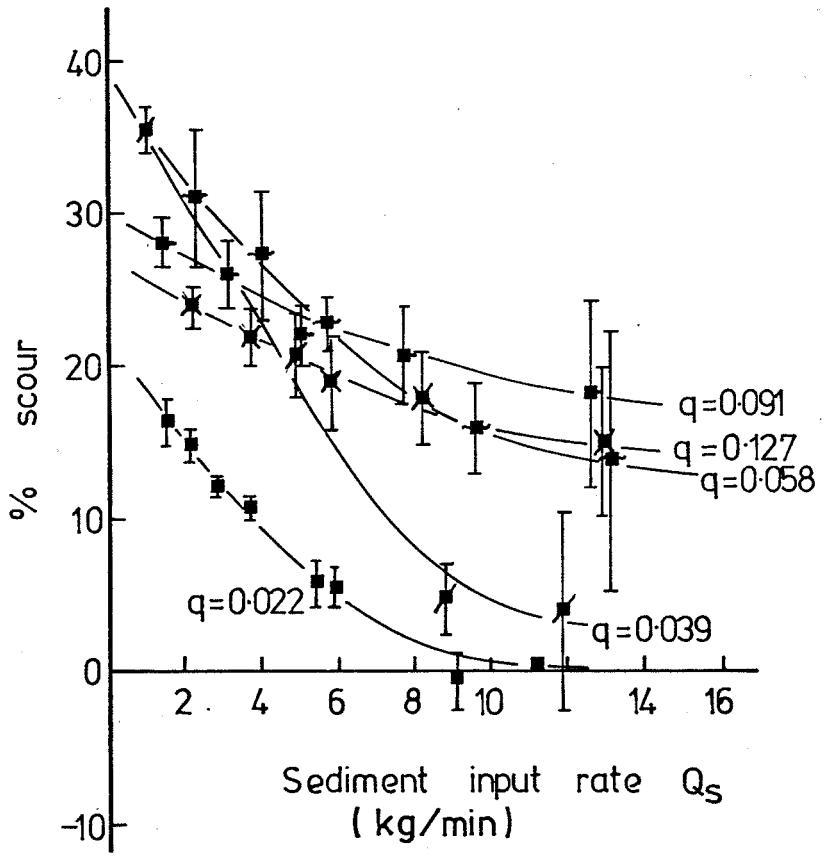

Figure 3-7(b): Plot of % scour versus sediment input rate (J = 0.098).

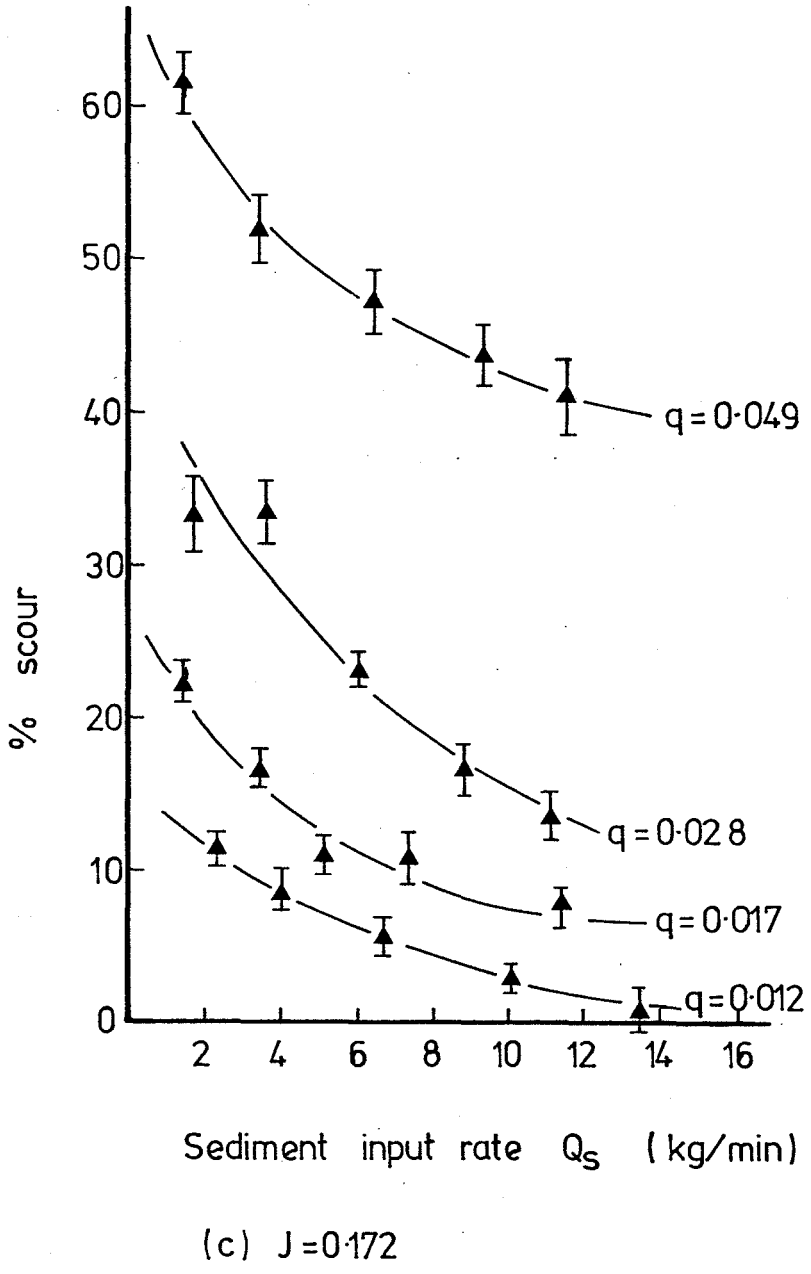

Figure 7-3(c): Plot of % scour versus sediment input rate (J = 0.172).

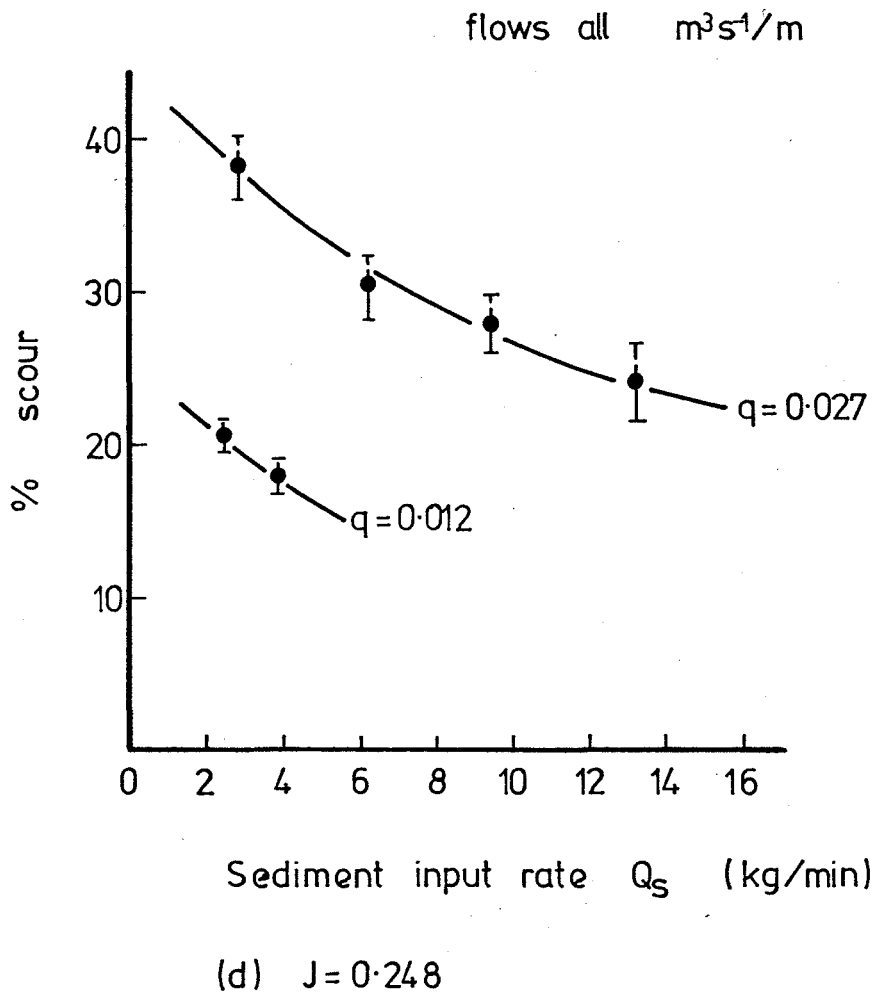

Figure 7-3(d): Plot of % scour versus sediment input rate (J = 0.248).

relationship (see section 7.5.1). The lower two flow rates, both with the initial regime of stable tumbling flow, show threshold sediment transport rates above which scour ceases, and deposition of sediment occurs. Similarly, the next higher flow rate, with the initial regime of unstable tumbling flow, exhibits a higher threshold again. However, the threshold required to produce deposition for the highest flow rate (initial regime is shooting flow) is reduced from that of the flow rate with the initial regime of unstable tumbling flow. Obviously the clockwise eddy (flow down the channel assumed to be from left to right) results in the shooting flow regime being less effective in transporting sediment through the stepped system, allowing filling of the scour zone at lower Q_s values.

Slope = 0.098

% scour decreases with increasing Q_s at about the same rate or less rapidly for this slope than assumed for slope = 0.027 (see fig. 7-3(b)). No net deposition occurred for any flow rates. Instead, the % scour associated with the lowest flow rate asymptotically approaches zero. Similarly, the next higher flow rate indicates a strong reduction in % scour with increasing Q_s toward an asymptotic value. The standard errors show, however, that strong sediment wave formation is occurring.

As the flow rate increases, a change in trend of % scour with Q_s is noticeable. The trend in % scour for the two highest flow rates (both with initial regime of unstable tumbling flow) suggests that very high transport rates would be required to reduce the % scour to zero. (Their relative positions reflect the respective values of % scour at $Q_s = 0$).

Slopes = 0.172 and 0.248

For these slopes, figs. 7-3(c) and (d) tend to indicate an almost linear relationship between % scour and sediment transport rate.

General

Fig. 7-3 tends to indicate a continuous trend in behaviour of scour reduction with increasing sediment transport rate and increasing slope. At slope = 0.027, the scour zone is easily swamped with gravel, while at higher slopes the system becomes much harder to inundate with gravel.

An interesting feature of the tests performed was that, with steady inputs of water and sediment not only the previously mentioned

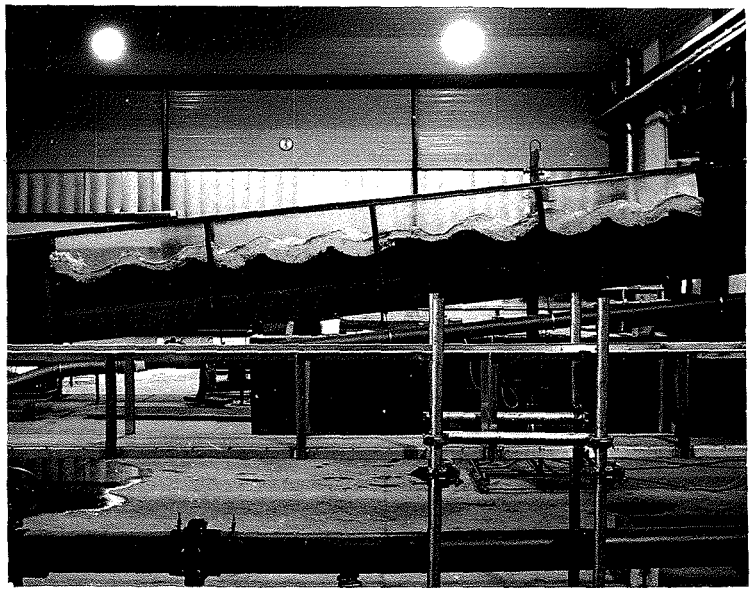

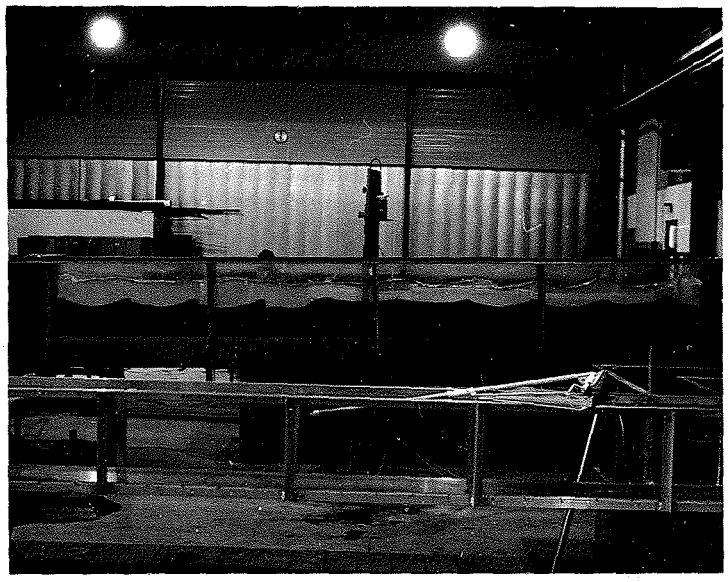

Figure 7-4: Sediment waves.

roll waves but also sediment waves occurred independently (see Appendix 5). The sediment waves were manifested by periodic variations in the degree of pool infilling along the channel, as is observable from the standard error values shown in fig. 7-3. Some of these waves are shown in fig. 7-4.

With an initial regime of stable tumbling flow, the waves of sediment sometimes precipitated flow instability by deforming the scour zone. However, with an initial regime of unstable tumbling flow, increasing sediment transport rate tended to damp the instability. At higher sediment transport rates when strong sediment waves were present, the flow modification due to the boundary sometimes caused complex patterns of flow instability.

As noted in section 2.4, sediment input to a step-pool channel is usually of a bulk nature. Further, these bulk inputs tend to travel through a step-pool system as discrete waves (Ashida et al, 1976; Hayward, 1978, 1980). However, while sediment waves moved through their sampling station, Ashida et al (1976) noted that there was a great variability in sediment transport rate, despite the averaged time rate of transport being essentially constant. This variability may be caused by waves such as observed in the model. Thus the long wave due to the bulk input is moved as a series of smaller waves. The actual mechanism of transport was seen to operate as follows:

Consider a pool at time t_1 (fig. 7-5)

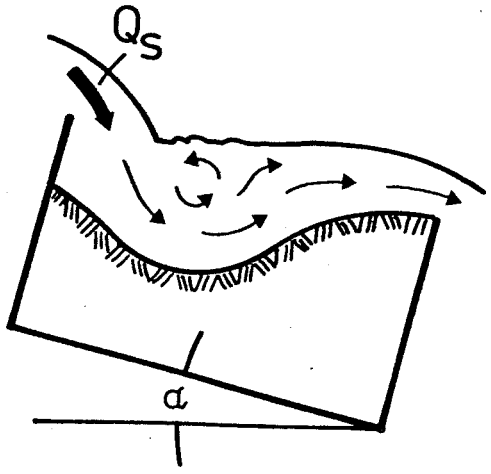

Figure 7-5: Pool at time t_1.

With sediment transport, sediment is not moved continuously through the step-pool system, but instead deposits on the downstream side of the pool (fig. 7-6), until at time t_2 the following situation is attained.

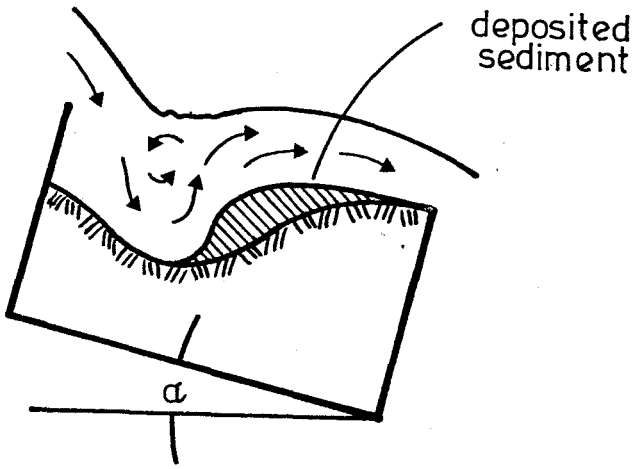

Figure 7-6: Pool at time t_2.

As with the mechanism causing the distortion of scour hole shape (section 6.5.3), this accumulation of gravel forces the scouring jet to rise prematurely. At some stage of the accumulation (say time t_2), however, the situation becomes unstable, and the extra sediment is washed out en mass, and the pool reverts to the shape it has at time t_1. In this way, sediment is moved through the system in discrete amounts. The distance the discrete amounts of gravel move, however, is determined by the flow and sediment transport rates.

At lower slopes the instability tends to transport the sediment out of the pool and deposit it over several pools. Thus long low waves form; at some value of sediment transport rate the differences in scour are observable over a length of channel. The process may be visualised

as follows (fig. 7-7).

The flow pattern change accompanying the sediment movement may be slight, and only observable as an oscillation in pool level with no change in direction of the eddy. Conversely, the instability may amplify over the sediment wave immediately downstream and develop into a roll wave proper.

At higher slopes, sediment is transported through the step-pool system more easily than at lower slopes. At low sediment transport rates, when the accumulated sediment does move it may be carried and deposited over several pools. As Q_s increases, the accumulation process accelerates, sediment moves more quickly, and the result is the two-tier pool structure shown in fig. 7-8. At all slopes with increasing sediment transport rate sediment wave length decreased and velocity of the sediment waves increased. Further, wavelength decreased with increasing slope.

Run 5 (slope = 0.098) was characterised by sediment almost 'choking' the channel. Flow occurred in waves, with no flow occurring between the waves (see fig. 7-9(a) and (b)). This behaviour of the step-pool system is seen to be similar to that of a type 2 debris flow as classified by Mizuyama (1981) (see section 7.2).

This development suggests that the sediment waves seen in natural channels (Hayward, 1978, 1980; Ashida et al, 1976) are retained in their coherent form as they pass along the channel by an intrinsic tendency toward non-uniformity in sediment motion.

7.5.3 Average and Maximum Velocities

Slope = 0.027

For a given flow rate q, average velocity v_m increased rapidly with Q_s, until a threshold was reached, corresponding to complete filling of the pools with sediment (see fig. 7-10). For higher values of Q_s there was essentially no further increase in v_m, and plane bed flow with deposition above the level of the baffles occurred.

The same trend is evident from fig. 7-11 for maximum velocities. Both average and maximum velocities increase with flow rate for a given sediment transport rate.

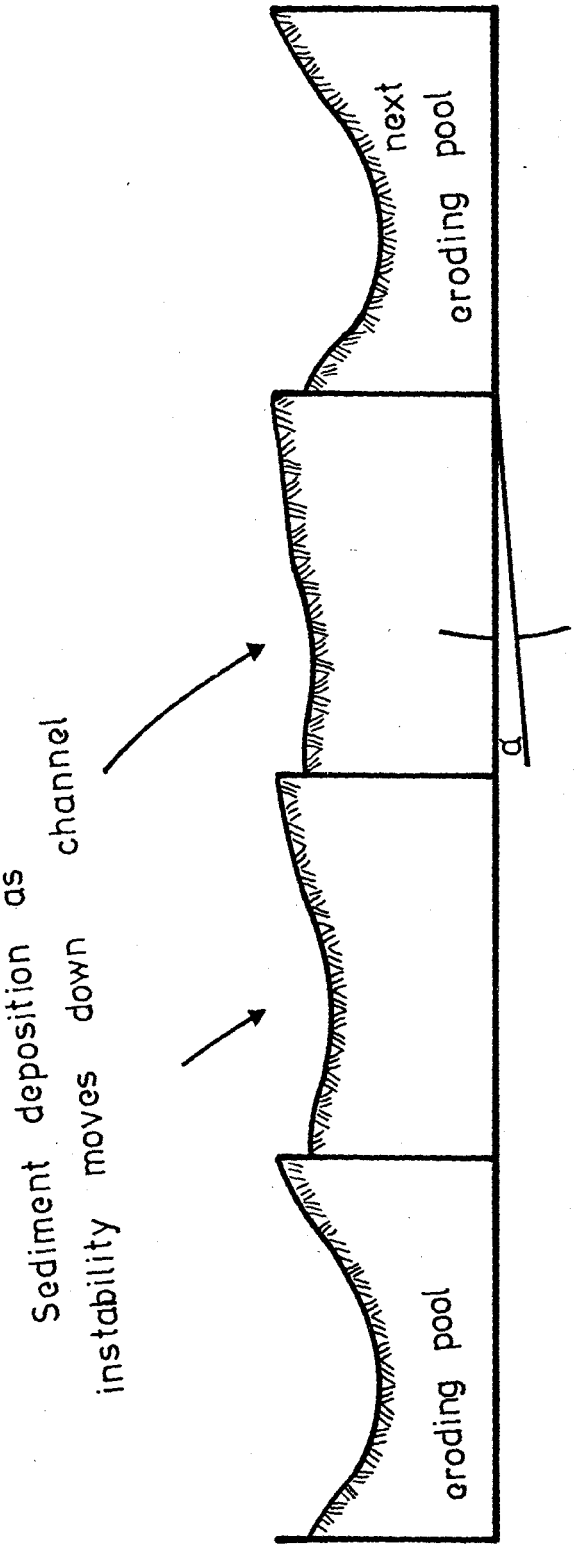

Figure 7-7: Sediment transport process causing long, low waves.

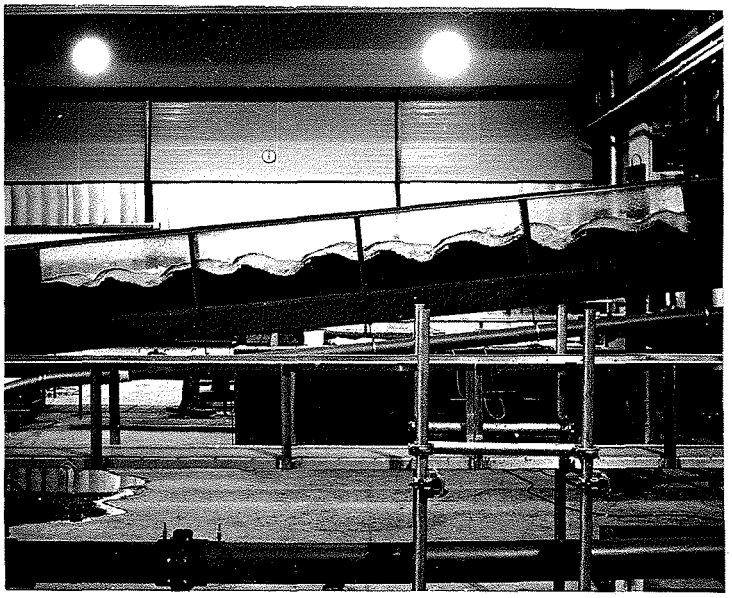

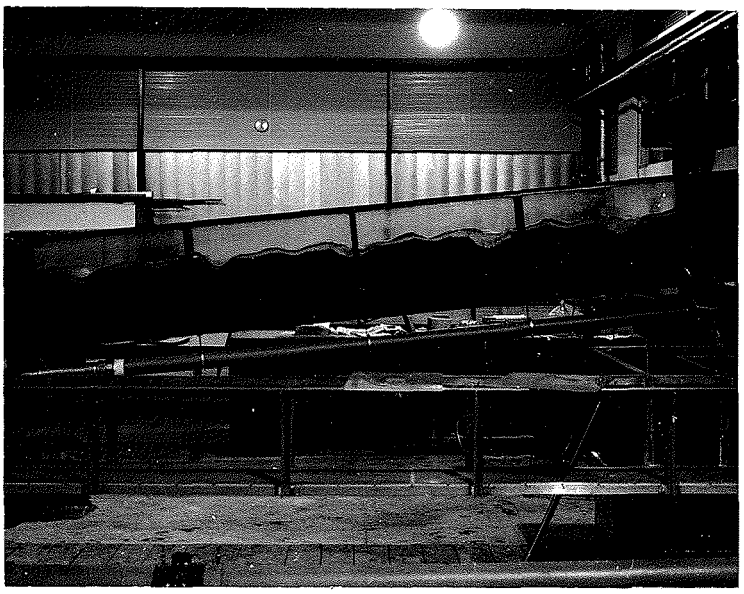

Figure 7-8: Two tier pool structure caused by sediment waves.

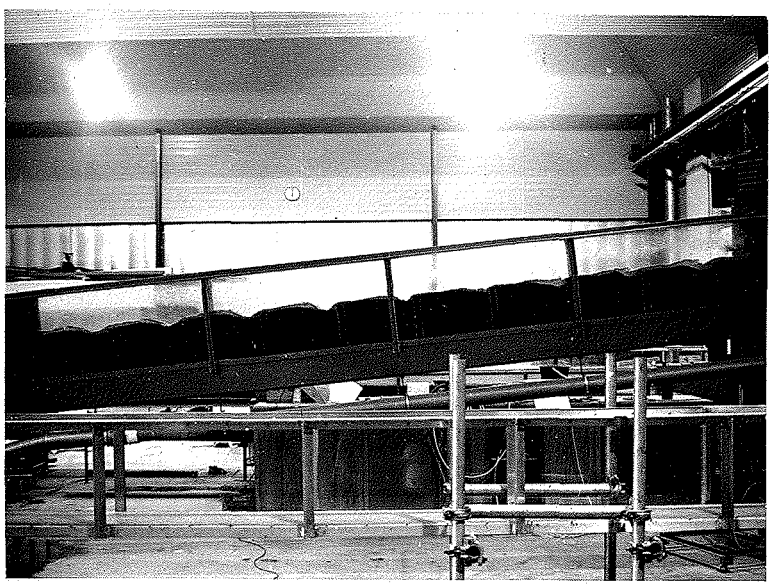

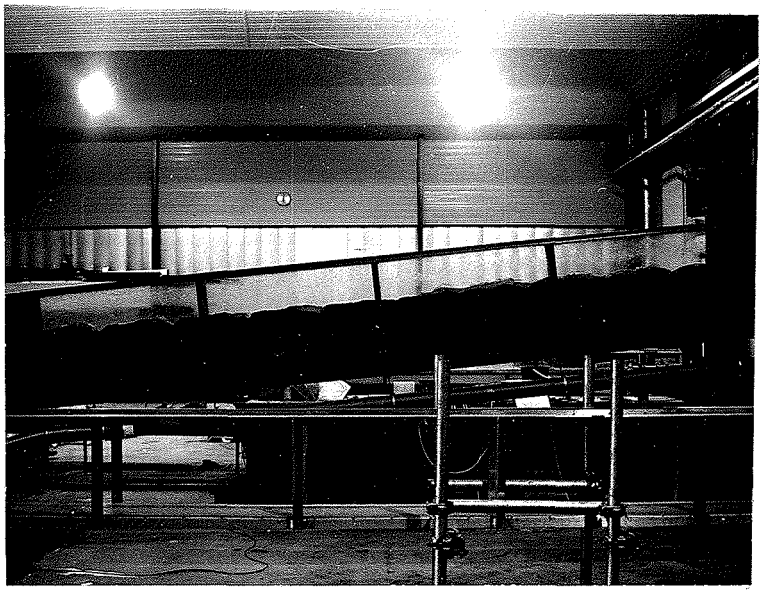

Figure 7-9: Choking of channel with sediment (Run 5).

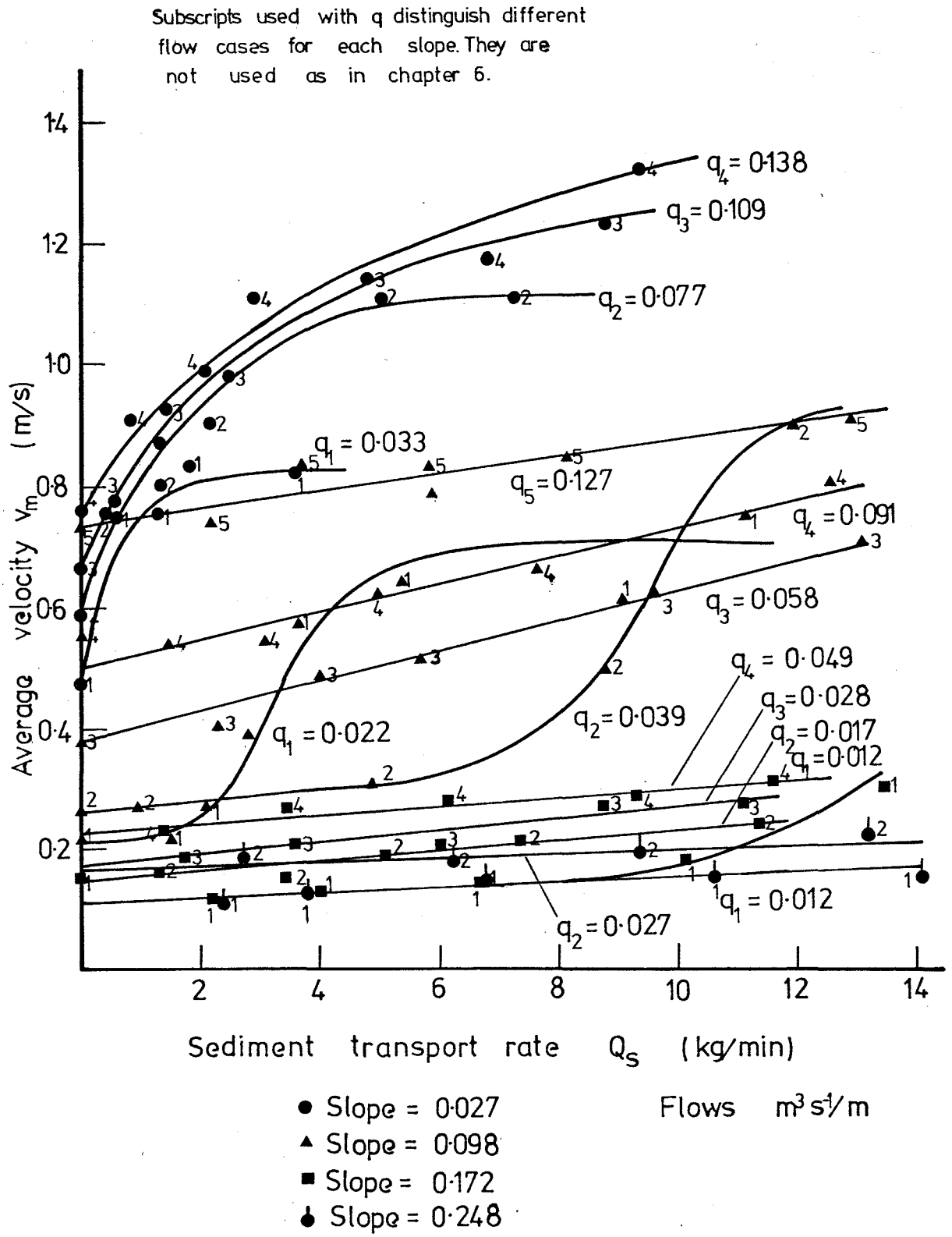

Figure 7-10: Plot of average velocity versus sediment transport rate (for various values of specific discharge).

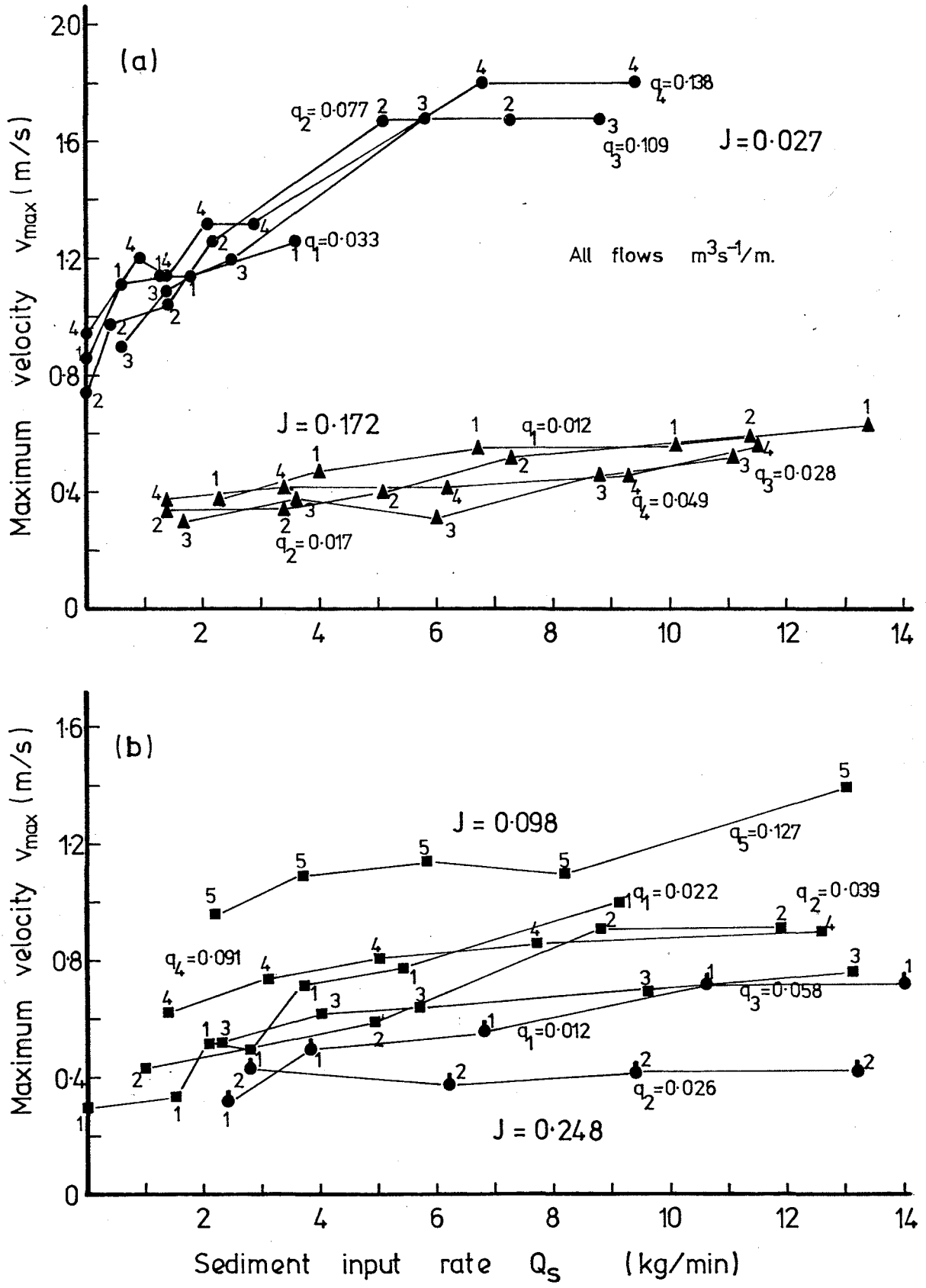

Figure 7-11: Plot of maximum velocity versus sediment transport rate (for various values of specific discharge).

Slope = 0.098

Initially v_m increased only slightly with Q_s (q constant) until with the two lowest flow rates, drowning of pools by sediment began to occur and v_m increased more rapidly (see fig. 7-10). Again a threshold was reached at which the pools were filled with sediment and the increase in v_m ceased. At higher flow rates no significant drowning of pools occurred and only a small increase in v_m was observed with increasing transport rate.

As at slope = 0.027, the trend in maximum velocities (see fig. 7-11) follows that of the average velocities.

Slopes = 0.172 and 0.248

Only the lowest flow at slope = 0.172 showed a significant increase in v_m, and that at a high value of Q_s. For the other flows, no significant drowning of the pools with sediment occurred, and v_m increased only slightly with Q_s.

At these slopes, however, maximum velocities deviate from the trend of the average velocities. Fig. 7-11 shows that for a given value of Q_s, v_{max} decreases with increasing flow rate.

General

For a given flow rate, it is seen that as pools become filled with sediment, an increase in v_m and v_{max}, and hence erosive capability, does indeed occur. However, drowning is much more difficult to achieve at steep slopes, requiring very large values of Q_s at moderate flows. Maximum values of v_m and v_{max} are attained when pools are completely drowned. Field studies (Hayward, 1978, 1980) describe and illustrate severe bank undercutting due to the drowning of pools by sediment. It is of particular interest that erosion is likely even at relatively low flow rates as pools become filled with sediment. It seems likely that a positive feedback may increase the erosive capability in that as the pools in a reach of stream are partly infilled, erosion of adjacent banks becomes possible, further increasing the degree of infilling and thereby bank erosion. Drowning of a step-pool system by a combination of high flow and sediment transport rates can easily occur in a 10 to 25 year event (Hayward, 1980).

7.5.4 Resistance to Flow

Slope = 0.027

Initial values of Darcy-Weisbach friction factor f (i.e. at $Q_s = 0$) reflect the trend shown in fig. 6-24 for the different flow rates. With increasing sediment transport rate, f decreases rapidly at first (see fig. 7-12(a)), and then more slowly. The rapid decrease occurs over the range of Q_s values where the pools become drowned with sediment (see fig. 7-3(a)). The slower decrease coincides with the region of plane bed flow caused by deposition of sediment.

Slope = 0.098

Again, initial values of f at $Q_s = 0$ reflect the trend shown in fig. 6-24. However, the rate of decrease of f with Q_s follows the trend for modification of % scour with Q_s (see fig. 7-3(b)). Thus the values of f for the lower flow rates decrease more quickly with Q_s than the values for higher flow rates (see fig. 7-12(b)).

Slopes = 0.172 and 0.248

Fig. 7-12(c) to (d) confirm the observations made for the other two slopes. That is, values of f at $Q_s = 0$ reflect the trends shown in fig. 6-24, and f decreases more quickly with Q_s for lower flow rates.

General

Fig. 7-12 shows that greater resistance to flow occurs at higher slopes than lower. Further, resistance to flow at any slope depends on the extent of the scour hole. Thus, at lower flow rates where the scour hole size decreases rapidly with sediment transport rate, resistance to flow also decreases rapidly.

This behaviour confirms the conclusions drawn about a step-pool channel's erosive capability from average and maximum velocity values. That is, a step-pool channel may suddenly increase in erosive capability by dissipating much less energy through resistance to flow at flow rates where sediment transport begins to drown the pools. This confirms Hayward's (1978, 1980) hypothesis of decreasing energy dissipation efficiency of pools as they become drowned.

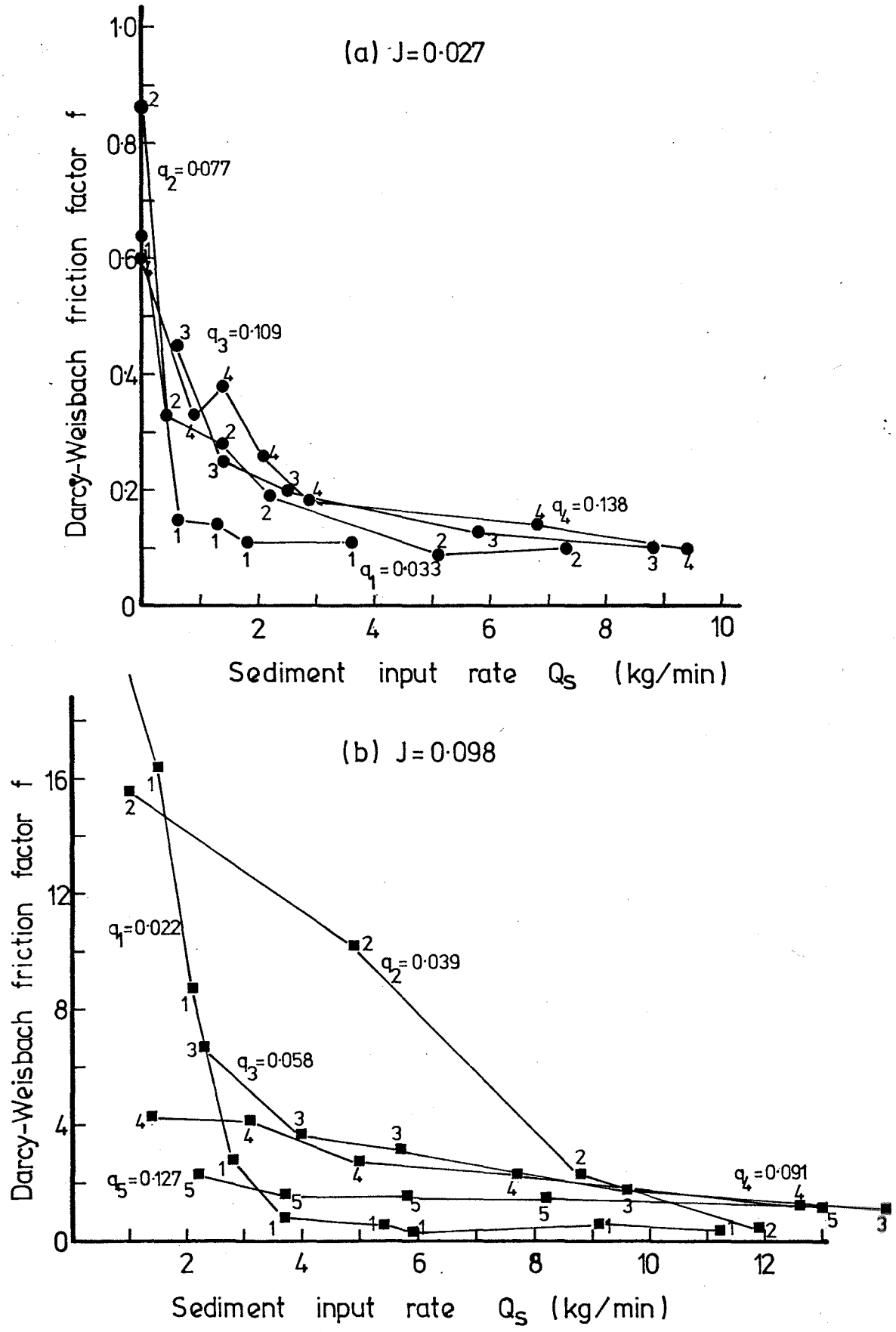

Figure 7-12: Plot of Darcy-Weisbach friction factor f versus sediment transport rate (for various values of specific discharge).

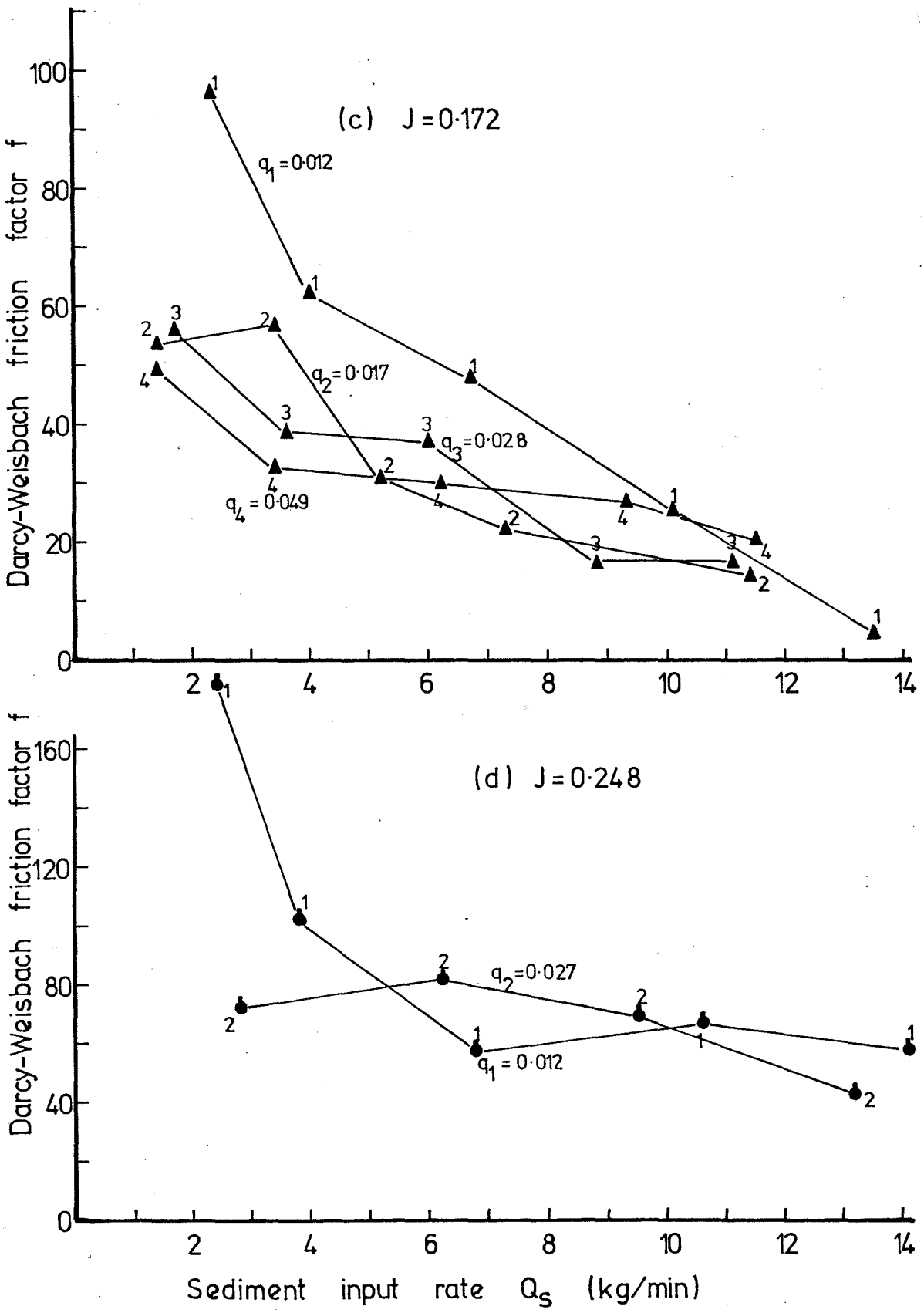

Figure 7-12: (Continued....)

7.6 APPLICABILITY OF SEDIMENT TRANSPORT FORMULAE TO STEP-POOL CHANNELS.

The Meyer-Peter and Müller formula, expressed in the form of equation 7.12, may be written

$$\phi_b = 8\ (\phi - 0.047)^{3/2} \qquad ...7.24$$

This is equivalent to

$$\phi_b = 8\ (\theta - \theta_{cr})^{3/2} \qquad ...7.25$$

where θ_{cr} is the relative shear stress at $\phi_b = 0$. As noted above, if the flow deviates from uniform and form losses occur, θ is replaced by θ' as shown in equation 7.13. The quantity

$$\left(\frac{k_s}{k_r}\right)^{3/2} J$$

is an adjusted slope so that only the portion of J due to grain resistance (i.e. J') is responsible for bedload movement (Graf, 1971).

Thus

$$\left(\frac{k_s}{k_r}\right)^{3/2}$$

is equivalent to the multiplier m defined in equation 7.2. The division of the bed resistance into its components, the one due to grain resistance J' and the other due to bedform resistance J", is accomplished by holding the hydraulic radius R_s constant and dividing the energy slope J (Graf, 1971). Correctly, this results in

$$\frac{J'}{J} = \left(\frac{k_s}{k_r}\right)^{2} \qquad ...7.26$$

but test results showed the relationship to be of the form

$$\frac{J'}{J} = \left(\frac{k_s}{k_r}\right)^{3/2} \qquad ...7.27$$

However

$$\frac{R'}{R_s} = \left(\frac{k_s}{k_r}\right)^{3/2} \qquad ...7.28$$

It appears that the effect of form roughness on sediment transport is more correctly described by dividing the hydraulic radius into components rather than the energy slope.

Now
$$k_r = \frac{26}{6\sqrt{D_{90}}} \qquad ...7.29$$
(Graf, 1971; Jäggi, 1978)

From the Manning (or Strickler) formula

$$k_s = \frac{v_m}{R_s^{2/3} J^{1/2}} \qquad ...7.30$$

Equation 7.25 then becomes (allowing for form roughness)

$$\phi_b = 8 (\theta' - \theta_{cr})^{3/2} \qquad ...7.31$$

Implicit in the preceding development is that sediment transport is considered to be affected by that part of the energy slope due to grain resistance only. That is, none of the flow energy lost through form resistance is available for bedload transport. However, in many sand or fine gravel situations, moving bedforms (which are responsible for form losses) constitute a major part of the bedload, and the applicability of the Meyer-Peter formula is therefore questionable in such circumstances.

In a step-pool system, a reduction in form loss does accompany sediment transport. But at $\phi_b = 0$, the flow is very non-uniform, and loss of fluid energy due to eddying in pools is a major feature of the flow. For q constant, increasing sediment transport reduces form loss (and % scour) by increasingly using this energy being dissipated in the pools.

This could be expressed in a formula as

$$\phi_b = f (\zeta_{\phi=0} - \zeta) \qquad ...7.32$$

where f = a function

and ζ = some dimensionless inverse function of form loss or scour hole size.

Because of the rapid acceleration of the flow in pools due to the changing flow geometry, large convective shear stress values negate the concept of a uniform and steady shear stress. Thus the Meyer-Peter and Müller formula can not be applied (even with allowance for form loss) to

such a non-uniform case as a step-pool channel.

The Einstein (1950) formula is written as shown in equation 7.14. Over a reasonable range of values of ψ (i.e. $\frac{1}{\theta}$) and ϕ_b, equation 7.14 behaves like the Meyer-Peter and Müller equation without the form roughness compensation (see fig. 7-13).

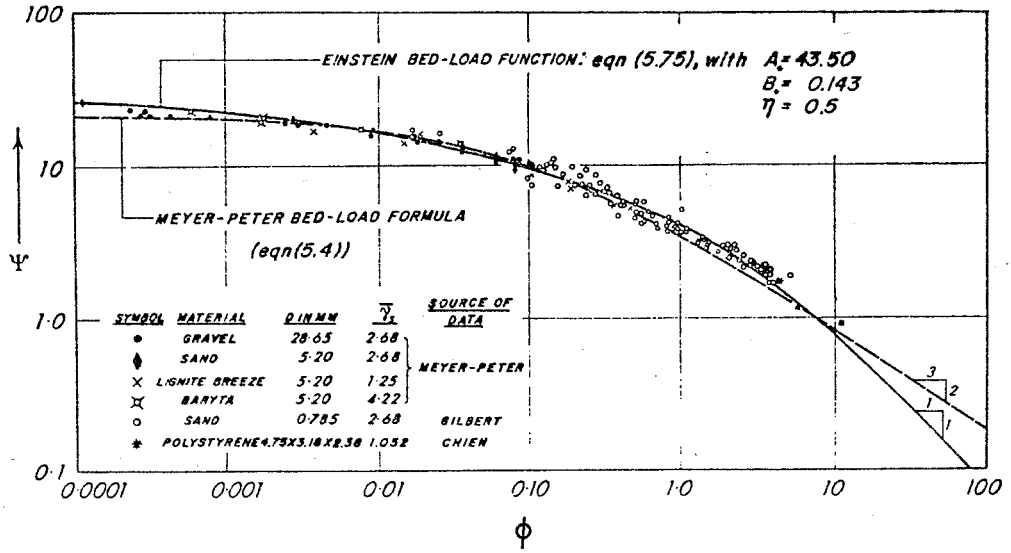

Figure 7-13: Comparison of behaviour of the Meyer-Peter and Müller bedload formula, and the Einstein bedload function (After Yalin, 1977, p.133).

Einstein, like Meyer-Peter and Müller, assumes that energy dissipated by form roughness is not available for grain movement. Equation 7.16 which takes account of this can be written

$$\psi' = \frac{(s-1)\ D_{35}}{\left(\frac{R'}{R_s}\right) R_s\ J} \qquad \ldots 7.33$$

From equations 7.13 and 7.28, it can be seen that this is the same adjustment used by Meyer-Peter and Müller.

However, unlike the Meyer-Peter and Müller equation, with the Einstein equation one can never arrive at an expression that would yield the Shields relation for $q_b = 0$. This is because according to the mathematical model adopted by Einstein, detachment is caused only by fluctuating forces F_y (the possibility of detachment by non-fluctuating (viscous) forces being completely excluded (Yalin, 1977, p. 142)). Therefore the term $\pm$ (0.143 ψ - 2), or more generally $\pm \left(B\psi - \frac{1}{\eta}\right)$ where η is a function of pressure fluctuations, can not be replaced by some function of an expression like equation 7.32 which involves steady quantities.

Equation 7.9 may be written

$$e_b = \sqrt{\frac{\tau_o - \tau_{ocr}}{\tau_o}} \left(\frac{\bar{h}}{D}\right)^{-2/3} \qquad ...7.34$$

As in the Meyer-Peter and Müller formula, the quantity $\tau_o - \tau_{ocr}$ (i.e. $\theta - \theta_{cr}$) is involved. As was shown above, convective accelerations in the scour pool due to the rapidly changing flow geometry make any concept of a steady shear stress inapplicable. Further, depth varies so markedly over a pool sequence that $\bar{h}$ is not really indicative of an average depth condition.

It is thus apparent that the efficiency e_b for Bagnold's stream power approach can not be calculated theoretically because of non-uniform flow, as well as the unknown qualitative effect due to falls and pools mentioned in section 7.2

Bagnold's stream power approach can not even be applied with an empirically determined efficiency e_b. Equation 7.7 shows that the bed-load transport rate equation involves stream power ω separately from e_b. Severe non-uniformities make its determination highly questionable.

It can thus be seen that until the mechanics of rapidly varied flow in the scour zone can be adequately described, conventional sediment transport formulae remain inapplicable to step-pool channels.

7.7 POSSIBLE EXPLANATION FOR THE HYDRAULIC BEHAVIOUR OF STEP-POOL TORRENTS (AND OTHER ALLUVIAL SYSTEMS)

Many aspects of the behaviour of sediment transporting turbulent flows are reminiscent of such intrinsic non-uniformities as the sediment

and roll waves discussed above. They include the development of bed forms, meanders, and riffle-pool sections in initially uniform channels. Current theories of sediment transport and channel formation tend to account for such non-uniformities by means of empirical coefficients. The steady state theory of geomorphology (being a linear thermodynamic approach) is such a theory. In the steady state theory, a stream system is assumed to tend toward the most probable energy distribution. This is attained through a compromise between two opposing tendencies; one toward a uniformly distributed rate of energy expenditure, and the other toward minimum work (formulated in terms of Prigogine's rule of minimum entropy production). The most probable condition will be characterised by a minimum total variance of the system components (given certain boundary conditions), implying a self- stabilising 'negative' feedback, or Le Châtelier moderation (Karcz, 1980).

However, the Prigogine minimum entropy production and Le Châtelier moderation theorems indicate that the geomorphic steady state is inherently restricted to near-equilibrium situations where the regime is linear (Karcz, 1980). This is applicable to laminar flow but not to turbulent flow where non-linearities due to inertial effects dominate (Davy and Davies, 1979).

By contrast, the behaviour of natural streams seems strikingly similar to the behaviour of non-linear thermodynamic systems (Davy and Davies, 1980; Karcz, 1980; Whittaker and Davies, 1982) such as those described by, for instance, Nicolis and Prigogine (1977).

Briefly, a linear thermodynamic system returns to a uniform state when slightly disturbed. This behaviour is restricted to conditions close to equilibrium. The state of continuation of this equilibrium-like behaviour is called the 'thermodynamic branch'. Farther from equilibrium, a bifurcation point is reached on the thermodynamic branch. Beyond this point a disturbance may generate an instability which, with positive feedback, drives the system to a new dynamic equilibrium in which large scale structural order is present. Here the processes are irreversible. This non linear behaviour leads to a new state which is called a 'dissipative structure ' (Prigogine, 1978), and can only be maintained by a sufficient flow of energy and matter.

Bed forms develop from an initial disturbance which is amplified: in the same way a dissipative structure is the result of a perturbation which is amplified by non-linear processes. That alluvial channel form

arises from this behaviour is supported by Parker et. al. (1982). They showed that a non-linear stability analysis can reproduce the shape of meanders in streams and rivers much more realistically than can linear stability analysis; also the non-linear analysis can accomodate perturbations of large amplitude.

The sediment and water waves observed in the present tests thus seem likely to have arisen from such non-linear processes (Whittaker and Davies, 1982; Parker et. al., 1982). In this case, the inability of current, essentially linear, theories of sediment transport to adequately describe the behaviour of step-pool systems is understandable. It is clear that a non-linear approach is needed to fully understand many (or even all) aspects of loose boundary flow; as shown by Parker et. al. (1982) techniques for such analysis are still in their infancy.

7.8 CONCLUSIONS

The main conclusions from the tests of sediment transport through an artificial step-pool channel are as follows:

(1) The flow regimes observed for clear water flow and clear water scour hold only at low sediment transport rates. The deviation from the expected flow regimes was much less at higher slopes.

(2) For flow rates with an initial regime of unstable tumbling flow, flow instability decreased with increasing transport rate.

(3) At higher sediment transport rates, sediment tended to move as waves. For a few flow rates with an initial regime of stable tumbling flow, this caused a flow instability.

(4) Unstable tumbling flow will occur only rarely in natural step-pool channels.

(5) % scour decreases with sediment transport rate. The rate of decrease in % scour with Q_s is related to the flow regime at $Q_s = 0$. Tests with a stable tumbling flow regime at $Q_s = 0$ showed a much stronger decrease with Q_s than did those with an unstable tumbling flow regime.

(6) Sediment transport in a step-pool channel may be seen as occurring as discrete pulses or waves of sediment, which translate slowly down the channel.

(7) Average and maximum velocities reflect % scour in the pools. As a pool fills with sediment to the point of inundation, average and

and maximum velocities increase suddenly. There is essentially no increase of average or maximum velocity with increasing sediment transport rate as plane bed flow occurs.

(8) From (7), it may be inferred that a step-pool channel will quickly increase its erosive capability as pools fill with sediment to the point of drowning.

(9) Resistance to flow follows closely the trend in % scour with increasing sediment transport rate.

(10) Sediment transport through a step-pool system can not be predicted by conventional sediment transport formulae, even with allowance for form losses. The rapidly varying nature of the flow violates the conditions of derivation of the formulae.

(11) Instability manifested as water or sediment waves is explicable in terms of recent advances in the thermodynamics of non-linear systems. The instabilities can be seen to be 'dissipative structures', maintained at far from thermodynamic equilibrium conditions by a sufficient flux of energy and material.

CHAPTER EIGHT

SUMMARY AND CONCLUSIONS

8.1 FORMATION OF STEP-POOL SYSTEMS IN STEEP MOUNTAIN STREAMS

8.1.1 Conditions of Origin of Steps and Pools

Steps and pools are recognised as reaches of alternatively steeper and flatter slope respectively in steep mountain streams. Such bedforms can be generated in the laboratory from a plane bed of heterogeneous material on a steep slope by sediment moving discharges. Once equilibrium is attained (i.e. no more sediment movement), subsequent lower flow rates reveal a step-pool aspect. These laboratory step-pools are similar to those observed in natural streams.

Thus step-pool structures are disequilibrium bed forms. That is, they are formed by high intensity, low return period events rather than by the flows which give them their step-pool appearance.

8.1.2 The Formative Process

The formation of the laboratory steps and pools involved a combination of antidune formation and armouring/paving. At low slopes (less than about 7.5%) very regular antidunes formed, and the bed surface was armoured. At slopes greater than about 7.5%, the antidune process was distorted by large bed elements, and the bed surface was paved.

8.1.3 Characteristics of the Deformed Bed

The bed forms resulting from the action of the sediment moving discharges tended to have a roughness concentration corresponding to a maximum resistance coefficient.

8.1.4 Practical Application

Immediately obvious is that the laboratory generated step-pools which achieved stability under the formative process are then extremely stable under reduced flow rates. Thus, step-pool mountain streams can be considered to be extremely stable under normal flow conditions. With this structural stability, bedload will usually be finer than the bed

stock, unless an unusually high intensity event breaks the structure down. Consequently, any artificial structures built on steep mountain streams will have a low risk of structural failure caused by the stream's own structural failure. However, artificial structures may be affected by finer bedload moved through the stable step-pool system.

Further to this normal stability, and bearing in mind the fairly regular positioning of steps in some steep channel reaches (as shown by the antidune analysis of test results) it seems reasonable to represent mountain streams by a succession of discrete weirs. This is confirmed by Rouse (1965). A channel composed of such discrete weirs can thus be used to investigate the behaviour of steep mountain streams.

8.2 IDEALISATION OF STEP-POOL MOUNTAIN STREAMS

A laboratory channel 0.132 m wide with baffles (0.285 m x 0.130 m x 0.033 m) placed at 0.5 m intervals was used to represent a steep mountain stream. Tests were performed with clear water flow, clear water scour, and sediment transport through this idealised step-pool system. Observations were made to distinguish those behavioural aspects due to the idealisation from those that represent flow in steep step-pool streams.

8.2.1 Flow Regimes

Three flow regimes were observed in the idealised step-pool system for clear water flow and clear water scour, namely:

(a) Stable tumbling flow

(b) Unstable tumbling flow

and (c) Shooting (or rapid) flow.

Stable tumbling flow, in which water tumbles from pool to pool over intervening steps, has long been recognised as characterising flow in steep mountain streams. Shooting flow is far less common, but has been observed (especially in conjunction with high bedload transport rates). However, unstable tumbling flow with its characteristic roll waves has not been reported in literature on steep mountain streams.

Stable tumbling flow occurs at relatively low flow rates. At a certain threshold flow rate which is a function of slope, the flow becomes unstable. The instability increases in magnitude with increasing

flow until at another threshold flow rate (again a function of slope) the flow becomes shooting.

The respective thresholds were higher for the clear water scour test runs than for the clear water flow test runs (see fig. 6-7). Unstable tumbling flow (for both clear water flow and clear water scour) arises from a different mechanism than that causing 'roll-wave' instability generated in uniform flow on steep slopes at Froude numbers of approximately 1.6 or greater.

At a slope of 0.027, unstable tumbling flow (clear water flow case) is caused by the breaking of standing waves at a theoretical maximum steepness of about 0.142. For this slope with clear water scour, unstable tumbling flow seems to be caused by the inability of the step-pool system to pass the imposed discharge according to the hydraulic principles of submerged weir flow. A surface nappe characterised both these situations.

At slopes greater than 0.098, unstable tumbling flow for both clear water flow and clear water scour is caused by the physical system boundaries constraining a submerged hydraulic jump to the point where it no longer has length available to be able to develop fully. The onset of unstable tumbling flow can be predicted on this basis. A plunging nappe characterised the flow at these slopes. The slope which results in the lowest flow rate for which unstable tumbling flow will occur is about J = 0.10. A comparison with field results shows that such a flow may correspond to greater than a 25 yr flood, and thus for clear water flow or clear water scour, unstable tumbling flow is unlikely to be observed in natural step-pool streams. A disordered step length inhibits the growth of roll waves; because natural step-pool systems have a somewhat disordered step length pattern, it is further unlikely that unstable tumbling flow will be observed in the field.

The clearly defined flow regimes observed for the clear water flow and clear water scour tests were radically altered by sediment transport. Sediment was often moved through the artificial step-pool channel in waves. The transport rate required to produce sediment waves increased with increasing slope (see fig. 7-2(a) to (c)). At slope = 0.027 (with an initial flow regime of stable tumbling, i.e. at zero input rate), % scour decreased as sediment transport rate increased until the sediment waves gave way to a plane bed. For flow rates with an initial regime of unstable tumbling flow, the flow instability decreased

with increasing transport rate. This trend was also noted at slope = 0.098.

However, at slope = 0.098, some flows with an initial regime of stable tumbling flow developed unstable flow because of strong sediment wave formation. From this it was apparent that unstable tumbling flow could occur in natural step-pool streams, in sections of the channel inundated with gravel, at lower flow rates than indicated by the no sediment transport case. However, any roll waves so produced would not persist in the non-inundated channel downstream.

8.2.2 Scour in an Artificial Step-Pool Channel

Scour in an artificial step-pool channel is clearly influenced by flow regime. Because flow regime is caused by the physical system constraints, scour is then influenced (that is, distorted) by these constraints.

% scour increased with increasing discharge in all cases, until the influence of the downstream step caused % scour to decrease as flow continued increasing. % scour subsequently increased again with shooting flow. Scour uninfluenced by the downstream step (and corresponding to a plunging nappe) is described by the equation

$$S_o = 7.72 \frac{q^{0.852} H_s^{0.495}}{g^{0.436} D_{90}^{0.333}} \qquad \ldots 6.28$$

This corresponds to the ultimate static limit of scour, where all material in suspension is removed from the scour zone.

Sediment transport influences scour markedly. At slope = 0.027, % scour for all flows tends, with increasing sediment transport, toward zero. This decrease in % scour is aided by the surface nappe profile, which is less effective than the plunging nappe in its scouring action. For slope = 0.098, % scour for stable tumbling flows decreases rapidly with increasing sediment transport rate. However, for unstable tumbling and shooting flows, % scour decreases much less rapidly with transport rate. This behaviour occurs for all regimes at higher slopes.

8.2.3 Erosive Potential of Step-pool Systems

Stream power is indicative of the ability of a stream to transport sediment. Further, stream power is closely correlated with mean flow

velocity. Thus, mean velocity is indicative of a stream's erosive potential.

Maximum velocity is indicative of the maximum material size a flow is capable of moving, and so in this way is also representative of a stream's erosive potential.

Darcy-Weisbach friction factor f is a measure of the fluid energy being dissipated by a rough bed. Thus, low f values and high values of mean and/or maximum velocity indicate a stream which has a high erosive potential.

For clear water flow, maximum velocities indicate that a stream will experience a sudden increase in erosive potential for flows in the upper range of unstable tumbling flows. For clear water scour, mean and maximum velocities suggest that natural step-pool streams will increase in erosive potential at flow rates for which the downstream step begins to limit development of the scour hole. These flow rates are lower than those causing the increase in erosive potential for the clear water flow case. With sediment transport, an increase in erosive potential was noted at much lower flow rates again. This increase occurred as pools became drowned with sediment, reducing the energy dissipation between steps. Thus, a stretch of stream channel inundated with sediment will tend to erode further material from the channel sides.

Resistance to flow can be predicted by empirical logarithmic laws, despite the fact that the flow is highly non-uniform. For clear water flow, Darcy-Weisbach friction factor f is given by

$$\sqrt{\frac{8}{f}} = 5.657\ A \log\left(\frac{R}{k'}\right) + B \qquad \ldots 5.53$$

where $A = (1.676 - 5.715\ J')$

and $B = (0.630\ J' - 0.057)$

For clear water scour, resistance to the flow increases with increasing discharge until the flow rate at which the influence of the down-stream step is strong enough to cause depth of scour to decrease. With increasing discharge beyond this flow rate, resistance to flow then decreases. Here Darcy-Weisbach friction factor f is given by

$$\sqrt{\frac{8}{f}} = 5.657\ A \log\left(\frac{S_o}{S}\right) + B \qquad \ldots 6.33/35$$

where $B = \phi$ (slope).

and $A = \phi(\text{slope})$ for increasing resistance
or A = const. for decreasing resistance.

8.2.4 Practical Application

The main application of the results on flow regime is in the design of channels used to take water safely down steep slopes. Highway drainage chutes and fish ladders are specific examples of such channels. Many stepped channels have been designed by 'feel' and experience rather than on a quantitative basis because of the lack of design rules with respect to the onset of unstable tumbling flow.

For totally artificial stepped channels, or channels with weirs incorporated into alluvium at regular intervals, the results presented herein give a basis for design so that unstable tumbling flow and shooting flow (which are dangerously erosive) may be avoided at the design discharge. Further, eliminating the unstable tumbling flow regime means that associated hydraulic structures are at less risk of failure due to rapidly varying forces.

Sediment transport is seen to bring difficulties to the design of such channels. As well as reducing the efficiency of energy dissipation, flow instability can occur at still lower discharges if sediment waves develop. Clearly, these channels should only be used where sediment transport will be minimal or avoided all together.

The information on scour in an artificially stepped torrent indicates that such structures scour (for flow rates where the scour hole is not distorted by the downstream step) to a maximum possible extent under the given conditions. Armouring or paving would of course reduce this scour. For higher flow rates where the downstream step distorts the scour hole shape, scour depth decreases, and scour begins to occur on the upstream side of the downstream sill. Clearly, such channels should have a design discharge at which the downstream sill does not distort the scour hole shape. The scour will be deeper than at some higher flow rates (with consequently more energy dissipation, lower mean velocities, and thus less erosive potential), the downstream sill will not be endangered by scour on its upstream side, and unstable tumbling flow will be avoided.

The tests show that for stable tumbling flows, if the sediment transport rate is zero or small, steep mountain step-pool streams will rarely develop unstable tumbling flow. However, instabilities may

develop in lengths of channels inundated with sediment, although the nonuniformity of step length reduces this likelihood. Where pools become inundated with sediment, average and maximum velocities indicate that the erosive potential suddenly becomes high. Not only are hydraulic structures then vulnerable to inundation with gravel, but adjacent side slopes are vulnerable to erosion by the flow.

Where a stream channel is adjacent to the toe of a slope, measures can be taken to prevent erosion by the flow under the conditions described above. Protection structures such as sediment check dams, groynes or rock mattresses could be placed so as to deny access to the slope. This is, however, sometimes not possible.

8.3 PHILOSOPHY OF APPROACH TO TWO-PHASE PROBLEMS

In the tests with sediment transport, the steps in the channel sometimes resulted in both water waves and sediment waves occurring, often independently. The response of the system to uniform inputs of water, sediment, and energy was clearly non-linear. On a macro-scale, the system could be considered to be amenable to linear analysis, but this avoids the difficulty posed by the processes operating, and is perhaps a 'black-box' approach.

Recent advances in non-linear thermodynamics appear to offer a more reasonable way of analysing the behaviour of such non-linear systems. In such an approach, the non-linear but quasi-steady sediment and water waves can be interpreted to be dissipative structures, maintained by constant and sufficiently high input rates of energy and matter.

8.4 SUGGESTION FOR FURTHER WORK

The channel used in the present tests was an idealisation of natural step-pool mountain streams. The results are thus not directly applicable to the field situation. Observation of steep mountain step-pool streams has enabled a number of reasonable inferences to be made from the test results regarding the natural situation. The next logical step is to study the behaviour of natural step-pool streams in response to various water and sediment inputs in the light of these detailed

tests. This will be difficult, and require considerable money and, one suspects, years of effort. However, the test results reported herein will enable researchers to concentrate on aspects of stream behaviour shown to be important in the idealised case, and likely to be of significance to the understanding of erosion processes in step-pool streams.

REFERENCES

ADACHI, S . 1964. On the artificial strip roughness. *Bull. Disaster Prev. Res. Inst. Kyoto Univ.*, No. 69, 20 p.

ALBERTSON, M.L.; BARTON, J.R. and SIMONS, D.B. 1960. Fluid Mechanics for Engineers. Prentice-Hall, Inc., Englewood Cliffs, N.J., U.S.A. 567 p.

AL-KHAFAJI, A. 1961. The dynamics of two-dimensional flow in steep, rough, open channels. Ph.D. thesis, Utah State Univ., Logan, Utah, U.S.A., 90 p.

ALLEN, J.R.L. 1976. Bed forms and unsteady processes: some concepts of classification and response illustrated by common one-way types. *Earth Surface Processes*, Vol. 1, pp 361-374.

ANDREWS, E.D. 1977. Hydraulic adjustment of an alluvial channel to the supply of sediment. Ph.D. thesis, University of California, Berkeley, California, U.S.A., 152 p.

APMANN, R.P., and BLINCO, P.H. 1969. Experiences with bed sills in stream stabilisation. *Journal of the Waterways and Harbors Div. A.S.C.E.*, Vol. 95, No. W.W. 3, pp 319-328.

ASHIDA, K. and BAYAZIT, M. 1973. Initiation of motion and roughness of flows in steep channels. *Proc. 15th Congress I.A.H.R.*, Vol. 1, pp 475-484.

ASHIDA, K.; TAKAHASHI, T. and SAWADA, T. 1976. Sediment yield and transport on a mountainous small watershed. *Bull. Disaster Prev. Res. Inst. Kyoto Univ.* Vol. 26, Pt 3, No. 240, pp 119-144.

ASHIDA, K.; TAKAHASHI, T. and SAWADA, T. 1981. Processes of sediment transport in mountain stream channels. In: *Erosion and Sediment Transport in Pacific Rim Steeplands* (Proc. I.A.H.S. Christchurch Symposium, Jan. 1981). (Ed. by T.R.H. Davies and A.J. Pearce), pp 166-178.

BAGNOLD, R.A. 1954. Experiments on a gravity-free dispersion of large solid spheres in a Newtonian fluid under shear. *Proc. Roy. Soc. Lond. A*, Vol. 225, pp 49-70.

BAGNOLD , R.A. 1956. The flow of cohesionless grains in fluids. *Philosophical Trans. Roy. Soc. London, A*, Vol. 249, No. 964, pp 235-297.

BAGNOLD, R.A. 1960. Sediment discharge and stream power. *United States Geological Surv. Circ. 421,* Washington, D.C.

BAGNOLD, R.A. 1966. An approach to the sediment transport problem from general physics. *United States Geological Surv. Prof. Paper 422-1,* Washington, D.C. 37 p.

BAGNOLD, R.A. 1968. Deposition in the process of hydraulic transport. *Sedimentology,* 10, pp 45-56.

BAGNOLD, R.A. 1977. Bedload transport by natural rivers. *Water Resources Research,* Vol. 13, No. 2, pp 303-312.

BAGNOLD, R.A. 1980. An empirical correlation of bedload transport rates in flumes and natural rivers. *Proc. Roy. Soc. Lond., A,* Vol. 372, pp 453-473.

BAKHMETEFF, B.A. and MATZKE, A.E. 1938. The hydraulic jump in sloped channels. *Trans. A.S.M.E.,* Vol. 60, pp 111-118.

BATHURST, J.C. 1978. Flow resistance of large-scale roughness. *Journal of the Hydraulics Div. A.S.C.E.,* Vol. 104, HY 12, pp 1587-1603.

BATHURST, J.C. 1982. Theoretical aspects of flow resistance. In: *Gravel-bed rivers: Fluvial Processes, Engineering and Management.* (Ed. by R.D. Hey, J.C. Bathurst and C.R. Thorne.) Wiley, England, in press.

BATHURST, J.C.; LI, R.M. and SIMONS, D.B. 1981. Resistance equation for large-scale roughness. *Journal of the Hydraulics Div. A.S.C.E.,* Vol. 107, HY 12, pp 1593-1613.

BAYAZIT, M. 1975. Free surface flow in a channel of large relative roughness. *Journal of Hydraulic Research,* Vol. 14, No. 2, pp 115-126.

BENNET, J.P. and NORDIN, C.F. 1977. Simulation of sediment transport and armouring. *Hydrological Sciences Bull.,* Vol. 22, No. 4, pp 555-569.

BESCHTA, R.L. 1981. Patterns of sediment and organic-matter transport in Oregon coast range streams. In: *Erosion and Sediment Transport in Pacific Rim Steeplands.* (Proc. I.A.H.S. Christchurch Symposium, Jan. 1981.) (Ed. by T.R.H. Davies and A.J. Pearce), pp 179-188.

BEVEN, K.; GILMAN, K. and NEWSON, M. 1979. Flow and flow routing in upland channel networks. *Hydrological Sciences Bulletin,* Vol. 24, No. 3, pp 303-325.

BOOTHROYD, J.C. 1970. Recent braided-stream sedimentation, South-central Alaska (Abst). *American Assoc. of Petroleum Geologists Bull.*, Vol. 54, p 836.

BOOTHROYD, J.C. and ASHLEY, G.M. 1975. Processes, bar morphology, and sedimentary structures on braided outwash fans, Northeastern Gulf of Alaska, In: *Glaciofluvial and Glaciolacustrine Sedimentation.* (Ed. by A.V. Jopling and B.C. McDonald), Society of Economic Paleontologists and Mineralogists, Special Publication No. 23, pp 1282-1301.

BRATER, E.F. and KING, H.W. 1976. Handbook of Hydraulics (6th Edition), McGraw-Hill, N.Y.

BRAY, D.I. and CHURCH, M. 1980. Armored versus paved gravel beds. *Technical note: Journal of the Hydraulics, Div. A.S.C.E.*, Vol. 106, HY 11, pp 1937-1940.

BREN, L.J. and TURNER, A.K. 1978. Wave propagation in steep, rough mountain streams. *Journal of the Hydraulics Div. A.S.C.E.*, Vol. 104, HY 5, pp 745-754.

CALKINS, D. and DUNNE, T. 1970. A salt tracing method for measuring channel velocities in small mountain streams. *Journal of Hydrology (Netherlands)* 11, pp 379-392.

CARSTENS, M.M. 1966. Similarity laws for localised scour. *Journal of the Hydraulics Div. A.S.C.E.*, Vol. 92, HY 3, pp 13-36.

CHOW, V.T. 1959. Open-channel hydraulics. McGraw-Hill, N.Y., 680 p.

CHURCH, M. and GILBERT, R. 1975. Proglacial fluvial and lacustrine environments. In: *Glaciofluvial and Glaciolacustrine Sedimentation.* (Ed. by A.V. Jopling and B.C. McDonald.) Society of Economic Paleontologists and Mineralogists, Special Publication, No. 23.

CHURCH, M. and KELLERHALS, R. 1970. Stream gauging in isolated areas using portable equipment. *Canada Dept of Energy, Mines and Resources, Inland Waters Branch, Tech. Bull. No. 25,* 90 p.

CORNISH, V. 1910. Waves of the sea and other water waves. The Open Court Publishing Co., La Salle, Ill., and T. Fisher Unwin, London.

COX, G.N. 1928. The submerged weir as a measuring device. *Bull. of the Univ. of Wisconsin Engineering Experiment Station.* Series No. 67, 155 p.

DAVIES, T.R.H. 1980. Bedform spacing and flow resistance. *Journal of the Hydraulics Div. A.S.C.E.*, Vol. 106, HY 3, pp 423-433.

DAVIES, T.R.H. and JÄGGI, M.N.R. 1981. Precise measurement of flow resistance. *Proc. 19th Congress, I.A.H.R.*, New Delhi, Feb. 1981.

DAVIES, T.R.H. and SUTHERLAND, A.J. 1980. Resistance to flow past deformable boundaries. *Short communication; Earth Surface Processes*, Vol. 5, pp 175-179.

DAVY, B.W. and DAVIES, T.R.H. 1979. Entropy concepts in fluvial geomorphology. A re-evaluation. *Water Resources Research*, Vol. 15, No. 1, pp 103-106.

DAVY, B.W. and DAVIES, T.R.H. 1980. Entropy concepts in fluvial germophology: A re-evaluation. *Comment and reply; Water Resources Research*, Vol. 16, No. 1, pp 250-251.

DAY, T.J. 1969. The channel geometry of mountain streams. M.A. thesis. University of British Columbia, Vancouver, Canada, 59 p.

DAY, T.J. 1972. The channel geometry of mountain streams. In: *Mountain Geomorphology (Geomorphological processes in the Canadian Cordillera)*. (Ed. by O. Slaymaker and H.J. McPherson) British Columbia. Geographical Series No. 14. Tantalus Research Ltd, pp 141-149.

DAY, T.J. 1977. Field procedures and evaluation of a slug dilution gauging method in mountain streams. *Journal of Hydrology* (N.Z.), Vol. 16, No. 2, pp 113-133.

DAY, T.J. 1981. An experimental study of armouring and hydraulic properties of coarse bed material channels. In: *Erosion and Sediment Transport in Pacific Rim Steeplands*. (Proc. I.A.H.S. Christchurch Symposium, Jan. 1981) (Ed. by T.R.H. Davies and A.J. Pearce), pp 236-251.

DEMENT'EV, V.V. 1962. Investigations of pulsation of velocities of flow of mountain streams and of its effect on the accuracy of discharge measurements. *Soviet Hydrology*, Vol. 1, No. 6, pp 588-623. (Publ. by Am. Geophysical. Union.)

DIETRICH, W. and DUNNE, T. 1978. Sediment budget for a small catchment in mountainous terrain. *Z. Geomorph. Suppl. Bd.*, 29, pp 191-206.

DODDIAH, D.; ALBERTSON, M.L. and THOMAS, R. 1953. Scour from jets. *Proc. 5th Meeting I.A.H.R.*, University of Minnesota, Minneapolis, U.S.A., pp 161-169.

DRESSLER, R.F. 1949. Mathematics solution of the problem of roll-waves in inclined open channels. *Communications on Pure and Applied Mathematics*, 2, pp 149-194.

EDWARDS, R.E. 1970. Sediment transport and channel morphology in a small mountain stream in Western Oregon. M.Sc. thesis, Oregon State University, Corvallis, U.S.A., 114 p.

EINSTEIN, H.A. 1942. Formulae for the transportation of bedload. *Trans. A.S.C.E.*, Vol. 107, pp 561-573.

EINSTEIN, H.A. 1950. The bedload function for sediment transportation in open channel flow. *U.S.D.A., Soil Conservation Service, Tech. Bull. 1026*, 81 p.

FAHNESTOCK, R.K. and HAUSHILD, W.L. 1962. Flume studies of the transport of pebbles and cobbles on a sand bed. *Geol. Soc. Amer. Bull.*, Vol. 73, pp 1431-1436.

FOLEY, M.G. and VANONI, V.A. 1977. Pulsing flow in steep alluvial streams. *Journal of the Hydraulics Div. A.S.C.E.*, Vol. 103, HY 8, pp 843-850.

FORSTER, J.W. and SKRINDE, R.A. 1950. Control of the hydraulic jump by sills. *Trans. A.S.C.E.*, Vol. 115, pp 973-987.

FRANKE, P.G. 1960. L'affouillement: Méchanisme et formes. *Oesterreichische Wasserwirtschaft*, Jan. 1960.

GESSLER, J. 1965. The beginning of bedload movement of mixtures investigated as natural armouring in channels. *Report No. 69 of the Laboratory of Hydraulic Research and Soil Mechanics of the Swiss Federal Institute of Technology*, Zürich, Switzerland, 89 p.

GESSLER, J. 1970. Self stabilising tendencies of alluvial channels. *Journal of the Waterways and Harbors Div., A.S.C.E.*, Vol. 96, W.W. 2, pp 235-249.

GOLUBTSOV, V.V. 1976. Dependence of the Coriolis and Boussinesq coefficients on the slope of a mountain stream. *Soviet Hydrology*, Vol. 15, No. 1, pp 41-43. (Publ. by Am. Geophysical Union.)

GRAF, W.H. 1971. Hydraulics of sediment transport. McGraw-Hill, N.Y., 513 p.

GRAF, W.L. 1979. Rapids in canyon rivers. *Journal of Geology*, Vol. 87, pp 533-551.

GREGORY, K.J. and WALLING, D.E. 1973. Drainage basin form and process. Wiley and Sons.

GRIFFITHS, G.A. 1980. Stochastic estimation of bedload yield in pool and riffle mountain streams. *Water Resources Research,* Vol. 16, No. 5, pp 931-937.

GUSTAVSON, T.C. 1974. Sedimentation on gravel outwash falls, Malaspina Glacier foreland, Alaska. *Journal of Sedimentary Petrology,* Vol. 44, No. 2, pp 374-389.

HARTUNG, F. and SCHEUERLEIN, H. 1967. Macroturbulent flow in steep, open channels with high natural roughness. *Proc. 12th Congress of the I.A.H.R.,* Vol. 1, Colorado, U.S.A., pp 1-8.

HAYWARD, J.A. 1978. Hydrology and stream sediments in a mountain catchment. Ph.D. thesis, (Vols 1-3), University of Canterbury, Christchurch, New Zealand.

HAYWARD, J.A. 1980. Hydrology and stream sediment from Torlesse Stream catchment. *Tussock Grasslands and Mountain Lands Inst. Lincoln College, (N.Z.), Special Publication No. 17,* 236 p.

HEEDE, B.J. 1972a. Flow and channel characteristics of two high mountain streams. *U.S.D.A., Forest Service Research Paper RM 92,* 12 p.

HEEDE, B.J. 1972b. Influences of a forest on the hydraulic geometry of two mountain streams. *Water Resources Bull.,* Vol. 8, No. 3, pp 523-530.

HENDERSON, F.M. 1966. Open channel flow. Macmillan, N.Y., 522 p.

HERBICH, J.B. and SHULITS, S. 1964. Large-scale roughness in open channel flow. *Journal of the Hydraulics Div. A.S.C.E.,* Vol. 90, HY 6, pp 203-230.

HEY, R.D. 1979. Flow resistance in gravel-bed rivers. *Journal of the Hydraulics Div. A.S.C.E.,* Vol. 105, HY 4, pp 365-379.

HOLMES, W.H. 1936. Travelling waves in steep channels. *Civil Engineering,* Vol. 6, pp 467-468.

ISHIHARA, J.; IWAGAKI, Y. and ISHIHARA, Y. 1952. On the roll-wave trains appearing in the water flow on a steep slope surface. *Memoirs of the Faculty of Engineering, Kyoto University,* Japan, Vol. XIV, No. 2, pp 83-91.

JACKSON, W.L. 1981. Bed material routing and streambed composition in alluvial channels. Ph.D. thesis, Oregon State University, Corvallis, U.S.A., 164 p.

JÄGGI, M.N.R. 1978. Die Sedimenttransportformeln von Meyer-Peter, Einstein und Engelund (Vergleich, Gültigkeitsbereiche, praktische anwendung). *Arbeitsheft Nr 4, Versuchsanstalt für Wasserbau, Hydrologie und Glaziologie, E.T.H., Zürich,* Switzerland, 88 p.

JAROCKI, W. 1957. A study of sediment (Bodanie Rumowski). *Wyda wriictwo Morskie,* Poland (Quoted by Gregory and Walling, 1973).

JEFFREYS, H. 1925. The flow of water in an inclined channel of rectangular section. *London, Edinburgh and Dublin Philosophical Magazine and Journal of Science,* Vol. 49, Ser. 6, pp 793-807.

JOHNSON, C.O. 1950. Similarity in scour below a spillway. M.Sc. thesis, University of Minnesota, Minneapolis, U.S.A., 64 p.

JOHNSON, G. 1967. The effect of entrained air on the scouring capacity of water jets. *Proc. 12th Congress of the I.A.H.R.*, Vol. 3, Colorado, U.S.A., pp. 219-226.

JUDD, H.E. 1964. A study of bed characteristics in relation to flow in rough, high-gradient natural channels. Ph.D. thesis, Utah State University, Logan, U.S.A., 182 p.

JUDD, H.E. and PETERSON, D.F. 1969. Hydraulics of large bed element channels. *Utah Water Research Laboratory PRWG 17-6,* College of Engineering, Utah State University, Logan, U.S.A., 115 p.

KARCZ, I. 1980. Thermodynamic approach to geomorphic thresholds. In: *Thresholds in Geomorphology (9th Geomorphology Symposium, 1978, Binghampton, N.Y.),* (ed. by D.R. Coates and J.D. Vitek). George Allen and Unwin, pp 209-226.

KELLER, E.A. 1971. Areal sorting of bedload material: The hypothesis of velocity reversal. *Geological Society of America Bull.*, Vol. 82, pp 753-756.

KELLER, E.A. and MELHORN, W.N. 1978. Rhythmic spacing and origin of pools and riffles. *Geological Society of America Bull.*, Vol. 89, pp 723-730.

KELLER, E.A. and SWANSON, F.J. 1979. Effects of large organic material on channel form and alluvial processes. *Earth Surface Processes,* Vol. 4, pp 361-380.

KELLERHALS, R. 1970. Runoff routing through steep natural channels. *Journal of the Hydraulics Div. A.S.C.E.*, Vol. 96, HY 11, pp 2201-2217.

KELLERHALS, R. 1972. Hydraulic performance of steep natural channels. In: *Mountain Geomorphology (Geomorphological processes in the Canadian Cordillera)* (ed. by O. Slaymaker and H.J. McPherson). British Columbia Geographical Series No. 14. Tantalus Research Ltd, pp 131-139.

KELLERHALS, R. 1973. Hydraulic performance of mountain streams. *Proc. 15th Congress of the I.A.H.R.*, Istanbul, Turkey, pp 467-473.

KELLERHALS, R. and BRAY, D. 1971. Sampling procedures for coarse fluvial sediment. *Journal of the Hydraulics Div. A.S.C.E.*, Vol. 97, HY 8, pp 1165-1180.

KENNEDY, J.F. 1961. Stationary waves in alluvial channels. *(Final report to U.S.D.A.). Report No. KH-R-2, W.M. Keck Laboratory of Hydraulics and Water Resources, California Inst. of Technology.* Pasadena, U.S.A, 146 p.

KENNEDY, J.F. 1963. The mechanics of dunes and antidunes in erodible-bed channels. *Journal of Fluid Mechanics*, Vol. 16, No. 4, pp 521-545.

KEULEGAN, G.H. and PATTERSON, G.W. 1940. A criterion for instability of flow in steep channels. *Trans. Am. Geophysical Union*, Vol. 21, pt. 2, pp 594-596.

KINDSVATER, C.E. 1944. The hydraulic jump in sloping channels. *Trans. A.S.C.E.*, Vol. 109, pp 1107-1120.

KNIGHT, D.W. and MacDONALD, J.A. 1979. Hydraulic resistance of artificial roughness. *Journal of the Hydraulics Div. A.S.C.E.*, Vol. 105, HY 6, pp 675-690.

KNIGHTON, A.D. 1981. Channel form and flow characteristics of supraglacial streams. Austre Okstindbreen, Norway. *Arctic and Alpine Research*, Vol. 13, No. 3, pp 295-306.

KOLOSEUS, H.J. 1958. The effect of free surface instability on channel resistance. Ph.D. thesis, State University of Iowa, U.S.A.

KOLOSEUS, H.J. and DAVIDIAN, J. 1961. Flow in an artificially roughened channel. In: *Short Papers in the Geologic and Hydrologic Sciences, Articles 1-146, U.S. Geol. Surv. Prof. Paper 424-8*, Art 12, pp 25-26.

KOLOSEUS, H.J. and DAVIDIAN, J. 1966a. Free surface instability correlations. *Geological Survey Water-Supply Paper 1592-C*, Washington D.C., U.S.A., 72 p.

KOLOSEUS, H.J. and DAVIDIAN, J. 1966b. Roughness concentration effects on flow over hydrodynamically rough surfaces. *Geological Survey Water-Supply Paper 1592-D.* Washington D.C., U.S.A., 21 p.

KOO, E.Y.T. 1963. Roll waves in a steep, rough channel. M.Sc. thesis, Virginia Polytechnic Inst., U.S.A., 40 p.

KOO, E.Y.T. 1967. One-dimensional stability analysis of unstable flow in a steep, rough channel. Ph.D. thesis, Virginia Polytechnic Inst., U.S.A.

KOSTER, E.H. 1978. Transverse ribs: Their characteristics, origin and paleohydraulic significance. In *Fluvial Sedimentology.* (Ed. by A.D. Miall). Canadian Society of Petroleum Geologists. Memoir 5. Calgary, Canada, pp 161-186.

KOTOULAS, D. 1967. Das kolkproblem unter besonderer Berücksichtigung der Faktoren Zeit und Geschiebemischung im Rahmen der Wildbach-verbauung. *Mitteil. Anst. für das forstl. Versuchswesen Bd.,* Vol. 43, Heft 1.

LARONNE, J.B. and CARSON, M.A. 1975. Inter-relationships between bed morphology and bed-material transport for a small, gravel-bed channel. *Sedimentology,* 23, pp 67-85.

LAURSEN, E.M. 1952. Observations on the nature of scour. *Proc. of the 5th Hydraulics Conf.,* June 9-11, Iowa State University, U.S.A.

LEOPOLD, L.B. and EMMETT, W.W. 1976. Bedload measurements, East Fork River, Wyoming. *Proc. Nat. Acad. Sci., U.S.A.,* Vol. 73, No. 4, pp 1000-1004.

LEOPOLD, L.B. and MADDOCK, T. Jnr. 1953. The hydraulic geometry of stream channels and some physiographic implications. *U.S. Geol. Surv. Prof. Paper 252,* Washington D.C., U.S.A.

LEOPOLD, L.B. and WOLMAN, M.G. 1957. River channel patterns: Braided, Meandering and Straight. *U.S. Geol. Surv. Prof. Paper 282-B,* Washington D.C., U.S.A.

LEOPOLD, L.B.; WOLMAN, M.G. and MILLER, J.P. 1964. Fluvial processes in geomorphology, W.H. Freeman and Co., San Francisco, U.S.A., 522 p.

LI, W.H. 1955. Criteria for simlitude of scour below hydraulic structures. Proc. *6th General Meeting of the I.A.H.R.,* The Hague, Netherlands.

LIGGETT, J.A. 1975. Stability. In: *Unsteady Flow in Open Channels.* (Vol. 1), (Ed. by K. Mahmood and V. Yevjevich.) Water Resources Publications, Colorado, U.S.A., pp 259-282.

LISLE, T. 1979. A sorting mechanism for a riffle-pool sequence. *Geological Society Am. Bull.* Vol. 90, pt 2, pp 1142-1157.

MacMURRAY, H.L. 1982. Development and evaluation of the salt-velocity method for the measurement of friction factor in rough boundary open channels. M.E. thesis, University of Canterbury, Christchurch, N.Z. (In prep.)

MacPHERSON, H.J. 1971. Dissolved, suspended and bedload movement patterns in Two O'Clock Creek, Rocky Mountains, Canada. Summer, 1969. *Journal of Hydrology, 12,* pp 84-96.

McDONALD, B.C. and BANERJEE, I. 1970. Sedimentology studies on the outwash plain below Peyto Glacier, Alberta. *Geol. Surv. Can.,* Paper 70-1A, p 199.

McDONALD, B.C. and BANERJEE, I. 1971. Sediments and bed forms on a braided outwash plain. *Canadian Journal of Earth Sciences,* Vol. 8, pp 1282-1301.

McDONALD, B.C. and DAY, T.J. 1978. An experimental flume study on the formation of transverse ribs. *Current Research, Part A, Geol. Surv. Can. Paper 78-1A,* pp 441-451.

MAYER, P.G. 1959. Roll waves and slug flows in inclined open channels. *Journal of the Hydraulics Div. A.S.C.E.,* Vol. 85, HY 7, pp 99-141.

MEADE, R.H.; EMMETT, W.W. and MYRICK, R.M. 1981. Movement and storage of bed material during 1979 in East Fork River, Wyoming, U.S.A. In: *Erosion and Sediment Transport in Pacific Rim Steeplands.* (Proc. I.A.H.S. Christchurch Symp., Jan. 1981.) (Ed. by T.R.H. Davies and A.J. Pearce.) pp 225-235.

MEGAHAN, W.F. 1976. Sediment storage in channels draining small forested watersheds in the mountains of Central Idaho. *Proc. 3rd Federal Inter-Agency Sedimentation Conf.,* Denver, Colorado, U.S.A. pp 4-115 - 4-126.

MEYER-PETER, E. and MÜLLER, R. 1948. Formulas for bedload transport. *Proc. 2nd Congress of the I.A.H.R.,* Stockholm, Sweden, pp 1-26.

MEYER-PETER, E. and MÜLLER, R. 1949. Eine formel Zur Berechnung des Geschiebetriebes. *Schweiz. Bauzeitung.* 67 Jg., Zürich, Switzerland.

MIDDLETON, G.V. and SOUTHARD, J.B. 1975. Depositional environments as interpreted from primary sedimentary structures and stratification sequences. *S.E.P.M. Short Course No. 2, Dallas.* Society of Economic Paleontologists and Mineralogists.

MILHOUS, R.T. and KLINGEMAN, P.C. 1971. Bedload transport in mountain streams. *Proc. 1971 Hydraulics Div. Speciality Conf., A.S.C.E.,* University of Iowa, U.S.A.

MILHOUS, R.T. and KLINGEMAN, P.C. 1973. Sediment transport in a gravel-bottomed stream. *Proc. 1973 Hydraulics Div. 21st Speciality Conf.,* Montana State University, U.S.A., pp 293-303.

MILLER, J.P. 1958. High mountain stream: Effects of geology on channel characteristics and bed material. *Memoir 4, State Bureau of Mines and Mineral Resources,* New Mexico Inst. of Mining and Technology, Socarro, U.S.A.

MILNE-THOMSON, L.M. 1968. Theoretical hydrodynamics (5th Edition). Macmillan, London, 743 p.

MIZUYAMA, T. 1981. An intermediate phenomenon between debris-flow and bedload transport. In: *Erosion and Sediment Transport in Pacific Rim Steeplands.* (Proc. I.A.H.S. Christchurch Symposium, Jan. 1981.) (Ed. by T.R.H. Davies and A.J. Pearce.) pp 212-224.

MOHANTY, P.K. 1959. The dynamics of turbulent flow in steep, rough, open channels. Ph.D. thesis, Utah State University, Logan, U.S.A. 90 p.

MOORE, W.L. 1943. Energy loss at the base of a free overfall. *Trans. A.S.C.E.,* Vol. 108, pp 1343-1360.

MORRIS, H.M. 1955. Flow in rough conduits. *Trans. A.S.C.E.,* Vol. 120, pp 373-398.

MORRIS, H.M. 1959. Design methods for flow in rough conduits. *Journal of the Hydraulics Div. A.S.C.E.,* Vol. 85, HY 7, pp 43-62.

MORRIS, H.M. 1968. Hydraulics of energy dissipation in steep, rough channels. *Bull. No. 19, Research Div. Virginia Polytechnic Inst.* Blacksburg, U.S.A., 108 p.

NANSON, G.C. 1974. Bedload and suspended-load transport in a small, steep, mountain stream. *Amer. Journal of Science,* Vol. 274, pp 471-486.

NEWSON, M.D. 1981. Mountain Streams. In: *British Rivers.* (Ed. by J. Lewis.) George Allen and Unwin, pp 59-89.

NICOLIS, G. and PRIGOGINE, I. 1977. Self organisation in non-equilibrium systems. Wiley and Sons, N.Y.

NIKURADSE, J. 1932. Gesetzmässigkeiten der turbulenten Strömung in glatten Rohren. *V.D.I. Forschungsheft 356*. Berlin, Germany.

NOVÁK, P. 1955. Study of stilling basins with special regard to their end sill. *Proc. 6th General Meeting of the I.A.H.R.* The Hague, Netherlands.

NOVÁK, P. 1961. Influence of bedload passage on scour and turbulence downstream of a stilling basin. *Proc. 9th Convention of the I.A.H.R.*, Belgrade.

O'LOUGHLIN, C.L. 1969. Streambed investigations in a small mountain catchment. *N.Z. Journal of Geology and Geophysics*, Vol. 12, No. 4.

O'LOUGHLIN, E.M. and MacDONALD, E.G. 1964. Some roughness concentration effects on boundary resistance. *La Houille Blanche*, No. 7, pp 773-782.

PARKER, G.; SAWAI, K. and IKEDA, S. 1982. Bend theory of river meanders. Part 2. Nonlinear deformation of finite-amplitude bend. *Fluid Mechanics*, Vol. 115, pp 303-314.

PETERSON, D.F. and MOHANTY, P.K. 1960. Flume studies of flow in steep rough channels. *Journal of the Hydraulics Div. A.S.C.E.*, Vol. 86, HY 9, pp 55-76.

PRIGOGINE, I. 1978. Time, structure and fluctuations. *Science*, Vol. 201, No. 4358, pp 777-785.

PROFFITT, G.T. and SUTHERLAND, A.J. 1980. Self-armouring of non-uniform alluvial sediments. *7th Australasian Hydraulics and Fluid Mechanics Conf.*, Aug. 18-22, Brisbane, Australia, pp 225-228.

RAJARATNAM, N. and BELTAOS, S. 1977. Erosion by impinging circular turbulent jets. *Journal of the Hydraulics Div. A.S.C.E.*, Vol. 103, HY 10, pp 1191-1205.

RAJU, K.G.R. and GARDE, R.C.J. 1970. Resistance to flow over strip roughness. *Journal of the Hydraulics Div. A.S.C.E.*, Vol. 96, HY 3, pp 815-834.

RAUDKIVI, A.J. and ETTEMA, R. 1977. Effect of sediment gradation on clear water scour. *Technical note: Journal of the Hydraulics Div., A.S.C.E.*, Vol. 103, Hy 10.

RICHARDS, K.S. 1976. The morphology of riffle-pool sequences. *Earth Surface Processes*. Vol. 1, pp 77-88.

RICHARDS, K.S. 1978. Simulation of flow geometry in a riffle-pool stream. *Earth Surface Processes*, Vol. 3, pp 345-354.

ROUSE, H. 1938. Fluid Mechanics for Hydraulic Engineers. Dover Publications.

ROUSE, H. 1939. Criteria for the similarity in the transportation of sediment. *Proc. 1st Hydraulics Conf.*, University of Iowa, U.S.A., pp 33-49.

ROUSE, H. 1965. Critical analysis of open channel resistance. *Journal of the Hydraulics Div. A.S.C.E.*, Vol. 91, HY 4, pp 1-25.

SABOL, G.V. and NORDIN, C.F. 1978. Dispersion in rivers as related to storage zones. *Journal of the Hydraulics Div. A.S.C.E.*, Vol. 104, HY 5, pp 695-708.

SAYRE, W.W. and ALBERTSON, M.L. 1963. Roughness spacing in rigid open channels. *Trans. A.S.C.E.*, Vol. 128, pp 343-372.

SCHEUERLEIN, H. 1973. Mechanics of flow in steep, rough, open channels. *Proc. 15th Congress of the I.A.H.R.*, Vol. 1, Istanbul, Turkey, pp 457-465.

SCHLICHTING, H. 1936. Experimentelle Untersuchungen zum Rauhigkeitsproblem. *Ingenieur Archiv.*, Vol. 7.

SCHMID, W. 1972. Die allge-meine dreidimensionale Kolkentwicklung unter besonderer Berücksichtigung des Geschiebetriebs und der Zeit. *Diss. Nr 4859, Versuchsanstalt für Wasserhau, Hydrologie und Glaziologie, E.T.H.*, Zürich, Switzerland, 224 p.

SCHMID, W. 1973. General, three-dimensional local scour development below a free overfall weir considered as a bedload transport problem. *Proc. 15th Congress of the I.A.H.R.*, Vol. 1, Istanbul, Turkey, pp 573-580.

SCHOKLITSCH, A. 1935. Stauraumberlandung und Kolkbwehr. Julius Springer, Berlin. (Translated from the German by E.F. Wilsey, Bureau of Reclamation, Denver, 1937.)

SCHOPPMANN, B. 1975. The mechanics of flow and transport of a progressive scour. *Proc. 16th Congress of the I.A.H.R.*, Vol. 2, Sao Paulo, pp 189-195.

SCHUMM, S.A.; BEAN, D.W. and HARVEY, M.D. 1982. Bed-form-dependent pulsating flow in Medano Creek, Southern Calorado. *Earth Surface Processes and Landforms*, Vol. 7, pp 17-28.

SEDDON, J. 1900. River hydraulics. *Trans. A.S.C.E.*, Vol. 43, pp 179-243.

SHAW, J. and KELLERHALS, R. 1977. Paleohydraulic interpretation of antidune bedforms with applications to antidunes in gravel. *Journal of Sedimentary Petrology*, Vol. 47, No. 1, pp 257-266.

SILVERSTON, E. and LAURSEN, E.M. 1976. Patterns of scour and fill in pool-rapid rivers. *Proc. 3rd Federal Inter-Agency Sedimentation Conf.*, Colorado, U.S.A., pp 5-125 - 5-136.

SUTHERLAND, A.J. and WILLIMAN, E.B. 1977. Development of armoured surfaces in alluvial channels. *6th Australasian Hydraulics and Fluid Mechanics Conf.*, Dec. 5-9, Adelaide, Australia, pp 352-355.

TAKAHASHI, T. 1978. Mechanical characteristics of debris flow. *Journal of the Hydraulics Div. A.S.C.E.*, Vol. 104, HY 8, pp 1153-1169.

THOMAS, H.A. 1940. The propagation of waves in steep prismatic conduits. *Proc. of the Hydraulic Conf., State University of Iowa, Studies in Engineering, Bull. 20*, March 1940.

THOMAS, R.K. 1953. Scour in a gravel bed at the base of a free overfall. M.Sc. thesis, A & M. College, Fort Collins, Colorado, U.S.A., 117 p.

THOMPSON, S.M. and CAMPBELL, P.L. 1979. Hydraulics of a large channel paved with boulders. *Journal of Hydraulic Res.*, Vol. 17, No. 4, pp 341-354.

UNITED STATES DEPARTMENT OF THE INTERIOR (BUREAU OF RECLAMATION). 1951. Water Measurement Manual, 2nd Edition, 1981 printing. Denver, Colorado, U.S.A.

VALENTINE, E.M. and WOOD, I.R. 1977. Longitudinal dispersion with dead zones. *Journal of the Hydraulics Div. A.S.C.E.*, Vol. 103, HY 9, pp 975-990.

VALENTINE, E.M. and WOOD, I.R. 1979. Experiments in longitudinal dispersion with dead zones. *Journal of the Hydraulics Div. A.S.C.E.*, Vol. 105, HY 8, pp 999-1016.

VANONI, V.A. (Ed.) 1975. Sedimentation Engineering. *A.S.C.E. - Manuals and Reports on Engineering Practice - No. 54,* 745 p.

VEDERNIKOV, V.V. 1945. Conditions at the front of a translation wave distributing a steady motion of a real fluid. *Comptes rendus (Doklady) de l'Académie des Sciences de l'U.R.S.S.,* Vol. 48, No. 4, pp 239-242.

VENNARD, J.K. and WESTON, R.F. 1943. Submergence effect on sharp crested weirs. *Engineering - News Record,* Vol. 130, No. 22, pp 118-120.

VILLEMONTE, J.R. 1947. Submerged-weir discharge studies. *Engineering-News Record,* Vol. 139, No. 26, pp 54-57.

VOLKART, P. 1972. Die Stabilisierung von flussläufen mittels einer folge von querschwellan. *Nr 6, Mitteilungen, Versuchsanstalt fur Wasserbau, Hydrologie und Glaziologie, E.T.H.,* Zürich, Switzerland, 58 p.

VOLKART, P.; TSCHOOP, J. and BISAZ, E. 1973. The effect of sills on riverbed. *I.A.H.R. Symposium on River Mechanics,* Jan. 9-12, Bangkok, Thailand, pp 167-178.

WHITTAKER, J.G. and DAVIES, T.R.H. 1982. Erosion and sediment transport processes in step-pool torrents. *1st I.A.H.S. Scientific General Assembly (Symposium 4: Recent developments in the explanation and prediction of erosion and sediment yield).* Exeter, U.K.

WHITTAKER, J.G. and JÄGGI, M.N.R. 1982. Origin of step-pool systems in mountain streams. *Journal of the Hydraulics Div. A.S.C.E.,* Vol. 108, In press.

WOLMAN, M.G. 1977. Changing needs and opportunities in the sediment field. *Water Resources Research, Amer. Geophysical Union,* Vol. 13, No. 1, pp 50-54.

YALIN, M.S. 1977. Mechanics of Sediment Transport. (2nd Edition.) Pergamon Press, Oxford, 298 p.

YANG, C.T. 1971. Formation of riffles and pool. *Water Resources Research,* Vol. 7, No. 6, pp 1567-1574.

YANG, C.T. 1972. Unit stream power and sediment transport. *Journal of the Hydraulics Div. A.S.C.E.,* Vol. 98, HY 10, pp 1805-1826.

YANG, C.T. 1976. Minimum unit stream power and hydraulics. *Journal of the Hydraulics Div. A.S.C.E.*, Vol. 102, HY 7, pp 919-934.

YANG, C.T. and STALL, J.B. 1976. Applicability of unit stream power equation. *Journal of the Hydraulics Div. A.S.C.E.*, Vol. 102, HY 5, 559-568.

APPENDIX 1

ANALYSIS OF AVERAGE VELOCITY FROM CONDUCTIVITY TRACES.

Average flow velocity was calculated from equation 3-2

$$\text{i.e. } v_m = \frac{x_2 - x_1}{\bar{t}_2 - \bar{t}_1} \qquad \ldots 1$$

where symbols are as defined in Chapter 3. For the present tests, $x_2 - x_1$ was a measured value. The quantity $\bar{t}_2 - \bar{t}_1$ is the distance between the centroids of the conductivity-time curves from the chart recorder traces corresponding to measurements of conductivity at locations x_1 and x_2, divided by the speed of the chart paper through the chart recorder.

Each pair of conductivity curves was analysed as follows: a false origin was established, and the area under each of the associated curves divided into strips (fig. 1).

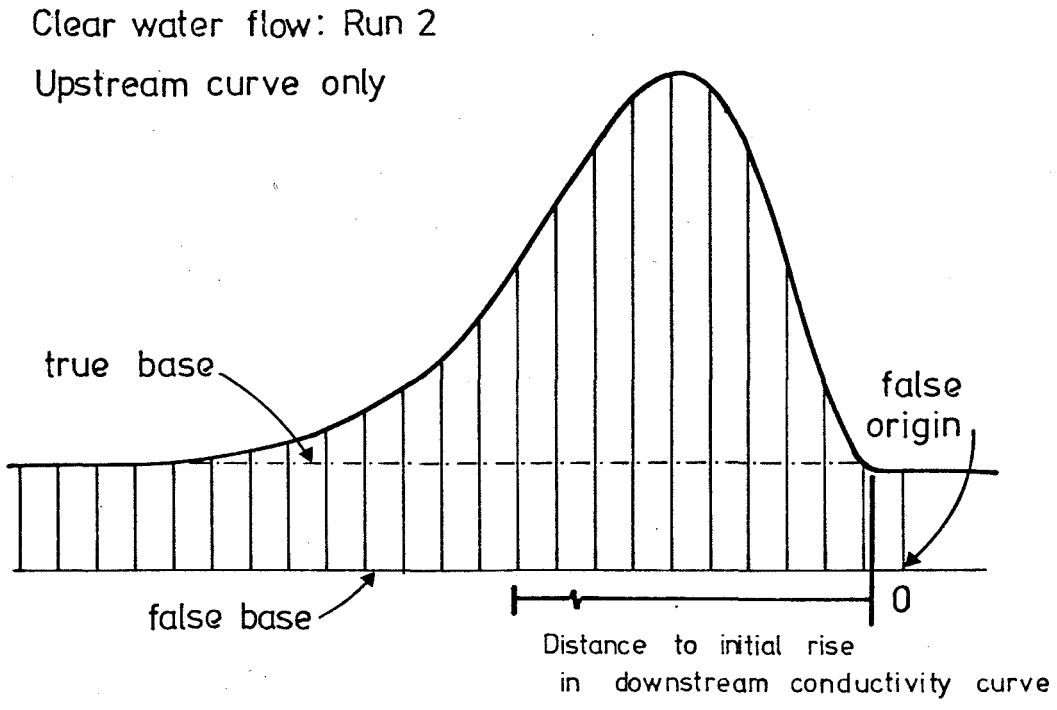

Figure 1: Treatment of conductivity curve for analysis of centroid.

The distance of the centroid of the area under each curve from the false origin was calculated as

$$x_m = \frac{\Sigma\ (A_i\ x_i)}{\Sigma\ A_i} \qquad \ldots 2$$

Strip areas (Ai's) under each conductivity trace were evaluated from a false base (as shown in fig. 1). The area from this base to the level of the tail of each conductivity curve was then subtracted, to give the A_i value. The level of the tail of each conductivity curve was established by averaging many strip area values from the essentially constant tail portion of each curve. In this way, the effect of dead zones on mean flow velocity was removed (see section 3-5 and fig. 3-12).

$x_{m2} - x_{m1}$ is thus the distance between the associated centroids, and is independent of the position of the false origin. The time between the two centroids is then

$$\bar{t}_2 - \bar{t}_1 = \frac{x_{m2} - x_{m1}}{v'} \qquad \ldots 3$$

where v' = speed of paper through the chart recorder.

An example of an analysed trace is shown in fig. 2.

With unstable tumbling flow, wave effects on the conductivity trace patterns became marked (see fig. 3). Most of the conductivity curves of this sort were analysed in the manner described above.

Sediment transport resulted in a different change to the conductivity trace patterns. This was due to oscillating pool levels at the probe stations associated with the sediment transport mechanism outlined in section 7-5-2. An example of a conductivity trace influenced in this way is shown in fig. 4. The strip areas under curves influenced by the transport mechanism were sometimes evaluated as follows. The trend in conductivity from before the tracer was introduced was continued through to the tail of the conductivity curve (see fig. 4). Strip areas were then evaluated by subtracting areas below this curve from the strip areas between the conductivity trace and the false base.

When unstable tumbling flow occurred with sediment transport, the downstream conductivity trace sometimes showed 'beating' (i.e., the pattern resulting from the superposition of two wave forms of different frequency). An example is shown in fig. 5.

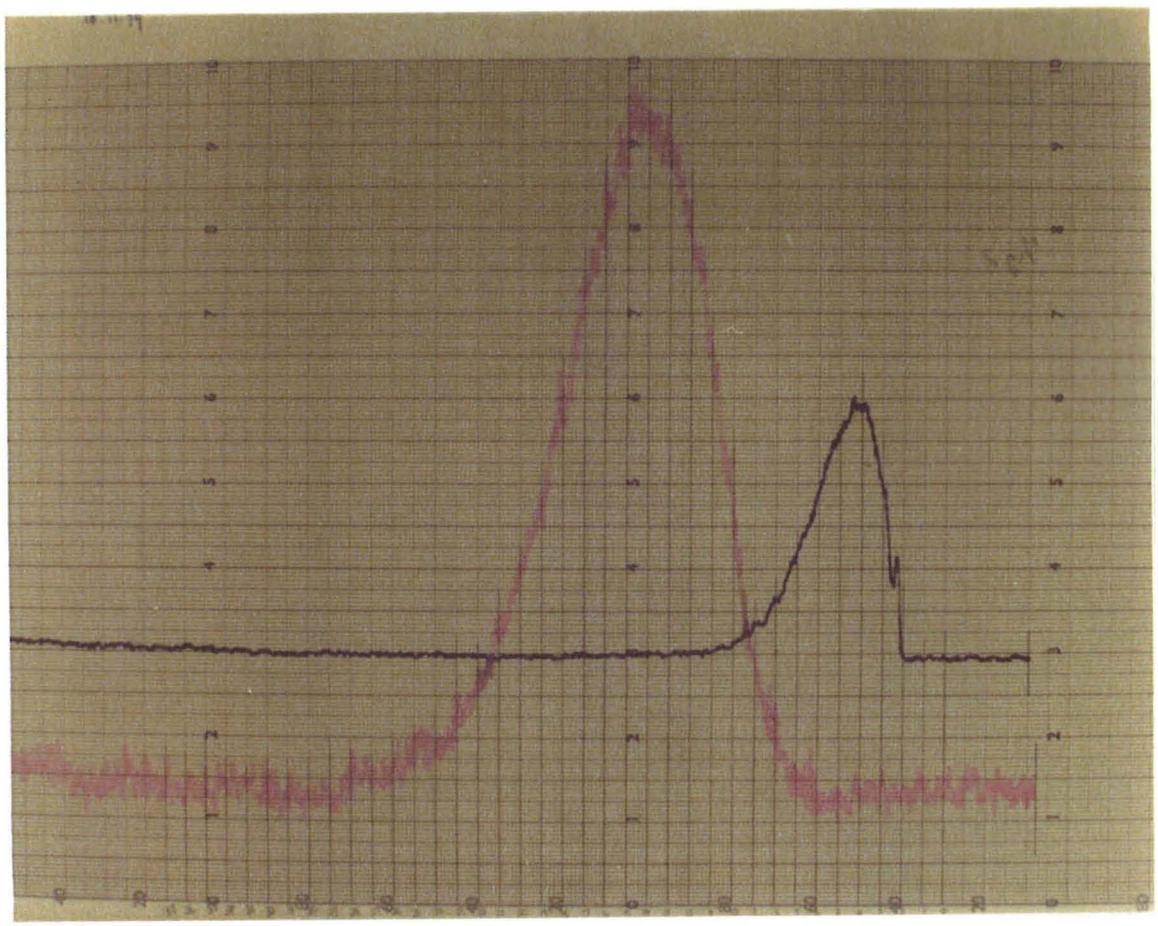

Figure 2: An example of an analysed trace.

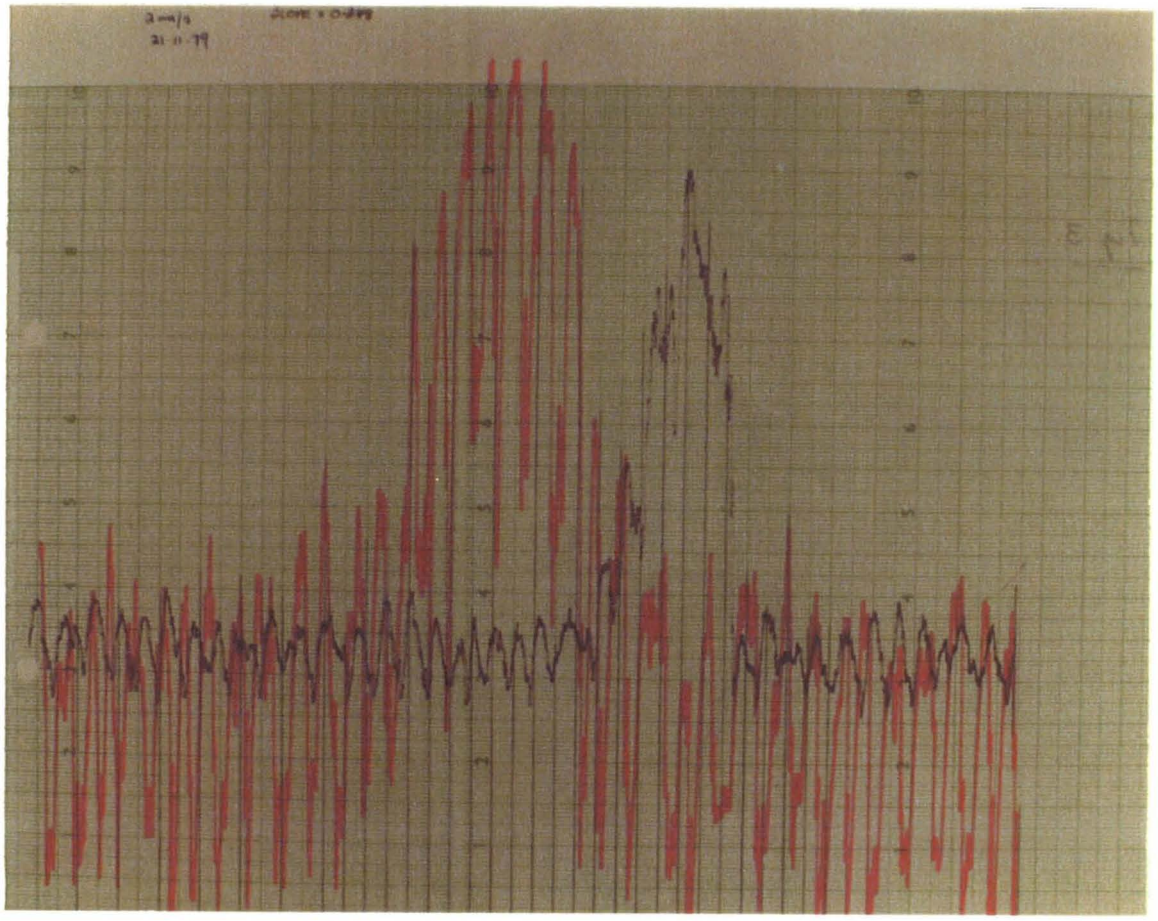

Figure 3: Effect of roll waves on conductivity trace patterns.

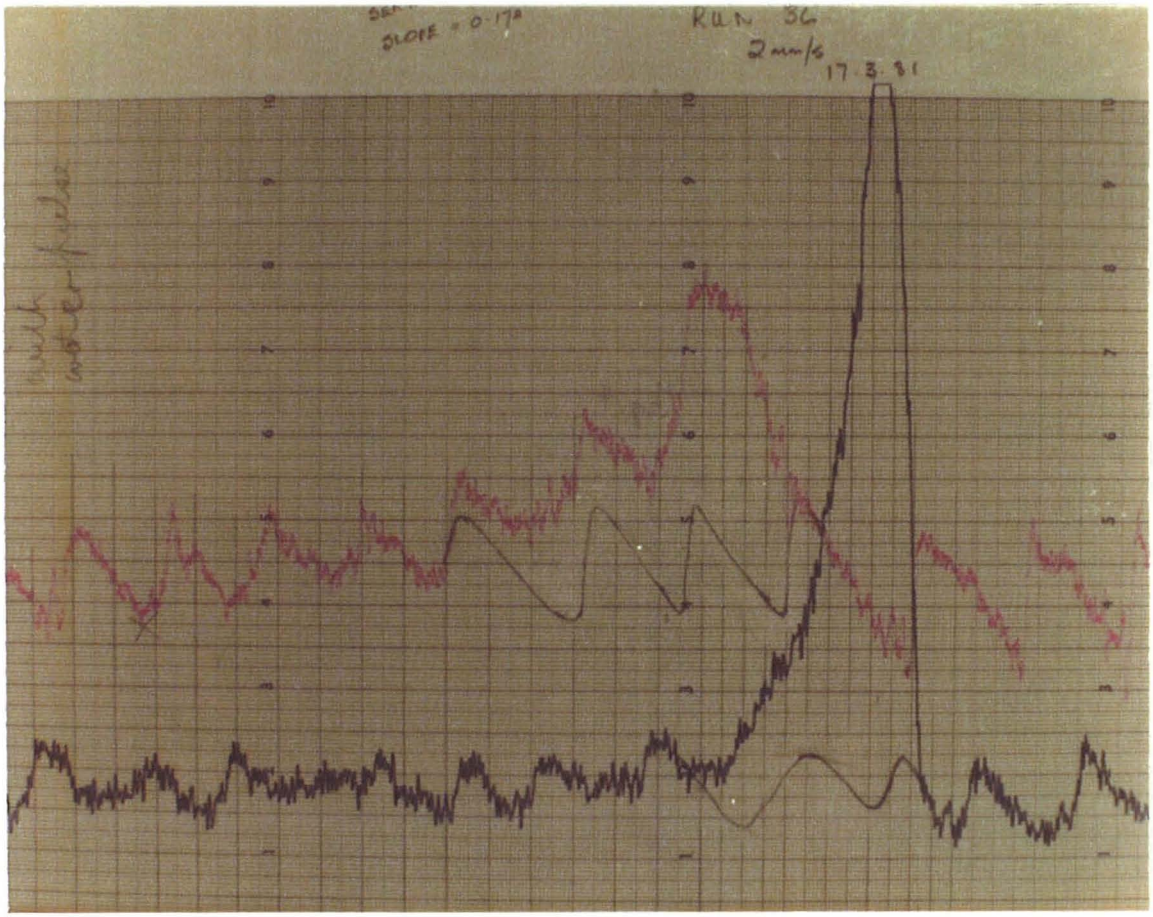

Figure 4: Conductivity traces influenced by oscillating pool levels associated with the sediment transport mechanism.

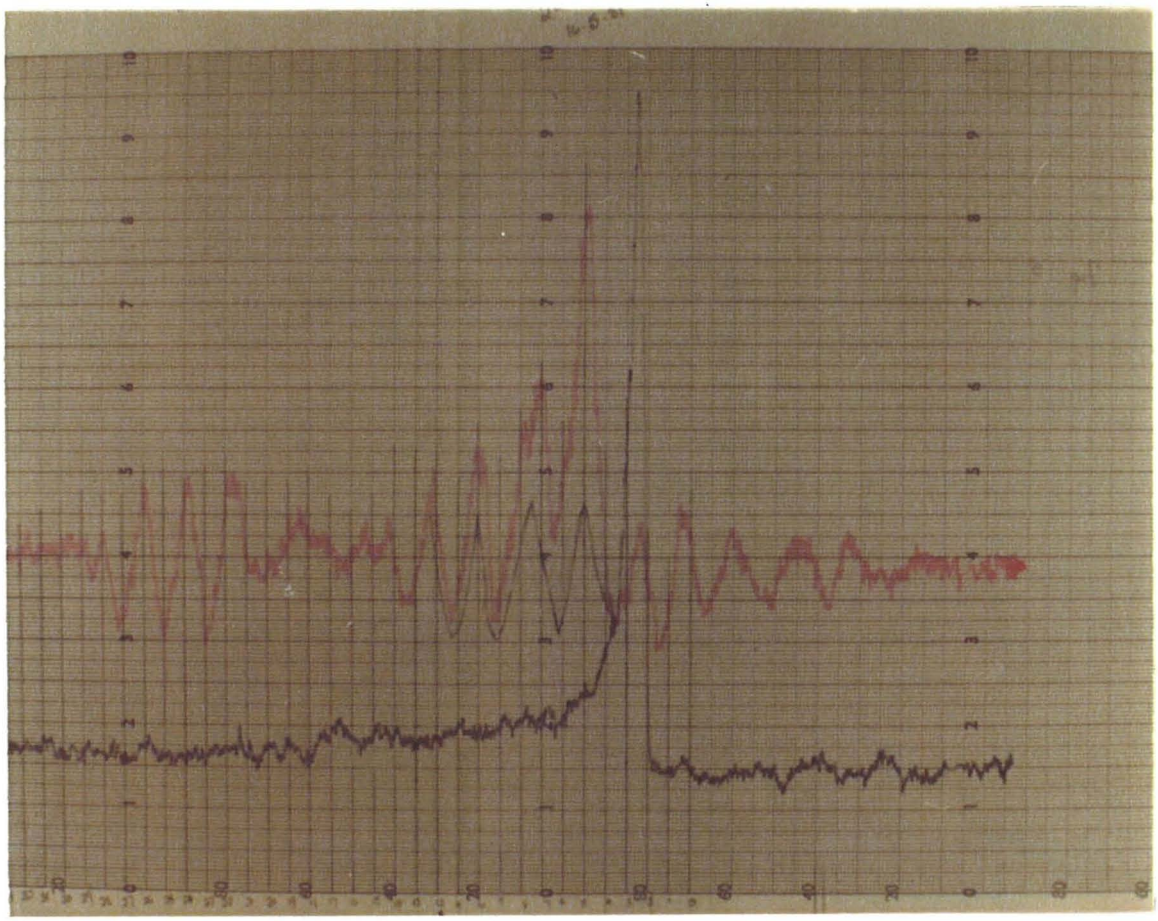

Figure 5: 'Beating' shown in conductivity trace.

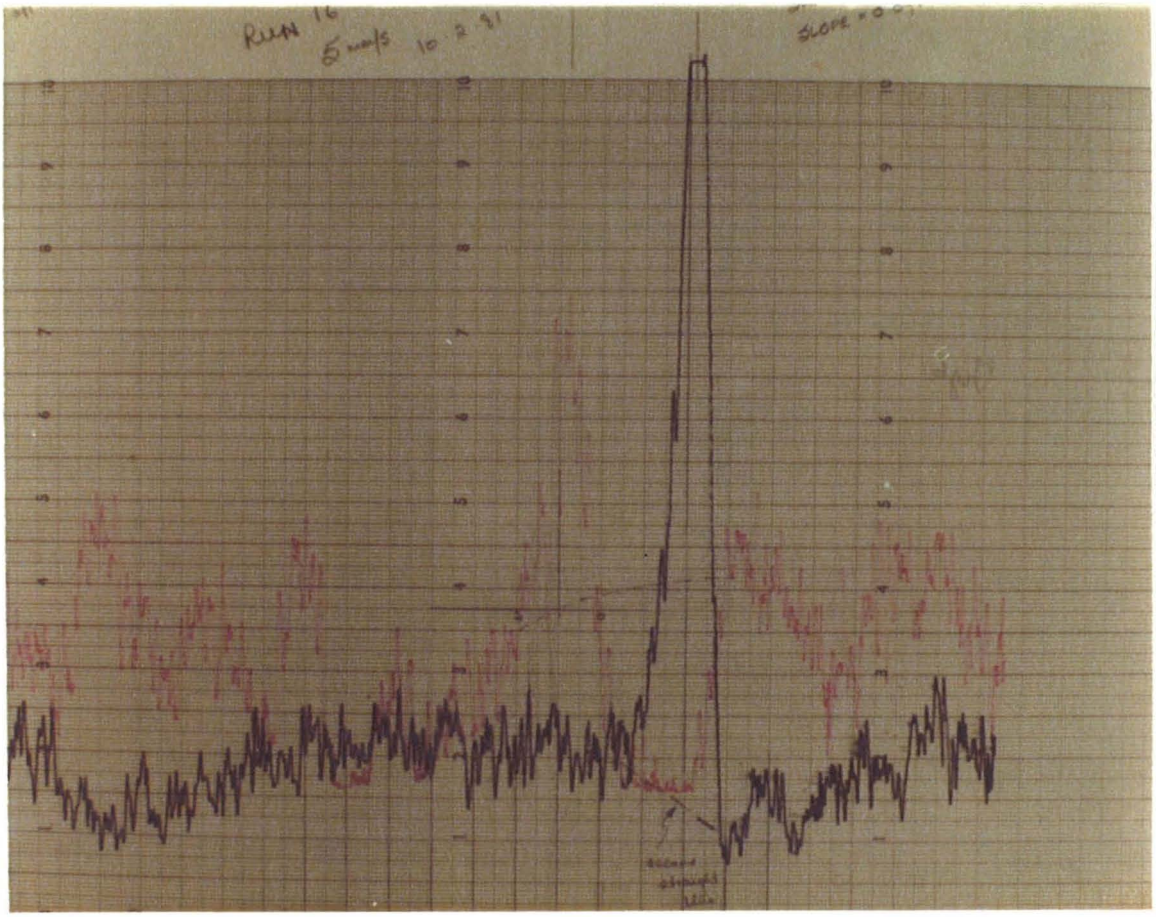

Figure 6: Conductivity traces with long-term trends.

At other times, the conductivity traces resulting from sediment waves and unstable tumbling flow produced patterns with long-term trends. To analyse these, the trend was continued and the strip areas A_i were evaluated as those between these lines and the conductivity traces (fig. 6).

With sediment transport, some flow rates which had large variations in conductivity curve pattern at low Q_s values produced quite smooth conductivity traces at high Q_s values. This is due to the lessening of flow instability with Q_s, and also because the change in water level associated with the transport mechanism was small as % scour became very small.

Although the form of the conductivity-time curves sometimes makes the derivation of accurate mean velocities difficult, there is little doubt that with flow instability and sediment waves occurring, this is the best available method of obtaining the information.

Maximum velocities for each test run were obtained by measuring the distance between the initial rise of conductivity trace of the upstream and downstream conductivity-time curves (see fig. 1). This distance was divided by the speed of the paper in the chart recorder to give a time t_{min} taken by the fastest tracer particles (and thus, by the fastest water particles) between the two probe stations.

Thus,

$$v_{max} = \frac{x_2 - x_1}{t_{min}} \qquad \ldots 4$$

APPENDIX 2

MANUSCRIPT OF THE PAPER 'ON THE ORIGIN OF STEP-POOL SYSTEMS IN MOUNTAIN STREAMS' (BY WHITTAKER AND JÄGGI), CURRENTLY IN PRESS.

The manuscript as presented here differs from the contents of Chapter 4. This difference is due to a methodological error in the work presented in this appendix that was discovered during writing of the thesis.

Average velocities v_m given in this appendix were not compensated for their underflow component. The true average velocity of the surface flow deforming the bed v_u is given by

$$v_u = \frac{q_t}{q_{D_u}} \left(v_m - \frac{q_{und} \, v_{und}}{q_t} \right) \qquad \ldots \; 1$$

where q_t = total specific discharge

q_{und} = specific discharge of underflow

v_{und} = velocity of underflow

and $q_{D_u} = q_t - q_{und}$ ... 2

The difference between v_u and v_m was insignificant at low slopes, but major at high slopes. Consequently, values of shear stress and friction factor are also quite different for high slopes. Despite this, the predicted armour layers (final conditions) were almost identical, with the worst error for any grain size being about 5%. Using v_u instead of v_m focussed the antidune results a little more clearly, strengthening the assertions regarding the role of antidune formation in the origin of step-pool systems.

Thus, while the difference in analysis changed some of the hydraulic variables, the results are fairly much the same.

ORIGIN OF STEP-POOL SYSTEMS IN MOUNTAIN STREAMS

by

Jeffrey G. Whittaker[1]
Martin N.R. Jäggi[2]

Summary

Experiments show that in steep mountain streams a bed-deforming process exists giving the low-flows a step-pool aspect. Steps and pools are the result of a combined action of self armouring and antidune formation which results in an important increase in flow resistance.

[1] Research Fellow, Dept of Agr. Engrg., University of Canterbury, Lincoln College, Canterbury, New Zealand

[2] Sen. Research Engr., Lab. of Hydraulics, Hydrology and Glaciology, Fed. Inst. of Technology, Zurich, Switzerland

Keys Words: bedforms, mountain streams, self armouring, sediment transport

Abstract: Mountain streams very often present a step-pool aspect. Antidune formation alone; dispersion and sorting theory or velocity reversal as advocated for the origin of riffle-pool sequences do not explain how steps and pools form. Experiments have been conducted to clarify their origin. If was found that the step-pool aspect appears after high flows had deformed the bed. During the presented tests a self armouring process occurred which resulted in a stabilization of the bed. When coarsening of the top layer was little classic antidunes resulted. An important coarsening was accompanied by a structuring of the bed into roughness elements whose spacing did correspond to maximum flow resistance. The substantial increase in resistance was an essential factor in bed-stabilization.

INTRODUCTION

Longitudinal stream profiles do not usually show a smoothly varying slope, but take the form of reaches of alternately flatter and steeper slope, due respectively to deep and shallow sections. The tendency for this development is a fundamental characteristic of many streams, and is largely independent of channel bed or bank material (23). In steep mountain streams, this tendency has frequently been reported (15, 16, 20, 21, 34, 46). In these streams, the alternating sections are often called steps and pools, because of their stair-like appearance. Until a fundamental understanding of the development and characteristics of step-pool sequences is gained, solutions to problems of hydraulics in steep mountain streams will rest on vague empiricism. The objective of this paper is to clarify the origin of step-pool sequences, and to assess their effect on the stability of the bed.

STEP-POOL SYSTEM STRUCTURE

Steep mountain streams tend to have a distinctive order to their structure, the characteristic units of which are steps and pools (see fig. 1(a)). Streams containing steps and pools are usually described either morphologically, or from the perspective of flow characteristics. In a morphological description, the stream channel configuration is said to be stair-like. Water flows over steps formed by the arrangement of boulders and large sized sediments across the stream channel, and falls into pools where a significant part of the fluid energy is consumed be roller eddies (3, 15, 16, 34, 40). In forested areas, the channel often has steps resulting from obstructions to the flow caused by logs that have fallen into the stream bed (17, 18, 24). Some authors have called steps "transverse ribs" (7, 33, 35, 36). When the stream is described in terms of its flow characteristics, the flow is seen as a series of more or less regularly spaced cascades (25, 26, 47) characterised by locally high velocities and intense turbulence, often combined with air entrainment (1, 20, 39, 41, 46) (see fig. 1(b)).

An analogy exists between step-pool systems and riffle-pool sequences. Riffle-pool sequences are found in rivers with a flatter slope and are mainly associated with bar formation and meandering (22, 34, 43, 44). The common feature of riffle-pool sequences is that their spacing corresponds

to approximately 5-7 channel widths. Step-pool systems have a much shorter wavelength which shows no such correlation with channel width. The analogy between riffle-pool and step-pool sequences exists, however, in view of the similar periodic flow disturbance and the differential grain size distribution between pools and riffles or steps. Hayward (15, 16) distinguishes different forms of steps, for instance those whose visual aspect is close to a riffle are called riffle steps.

POSSIBLE MECHANISMS FOR STEP-POOL FORMATION

General features of any theory of origins:

Any theory attempting to explain the origin of step-pool systems must take into account the fact that they are disequilibrium bed forms in the sense proposed by Allen (2) and Middleton and Southard (37). The structures are not created by the low flows which give the visual step-pool appearance and which move very little bed sediment; rather their formation is associated with flow conditions during high-intensity, low frequency flood events.

A necessary factor for step-pool formation is that there must be heterogeneity of bed material size (34). Such material may be derived from a variety of sources, for example weathering of steep cliffs, glaciation deposits (38), and tributary streams (14), as well as that transported by the stream. Thus both the material size and its source are independent variables (similarly for log steps). This coarse material is restructured into step-pool patterns. Boulders are swept out of incipient pools and collected in incipient riffles (34). Armouring of the bed is a feature of this restructuring. Step-pool formation may also be affected by the influence of past and present climatic/hydrologic regimes. Some mountain streams investigated have, in the past, been subjected to much higher flows than those experienced at present. However, apparently immovable bed material such as that reported by Miller (38) may in fact be capable of responding to a low-interval flood. Hence, it can be seen that step-pool systems are generally not in equilibrium with "normal flow" conditions. In this context some existing theories of step-pool origin are now examined.

The antidune theory of origin:

Features in shallow gravel channels which have been called transverse ribs (35) correspond to step-pool sequences in steep cobble channels (7). Many authors (5, 6, 7, 32) consider these transverse ribs to be antidunes. Shaw and Kellerhals (48) found a striking similarity between bed forms in the field and gravel antidunes developed in the laboratory, both in rather uniform material.

The difficulty in equating transverse ribs (and thus steps) with antidunes lies not in the validity of the proposal (as is shown subsequently by the writers), but in the mechanism proposed to explain the formation of transverse ribs. Firstly, antidunes are formed in association with a standing wave, where the waveform of the bed is in phase with the form of the water surface (29). Transverse ribs on outwash areas are reported to have formed when material introduced locally generated an accompanying surface wave (32). This introduced bed material is atypical of the bed material and so the bed forms are not true bedwaves as proposed by Kennedy (29). Secondly, the mechanism proposed by Koster (32) involves growth of a ribbed sequence proceeding upstream in response to a water disturbance migrating upstream in discrete steps. According to Kennedy (29), an antidune wavetrain propagates downstream, regardless of the direction of movement of the antidunes.

A variation on this theme is a mechanism proposed by McDonald and Day (36) in which transverse ribs are formed by a process in which a hydraulic jump travels rapidly upstream in an episodic fashion. Pebbles accumulate just downstream of the hydraulic jump during the intervals when it is stationary. As pointed out by McDonald and Day (36), it is difficult to transfer this formative mechanism to natural channels, and it has never been reported in the literature.

Dispersion and sorting theory:

Yang (52) developed a theory that riffle-pool sequences (and thus, by analogy, step-pool sequences) occur because "natural streams minimise their time rate of potential energy expenditure per unit mass of water in accordance with the law of least time rate of energy expenditure". Yang further suggests that in riffles, where the local energy gradient is higher than average, there would be a high rate of shearing of bed material. Bed elevation would consequently increase with migration of coarse material

to the surface due to a grain dispersion process reported by Bagnold (4). For these effects to occur, however, the whole bed must be in a state of general shearing motion to a considerable depth. In a gravel river this would occur only under debris flow conditions.

Velocity reversal theory:

This theory, although developed for riffles and pools, can by analogy be considered to apply to steps and pools. Keller (22) measured velocities in pools and riffles for different discharges. He reported that with increasing discharge, there was a greater increase of velocity in the pools than in the riffles. He concluded from extrapolation of this data, that there would be a velocity reversal at high flows which would move coarse grains quickly from a riffle, through the subsequent pool to be deposited in the next riffle, thus maintaining these features.

There is no evidence that this reversal actually occurs. The data used does not show a velocity reversal, only a velocity equalisation. Further the mechanism proposed from the anticipated velocity reversal is essentially one of maintenance of riffle-pool and step-pool forms; it does not account for development of the bedforms from an initially plane bed.

TESTS

Tests were performed to clarify the process of the origin of step-pool sequences. Bed-forming and grain sorting processes were expected to occur under appropriate flow conditions. It was thought that either or both tendencies would eventually stabilise the bed for flows capable of deforming an initially plane bed.

Test procedure:

The laboratory tests were performed in a tilting, recirculating channel, 10m long, 0.132m wide and 0.5m deep. A graded sediment ranging between 2mm and 50mm in size (see fig.5), initially arranged as a plane bed, had a sediment-moving discharge passed over it. No sediment was fed at the upstream end of the flume; thus parallel and rotational degradation occurred as the bed was eroded. Because of the steep slopes used, the change in slope associated with rotational degradation was, where it occurred and the

bed also stabilized, comparatively small. For most of the selected discharges the bed achieved a stable condition when sediment motion ceased.

Stabilization was favoured because of increased resistance to flow, for most of the test runs. This increase was due to an increase in form resistance as well as armouring of the bed. To estimate resistance to flow, measurements of mean flow velocity were made, using an adaption of the salt-velocity measurement technique (9).

When the bed had stabilized under the deforming flow, to what are subsequently referred as final conditions, the discharge was reduced to study the low flow appearance of the bed. This allowed a visual comparison with the field situation, commensurate with the disequilibrium concept mentioned above.

At the completion of each run, the longitudinal profile of the bed was measured. Bed armouring was seen to be a significant factor, so areal bed samples were taken. A proportion of bed surface was sprayed with paint, the painted stones removed by hand, and a sieve analysis of these stones performed. The areas sampled extended over at least one bedform, therefore represent an average and not a local grain size distribution.

Discharge measurements were made with a calibrated orifice plate inserted in the return pipe. A summary of experimental data is found in table 1.

EXPERIMENTAL OBSERVATIONS

Within the ranges of slopes (2.5% to 25%) for which experimental flume runs were performed, two clearly defined cases were observed:

At lower slopes, for relatively high flow rates, antidunes formed which were similar to those reported by Shaw and Kellerhals (48). As the flow rate was subsequently reduced, a hydraulic jump formed in the existing trough region. The visual impression at a low flow rate was more that of a riffle-pool sequence, although the wavelength was obviously determined by that of the original antidunes. Fig.2(a) illustrates conceptually a run with the progression from bed-forming flow to low flow.

At higher slopes and relatively small flows, the coarser grains had a considerable effect on the bed deforming process. The flow initially formed regular wavetrains, but with some degradation the flow pattern subsequently developed increasingly in response to the location of larger individual roughness elements. These larger elements anchored some of the waves, preventing migration. Some of the "steps" so formed, occasionally broke down, setting in motion a short-lived "slug" of sediment. At a low flow rate, relative to the deforming flow, the flow pattern closely resembled step-pool sequences as seen in natural situations (see fig.2(b)).

The transitions slope between the two above mentioned cases was about 0.075.

RESULTS

The main results of the tests are listed in table 1. A side-wall correction procedure, for estimating friction losses due to the flume walls, was applied after Gessler (11).

From the test results the friction factor, f_s, the average bottom shear stress, $\bar{\tau}$, and the hydraulic radius with respect to the bed, r_s, were calculated.

For a comparison of the results, f_s, d and r_s values were computed for the plane bed case at the beginning of the tests. Because of rapid initial bed deformation, it was not possible to measure these parameters. Thus, for computation of resistance to flow in this case, the Keulegan logarithmic resistance law was used. The occurrence of wake interference losses in the lee of larger roughness elements necessitated the use of a roughness height of $3.5D_{84}$ in the Keulegan computation (Hey (19)). Thompson and Campbell (50), noting this blocking effect, have suggested $k_s = 4.5D$, where D is the median boulder diameter. From a theoretical perspective, the choice of a coefficient of 3.5 is somewhat arbitrary. Thus, the values of $\sqrt{f_{so}/f_s}$ are not precise. This explains why some of these values (tests 11/14/17) are slightly greater than unity.

Because of the high gradients in the experiments, sin θ was used for the energy slope instead of tan θ (46).

Wavelength of observed bedforms:

Kennedy (29,30) developed an analysis of antidune bedforms, which related the Froude number F of the flow to the wave number k ($k = 2\pi/L$ where L is the wavelength of the bedform) and the flow depth d. He found that the region for possible antidune formation is delineated by equations for maximum and minimum Froude number F_m and F_a. These two defining envelopes are shown in fig.3; the enclosed region is that denoted by the letters ABC.

The experimental values of bed wavelength L were calculated from a zero-crossing analysis of the measured bed profile. Photographs of runs taken at slopes less than 0.075 gave wavelengths that were different from those indicated by zero-crossings analysis; the rough sediment profile yielded more zero-crossings than the fluid pattern showed. Both values of wavelength are shown in table 2. Using the value d_o, (the computed flow depth at the beginning of the tests), for the determination of F and k, results were obtained as shown in fig.3. The points fall within, or are close to, the region of antidune formation. However, using d, the flow depth derived from velocity measurements at the end of the tests, only the tests on slopes less than 0.075 give points that are consistent with antidune formation. Other points fall well outside this region because the bed deformation increased d and decreased F from their initial values. This supports the observation that at slopes greater than 0.075, initially regular wavetrains were subsequently modified by the flow, which was increasingly influenced by the presence of larger individual roughness elements as degradation occurred.

The Froude number F was calculated from the formula $F = u_m/\sqrt{(gd \cos \theta)/\alpha}$ which allows for steep slope effects. The coriolis coefficient α was calculated from the mean value given by the equations of Obrazosvskiy and Morozov (13)

In fig.3 points corresponding to the initial depth d_o were plotted only if there was a substantial difference to the values deduced from the final depth d.

Steepness of observed bedforms:

Bedforms are not only characterised by their wavelength, but also by their steepness, i.e. the ratio of their height to their wavelength. In a more general way this value has been called roughness spacing when considering isolated roughness elements and their concentration over the bed (45).

An ideal spacing, which corresponds to a local maximum of the resistance coefficient (10), has been reported for artificial roughness elements and lower regime bedforms (8, 45, 51). Upper regime bedforms, i.e. antidunes tend to develop a steepness that lies within the range given by Rouse (45) as corresponding to a maximum of resistance for artificial roughness elements, but this steepness is only achieved when the surface waves are on the point of breaking. The ideal steepness is thus only reached cyclically, and usually only occurs over a portion of the bed. The mean steepness of antidunes thus tends to be less than the 'ideal' value.

For an armoured bed, Sutherland and Williman (49) again found such a tendency towards an ideal spacing. They used a zero crossing analysis to define element size, or height, as the maximum difference in elevation between successive upward zero crossings defining the element. The mean height of all elements is a measure of the effective roughness size of the surface. Effective roughness concentration e was defined as the sum of the heights of all elements divided by the length of the sample. For the tests reported herein, each maximum height between successive upward zero crossings was divided by the distance between the same upward zero crossings, and the mean of the resultant steepness values taken to give an effective roughness concentration e. The results are shown in table 3.

Resistance to flow:

During formation of step-pool systems (as simulated by these tests), bedform generation and grain sorting increased the resistance to flow. The grain sorting resulted in an armoured stable bed, with larger grains acting as isolated roughness elements. The increase in flow resistance can be characterised by the ratio $\sqrt{f_{so}/f_s}$, where f_s is calculated from the test results, and f_{so} from the computed initial flow velocities. Values of this ratio are listed in table 1.

The tests with low slope and high discharge showed no appreciable change in resistance. However, for the test runs at higher slopes, with lower discharges, the increase in resistance was very large. This is despite the fact that for these runs (i.e. the tests at slopes greater than 0.075), large scale roughness effects were considered in calculating the initial resistance coefficient by virtue of using the modification to the Keulegan resistance law as proposed by Hey (19).

Bed armouring:

In widely graded materials, the flow causes grain sorting. This leaves a coarser top layer by preferentially eroding more of the finer materials than the coarser. Gessler (11, 12), approached the problems from a probabilistic perspective. There is a probability q of remaining in the top layer, which is function of the flow conditions. If p is the grain size distribution curve for the original material, then $dp_a = q\ dp/({}_o\int^1 q\ dp)$ defines the grain size distribution of the top layer. Further, an average probability $\bar{q}$ is defined (12), where $\bar{q} = {}_o\int^1 q\ dp_a)$. If this value exceeds 0.5, then a stable top layer can be formed. The analysis (11) for predicting the armoured top layer was applied to a sample of the original material used in the experimental runs previously described. Results are shown for three runs in fig.4, compared with the corresponding measured armour layer, where runs 3 and 18 present maximum difference between predicted and measured distribution of all the tests. Table 4 lists the values of $\bar{q}$ corresponding to initial conditions.

For slopes larger than 0.075 all values of $\bar{q}$ are far lower than the limit of bed stabilization 0.5. Stabilization was therefore possible only due to increase in flow resistance, as also illustrated by the values of $\sqrt{f_{so}/f_s}$. For the runs with flatter slopes no noticeable increase of flow resistance was found. The corresponding values of table 4 fall close to 0.5, the differences are believed to be attributed to the precision of the measurements.

The effect of the sampling procedure and corresponding correction procedures have been discussed by Kellerhals and Bray (28), later by Proffitt and Sutherland (42). In fig.5 some armour layer grain size distribution curves (areal sampling) are modified to allow comparison with the original curve (volume sampling).

DISCUSSION OF RESULTS

The values of the Darcy-Weisbach friction fact f_s, found in the above experiments after stabilization, are extremely high. However, they are similar to values obtained by other researchers for flow in similar channels. as reported by Scheuerlein (46).

For the low-slope runs 11, 12, 14, 17 and 18, the change in resistance to flow was negligible over the duration of the tests. These runs yielded classic antidunes, which in the precision of measurement conformed to the equations derived by Kennedy (29, 30). The average e value of 0.054 for these runs lies well outside the general range given by Rouse as corresponding to the maximum roughness concentration of many roughness forms. However, no values for steepness of antidunes have been reported corresponding to maximum roughness. The maximum steepness of antidunes is theoretically reached when the water surface wave amplitude reaches a critical value of 0.142 L (i.e. e = 0.142). At this point the antidunes wash out. A photograph of an individual breaking antidune in run 14 showed a value of e = 0.151 - close to the theoretical value. Thus for these runs, the e values reflect an average condition, where some of the bed is essentially plane, and some of it will have antidunes at less or at the maximum amplitude. Observation showed that armouring did occur for these runs. However, the predicted and the measured armour layers are not as well correlated as for the other runs, since the predicted armour layers for initial and final conditions tend to be too coarse (fig.4). These predicted armour layers are virtually identical because there was very little change in shear stress over the duration of the bed deforming process. On correcting the measured armour layer to enable comparison with the original bed material, using the Proffitt and Sutherland correction (kellerhals and Brays correction over-compensates), it is apparent that little coarsening had occurred. For these runs, action of the flow on the surface consists more of a rearrangement of the bed material, rather than coarsening. This suggestion is supported by the very low bedload transport rates that occurred for these runs, implying that classic antidunes were formed because coarsening of the top layer was minimal.

For the remaining runs (i.e. 1-5, 7, 8, 10, 15 and 16) resistance to flow increased during the run. Using initial conditions, the plot of F vs kd in fig.3 indicates that the bed waves at the beginning of these runs were antidunes. Using final conditions, the points from a plot of F vs kd lie in the region of fig.3 labelled by Yalin (51) as a region of non-antidunes.

However, reasonably good correlation was obtained between the measured and predicted armour layer for these runs as shown for tests 3 and 8 in fig.4. That there is little difference between the armour layers predicted from initial and final conditions shows that Gesslers method is, for these tests,

reasonably insensitive to change in shear stress. The armour layer calculated from initial conditions tends to give the better correlation with the measured armour layer, which could be expected since form drag could not be considered in the calculation for final condition.

The average e value for runs 1-5, 7, 8, 10, 15 is 0.129. This is lower than the mean value of 0.19 obtained by Sutherland and Williman (49) for their armouring tests. However, the maximum roughness height for long, square roughness elements and rectangular-bar roughness elements occurs at roughness-concentrations of just less than 0.1 and just greater than 0.1 respectively (31). The bedforms of the present tests, while recognised as distorted waves, can be considered to resemble rectangular elements. The e value of 0.129 then reflects a compromise between the value of 0.1 (Judd and Peterson (21), noted that the high gradient, rough channels they investigated tended to give maximum resistance at e = 0.1) due to the bedforms, and the value of 0.2 reported to characterize armour layer.

The role of bedforms associated with armouring explains why, although the $\bar{q}$ values for these tests indicated that stability would not be reached, in fact the bed did stabilize.

CONCLUSIONS

It has been possible to simulate, in a laboratory flume, a bed deforming process which resulted, after flow reduction, in step-pool sequences which resembled those found in mountain streams. On the basis of these simulations, it is postulated that the step-pool structures in the bed of a mountain stream are generated during high flows and not by the low flow which gives them the step-pool aspect. Thus, under usual flow conditions, the channel bed of steep mountain streams can be seen as being extremely stable.

The deforming process leading from an initial plane bed to step-pool formation is basically the same process as that which produced antidunes. However, effects due to the heterogeneity of bed sediments disturb the regularity of the process.

Where such disturbances occur (at slopes greater than 0.075 for the described experiments), bed deformation is accompanied by a large increase in resistance to flow which is accompanied by the formation of a coarse armour layer.

Where coarsening of the top layer is not a significant effect, regular antidunes occur (at slopes less than 0.075 in the present tests). Armouring for these cases involved rearrangement rather than coarsening of the top layer.

Thus the simulation of formation of step-pool structures involves a combination of antidune and armour layer formation. Values of roughness concentration tend to suggest that deformation may be that which gives a maximum resistance coefficient.

In view of the above proposed mechanism for generation of step-pool sequences, it should now be possible to attack the problem of predicting and understanding resistance to flow in steep mountain streams. This will give a better basis for prediction of sediment output from mountain regions, vital where agriculture and hydro-power generation are affected.

ACKNOWLEDGEMENTS

The writers wish to thank Dr T.R.H. Davies and Dr G.M. Smart for their constructive criticism of the paper. The practical assistance of Mr C. Tinker was of the utmost value. Appreciation is also expressed to Mr Isaac, of the Isaac Shingle and Sand Co. Ltd, for the gravel donated for experimental use. This study was supported by a Research Contract between the National Water and Soil Conservation Organisation of New Zealand and Lincoln College.

APPENDIX I - REFERENCES

1. AL-KHAFAJI, A., "The Dynamics of Two-Dimensional Flow in Steep, Rough, Open Channels." A dissertation submitted in partial fulfilment of the requirements for the degree of Doctor of Philosophy. Utah State University, Logan, Utah, 1961.

2. ALLEN, J.R.L., "Bed Forms and Unsteady Processes: Some Concepts of Classification and Response Illustrated by Common One-Way Types". Earth Surface Processes, Vol.1, 1976, pp 361-374.

3. ASHIDA, K., TAKAHASHI, T. and SAWADA, T., "Sediment Yield and Transport on a Mountainous Small Watershed." Bull.Disast.Prev.Res.Inst., Kyoto University, Vol.26, pt.3, No.240, Sept. 1976.

4. BAGNOLD, R.A., "Experiments on a Gravity-Free Disperson of Large Solid Spheres in a Newtonian Fluid Under Shear." Proc. Royal Soc. London, A. Vol. 225, 49; 1954.

5. BOOTHROYD, J.C., "Recent Braided-Stream Sedimentation, South Central Alaska (Abst)." American Assoc. of Petroleum Geologists Bulletin, Vol.54, 1970 pp 836.

6. BOOTHROYD, J.C. and ASHLEY, G.M., "Processes, Bar Morphology, and Sedimentary Structures on Braided Outwash Fans, North Eartern Gulf of Alaska." In 'Glaciofluvial and Glaciolacustrine Sedimentation: Ed. by A.V. Jopling and B.C. McDonald, Society of Economic Paleontologists and Mineralogists, Special Publ. No. 23, 1975.

7. CHURCH, M.A. and GILBERT, R., "Proglacial Fluvial and Lacustrine Environments", in 'Glaciofluvial and Glaciolacustrine Sedimentation', Ed. by A.V. Jopling and B.C. McDonald, Society of Economic Paleontologists and Mineralogists, Special Publ. No. 23; 1975.

8. DAVIES, T.R.H., "Bedforms Spacing and Flow Resistance", Journal of the Hydraulics Div, ASCE, Nol.106, No.HY3, Proc. Paper 15258, March 1980, pp 423-433.

9. DAVIES, T.R.H. and JAEGGI, M.N.R., "Precise Laboratory Measurement of Flow Resistance, "Proc., XIXth Congress IAHR, New Delhi, Feb. 1981.

10. DAVIES, T.R.H. and SUTHERLAND, A.J., "Resistance to Flow past Deformable Boundaries", Short communication, Earth Surface Processes, Vol.5, 1980, pp 175-179.

11. GESSLER, J., "Beginning of Bedload Movement of Mixtures Investigated as Natural Armouring in Channels", Report No. 69 of the Lab. of Hydr. Res. and Soil Mech. of the Swiss Fed. Inst. of Technology in Zurich, 1965.

12. GESSLER, J., "Self Stabilizing Tendencies of Alluvial Channels", Journal of Waterways and Harbours Division, ASCE WW2, May 1970 pp 235-249.

13. GOLUBTSOV, V.V., "Dependence of the Coriolis and Boussinesq Coefficients on the Slope of a Mountain Stream." Soviet Hydrology, Selected Papers, Vol. 15, No.1, 1976 (Publ. by Am. Geophys. Union).

14. GRAF, W.L., "Rapids in Canyon Rivers", Journal of Geology, Vol. 87, Sept. 1979, pp 533-551.

15. HAYWARD, J.A., "Hydrology and Stream Sediments in a Mountain Catchment". Ph.D. thesis, University of Canterbury, Christchurch, New Zealand, Vol. 1-3, 1978.

16. HAYWARD, J.A., "Hydrology and Stream Sediment from Torlesse Stream Catchment". Special Publ. No. 17, Tussock Grasslands and Mountain Lands Institute, Lincoln College, New Zealand, 1980.

17. HEEDE, B.H., "Flow and Channel Characteristics of Two High Mountain Streams", U.S.D.A. Forest Service Res. Paper R.M. 92, (1972a), p 12.

18. HEEDE, B.H., "Influences of a Forest on the Hydraulic Geometry of Two Mountain Streams", Water Resources Bull., Vol.8, No.3, June 1972b.

19. HEY, R.D., "Flow Resistance in Gravel Bed Rivers", Journal of the Hydraulic Division, ASCE, Vol.109, No.HY4, Proc.Paper 14200, April 1979, pp 365-379.

20. JUDD, H.E., "A Study of Bed Characteristics in Relation to Flow in Rough, High-Gradient, Natural Streams", a dissertation submitted in partial fulfilment of the requirements for the degree of Doctor of Philosophy, Utah State University, Logan, Utah, 1964.

21. JUDD, H.E. and PETERSON, D.F., "Hydraulics of Large Bed Element Channels", Utah Water Res. Lab., PRWG 17-6, College of Engineering, Utah State University, Logan, Utah 84321, August 1969.

22. KELLER, E.A., "Areal Sorting of Bed Load Material: The Hypothesis of Velocity Reversal", Geological Soc. of America Bull., Vol.82, March 1971, pp 753-756.

23. KELLER, E.A. and MELHORN, W.N., "Rhythmic Spacing and Origin of Pools and Riffles", Geol. Soc. of America Bull., Vol.89, May 1978, pp 723-730.

24. KELLER, E.A. and SWANSON, F.J., "Effects of Large Organic Material on Channel Form and Fluvial Process", Earth Surface Processes, Vol.4, 1979, pp 361-380.

25. KELLERHALS, R., "Runoff Routing Through Steep Natural Channels", Journal of the Hydraulics Division, ASCE, Vol.96, No.HY11, Nov. 1970.

26. KELLERHALS, R., "Hydraulic Performance of Steep Natural Channels", from 'Mountain Geomorphology (Geomorphological Processes in the Canadian Cordillera)', British Columbia Geographical Series, No.14; Ed. by O. Slaymaker and H.J. McPherson, Tantalus Research Ltd, 1972.

27. KELLERHALS, R., "Hydraulic Performance of Mountain Streams", Proc. 15th Congress of the IAHR, Vol.1, Istanbul, 1973.

28. KELLERHALS, R. and BRAY, D.I., "Sampling Procedures for Coarse Fluvial Sediment", Journal of the Hydraulic Division, ASCE, Vol.97, Aug. 1971, pp 1165-1180.

29. KENNEDY, J.F., "Stationary Waves and Antidunes in Alluvial Channels" (Final Report to U.S.D.A.) Report No. KH-R-2, January 1961, W.M. Keck Lab of Hydr. and Water Resources, California Institute of Technology.

30. KENNEDY, J.F., "The mechanics of Dunes and Antidunes in Erodible Bed Channels", Journal of Fluid Mechanics, Vol. 16, No.4, 1963.

31. KOLOSEUS, H.J. and DAVIDIAN, S., "Roughness Concentration Effects on Flow over Hydrodynamically Rough Surfaces", U.S. Geological Survey Water Supply Paper 1592-A, 1966.

32. KOSTER, E.H., "Transverse Ribs: Their Characteristics, Origin and Paleohydraulic Significance", from 'Fluvial Sedimentology', Ed. A.D. Miall, Canadian Soc. of Petroleum Geologists, Memoir 5, Calgary, Canada, August 1978.

33. LARONNE, J.B. and CARSON, M.A., "Inter-Relationships between Bed Morphology and Bed Material Transport for a Small, Gravel Bed Channel", Sedimentology 23, 1975, pp 67-85.

34. LEOPOLD, L., WOLMAN, G., MILLER, J., "Fluvial Processes in Geomorphology", W.H. Frieman and Company, 1964, 520p.

35. McDONALD, B.C. and BANERJEE, I., "Sediments and Bed Forms on a Braided Outwash Plain", Canadian Journal of Earth Science, 8, 1971 pp 1282-1301.

36. McDONALD, B.C. and DAY, T.J., "An Experimental Flume Study on the Formation of Transverse Ribs", Current Research, Part A, Geol. Survey Canada, Paper 78-1A, 1978, pp 441-451.

37. MIDDLETON, G.V. and SOUTHARD, J.B. eds., "Depositional Environments as Interpreted from Primary Sedimentary Structures and Stratification Sequences", S.E.P.M. Short Course, No. 2, Dallas 1975, Soc. of Economics Paleontologists and Mineralogists.

38. MILLER, J.P. "High Mountain Streams: Effects of Geology on Channel Characteristics and Bed Material", Memoir 4, State Bureau of Mines and Mineral Resources, New Mexico Institute of Mining and Technology, Socarro, New Mexico, 1958.

39. MOHANTY, P.K., "The Dynamics of Turbulent Flow in Steep, Rough Open Channels", a dissertation submitted in partial fulfilment of the requirements for the degree of Doctor of Philosophy, Utah State University, Logan, Utah, 1959.

40. O'LOUGHLIN, C.L. "Streambed Investigations in a small, Mountain Catchment", New Zealand Journal of Geology and Geophysics, Vol.12, No.4, Nov. 1969.

41. PETERSON, D.F. and MOHANTY, P.K., "Flume Studies of Flow in Steep Rough Channels", Journal of the Hydraulics Division, ASCE, Vol. 86, HY9, Nov. 1960.

42. PROFFITT, G.T. and SUTHERLAND A.J., "Self Armouring of Non Uniform Alluvial Sediments", 7th Australasian Hydraulics and Fluid Mechanics Conference, Brisbane, 1980.

43. RICHARDS, K.S. "The Morphology of Riffle-Pool Sequences", Earth Surface Processes, Vol.1, 1976, pp 71-80.

44. RICHARDS, K.S., "Simulation of Flow Geometry in a Riffle Pool Stream", Earth Surface Processes, Vol.3, 1978, pp 345-354.

45. ROUSE, H., "Critical Analysis of Open Channel Resistance", Journal of the Hydraulic Division, ASCE, Vol91, HY4, July 1965, pp 1-25.

46. SCHEUERLEIN, H., "Mechanics of Flow in Steep, Rough Open Channels", Proc. 15th Congress IAHR, Istanbul, 1973.

47. SEDDON, J., "River Hydraulics", Transactions of the ASCE, Vol.43, June 1900, pp 197-243.

48. SHAW, J. and KELLERHALS, R., "Paleohydraulic Interpretation of Antidune Bedforms with Application to Antidunes in Gravel", Journal of Sedimentary Petrology, Vol.47, No.1, March 1977, pp 257-266.

49. SUTHERLAND, A.J. and WILLIMAN, E.B., "Development of Armoured Surfaces in Alluvial Channels", 6th Australasian Hydraulics and Fluid Mechanics Conference, Adelaide, Australia, 1977.

50. THOMPSON, S.M. and CAMPBELL, P.L., "Hydraulics of a Large Channel Paved with Boulders", Journal of Hydraulic Research, Vol. 17, 1979, No.4, pp 341-354.

51. YALIN, M.S., "Mechanics of Sediment Transport", 2nd Edition, 1977, Pergamon Press.

52. YANG, C.T., "Formation of Riffles and Pools", Water Resources Research, Vol. 7, No. 6, Dec. 1971.

APPENDIX II - NOTATION

D = grain size

D_{84} = characteristic grain size, than which 84% of the mixture is smaller

d = flow depth

d_o = initial flow depth

e = roughness spacing

F = Froude number

F_a = minimum Froude number

F_M = maximum Froude number

f_s = bottom friction factor

f_{so} = initial bottom friction factor

g = gravity acceleration

k = wave number

k_s = roughness element size

L = wave length

p = grain size distribution function

p_a = armour coat grain size distribution function

Q = discharge

q = probability of a grain of remaining in the armour coat

$\bar{q}$ = average probability, stability factor for armour coat

r_s = hydraulic radius, referred to the bottom

u_m = average velocity

α = velocity distribution correction coefficient

θ = angle of inclination of the flume

$\bar{\tau}_s$ = average bottom shear stress of the flow

τ' = reduced shear stress

Run No.	Slope (sin θ)	Discharge Q in cubic meters	Average velocity u_m in meters per second	Depth d in meters	Hydraulic radius r_s in meters	Friction factor f_s	Shear Stress $\bar{\tau}_s$ in Newton per square meter	Initial depth d_o in meters	Initial friction factor f_{so}	$\frac{f_{so}}{f_s}$	Froude number F (final conditions)
(1)	(2)	(3)	(4)		(5)	(6)	(7)	(8)	(9)	(10)		(11)
1	0.0977	0.0039	0.360		0.082	0.081	4.78	77.39	0.038	0.52	0.33	0.521
2	0.0977	0.0041	0.375		0.083	0.082	4.45	78.28	0.040	0.52	0.24	0.539
3	0.0977	0.0045	0.356		0.096	0.095	5.72	90.63	0.042	0.47	0.29	0.476
4	0.0977	0.0054	0.395		0.103	0.101	4.98	97.03	0.046	0.42	0.29	0.510
5	0.0847	0.0062	0.427		0.110	0.108	3.93	89.63	0.049	0.39	0.32	0.529
6			unstable conditions									
7	0.163	0.0010	0.294		0.028	0.028	4.12	44.47	0.020	1.45	0.59	0.767
8	0.172	0.0008	0.321		0.019	0.019	2.47	31.82	0.018	1.94	0.89	1.024
9			unstable conditions									
10	0.2380	0.0004	0.169		0.018	0.018	11.74	41.92	0.013	4.57	0.62	0.569
11	0.0220	0.0148	0.867		0.129	0.109	0.251	23.59	0.098	0.10	0.63	0.931
12	0.0250	0.0182	1.250		0.110	0.085	0.106	20.77	0.108	0.098	0.96	1.460
13			unstable conditions									
14	0.0420	0.0108	1.174		0.070	0.060	0.144	24.81	0.075	0.24	1.29	1.762
15	0.1680	0.0012	0.248		0.037	0.037	7.89	60.65	0.019	1.13	0.38	0.563
16	0.2410	0.0008	0.136		0.044	0.044	44.91	103.84	0.015	1.87	0.20	0.293
17	0.025	0.0147	1.200		0.093	0.073	0.099	17.85	0.094	0.103	1.02	1.524
18	0.0260	0.0118	1.027		0.087	0.072	0.140	18.43	0.081	0.11	0.89	1.351

TABLE 2: WAVELENGTH OF BEDFORMS

Run No.	Wavelength in meters			Standard Deviation of meters
	Average	Max.	Min.	
(1)	(2)	(3)	(4)	(5)
1	0.171	0.497	0.045	0.104
2	0.169	0.640	0.049	0.119
3	0.227	0.814	0.038	0.163
4	0.247	0.903	0.082	0.170
5	0.258	0.618	0.049	0.134
6	unstable conditions			
7	0.225	0.759	0.065	0.169
8	0.239	0.686	0.091	0.153
9	unstable conditions			
10	0.272	0.700	0.061	0.186
11	(0.585) 0.402	1.026	0.120	0.248
12	(1.091) 0.502	1.062	0.110	0.268
13	unstable conditions			
14	(0.632) 0.416	0.979	0.104	0.255
15	0.286	1.107	0.084	0.236
16	longitudinal profile not measured			
17	(0.642) 0.433	1.215	0.124	0.299
18	(0.546) 0.457	1,352	0.188	0.280

(figures in brackets based on photographs)

TABLE 3: ROUGHNESS SPACING

Run No.	Roughness spacing e			Standard deviation
	Average	Max.	Min.	
(1)	(2)	(3)	(4)	(5)
1	0.146	0.436	0.031	0.074
2	0.138	0.311	0.040	0.078
3	0.118	0.288	0.031	0.068
4	0.126	0.217	0.086	0.051
5	0.100	0.190	0.011	0.039
6	unstable conditions			
7	0.149	0.335	0.040	0.063
8	0.129	0.250	0.045	0.057
9	unstable conditions			
10	0.130	0.356	0.039	0.071
11	0.065	0.136	0.022	0.030
12	0.046	0.087	0.022	0.019
13	unstable conditions			
14	0.051	0.125	0.012	0.027
15	0.127	0.293	0.036	0.063
16	longitudinal profile not measured			
17	0.052	0.141	0.020	0.029
18	0.055	0.116	0.017	0.023

TABLE 4: SELF ARMOURING STABILITY COEFFICIENT

Run No. (1)	$\bar{q}$ (2)
1	0.240
2	0.238
3	0.145
4	0.174
5	0.183
7	0.213
8	0.224
10	0.183
11	0.495
12	0.492
17	0.430
18	0.458

FIGURE CAPTIONS

Fig.1 : Steps and pools in the same reach of a steep mountain stream under differing flow conditions

Fig.2(a) : Conceptualisation of progression from antidune flow to the tumbling flow of a step-pool system

Fig.2(b) : Conceptualisation of progression from rough flow to the tumbling flow of a step-pool system

Fig.3 : Plot of dimensionless wave number kd vs Froude number F

Fig.4 : Plot of measured and predicted armour layer distribution

Fig.5 : Plot of original material distribution compared with corrected measured armour layer distribution

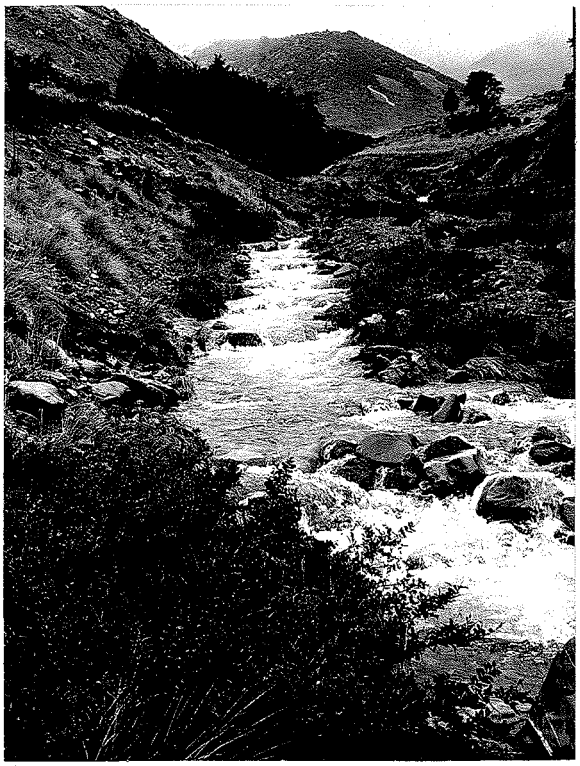

Figure 1: Steps and pools in the same reach of a steep mountain stream under differing flow conditions.

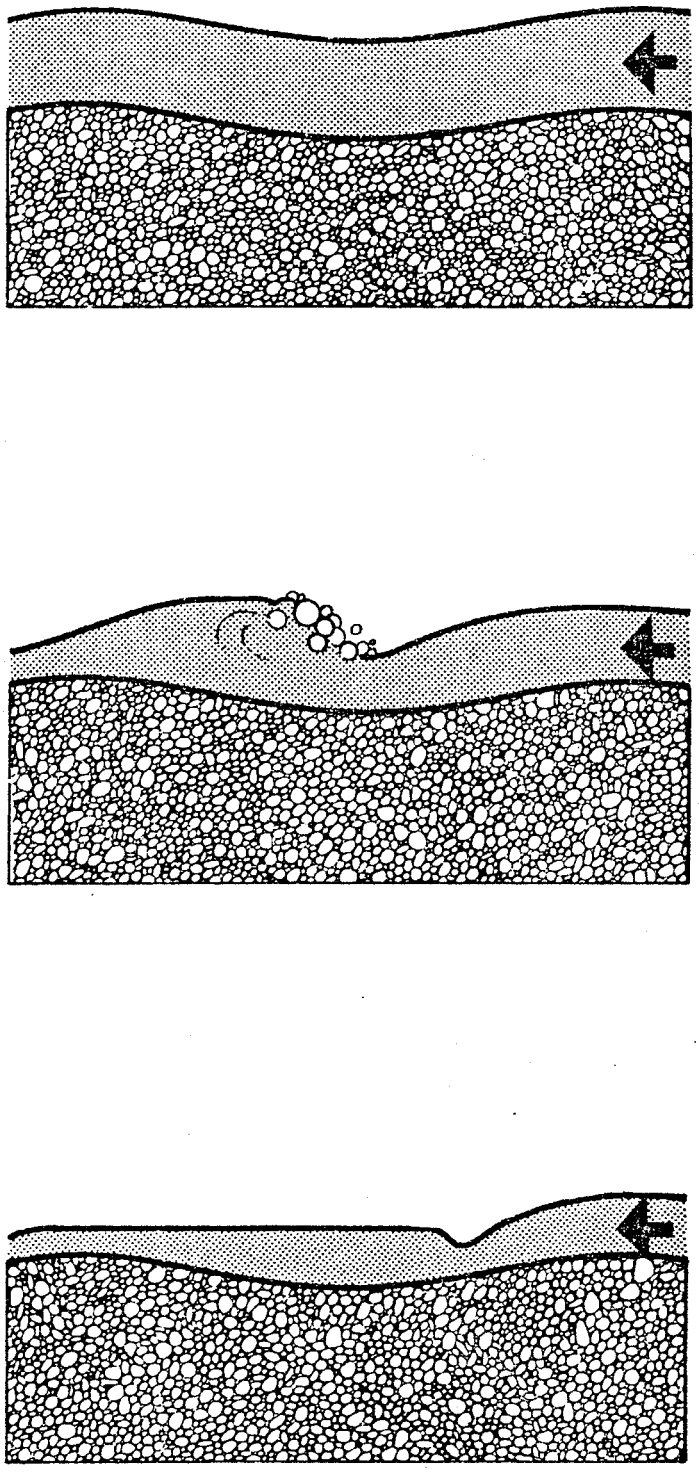

Figure 2(a): Conceptualisation of progression from antidune flow to the tumbling flow of a step-pool system.

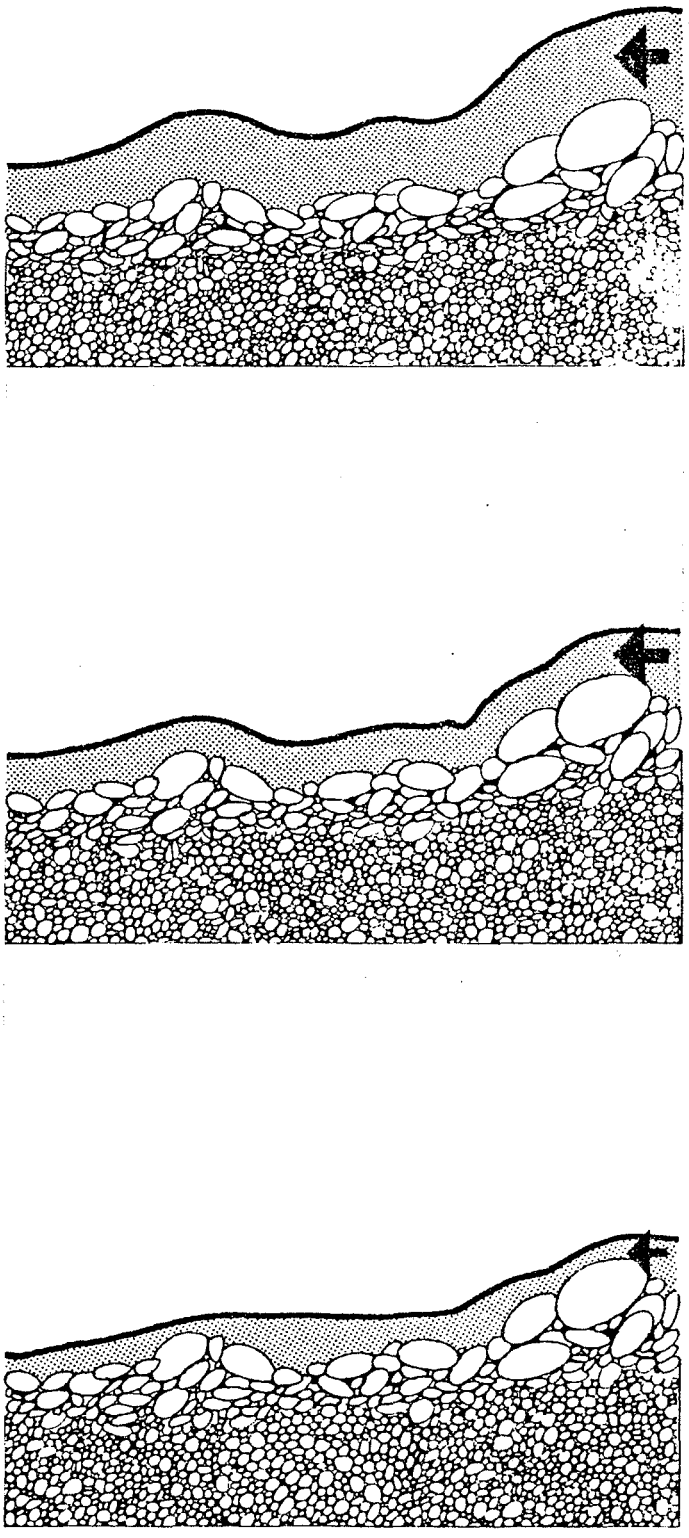

Figure 2(b): Conceptualisation of progression from rough flow to the tumbling flow of a step-pool system.

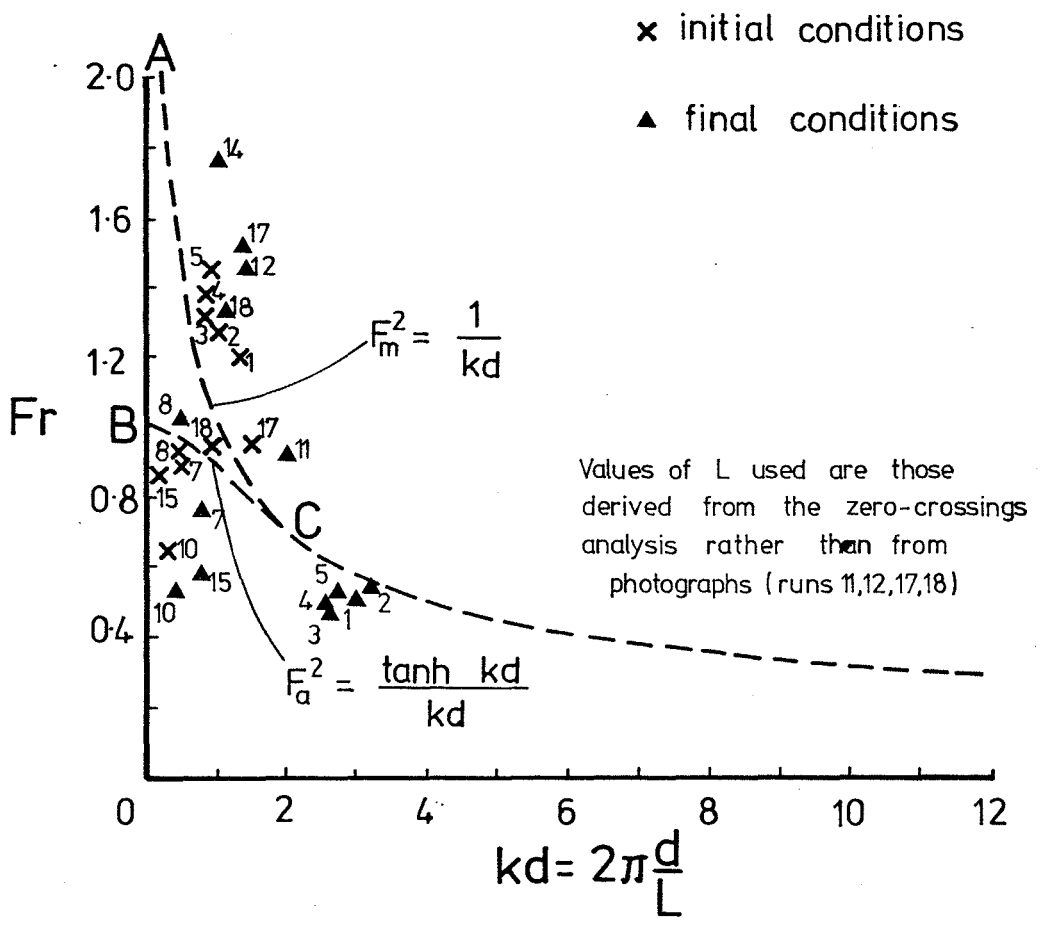

NB: Fr values for initial condition points were plotted as calculated from the formula $Fr = v_m/\sqrt{gd}$ rather than from the formula allowing for steep slope effects via the coriolis coefficient. Even so, the points for runs 11, 12, 15, 17, 18 were plotted incorrectly.

Figure 3: Plot of dimensionless wave number kd vs Froude number F.

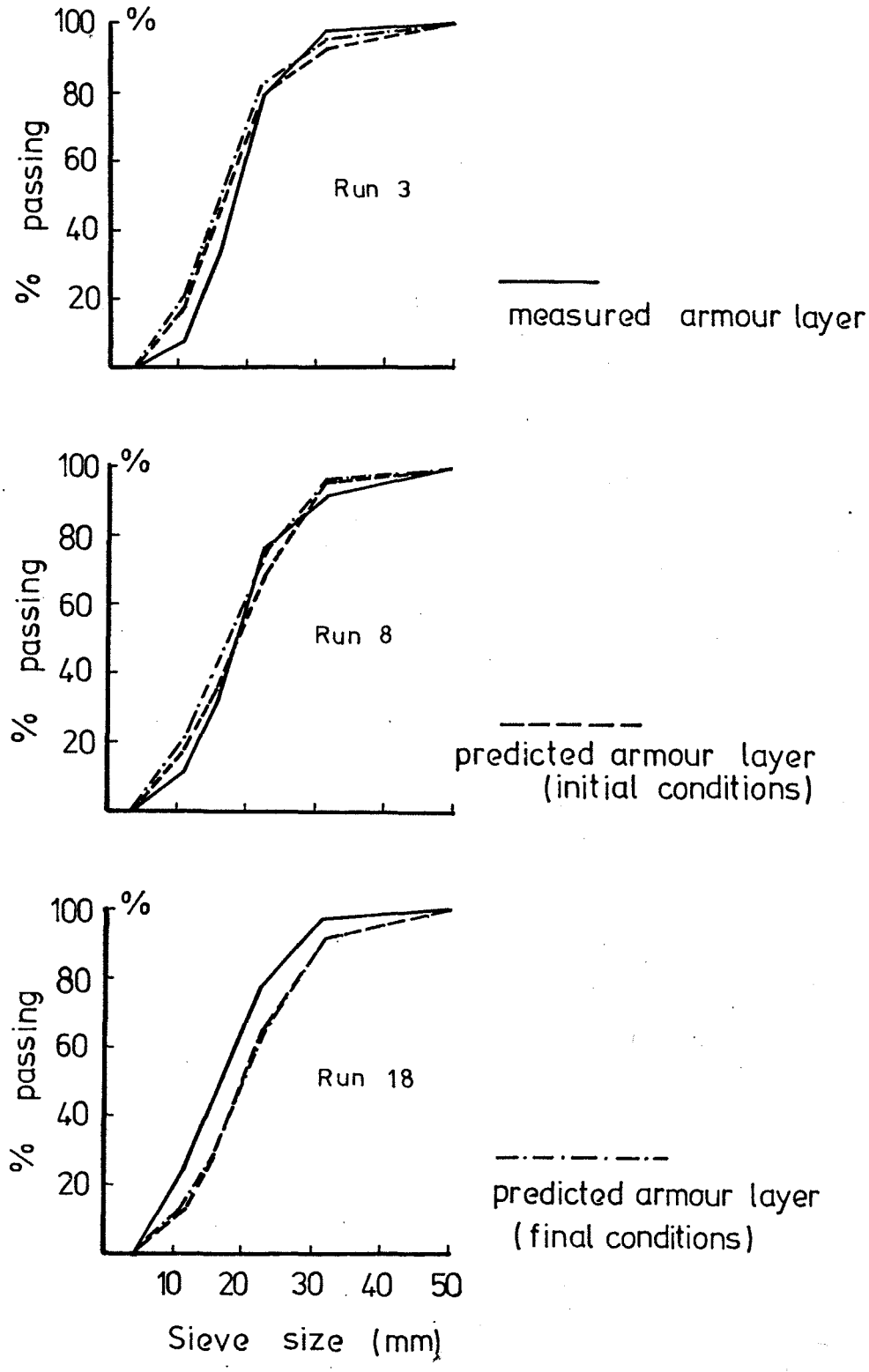

Figure 4: Plot of measured and predicted armour layer distributions.

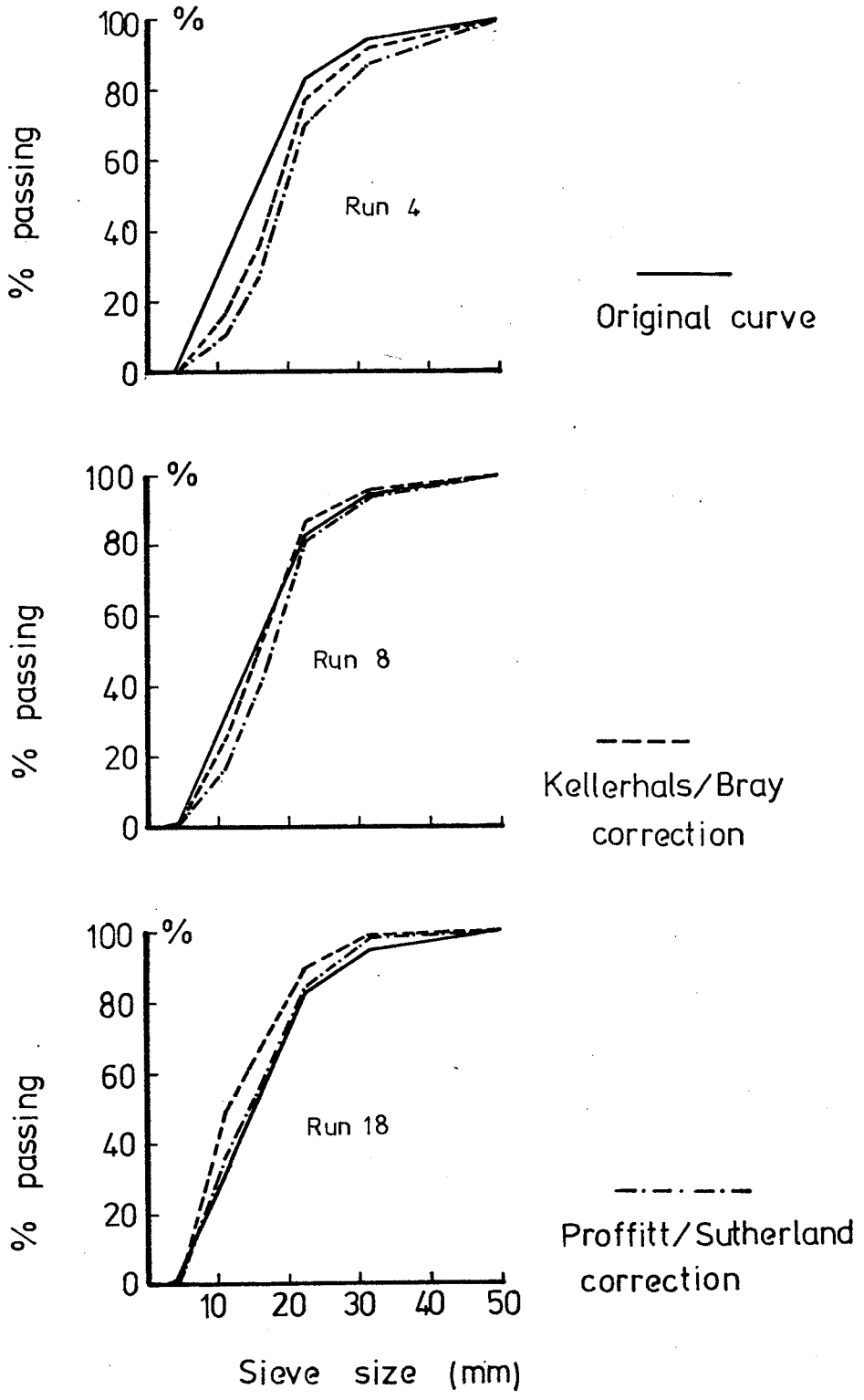

Figure 5: Plot of original material distribution compared with corrected measured armour layer distribution.

APPENDIX 3

EXAMPLE OF CALCULATION OF ARMOUR LAYER DISTRIBUTION AND STABILITY COEFFICIENT BY GESSLER'S METHOD

Bed deformation. Run 4. Gessler Calculation (final conditions).

k_1	k_i	$\overline{T}$	T_c	$\frac{T_c}{\overline{T}}$	q	ΔP_A	$q\Delta P_A$	ΔP_D	P_D	$q^2\Delta P_A$
2										
	3	1.760	0.047	0.027	0.046	0.0140	0.0006	0.0081		2.962×10^{-5}
4									0.0081	
	7.6	0.695	0.047	0.068	0.052	0.295	0.0153	0.2076		0.001
11.2									0.2157	
	13.6	0.388	0.047	0.121	0.062	0.196	0.0122	0.1655		0.001
16									0.3813	
	19.2	0.275	0.047	0.171	0.075	0.277	0.0208	0.2822		0.002
22.4									0.6635	
	26.95	0.196	0.047	0.240	0.093	0.113	0.0105	0.1425		0.001
31.5									0.8060	
	40.8	0.129	0.047	0.363	0.136	0.105	0.0143	0.1940		0.002
50									1.000	
							$\Sigma q\Delta P_A = 0.0737$		$\Sigma q^2\Delta P_A = 0.00606$	
								$\rightarrow \overline{q} = 0.08220$		

APPENDIX 4

MANUSCRIPT OF THE PAPER 'EROSION AND SEDIMENT TRANSPORT PROCESSES IN STEP-POOL TORRENTS' (BY WHITTAKER AND DAVIES) TO BE PRESENTED AT THE FIRST I.A.H.S. SCIENTIFIC GENERAL ASSEMBLY, EXETER, U.K., JULY, 1982

EROSION AND SEDIMENT TRANSPORT PROCESSES IN STEP-POOL TORRENTS

by

J.G. Whittaker
T.R.H. Davies

Agricultural Engineering Department
Lincoln College
University of Canterbury
New Zealand

ABSTRACT

In upland regions, streams often exhibit a step-pool morphology where water cascades between relatively deep pools. The capacity of such streams to entrain adjacent slope material depends not only on water flow rate and channel slope, but also on the degree of infilling of the pools by sediment. This situation has been idealised, using a laboratory channel containing regularly spaced baffles. The results appear consistent with findings of studies of real torrents. The laboratory investigation has revealed that the erosive capacity of step-pool streams reaches a maximum (for a given flow rate) when the pools are almost full of sediment; that is, when sediment transport rates are high. This behaviour is conducive to erosion of adjacent slopes and contrasts with that of lowland alluvial streams. Despite steady inputs, water and sediment outputs from the laboratory channel were often independently unsteady. Step-pool streams thus seem to display intrinsic unsteadiness, particularly of sediment movement. This parallels reports of coherent sediment 'waves' moving slowly through mountain torrents. Such behaviour is consistent with recent findings in the thermodynamics of non-linear systems. These findings seem to relate also to low-slope alluvial channel processes. Conventional linear analysis may be inappropriate to these situations.

INTRODUCTION

In the steep, upper catchment areas typical of many mountainous regions, valley side slopes commonly extend to the very banks of the stream in the valley bottom. Movement of material down such slopes is largely controlled by stream bank erosion and undercutting of the toe of the slope by the stream.

Steep mountain streams often exhibit a staircase appearance, where a series of rocky steps alternate with relatively deep pools. This step-pool structure acts as an energy dissipator at low flow rates. At high flows (or at moderate flows with a high sediment load where pools become filled with sediment), the structure is less effective as an energy dissipator, leading to higher flow velocities and a greater ability to entrain adjacent slope material.

In order to study this variation in the erosive capacity of a step-pool stream, the stream system has been idealised in a laboratory channel containing regularly spaced baffles. A tilting, recirculating flume of width 0.13 m and length 9.5 m was used, the slope of which could be varied up to 25%. Baffle plates 0.27 m high were spaced at 0.5 m intervals along the flume bed. A rotating tube sediment feed device capable of supplying 16 kg/min of 4 mm gravel was mounted on the upstream end of the flume. Mean flow velocities were measured using the salt-velocity method (Davies and Jaeggi (1981)). Mean flow velocity was used as an indicator of the stream's relative erosive capability, being directly proportional to unit stream power (Yang (1972)). Variation of erosive capability through a single step-pool unit is now being studied.

VARIATION IN EROSIVE ABILITY

Tests were performed at four slopes. At each slope, a series of flow rates was investigated, for each of which the variation of mean flow velocity $\langle v \rangle$ with sediment transport rate Q_s was examined. A test was considered to have achieved equilibrium when the measured sediment output rate from the tail of the flume equalled the input rate. Photographs were taken to allow examination of flow and scour depths. Results of these tests are shown in Fig.1.

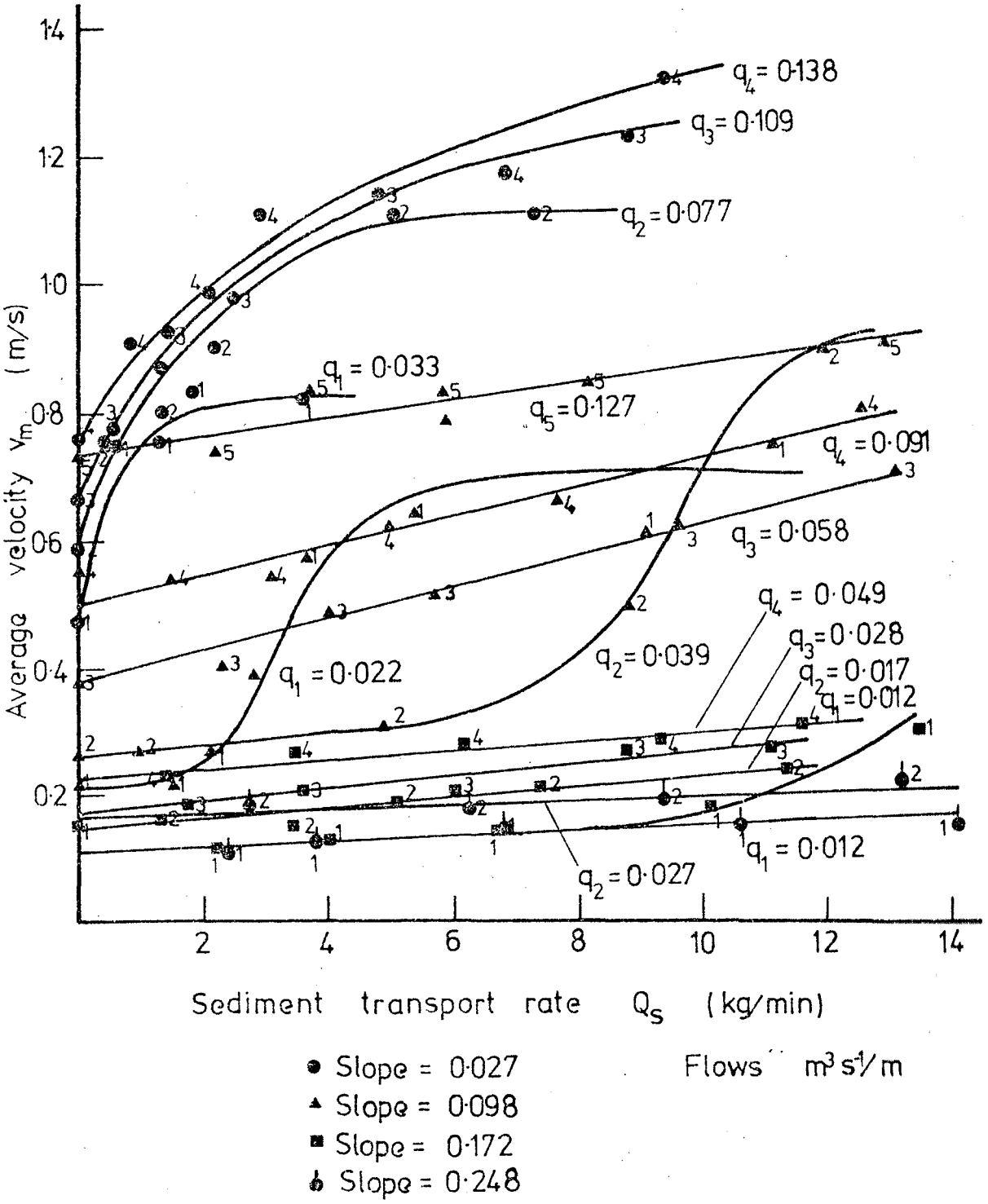

Figure 1: Average velocity versus sediment transport rate.

Slope = 2.7%

For a given flow rate Q, <v> increased rapidly with Q_s, until a threshold was reached, corresponding to complete filling of the pools with sediment. For higher values of Q_s there was no further increase in <v>, and plane bed flow with deposition above the level of the baffles occurred.

Slope = 9.9%

Initially, <v> increased only slightly with Q_s (Q const) until, with the two lowest flow rates, drowning of pools by sediment began to occur, and <v> increased more rapidly. Again, a threshold was reached at which the pools were filled with sediment and the increase in <v> ceased. At higher flow rates no significant drowning of pools or increase in <v> was observed.

Slope = 17.2%, 24.8%

Only the lowest flow at slope = 17.2% showed an increase in <v>, and that at a high value of Q_s. For the other flows, no significant drowning of the pools occurred.

For a given flow rate, it is seen that as pools became filled with sediment an increase in <v>, and hence erosive capability, does indeed occur; however, drowning is much more difficult to achieve at steep slopes, requiring very large values of Q_s at moderate flows. Maximum velocity is attained when the pools are completely drowned. It is significant that field studies (Hayward (1980)) describe and illustrate severe bank undercutting due to the drowning of pools by sediment. Of particular interest is that erosion is likely even at relatively low flows as pools become filled with sediment. It seems likely that a positive feedback may increase the erosion capability in that as the pools in a reach of stream are partly infilled, erosion of adjacent banks becomes possible, further increasing the degree of infilling and thereby bank erosion. This may explain the occurrence and movement of coherent 'slugs' of sediment through a stream system (Hayward (1980), Ashida, et. al. (1976), Beschta (1981)), although, as shown in the following section, such behaviour seems inherent in a step-pool stream. As yet, it has not been possible to relate laboratory flow rates closely to those causing equivalent behaviour of prototype streams. Visual appearance suggests that, in the field, flows high enough to drown a step-pool system without sediment input would be of the order of a 100 to 1000 yr flood. However, drowning by a combination of high flow and sediment transport rates can easily occur in a 10 to 25 yr event (Hayward (1980)).

Thus, at high sediment transport rates, a step-pool stream may, depending on the flow, become very erosive. This contrasts with the behaviour of lowland alluvial rivers, where low sediment input rates are generally thought to lead to bank and bed scouring.

UNSTEADINESS OF WATER AND SEDIMENT FLOW

It is well known (Morris (1968)) that clear water flow over regularly spaced baffles can give rise to periodic roll waves. This phenomenon was observed in some of the present tests. The roll waves occurred when the discharge coefficient for flow over a baffle increased due to the water surface in the pool upstream of the baffle rising beyond a certain level. This increase in discharge resulted in washing out of the hydraulic jump immediately upstream of the baffle into the pool downstream of the baffle. The water level in the upstream pool thus fell, while that in the inundated pool rose. The same process subsequently occurred with greater amplitude at the next baffle downstream: the region of high water level propagated and amplified through successive pools. The fall in the level of the original pool caused a decrease in outflow over the baffle. Because inflow then exceeded outflow, this level rose again, setting another wave in motion. These roll waves have never been reported in the literature on naturally-formed step-pool streams. This is probably because the irregularity of natural step-pool sequences tends to damp out such waves.

However, Dement'ev (1962), reported velocity pulsations in mountain rivers of the U.S.S.R. with periods down to the researcher's measuring limit of about 30 sec. Pulsations short enough to correspond to roll-waves could have occurred. The magnitude of the pulsations increased with roughness of the bed, and with increasing velocity of flow. Dement'ev (1962) inferred that the pulsations were due to turbulence.

It was noted in the present tests that, with steady inputs of water and sediment, both the water and sediment outputs were often independently unsteady. Slow moving sediment waves were manifested by periodic variations in the degree of pool infilling along the channel (Fig.2). A pattern was observable (Table 1).

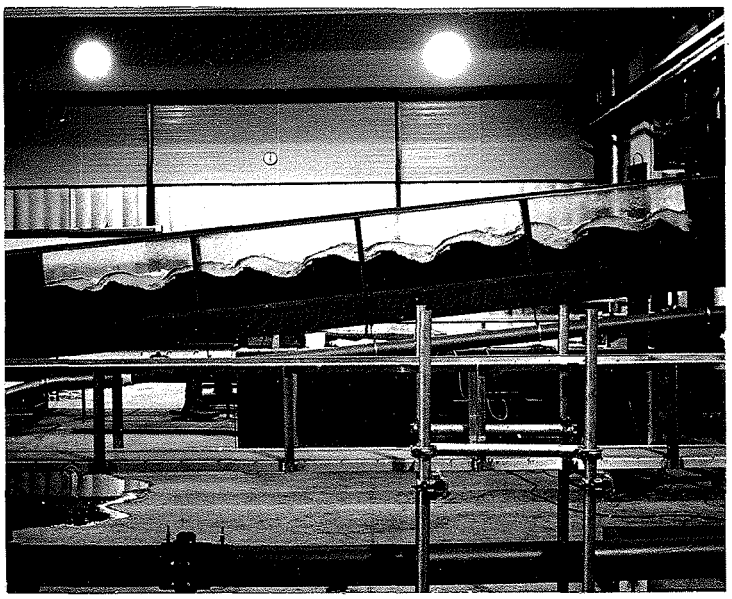

Run 11: Slope = 9.9 p.c. Q = 7.65 l/s

Q_s = 13.1 kg/min

Run 16: Slope = 9.9 p.c. Q = 12.07 l/s

Q_s = 12.6 kg/min

Figure 2: Sediment waves.

TABLE 1

Flow State	BEHAVIOUR OF MODEL WITH INCREASING Q_s
Stable	Sediment waves may develop; (these modify the flow with possible instability)
Periodic Roll Waves	The flow instability decreases. Sediment waves may develop, and with consequent flow modification lead to complex flow instability.

This suggests that the sediment 'slugs' seen in natural channels may be generated by localised bank erosion and be retained in their coherent form as they pass along the channel by an intrinsic tendency toward non-uniformity in sediment motion.

Many aspects of the behaviour of sediment-transporting turbulent flows point toward similar inherent non-uniformities. They include the development of bed forms, meanders and riffle-pool sections in initially uniform channels. Current theories of sediment transport and channel formation tend to account for such non-uniformities by means of empirical coefficients. Rather, the behaviour of natural streams seems strikingly similar to the behaviour of such non-linear thermodynamic systems (Davy and Davies (1980), Karcz (1981)) as described by, for instance, Nicolis and Prigogine (1977).

Very briefly, a linear thermodynamic system returns to a uniform state when slightly disturbed, as, for example, does a bed of sand under laminar flow. This behaviour is restricted to conditions close to equilibrium. Farther from equilibrium, where the thermodynamic system is non-linear, a disturbance may generate an instability which, with positive feedback, drives the system to a new dynamic equilibrium state in which large scale structural order is present. The new state is called a dissipative structure (Prigogine (1978)). Such a state can only be maintained by a sufficient flow of energy and matter. The analogy between non-linear behaviour and the development of bed forms is very clear. The bed form develops from an initial disturbance which is amplified; in the same way a dissipative structure is the result of a perturbation which is amplified by non-linear processes. In both cases, the result is a large scale (relative to the initial disturbance) spatial ordering. The sediment and

water waves observed in the present tests are seen to have arisen from such non-linear processes. Thus, the writers contend that attempts to derive analytical models for the behaviour of natural channels in both lowland and highland situations should involve recent advances in the understanding of non-linear system behaviour, rather than continuing to manipulate linear analyses to fit what are essentially non-linear conditions.

ACKNOWLEDGEMENTS

This study was supported by a Research Contract between the National Water & Soil Conservation Organisation of New Zealand and Lincoln College.

REFERENCES

ASHIDA, T., TAKAHASHI, T., & SAWADA, T. (1976) Sediment yield and transport on a mountainous small watershed. Bull. Disaster Prev. Res. Inst. Kyoto Univ. Vol. 26, Pt 3, No. 240.

BESCHTA, R.L. (1981) Patterns of sediment and organic-matter transport in Oregon coast range streams. In: Erosion and Sediment Transport in Pacific Rim Steeplands (Proc. Christchurch Symp., Jan. 1981), 179-188. I.A.H.S. Publ. No. 132.

DAVIES, T.R.H. & JAEGGI, M.N.R. (1981) Precise laboratory measurement of flow resistance. Proc. XIX Congress, I.A.H.R., New Delhi.

DAVY, B.W., & DAVIES, T.R.H. (1980) Reply: Entropy concepts in fluvial geomorphology: A re-evaluation. Water Resources Research. Vol. 16, No.1.

DEMENT'EV, V.V. (1962) Investigations of pulsations of velocities of mountain streams and of its effect on the accuracy of discharge measurements. Soviet Hydrology No. 6, 588-623.

HAYWARD, J.A. (1980) Hydrology and stream sediments in a mountain catchment. Tussock Grasslands and Mountain Lands Institute Special Publication No. 17,

Lincoln College, Univ. of Canterbury, New Zealand.

KARCZ, I. (1980) Thermodynamic approach to geomorphic thresholds. In: Thresholds in Geomorphology (ed. by D.R. Coates & J.D. Vitek) George Allen and Unwin.

MORRIS, H.M. (1968) Hydraulics of energy dissipation in steep, rough channels. Bull. No. 19, Research Division, Virginia Polytechnic Institute, Blacksburg, Virginia, U.S.A.

NICOLIS, G. & PRIGOGINE, L. (1977) Self organisation in non-equilibrium systems. Wiley and Sons, N.Y.

PRIGOGINE, L. (1978) Time, structure, and fluctuations. Science, Vol. 201, No. 4358, 777-785.

YANG, C.T. (1972) Unit stream power and sediment transport. Journal of the Hydraulics Div., A.S.C.E., Vol. 98, No. HY10, Proc. Paper 9295, 1805-1826.

APPENDIX 5

OBSERVATIONS OF FLOW AND SCOUR WITH SEDIMENT TRANSPORT IN A STEP-POOL SYSTEM (WITH PHOTOGRAPHS)

A. SLOPE = 0.027

A1 $q = 0.033\ m^3\ s^{-1}/m$ INITIAL STATE : Stable tumbling flow.

RUN	Q_s (kg/min)	DESCRIPTION
78	0.00	Very little scour. Flow stable tumbling (surface nappe). (See photograph)
77	0.599	Scour pattern is uneven. Part of the flow is stable tumbling, while the rest is essentially plane bed flow.
70	1.318	Minimal scour in some pools. The flow is plane bed flow.
22	1.827	As for Run 70.
23	3.642	Totally plane bed flow. Sediment has deposited above the level of the steps. (See photograph)

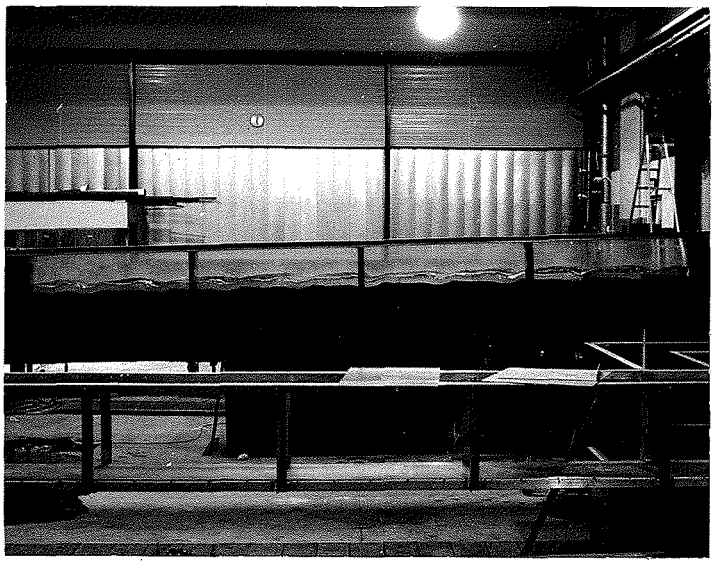

Run 78

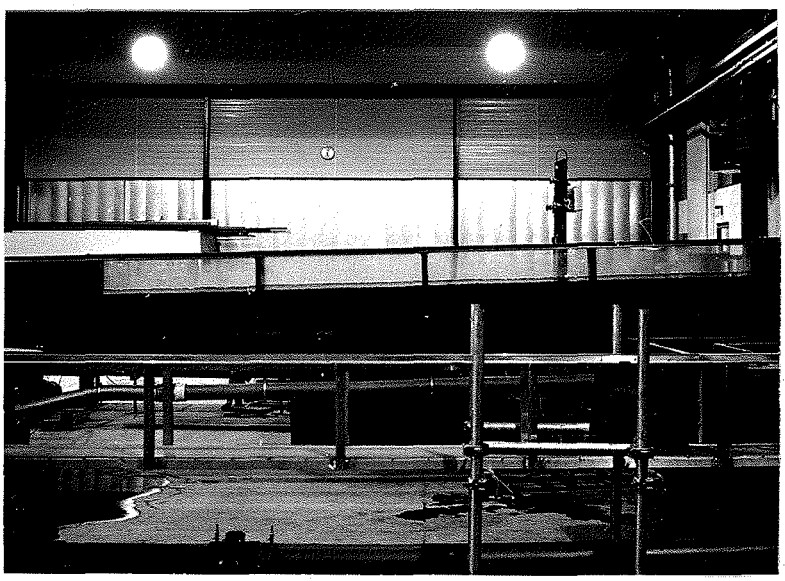

Run 23

A2 $q = 0.077\ m^3\ s^{-1}/m$ INITIAL STATE : Stable tumbling flow.

RUN	Q_s (kg/min)	DESCRIPTION
80	0.00	Point of maximum scour midway between steps. Stable (surface nappe) flow. (See photograph)
79	0.377	Scour reduced with small variations in scour pattern apparent. Flow stable.
71	1.377	Flow stable. Long, low waves beginning to appear. $c \simeq 0.1$ m/s.
24	2.181	Flow is stable, but partly smooth sinusoidal Long low sediment waves apparent. $L \simeq 2.5$ m. $c \simeq 0.13$ m/s. (See photographs)
25	5.052	Scour almost non-existent. Flow essentially plane.

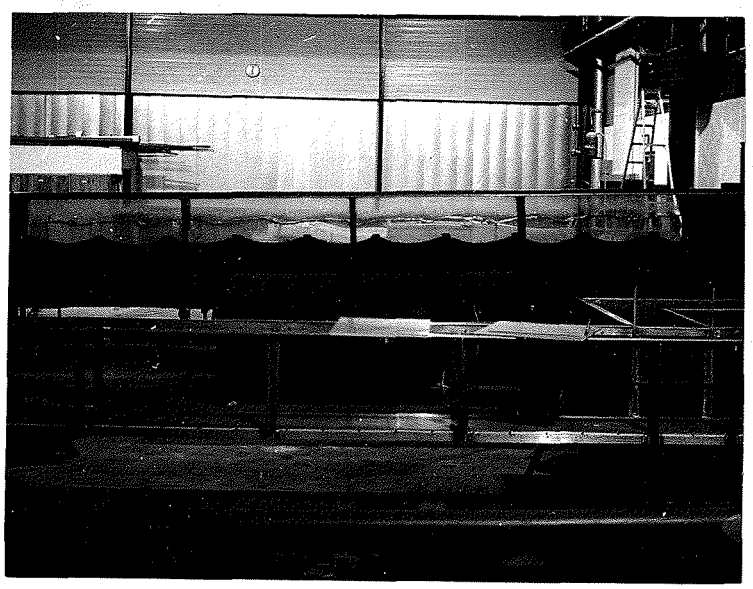

Run 80

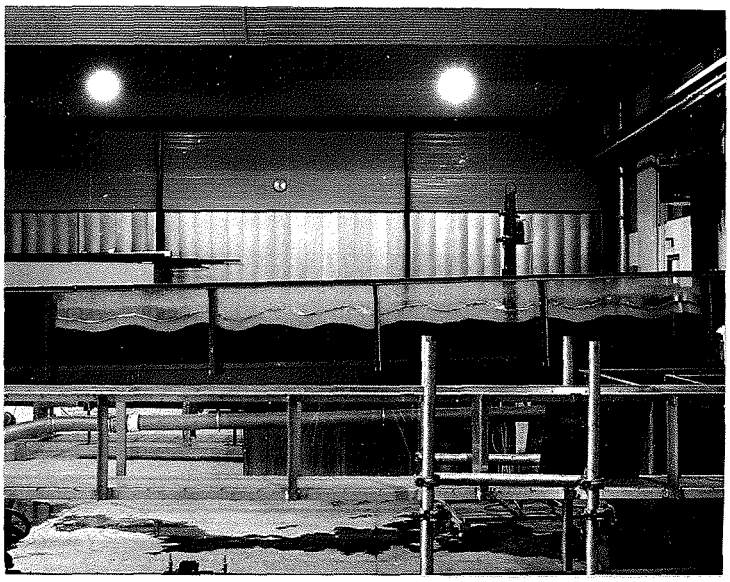

Run 24(a)

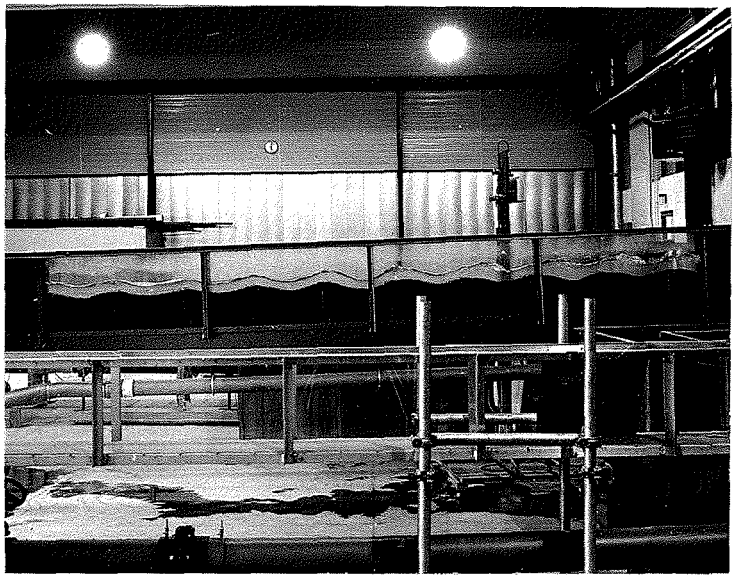

Run 24(b)

A3 $q = 0.110\ m^3\ s^{-1}/m$ INITIAL STATE : Unstable tumbling flow.

RUN	Q_s (kg/min)	DESCRIPTION
76	0.571	Flow is unstable. Discrete sediment waves observable. $L \simeq 3.5$ m. $c \simeq 0.02$ m/s. (See photograph)
72	1.414	Flow is unstable. Wave length is less distinct than for Run 76.
27	2.545	Flow is now practically stable. Sediment waves comprise a large proportion of the bed. $L \simeq 1.5$ m. $c \simeq 0.04$ m/s. (See photographs)
28	5.810	Large portion of the bed surface is plane. The flow is stable.

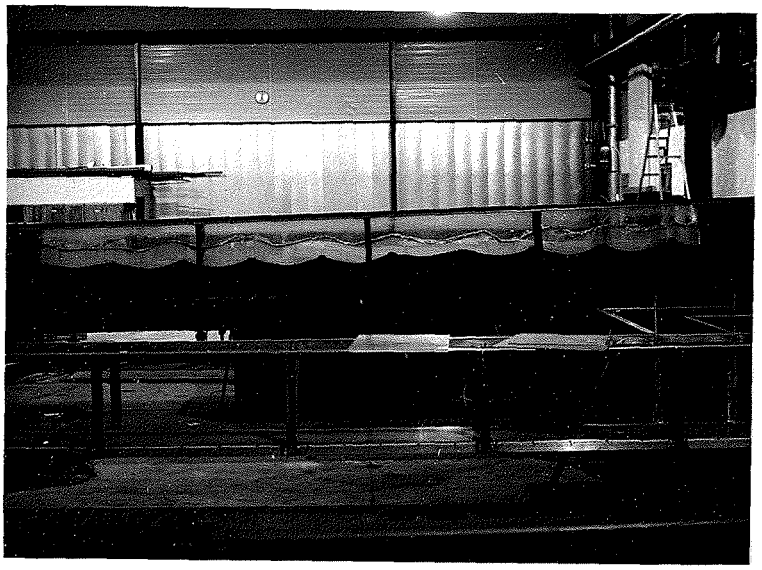

Run 76

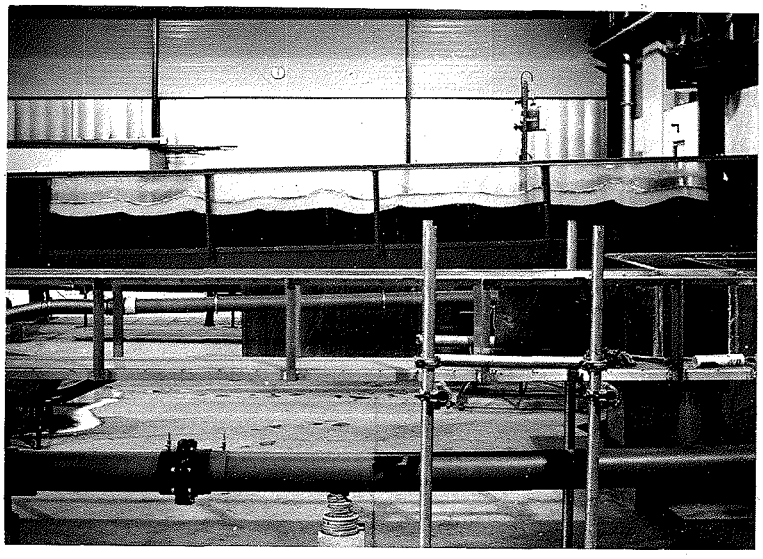

Run 27(a)

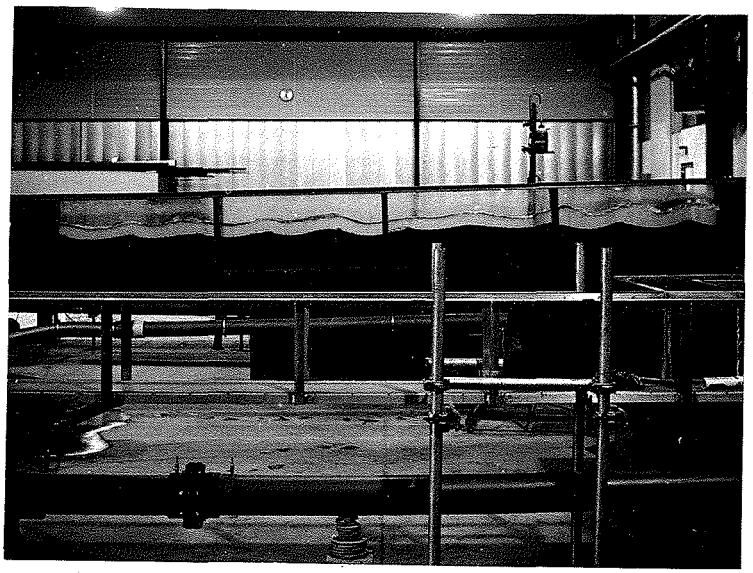

Run 27(b)

A4 $q = 0.138\ m^3\ s^{-1}/m$ INITIAL STATE : Shooting flow.

RUN	Q_s (kg/min)	DESCRIPTION
73	0.00	Shooting flow with some surface instability. Point of maximum scour midway between steps, although eroding just upstream of steps.
75	0.864	Discrete waves observable. Still some surface instability. $L > 3.5$ m. $c \simeq 0.006$ m/s.
31	1.363	Description as for Run 75. $L \simeq 2.5$ m. $c \simeq 0.005$ m/s. (See photographs)
74	2.137	Scour has decreased substantially from initial conditions. Sediment waves still observable. Flow essentially stable.
30	2.933	Bed is almost plane. Flow essentially stable.

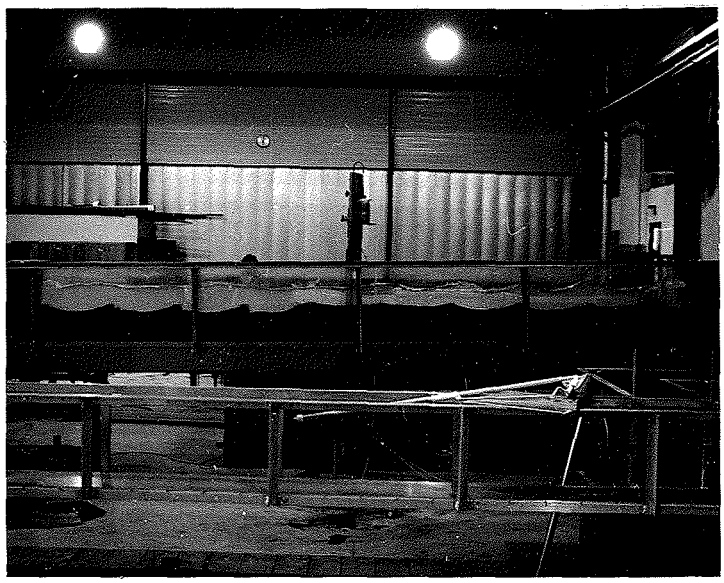

Run 31(a)

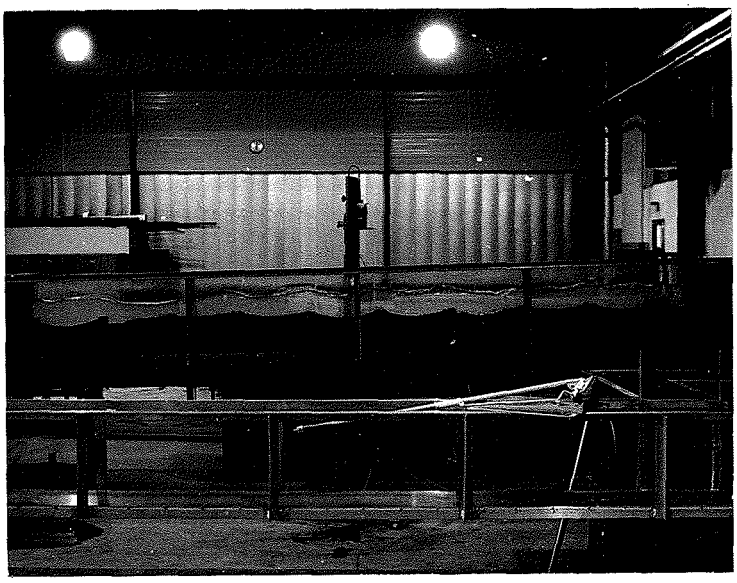

Run 31(b)

B. SLOPE = 0.098

B1 $q = 0.022\ m^3\ s^{-1}/m$ INITIAL STATE : Stable tumbling flow.

RUN	Q_s (kg/min)	DESCRIPTION
65	0.00	Flow is stable tumbling. Scour reflects plunging nappe profile. (See photograph)
64	1.525	Scour is reduced. Flow stable tumbling.
81	2.139	Scour reduced again. Flow still stable tumbling. Scour shapes accompanying sediment transport mechanism are observable. (See photograph)
1	2.791	Flow still stable. Scour again reduced.
2	3.678	Further reduction in scour. Flow stable.
4	5.352	As for Run 2.
3	5.852	Scour small. Flow stable (just).
5	9.096	System choked with sediment. Flow very unstable. (See photograph)

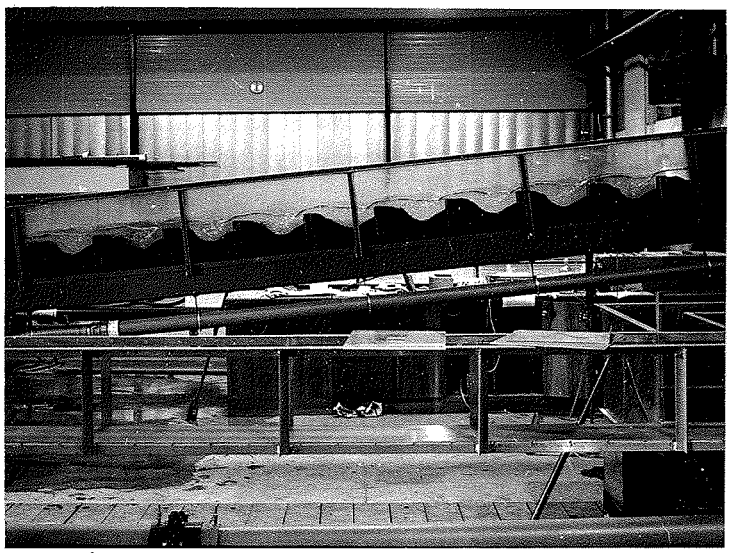

Run 65

Run 81

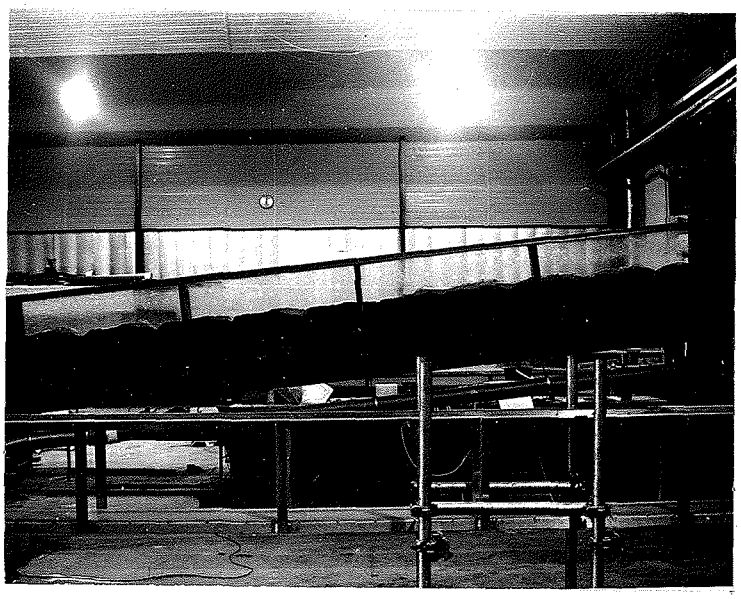

Run 5

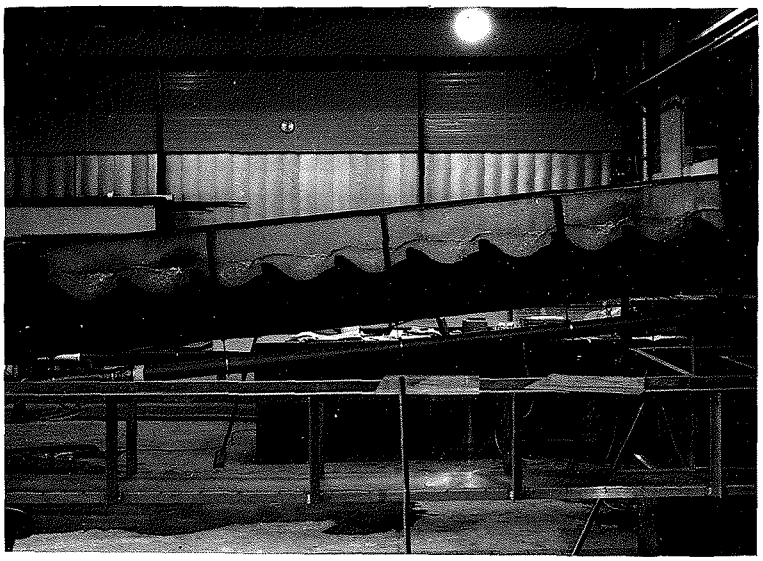

Run 66

B2 $q = 0.039\ m^3\ s^{-1}/m$ INITIAL STATE : Stable tumbling flow.

RUN	Q_s (kg/min)	DESCRIPTION
66	0.965	Flow stable (plunging nappe). Reasonably extensive scour. (See photograph)
67	4.862	Flow stable. Scour is reduced with sediment waves beginning to occur.
68	8.775	Sediment waves are apparent. Flow has become unstable.
69	11.878	Strong sediment waves. L ≃ 1 m. Flow is unstable. (See photograph)

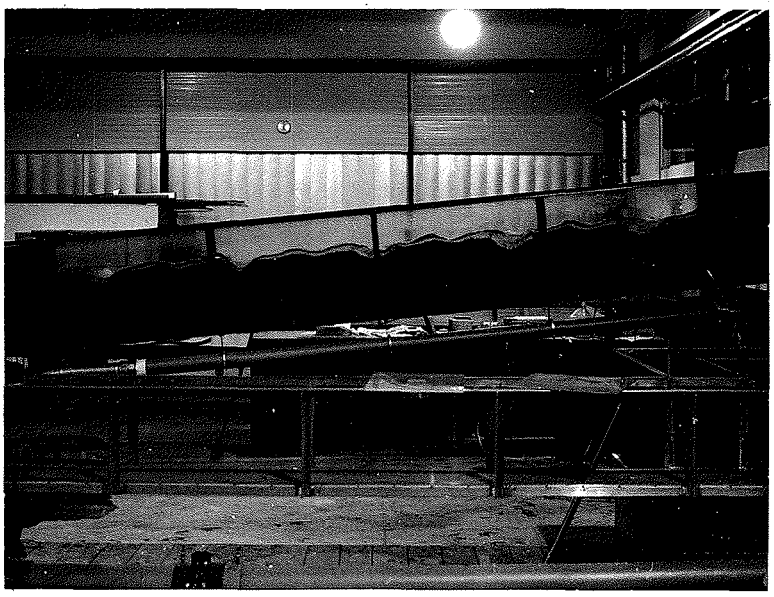

Run 69

B3 $q = 0.058\ m^3\ s^{-1}/m$ INITIAL STATE : Stable tumbling flow.

RUN	Q_s (kg/min)	DESCRIPTION
7	2.329	Flow is stable tumbling. Discrete sediment waves are already apparent.
8	3.991	Flow is stable. Discrete sediment waves.
9	5.688	Flow is still stable. Sediment waves are less apparent.
10	9.611	Sediment waves of L ≃ 1 m. Flow still stable (with some movement in pool associated with transport mechanism).
11	13.098	Strong sediment waves with two tier pool structure. L ≃ 1 m. Flow oscillating a little with transport mechanism, but there is no surging with roll waves. (See photograph)

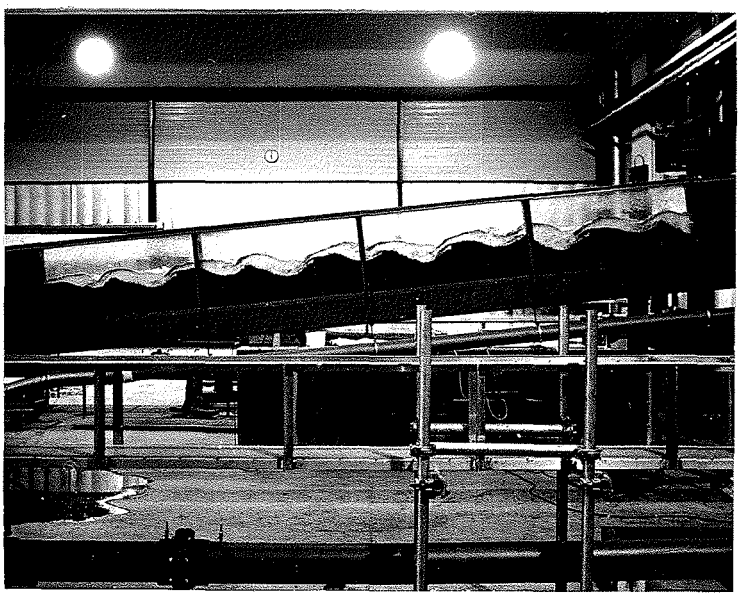

Run 11

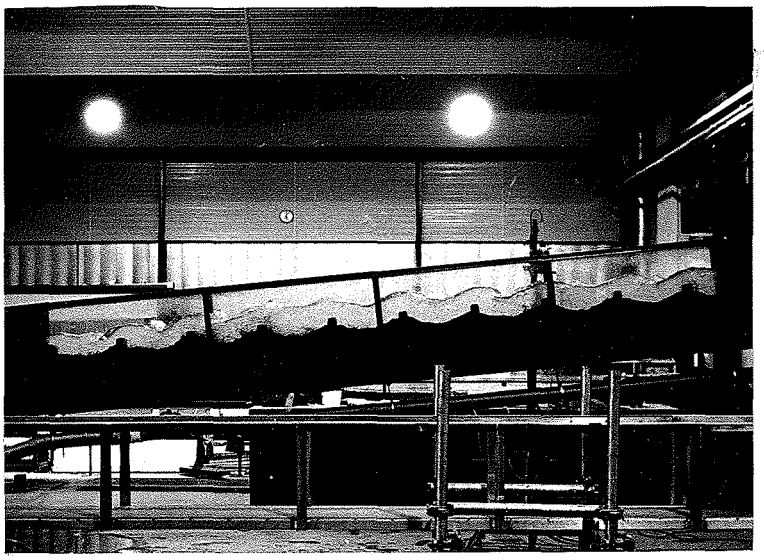

Run 12

B4 $q = 0.091\ m^3\ s^{-1}/m$ INITIAL STATE : stable tumbling flow.

RUN	Q_s (kg/min)	DESCRIPTION
12	1.441	Flow is unstable tumbling. Scour pattern is reasonably consistent. (See photograph)
13	3.059	Instability in the flow is not as marked as above. Scour pattern is reasonably consistent.
14	4.975	Flow instability is further diminished. Some variation in scour pattern is evident.
15	7.665	Flow is still unstable. Sediment waves are apparent. $L \simeq 2$ m. $c \simeq 0.05$ m/s.
16	12.558	Sediment waves with unstable flow. $L \simeq 2$ m. $c \simeq 0.05$ m/s. (See photographs)

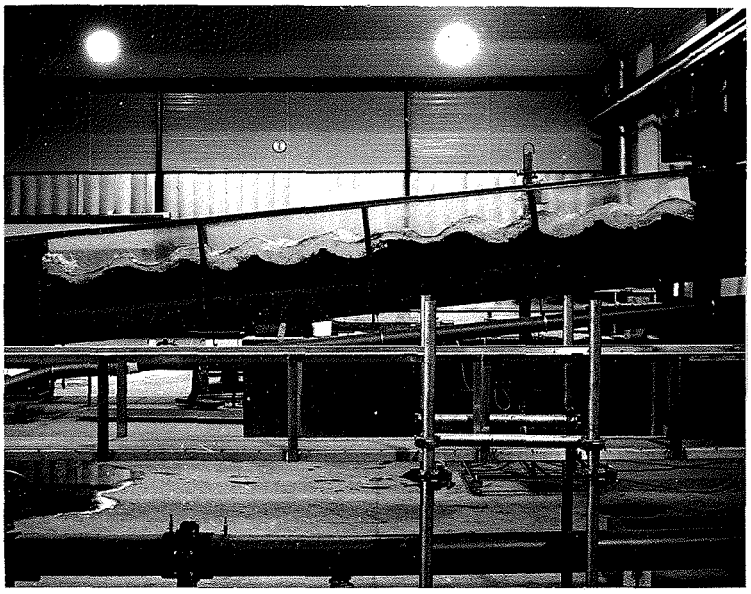

Run 16(a)

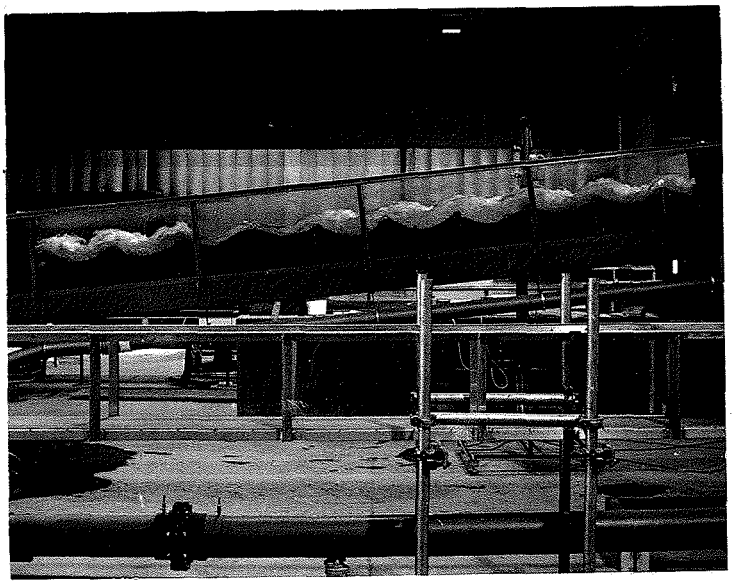

Run 16(b)

B5 $q = 0.127\ m^3\ s^{-1}/m$ INITIAL STATE : Unstable tumbling flow.

RUN	Q_s (kg/min)	DESCRIPTION
17	2.202	Flow is very unstable, with large roll waves. Scour pattern is reasonably consistent.
18	3.683	Flow still unstable with big roll waves. Reasonably consistent scour pattern.
19	5.817	Flow instability is less pronounded. Sediment is starting to travel in waves.
20	8.153	Flow is still unstable. Sediment waves apparent. $L \simeq 2.5$ m. $c \simeq 0.03$ m/s. (See photographs)
21	12.939	Flow still unstable, although again less pronounced. Sediment waves. $L \simeq 2$ m. $c \simeq 0.05$ m/s.

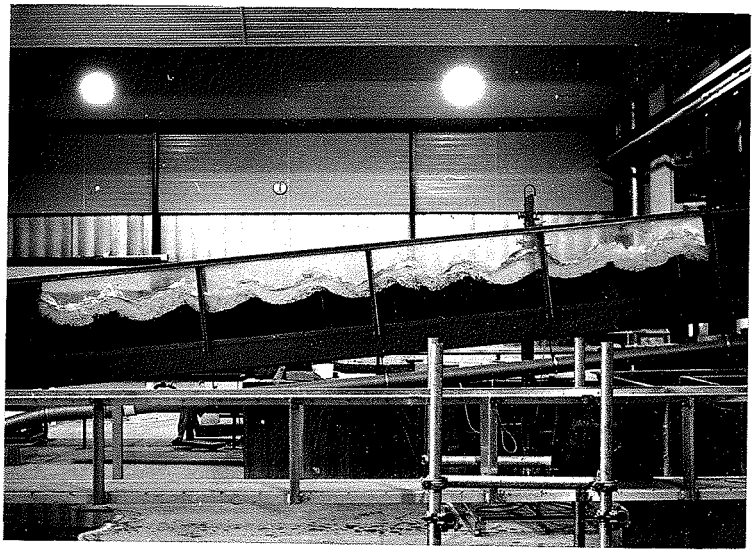

Run 20(a)

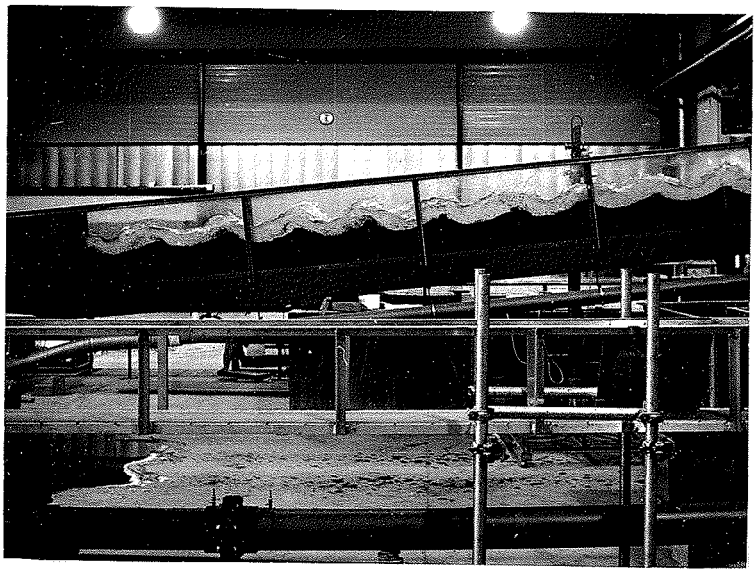

Run 20(b)

C. SLOPE = 0.172

C1 $q = 0.012\ m^3\ s^{-1}/m$ INITIAL STATE : Stable tumbling flow.

RUN	Q_s (kg/min)	DESCRIPTION
48	2.253	Small extent of scour. Flow stable. (See photograph)
49	3.995	Scour reduced. Flow stable.
50	6.730	Scour again reduced. Flow stable.
51	10.102	Two-tier sediment waves. Flow stable. (See photograph)
52	13.460	Same type of sediment waves as for Run 51, but almost choking system. Flow has become unstable. (See photograph)

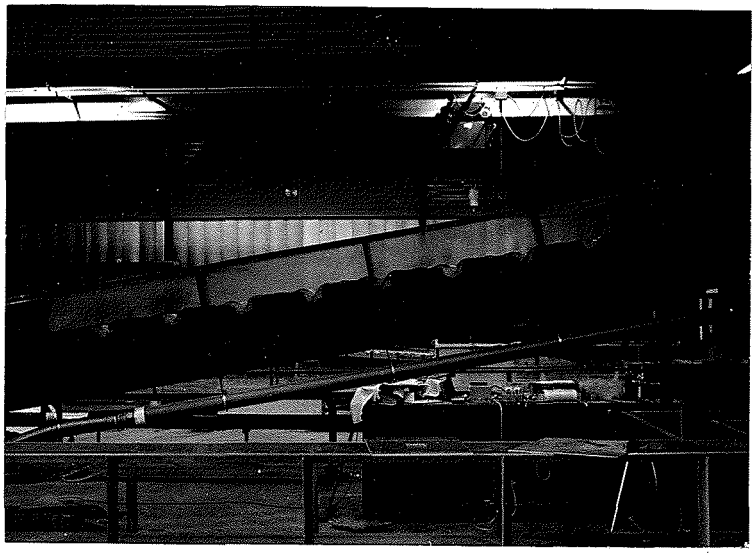

Run 48

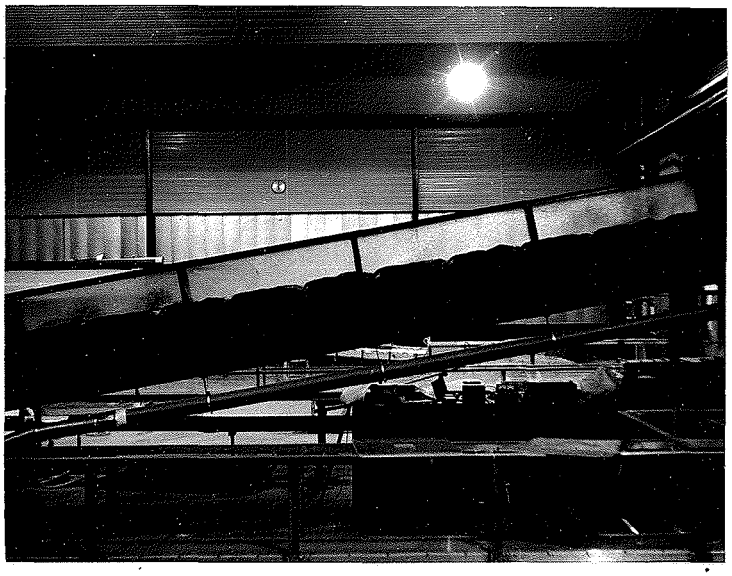

Run 51

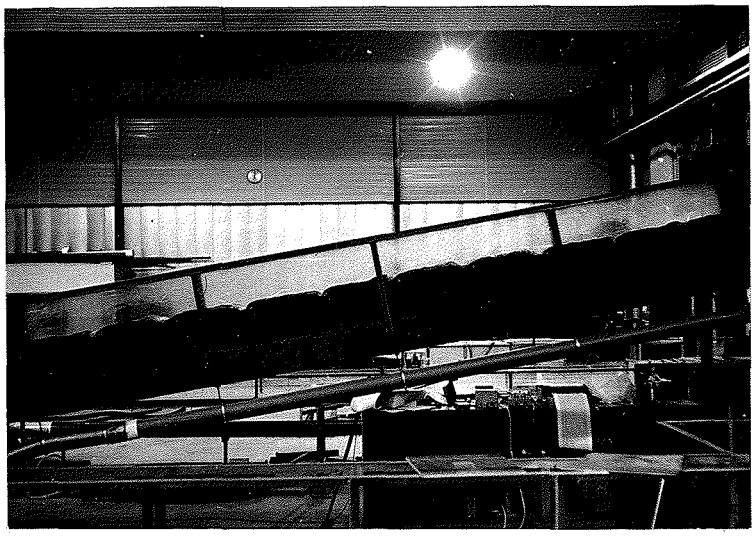

Run 52

C2 $q = 0.017\ m^3\ s^{-1}/m$ INITIAL STATE : Stable tumbling flow.

RUN	Q_s (kg/min)	DESCRIPTION
39	1.355	Flow stable. Reasonably consistent scour pattern. Period T of transport mechanism ≃ 23 secs.
40	3.408	Decrease in scour. Otherwise, same as for Run 39.
41	5.089	Stable flow. No sediment waves. (See photograph)
42	7.335	T ≃ 9 secs.) Comments as above.
43	11.384	T ≃ 5 secs.)

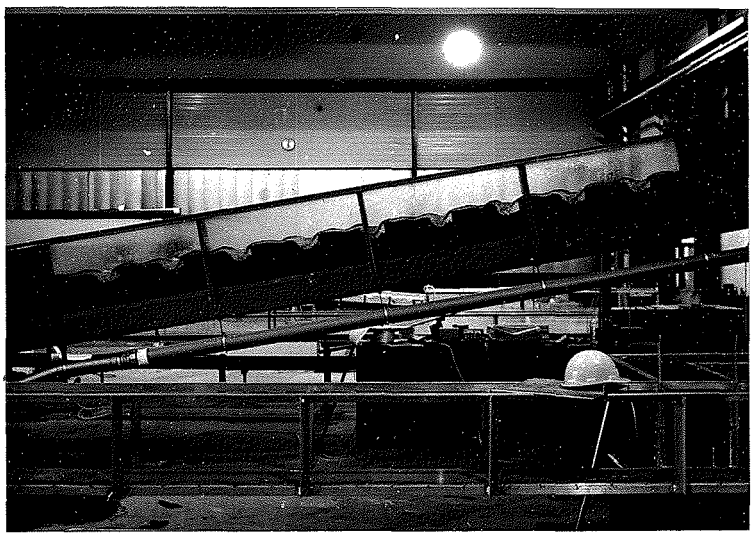

Run 41

C3 $q = 0.028\ m^3 \cdot s^{-1}/m$ INITIAL STATE : Stable tumbling flow.

RUN	Q_s (kg/min)	DESCRIPTION
34	1.706	Flow stable. No sediment waves. (See photograph)
35	3.592	As above. Period T associated with transport mechanism = 17 secs.
36	5.999	Flow stable. No sediment waves. T ≃ 12 secs.
37	8.781	Flow stable. No sediment waves.
38	11.068	Flow stable, no waves of sediment. (See photograph)

Run 34

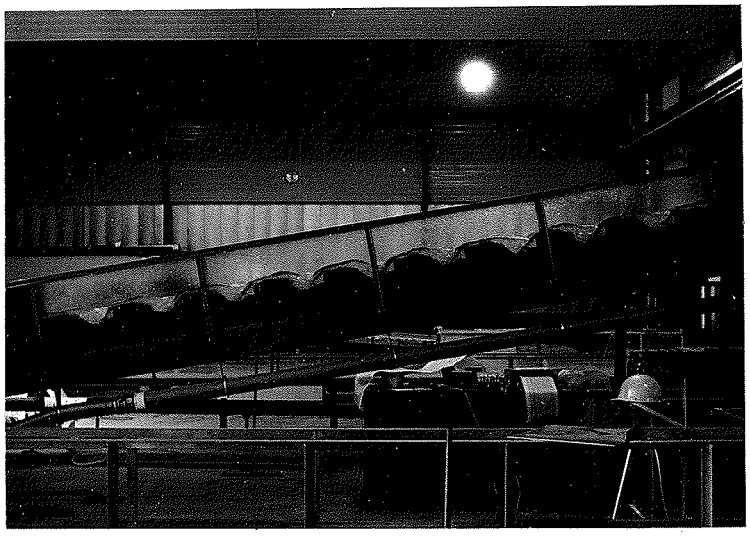

Run 38

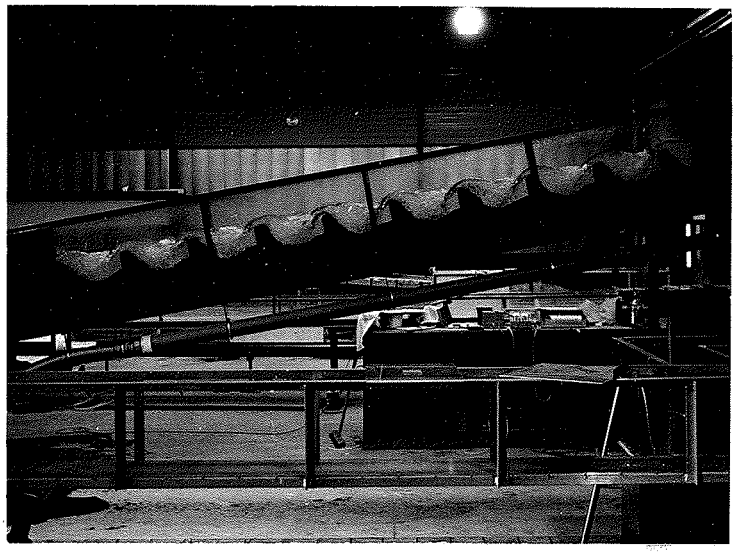

Run 46(a)

C4 $q = 0.049\ m^3\ s^{-1}/m$ INITIAL STATE : Stable tumbling flow.

RUN	Q_s (kg/min)	DESCRIPTION
44	1.401	All these runs had stable flow with no sediment waves. The transport mechanism was noted. (See photograph)
45	3.438	
46A	6.150	
46	9.265	
47	11.549	

D SLOPE = 0.248

D1 $q = 0.012\ m^3\ s^{-1}/m$ INITIAL STATE : Stable tumbling flow.

RUN	Q_s (kg/min).	DESCRIPTION
53	2.403	Consistent scour shape. Stable flow. (See photograph)
54	3.816	As for Run 53.

No photographs of Runs 55 to 58 were taken. Flow remained stable for all these runs. However, a two-tier pool shape denoted the presence of sediment waves for Runs 57 and 58.

Run 53

D2 $q = 0.027\ m^3\ s^{-1}/m$ INITIAL STATE : Stable tumbling flow.

RUN	Q_s (kg/min)	DESCRIPTION
59	2.780	All these runs had stable flow with no sediment waves. (See photograph)
60	6.223	
61	9.358	
62	13.201	

Run 60

APPENDIX 6

Amendments to thesis

LITERATURE REVIEW

It should be noted that nearly all quoted formulae for flow resistance (e.g. Judd and Peterson, Bathurst, Hey, and Keulegan) and sediment transport (e.g. Meyer-Peter and Müller, Einstein) were derived for rivers of different form from that of step-pool streams. As the processes of flow are different, it was not expected that these formulae would be directly applicable to step-pool channels. Rather, they are quoted to give an overview of the subject and to provide a comparison, illustrate previous techniques and so on. Almost no formulae for step-pool channels have been derived in previous studies.

The term $3.5D_{84}$ in the Keulegan equation (p 47) represents the equivalent roughness in terms of a measurable particle diameter. It is not in fact related to the blocking effect described by Thompson and Campbell which accounts for the funnelling of flow between boulders in channels with large relative roughness.

The equation of Volkart (eq. 6-12) is limited to a narrow test range as compared to that of this study. Consequently, the term defined as an error in Volkart's analysis reflects rather the limits of applicability of Volkart's equation.

EXPERIMENTAL ERRORS

Research into the salt-velocity technique by MacMurray (1983) has shown that errors in determining mean velocity in situations where mixing is slow and density differences between the tracer and water are of significance may be up to 10%. However, in tumbling flow, mixing is certainly not a problem.

Davies and Jaeggi (1981) show that the error in the determination of mean velocity for a steep stream situation depends mainly on the error in determining the travel time of the tracer between the probes. Given the nature of some of the conductivity trace patterns evaluated, a 10% error in the mean velocity and depth values is conceivable, indicating

a possible 15% error in the determination of $\sqrt{8/f}$. This error is still smaller than the observed variations in $\sqrt{8/f}$.

For step-pool streams the method is felt to be the best available and internally consistent, so the observed trends should be correct.

ANALYSIS OF RESULTS

The derived results and formulae are empirical and apply for the limited range of experimental conditions only. Consequently, application of the formulae (as opposed to the qualitative results) to flows in systems with different weir spacings and sediment sizes should be made with caution.

FROUDE NUMBERS

(See pages 78-81, 123-124). All the Froude numbers listed in the tables of results are less than unity. However, some of the corresponding tests are for the shooting flow regime where Froude numbers of greater than one could be expected. The salt-velocity value derived for these tests indicated that the lower section of the flow skimming over the step crests interacts strongly with the eddies between the steps. Thus, while the flow at or near the surface was certainly supercritical, the inclusion in the analysis of mean velocity of the much slower velocity components from near the weir crests resulted in average Froude numbers of less than unity.

JET ANGLE

θ is in fact not determined by the downstream step. Rather, the trends in θ with changing discharge are due to the fact that the nappes were nonaerated.